SANDIA REPORT
SAND2009-6944
Unlimited Release
Printed September 2010

Temperature and Heat Flux Datasets of a Complex Object in a Fire Plume for the Validation of Fire and Thermal Response Codes

Thomas Blanchat and Dann Jernigan

Prepared by
Sandia National Laboratories
Albuquerque, New Mexico 87185 and Livermore, California 94550

Sandia is a multiprogramming laboratory operated by Sandia Corporation,
a Lockheed Martin Company, for the United States Department of Energy's
National Nuclear Security Administration under Contract DE-AC04-94AL85000.

Approved for public release; further dissemination unlimited.

Sandia National Laboratories

Issued by Sandia National Laboratories, operated for the United States Department of Energy by Sandia Corporation.

NOTICE: This report was prepared as an account of work sponsored by an agency of the United States Government. Neither the United States Government, nor any agency thereof, nor any of their employees, nor any of their contractors, subcontractors, or their employees, make any warranty, express or implied, or assume any legal liability or responsibility for the accuracy, completeness, or usefulness of any information, apparatus, product, or process disclosed, or represent that its use would not infringe privately owned rights. Reference herein to any specific commercial product, process, or service by trade name, trademark, manufacturer, or otherwise, does not necessarily constitute or imply its endorsement, recommendation, or favoring by the United States Government, any agency thereof, or any of their contractors or subcontractors. The views and opinions expressed herein do not necessarily state or reflect those of the United States Government, any agency thereof, or any of their contractors.

Printed in the United States of America. This report has been reproduced directly from the best available copy.

Available to DOE and DOE contractors from
U.S. Department of Energy
Office of Scientific and Technical Information
P.O. Box 62
Oak Ridge, TN 37831

Telephone: (865) 576-8401
Facsimile: (865) 576-5728
E-Mail: reports@adonis.osti.gov
Online ordering: http://www.osti.gov/bridge

Available to the public from
U.S. Department of Commerce
National Technical Information Service
5285 Port Royal Rd.
Springfield, VA 22161

Telephone: (800) 553-6847
Facsimile: (703) 605-6900
E-Mail: orders@ntis.fedworld.gov
Online order: http://www.ntis.gov/help/ordermethods.asp?loc=7-4-0#online

SAND2009-6944
Unlimited Release
Printed September 2010

Temperature and Heat Flux Datasets of a Complex Object in a Fire Plume for the Validation of Fire and Thermal Response Codes

Thomas Blanchat and Dann Jernigan

Fire and Aerosol Sciences

Department Names
Sandia National Laboratories
P.O. Box 5800
Albuquerque, New Mexico 87185-1914

Abstract

It is necessary to improve understanding and develop temporally- and spatially-resolved integral scale validation data of the heat flux incident to a complex object in addition to measuring the thermal response of said object located within the fire plume for the validation of the SIERRA/FUEGO/SYRINX fire and SIERRA/CALORE codes. To meet this objective, a complex calorimeter with sufficient instrumentation to allow validation of the coupling between FUEGO/SYRINX/CALORE has been designed, fabricated, and tested in the Fire Laboratory for Accreditation of Models and Experiments (FLAME) facility.

Validation experiments are specifically designed for direct comparison with the computational predictions. Making meaningful comparison between the computational and experimental results requires careful characterization and control of the experimental features or parameters used as inputs into the computational model. Validation experiments must be designed to capture the essential physical phenomena, including all relevant initial and boundary conditions.

This report presents the data validation steps and processes, the results of the penlight radiant heat experiments (for the purpose of validating the CALORE heat transfer modeling of the complex calorimeter), and the results of the fire tests in FLAME.

CONTENTS

1. EXPERIMENT OBJECTIVE 1

1.1 Background 1

2. COMPLEX CALORIMETER 3

2.1 Design 3
2.2 Thermocouple Locations, Painting, and Assembly 8

3. PENLIGHT TESTING 14

3.1 Penlight Facility and Shroud 14
3.1.1 Penlight Shroud Extension 15
3.2 Penlight Characterization 22
3.3 Penlight Testing Overview 22
3.4 Test 1 – Nose In 1 26
3.5 Test 3 – Rear In 1 35
3.6 Test 6 – Nose Up 3 43
3.7 Summary of the Penlight Tests 52

4. FLAME TESTING 55

4.1 Experimental Facility Description 55
4.2 Experiment Measurements and Instrumentation 56
4.2.1 Facility Air Flow 57
4.2.2 Fuel Recession 60
4.2.3 Fuel Temperature Measurements 61
4.2.4 FLAME Wall Temperature 62
4.2.5 FLAME Wall Heat Flux and Fire Plume Heat Flux 63
4.2.6 Heat Flux to the Pool Surface 64
4.2.7 Photometric Fire Coverage 66
4.2.8 Wind Speed and Direction Measurement 66
4.2.9 Fuel Ignition 67
4.2.10 Summary of Instrumentation 68
4.3 Data Acquisition (DAQ) 69
4.4 Data Validation 70
4.5 Experiment Configuration and Matrix of Experiments in FLAME 71
4.6 Presentation of FLAME Facility Data from Test 15 – Nose Up 73
4.7 Presentation of Complex Calorimeter Data from Test 15 – Nose Up 80
4.8 Animation of the CC-15 Test Temperature Data – Nose Up 89
4.9 Animation of the CC-15 Test Surface Heat Flux Data – Nose Up 94

5. MEASUREMENTS OF BOUNDARY CONDITIONS AND MATERIAL PROPERTIES 101

5.1 Pan Heat Flux 101
5.2 Fuel Regression 102
5.3 Test-to-Test Variance in Calorimeter Surface Emissivity 103
5.4 Combustion Air Flow 105
5.5 Insulation and Stainless Steel Thermal Properties 107
5.6 Properties of JP-8 Jet Fuel 109

6. 109

7. MEASUREMENT UNCERTAINTY 111

7.1 Uncertainty of Overall System 111
7.2 Uncertainty of Calorimeter Sheathed Temperatures 112
7.3 MIMS Thermocouple Bias Errors 112

7.4 Heat Flux Measurements made by Sandia HFG Analyzer 113
7.5 Heat Flux Measurements made by Beck Engineering IHCP1D Code 113
7.6 Fuel Regression Measurements 114
7.7 Measurement Uncertainty Summary 114

8. QUANTIFY THE EXPERIMENTAL UNCERTAINTY – A POSTTEST VISIT WITH ANALYSTS 117

8.1 Insulation – Posttest Status and Variability in the Thermal Properties 118
8.2 Pyromark® Paint Emissivity – Large Uncertainty 119
8.3 Thermocouple Bias Errors 121
8.4 Posttest Thermocouple Attachment and Survivability 123
8.5 Experiment Repeatability 125

9. CONCLUSION 129

10. REFERENCES 130

APPENDIX A ENGINEERING DRAWINGS OF THE COMPLEX CALORIMETER 133

APPENDIX B COMPLEX CALORIMETER THERMOCOUPLE LOCATIONS 152

FIGURES

Figure 1 Example of a complex shape. 1
Figure 2 Complex calorimeter outer shell and support. 3
Figure 3 Complex calorimeter with outer shell removed. 4
Figure 4 Complex calorimeter with insulation layer removed. 4
Figure 5 Complex calorimeter with inner back cylinder removed. 5
Figure 6 Complex calorimeter cutaway showing blivet supports. 5
Figure 7 Construction and shop assembly photographs. 7
Figure 8 Thermocouple installation. 10
Figure 9 Pyromark paint application (pre-cure). 11
Figure 10 Pyromark paint after cure. 12
Figure 11 Final assembly. 13
Figure 12 Heated back and side, and unheated front views of Penlight. 14
Figure 13 The penlight shroud extension. 15
Figure 14 Penlight shroud and extension – isometric view 16
Figure 15 Penlight shroud and extension – front view 17
Figure 16 Penlight shroud and extension – back view 17
Figure 17 Penlight shroud and extension – left view 18
Figure 18 Penlight shroud and extension – right view 18
Figure 19 Penlight shroud and extension – top view 19
Figure 20 Penlight shroud and extension – bottom view 19
Figure 21 The complex calorimeter in the “nose in” orientation. 23
Figure 22 The nose up test utilizing the Penlight shroud extension. 23
Figure 23 The nose in configuration for Test 1. 26
Figure 24 Penlight Main Shroud – 2/10/05 27
Figure 25 Penlight Back Shroud - 2/10/05 27
Figure 26 Outer Cone – 2/10/05 28
Figure 27 Outer Bucket - 2/10/05 28
Figure 28 Outer Bucket Bottom Plate – 2/10/05 29
Figure 29 Inner Cone - 2/10/05 29
Figure 30 Inner Cone Bottom Plate – 2/10/05 30
Figure 31 Inner Bucket Outer Edge - 2/10/05 30
Figure 32 Inner Bucket Inner Edge – 2/10/05 31
Figure 33 Inner Bucket Bottom Plate - 2/10/05 31
Figure 34 Inner Bucket Blivet Plate – 2/10/05 32
Figure 35 Blivet Side - 2/10/05 32
Figure 36 Blivet Top (Cone Side) – 2/10/05 33
Figure 37 Blivet Bottom (Bucket Side) - 2/10/05 33
Figure 38 Penlight and calorimeter response (2280 s) in Test 1 34
Figure 39 Penlight Main Shroud – 2/23/05 35
Figure 40 Penlight Back Shroud - 2/23/05 35
Figure 41 Outer Cone – 2/23/05 36
Figure 42 Outer Bucket - 2/23/05 36
Figure 43 Outer Bucket Bottom Plate – 2/23/05 37
Figure 44 Inner Cone - 2/23/05 37

Figure 45 Inner Cone Bottom Plate – 2/23/05 38
Figure 46 Inner Bucket Outer Edge - 2/23/05 38
Figure 47 Inner Bucket Inner Edge – 2/23/05 39
Figure 48 Inner Bucket Bottom Plate - 2/23/05 39
Figure 49 Inner Bucket Blivet Plate – 2/23/05 40
Figure 50 Blivet Side - 2/23/05 40
Figure 51 Blivet Top (Cone Side) – 2/23/05 41
Figure 52 Blivet Bottom (Bucket Side) - 2/23/05 41
Figure 53 Calorimeter response (3400 s) in Test 3. 42
Figure 54 The nose up configuration for Test 6. 43
Figure 55 Penlight Main Shroud – 3/16/05 43
Figure 56 Penlight Back Shroud - 3/16/05 44
Figure 57 Outer Cone – 3/16/05 44
Figure 58 Outer Bucket - 3/16/05 45
Figure 59 Outer Bucket Bottom Plate – 3/16/05 45
Figure 60 Inner Cone - 3/16/05 46
Figure 61 Inner Cone Bottom Plate – 3/16/05 46
Figure 62 Inner Bucket Outer Edge - 3/16/05 47
Figure 63 Inner Bucket Inner Edge – 3/16/05 47
Figure 64 Inner Bucket Bottom Plate - 3/16/05 48
Figure 65 Inner Bucket Blivet Plate – 3/16/05 48
Figure 66 Blivet Side - 3/16/05 49
Figure 67 Blivet Top (Cone Side) – 3/16/05 49
Figure 68 Blivet Bottom (Bucket Side) - 3/16/05 50
Figure 69 Penlight and calorimeter response (3200 s) in Test 6. 51
Figure 70 Repeatability of penlight shroud temperatures. 52
Figure 71 Computed standard error for the outer bucket over 3 penlight tests. 53
Figure 72 Complex calorimeter on support stand in FLAME. 55
Figure 73 Side and top views of the flame facility with major dimensions. 56
Figure 74 The air source ring, fuel pan, and pedestal in FLAME. 59
Figure 75 The air source ring, fuel pan, and pedestal in FLAME. 59
Figure 76 TSI hot-wire velocity probes at the NE and SW locations. 60
Figure 77 Fuel differential pressure, regression rate, and pool mass loss rate. 61
Figure 78 Thermocouple array for fuel recession. 62
Figure 79 Thermocouples on the FLAME West Wall. 63
Figure 80 FLAME East wall heat flux array. 64
Figure 81 Fuel pan showing SNL HFGs, igniters, and rails. 64
Figure 82 Fuel pan rails, HFGs, and igniter shields removed. 65
Figure 83 The Sandia HFG. 65
Figure 84 Video cameras on the North Wall. 66
Figure 85 Fuel igniter setup 67
Figure 86 The mobile instrumentation trailer. 69
Figure 87 Ambient air monitor temperatures. 75
Figure 88 Fuel pan array temperatures. 75
Figure 89 Monitor temperatures for the CC support arm. 76
Figure 90 Fiducial signal for igniter. 76

Figure 91 FLAME wall and coolant temperatures. 77
Figure 92 Air ring velocity from the TSI anemometers. 77
Figure 93 Wind Speed and Direction near FLAME chimney. 78
Figure 94 Laser signal for soot concentration analysis. 78
Figure 95 Fuel pan differential pressure measurement. 79
Figure 96 Heat flux measurements from the wall-mounted gauges. 79
Figure 97 Flow rate from the four blowers supplying the air ring. 80
Figure 98 CC-15 outer cone temperatures. 81
Figure 99 CC-15 outer bucket temperatures. 82
Figure 100 CC-15 outer bucket bottom plate temperatures. 82
Figure 101 CC-15 inner cone temperatures. 83
Figure 102 CC-15 inner cone bottom plate temperatures. 83
Figure 103 CC-15 inner bucket outer edge temperatures. 84
Figure 104 CC-15 inner bucket inner edge temperatures. 84
Figure 105 CC-15 inner bucket bottom plate temperatures. 85
Figure 106 CC-15 inner bucket blivet plate temperatures. 85
Figure 107 CC-15 blivet side temperatures. 86
Figure 108 CC-15 blivet top (cone side) temperatures. 86
Figure 109 CC-15 blivet bottom (bucket side) temperatures. 87
Figure 110 Insulation wrapping the support arm. 88
Figure 111 CC-15 surface temperature contours at 0 s. 89
Figure 112 CC-15 surface temperature contours at 200 s. 90
Figure 113 CC-15 surface temperature contours at 400 s. 90
Figure 114 CC-15 surface temperature contours at 600 s. 91
Figure 115 CC-15 surface temperature contours at 800 s. 91
Figure 116 CC-15 surface temperature contours at 1000 s. 92
Figure 117 CC-15 surface temperature contours at 1200 s. 92
Figure 118 CC-15 surface temperature contours at 1400 s. 93
Figure 119 CC-15 surface temperature contours at 1600 s. 93
Figure 120 CC-15 surface temperature contours at 1800 s. 94
Figure 121 Calorimeter cutaway showing blivet supports and no mid insulation. 95
Figure 122 CC-15 surface incident heat flux contours at 0 s and 50 s. 95
Figure 123 CC-15 surface incident heat flux contours at 100 s and 150 s. 96
Figure 124 CC-15 surface incident heat flux contours at 200 s and 250 s. 96
Figure 125 CC-15 surface incident heat flux contours at 300 s and 350 s. 97
Figure 126 CC-15 surface incident heat flux contours at 400 s and 450 s. 97
Figure 127 CC-15 surface incident heat flux contours at 500 s and 550 s. 98
Figure 128 CC-15 surface temperature contours at 600 s and 650 s. 98
Figure 129 CC-15 surface incident heat flux contours at 700 s and 750 s. 99
Figure 130 CC-15 surface incident heat flux contours at 800 s and 850 s. 99
Figure 131 CC-15 surface incident heat flux contours at 900 s and 950 s. 100
Figure 132 Lower north wall camera: prestart, ignition, 4 minutes, 1 min average. 100
Figure 133 Temperature from pan SNL HFGs Pan in CC-1. 101
Figure 134 Incident heat flux from pan SNL HFGs Pan in CC-1. 101
Figure 135 Fuel DP data. 102
Figure 136 Fuel regression profiles. 103

Figure 137 Templates for emissivity measurements. 104
Figure 138 Complex Calorimeter surface spot emissivity..... 104
Figure 139 Average surface emissivity..... 105
Figure 140 Combined transient blower flow rate. 106
Figure 141 Air ring standard and actual air velocity (all tests)..... 106
Figure 142 Thermal properties for 8 pcf Cerablanket. 108
Figure 143 Thermal properties for 304 stainless steel. 108
Figure 144 Schematic of a typical TC data acquisition system. 111
Figure 145 Cross section and fine mesh TFNS solution for the calorimeter in the FLAME facility. 117
Figure 146 Post test status of insulation. 118
Figure 147 Testing of thermal properties of ceramic fiber insulation. 119
Figure 148 The Cary-Integrating Sphere and SOC-100 Hemispherical Directional Reflectometers. 120
Figure 149 Emissivity data for 304SS with Pyromark paint. 120
Figure 150 Schematic of thermocouple mounted on outer shell. 121
Figure 151 Measured and corrected temperatures at location 53 for CC-15. 123
Figure 152 Pretest and posttest views of thermocouple attachments. 123
Figure 153 Procedure to analyze thermocouple attachment. 124
Figure 154 Inner shell thermocouple attachment analysis. 124
Figure 155 Comparison of fuel regression in CC-15, CC-17, and CC-18. 126
Figure 156 Blivet response repeatability. 126
Figure 157 Cone and cylinder response repeatability. 127
Figure 158 Relative difference of the experiments used for model prediction. 128

TABLES

Table 1 Penlight Shroud and Extension Thermocouple Locations 20
Table 2 List of penlight experiments. 25
Table 3 Average Air Source Velocity as a function of the ganged blower speed. 58
Table 4 Instrumentation List 68
Table 5 Experiment Matrix for FLAME Tests 71
Table 6 Boundary Conditions for the FLAME experiments. 72
Table 7 Air Ring Flow and Velocity 107
Table 8 Properties of JP-8 Jet Fuel 109
Table 9 Measurement Uncertainty Summary 115
Table 10 Percent correction of absolute temperature for given plate temperatures. 122
Table 11 Thermocouples failing attachment criteria. 125

NOMENCLATURE

AF&F	Arming, Fuzing and Firing
ASC	Advanced Strategic Computing
ASME	American Society of mechanical Engineers
CARS	Coherent Anti-Stokes Raman Scattering
DAQ	Data Acquisition
DAS	Data Acquisition System
DP	Differential Pressure
DSW	Directed Stockpile Work
FLAME	Fire Laboratory for Accreditation of Models and Experiments
FRH	FLAME/Radiant Heat facility
HFG	Heat Flux Gauge
HP	Hewlett Packard
ID	Inner Diameter
LAN	Local Area Network
LCBS	Lurance Canyon Burn Site
LEP	Lifetime Extension Program
M&S	Modeling and Simulation
MIMS	Mineral-Insulated Metal-Sheathed
MIU	Mobile Instrument Trailer
MTE	Major Technical Element
MUX	Multiplexer Units
NI	National Instrument
NIST	National Institute of Standards and Technology
OD	Outer Diameter
PIRT	Phenomena Identification and Ranking Table
PIV	Particle Image Velocimetry
PSL	Primary Standards Laboratory
RANS	Renyolds-Average Navier-Stokes
RHF	Radiant Heat Facility
RSS	Root-Sum-Square
SNL	Sandia National Laboratories
STS	Stockpile to Target Sequence
TC	Thermocouple
TTC	Thermal Test Complex
UPS	Uninterruptible Power Supply
V&V	Verification and Validation
WSEATC	Weapons Systems Engineering Assessment Technology Campaign
WSECC	Weapons Systems Engineering Certification Campaign

ACKNOWLEDGEMENTS

The authors want to acknowledge and thank Chuck Hanks for developing the hardware and performing the novel thermocouple attachment check – outstanding! Marty Sherman performed numerous analyses in preparation for sending the data to the Calore team for thermal response comparisons, including looking at thermocouple conduction and natural convection effects. Kevin Dowding reviewed thermocouple bias errors and also provided the method to assess the thermocouple attachment error. In addition, Kevin provided insight on presentation of experiment variability.

As always, these experiments could not have been performed without the support of the extremely capable technologists in the Fire and Aerosol Sciences Department and the TMSS support group who assembled the hardware and ran the tests.

Lastly, I want to thank those who performed the peer-review of this report, Sheldon Tieszen, Jim Nakos and Kevin Dowding.

1. EXPERIMENT OBJECTIVE

1.1 Background

It is necessary to improve understanding and develop validation data for the heat flux incident to a complex object located within the fire plume for the validation of SIERRA/FUEGO/SYRINX fire and SIERRA/CALORE [Bova et al.] thermal response codes. To meet this objective, a complex calorimeter with sufficient instrumentation to allow validation of the coupling between FUEGO/SYRINX/CALORE was designed and fabricated, in preparation for fire testing in the Fire Laboratory for Accreditation of Models and Experiments (FLAME) facility. Refer to Blanchat et al. [2005] for the detailed test plan describing the steps and requirements for this formal validation test activity.

The complex calorimeter was designed to enable validation of the coupling between FUEGO/SYRINX/CALORE. The need to measure incident heat flux to prototypic devices in actual fire conditions guided the shape (Figure 1) and instrumentation of the complex calorimeter. In addition, the complex calorimeter contains sufficient complexity and instrumentation to allow meaningful exercise and assessment of the code coupling. Data sets will be obtained to measure the incident total heat flux to the object, and the thermal response of a component within the complex object in a fully turbulent fire.

Figure 1 Example of a complex shape.

Pretest computational simulations were performed to guide the calorimeter and experiment design. Pretest fire simulations were performed with the VULCAN CFD fire codes [Luketa-Hanlin et al., 2004]). Design of the complex calorimeter for thermal response was performed using CALORE and a user-imposed heat flux boundary condition [Romero, C., 2004].

The goal of this report is to present a description of the complex calorimeter hardware, the results of the penlight experiments (for possible use in validation of the CALORE heat transfer models of the complex calorimeter), and the results of the fire experiments in the FLAME facility. In addition, data validation steps and processes, and measurement uncertainty will be discussed.

This report was written specifically with the end-user, the fire and thermal analyst, in mind. All of the experimental data is included on a DVD. Data and plots in Excel format provide a convenient interface for navigating the experiment data sets.

In addition to the numerical and graphical presentation of the data, animations of temperature and heat flux contour plots of the calorimeter and penlight shrouds were created to better visualize the fire insult (some animations are included on the CD). The DVD also contains some of the digitized movies from the video camera coverage of all

the fires. The digitized movies can be viewed with a standalone MPEG viewer, such as Windows Media Player. The Excel program and the video media are intended to provide a user-friendly archival database in support of model validation efforts.

The continued development of the model validation experiments to provide validated fire physics models (e.g. FUEGO) will eventually lead to an ability to predict the threat posed by fires, the response of objects in fires, and confidence in those predictions.

2. COMPLEX CALORIMETER

2.1 Design

The layout for the complex calorimeter is shown in Figures 2-6 below with some photographs from construction and shop assembly shown in Figure 7. The complex calorimeter is composed of three 304 stainless steel (SS) sections: a nose cone; a cylindrical center section; and a cylindrical base, each with an outer and an inner shell (concentric). A large SS mass (blivet) resides inside the inner shell of the cylindrical center section. Overall, it is approximately 3 ft. long and has a diameter of 15 inches. Construction drawings are provided in Appendix A. Note that material certifications were required from the manufacturer and all as-received parts were inspected for compliance with the drawings.

Thermocouples (TCs) (all thermocouples are 1/16-inch mineral-insulated metal-sheathed type-K) are attached to the inside of the outer shell (1/8-inch thick) of all three sections. Coincident thermocouples are attached to the inside shell (3/8-inch thick). These thermocouples, with the use of ceramic fiber insulation (1-inch thick Cerablanket™), allow reduction of the temperature data to absorbed heat flux via 1-D inverse heat conduction methods [Nakos, 2004].

While the calorimeter design is relatively simple (only two well-characterized materials and no water-cooled or gas-purged instrumentation), the complex calorimeter contains sufficient complexity (shape, multiple layers) and instrumentation to allow meaningful exercise and assessment of the FUEGO/SYRINX/CALORE coupling.

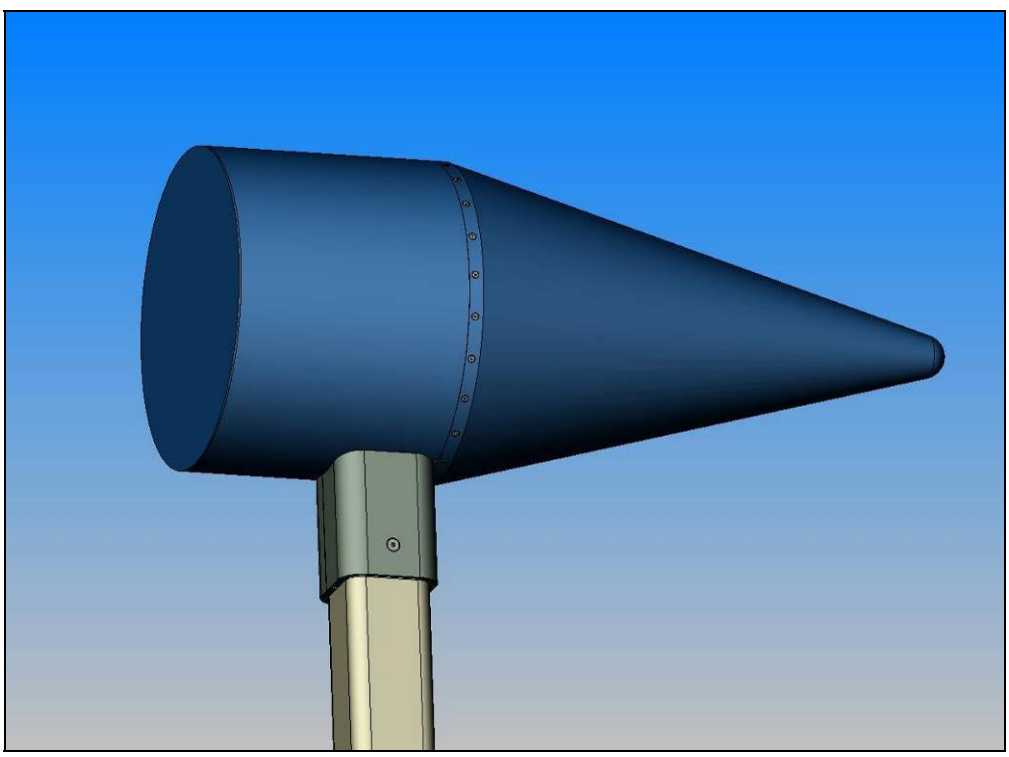

Figure 2 Complex calorimeter outer shell and support.

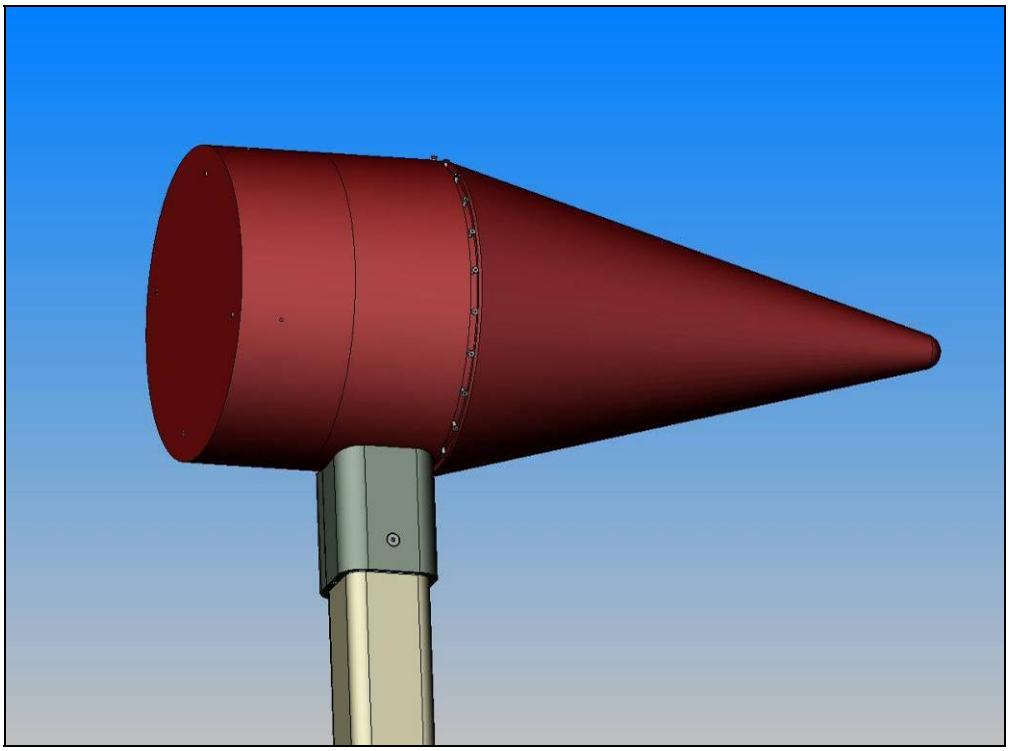

Figure 3 Complex calorimeter with outer shell removed.

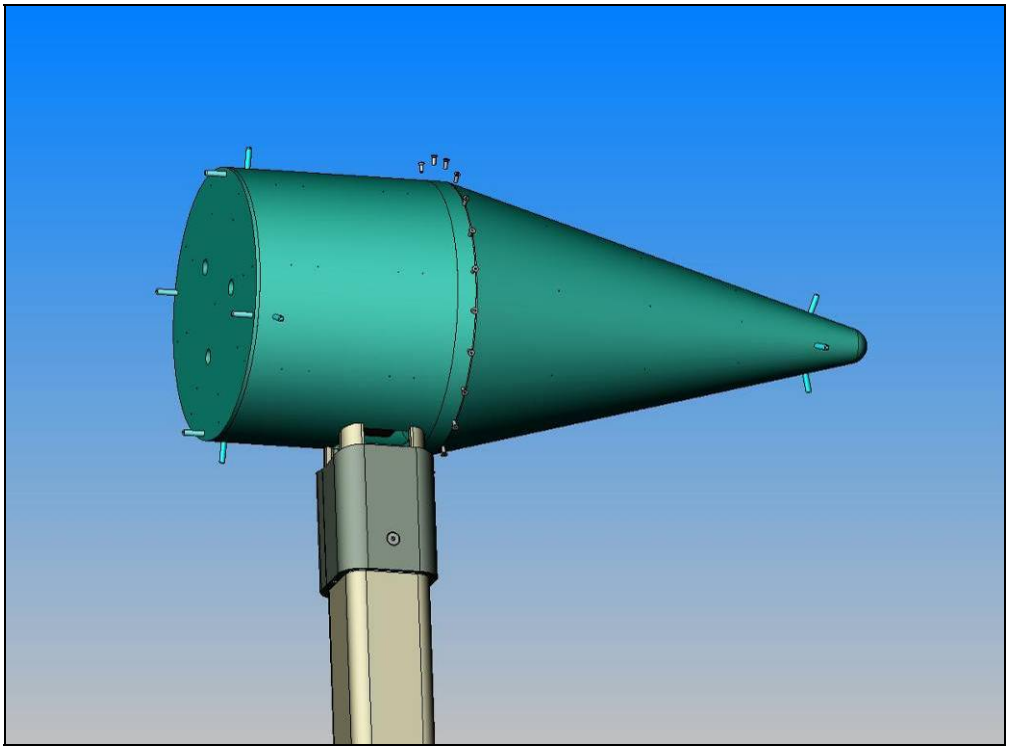

Figure 4 Complex calorimeter with insulation layer removed.

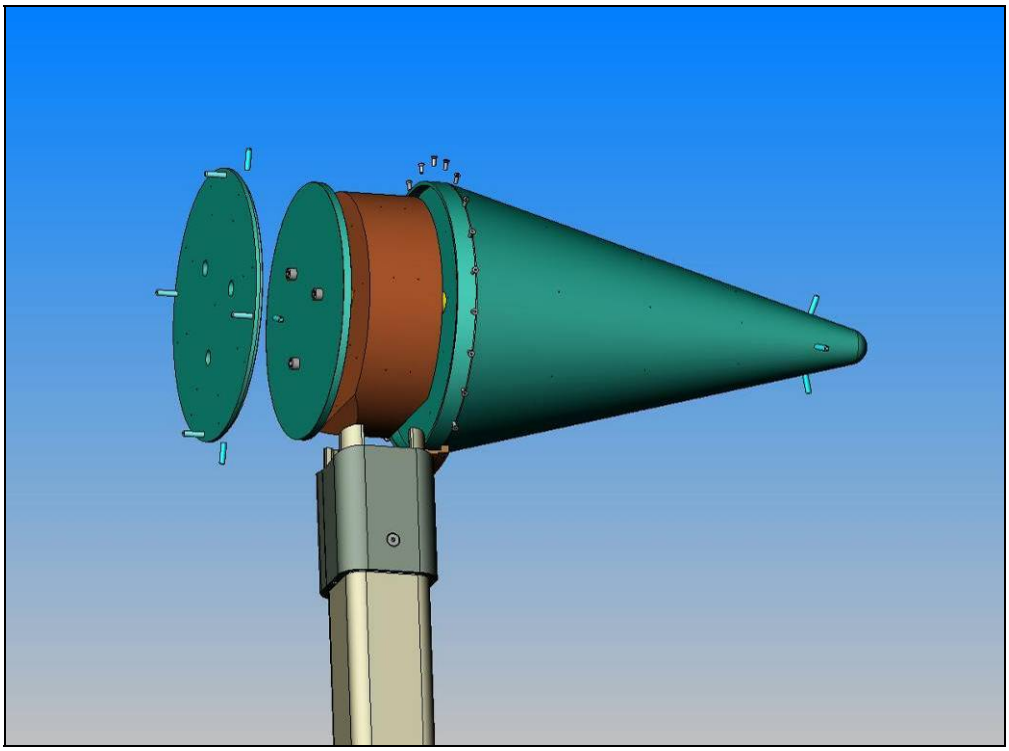

Figure 5 Complex calorimeter with inner back cylinder removed.

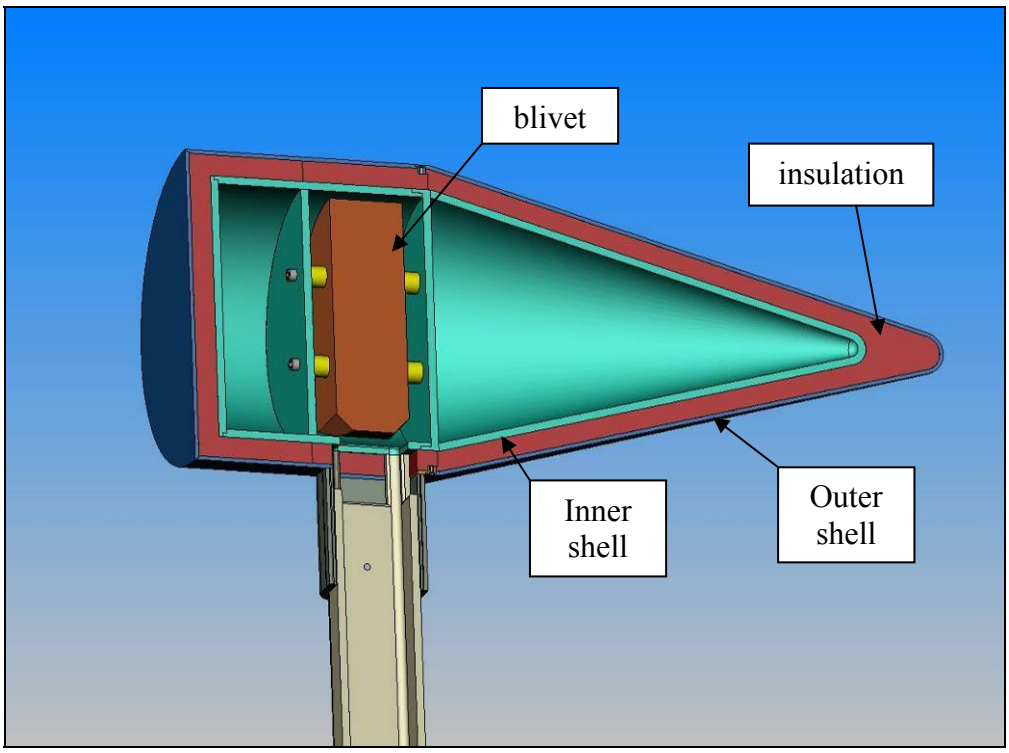

Figure 6 Complex calorimeter cutaway showing blivet supports.

Inner cylinder (inner bucket)

Inner cylinder welded to support arm

Outer cylinder (outer bucket)

View inside inner cylinder with blivet spacers

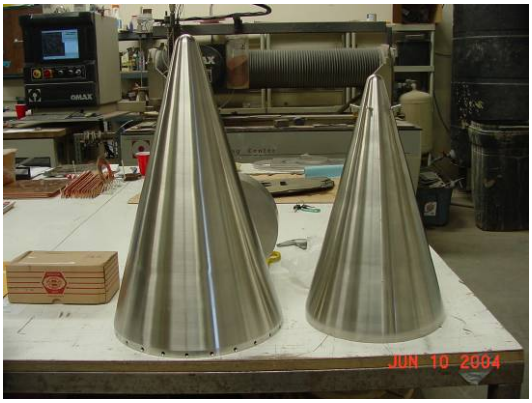

Outer and inner cone

Blivet placed in the inner cylinder

Inner cone bottom

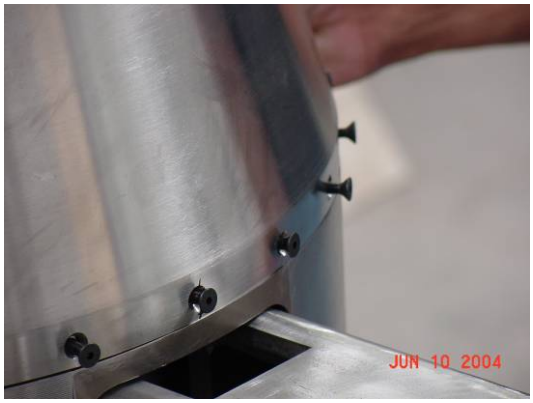

Attaching outer cone to outer cylinder

Inner cone attached to inner cylinder

Assembled calorimeter

Inner cone attachment close up

Figure 7 Construction and shop assembly photographs.

2.2 Thermocouple Locations, Painting, and Assembly

The temperature measurements are quite extensive, consisting of data from 254 thermocouples (TC), over all sections.

The response variable for FUEGO validation will be some norm or measure of incident heat flux (not including the portion of the incident reflected away) to the calorimeter outer surface. Incident heat flux is the sum of the absorbed flux plus the re-radiated flux and convective flux. The heat re-radiated from the calorimeter surface can be calculated from the surface temperature (a product from the inverse heat conduction calculation for absorbed heat flux) and the surface emissivity. The entire outer surface of the calorimeter is painted with a high temperature black paint (Pyromark 2500, emissivity = 0.85±0.09, see Nakos et al. [2004b]).

TC locations on the calorimeter inside surface of the *outer shell* are: **outer shell bottom surface -** three rings – 17 locations; **outer shell cylindrical surface -** four rows – 30 locations; **outer shell cone surface** – six rows – 36 locations (three rows have 8 TCs per row, 45° spacing, three rows have 4 TCs per row, 90° spacing) and 1 TC at the tip of the outer cone. This gives a total of **84** thermocouple locations on the outer shell.

TC locations on the calorimeter outer surface of the *inner shell* are: **inner shell bottom surface -** three rings – 17 locations; **inner shell cylindrical surface -** four rows – 30 locations; **inner shell cone surface** – three rows – 24 locations (three rows with 8 TCs per row, 45° spacing) and 1 TC at the tip of the inner cone. In addition, there are 14 TC locations on the calorimeter inner surface of the *inner shell*, located on the **inner shell cylindrical surface** – two rows – seven TC's per row, coincident with the TC's attached to the blivit. In addition, there are 17 coincident TCs attached to the **flat surface of the inner cone** and 17 coincident TCs attached to the **flat surface of the inner cylinder** that are opposite the matching two flat surfaces of the blivit, discussed below. This gives a total of **120** thermocouple locations on the inner shell.

The center section has been designed to provide primarily a radiant cavity environment to a central object ('blivet') for the CALORE simulation. The blivit is a solid disk of stainless steel, 11.17 inches in diameter and 3.5 inches thick. The blivet has three rings of TCs on each flat face (17 TCs, a center TC, a middle ring of eight, and an outer ring of eight) and two rows of TCs on the cylindrical face (16 TCs, eight per row, 45° spacing) for a total of **50** thermocouples.

The total number of TCs attached to the complex calorimeter is **254** (not counting telltales or support arm thermocouples). All thermocouple locations on the complex calorimeter are extensively documented in Appendix B.

Extensive checks were performed on the thermocouples upon receipt from the manufacturer, including resistance checks (lead to lead, + to sheath, - to sheath (megger at 200 volts, 1 s cycle, acceptance criteria > 100 MΩ)) and a water bath with 10 TCs/test in a stirred chiller at 2°C and 90°C (acceptance criteria of ±1°C to a calibrated TC).

All thermocouples were placed on the calorimeter per an operating procedure and by a qualified technologist. Placements were within ±0.0625 inches of the punch mark located during the machining process (Appendix A).

All inner stainless steel surfaces that predominately radiate to the central cavity and blivet (including the blivet) are painted with Pyromark® 2500 and then cured according to a recommended cure schedule. Emissivity measurements were taken on the outer shell surface (pre- and post-test). Photographs of thermocouple mounting, painting, and final assembly are given in Figures 8-11.

All parts of the CC (except for the 3 bolts through the blivet and the small screws attaching the outer cone to the outer cylinder) were fabricated using 304 SS. High temperature ceramic blanket insulation (1 inch thick, 8 lb/ft3 density Cerablanket from Thermal Ceramics®) is placed between the concentric inner and outer shells. The thermal properties for the calorimeter materials and the surface emissivity are discussed in detail in Section 5.

Figure 8 Thermocouple installation.

Figure 9 Pyromark paint application (pre-cure).

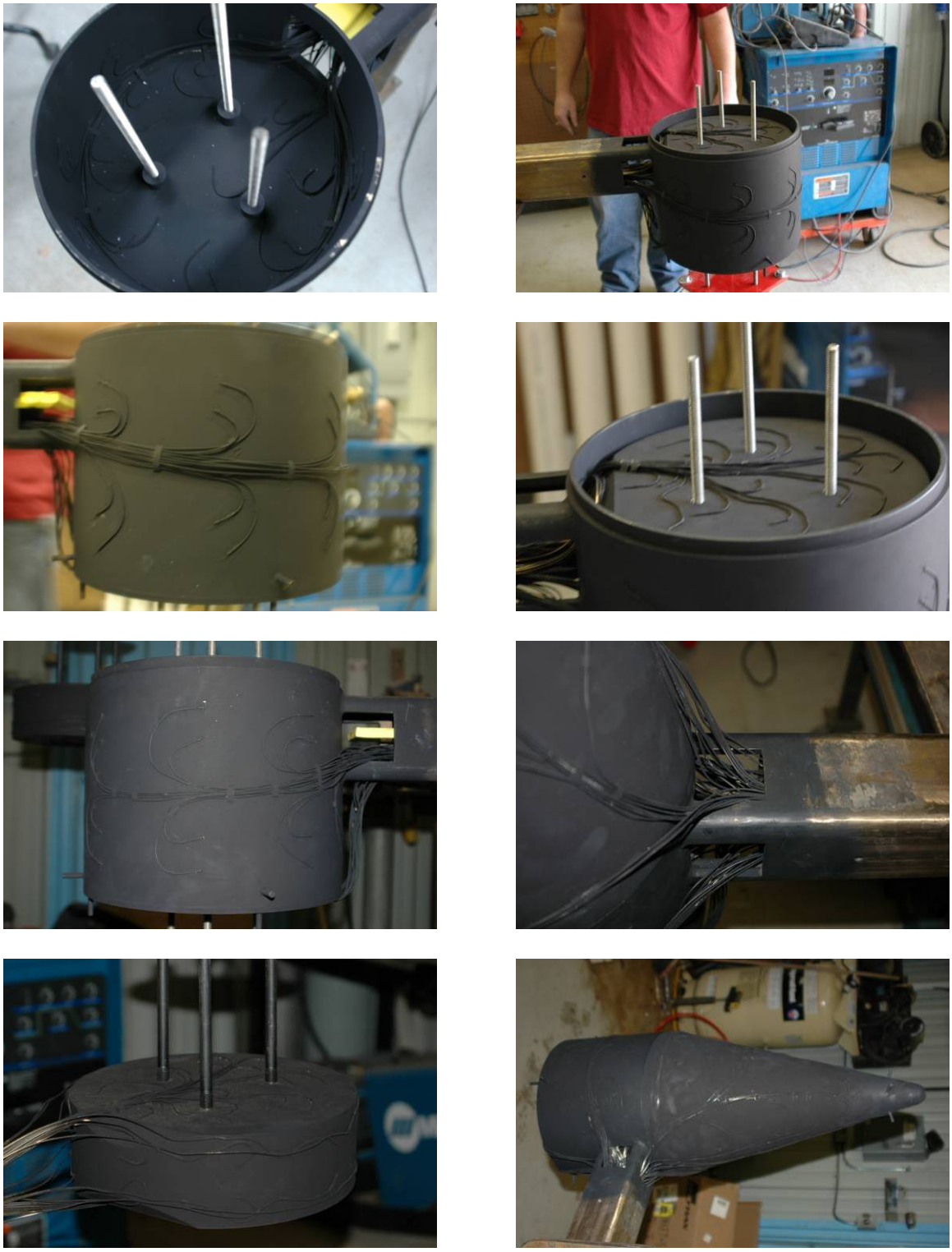

Figure 10 Pyromark paint after cure.

Figure 11 Final assembly.

3. PENLIGHT TESTING

A process was performed prior to fire testing to confirm the accuracy of the data. Data validity checks include description and locations of all instrumentation, as-received instrument checks, and data acquisition systems (DAS) calibrations. These are described in detail in following chapters. This section describes the results of the complex calorimeter tests in "Penlight." The main purpose of these tests was in-situ function tests of the attached thermocouples. In addition, the data could be used to validate the CALORE heat transfer modeling of the complex calorimeter.

3.1 Penlight Facility and Shroud

The complex calorimeter was tested in the Penlight apparatus (Figure 12).

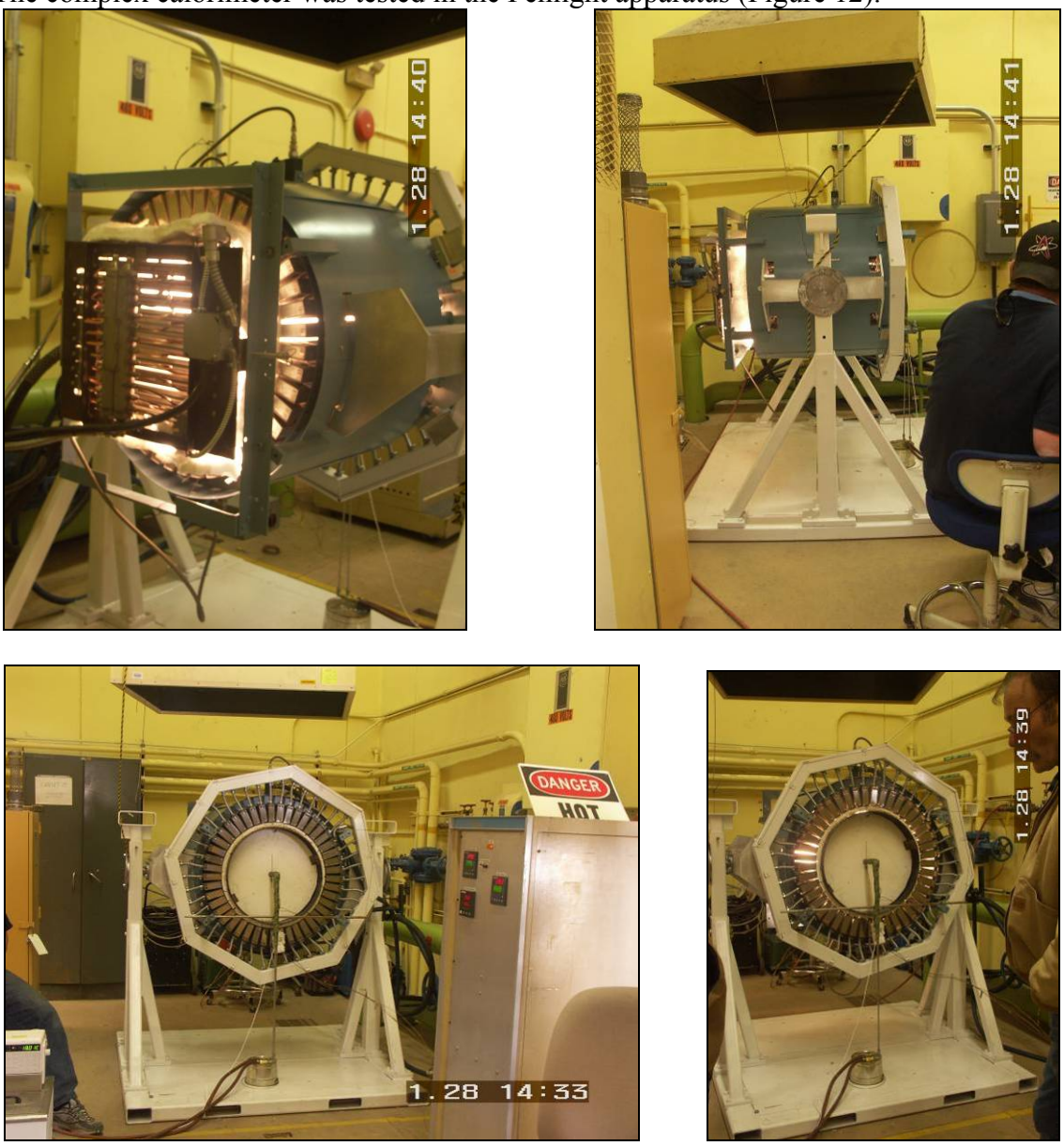

Figure 12 Heated back and side, and unheated front views of Penlight.

The Penlight apparatus is a radiantly heated cavity, 21.5 inches (546.1 mm) in diameter and 33 inches (838.2 mm) long. The cavity (a cylindrical inconel shroud) is heated on the back and cylindrical sides by quartz lamps, whose power is controlled by thermocouples attached to the shroud, maintaining the desired shroud temperature. The cavity front end is open. The shroud is fabricated from 1/8-inch thick rolled inconel. All interior surfaces of the shroud are painted with a high temperature black paint (Pyromark, emissivity = 0.86). Twenty eight thermocouples are attached to the inner surface of the shroud cylindrical section. From outside, looking at the open end, seven thermocouples are placed on each of the four orientations, top (0°), right side (90°), bottom (180°), and left side (270°). Note that additional thermocouples are used to both control the power to the lamps and provide over-temperature protection.

Eleven thermocouples are attached to the inner surface of the shroud back plate. From outside, looking in the open end, seven thermocouples are placed on a vertical centerline, three thermocouples are placed on the left side (270°) horizontal centerline, and one thermocouple is placed on the right side (90°) horizontal centerline. Note the control thermocouple (C) is located near the plate center.

3.1.1 Penlight Shroud Extension

A shroud extension (shown as green in Figure 13) was fabricated to accommodate the complex calorimeter nose up test. Four views (side, front, top, and bottom) showing the calorimeter half-engulfed by the extension are presented in Figure 13.

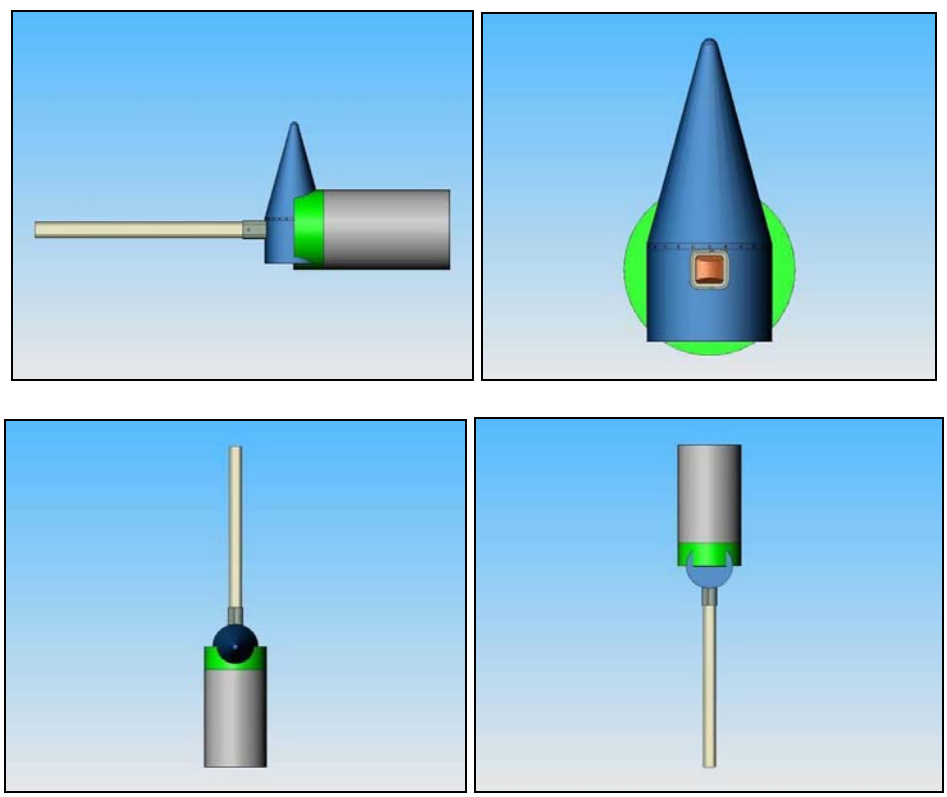

Figure 13 The penlight shroud extension.

The extension (Figure 14) consisted of four parts; a rolled cylindrical extension, and two flat side plates and a flat bottom plate that formed an end cap to the extension. All parts were fabricated using rolled and/or cut 1/16-inch thick stainless steel plate. All inside surfaces were painted with Pyromark.

Figures 15-20 give views and locations of the thermocouples on the shroud and shroud extension (14 thermocouples on the shroud extension (3 on the bottom end cap, 2 on each side end cap, and 7 on the cylindrical section)). The locations of the thermocouples are given in Table 1.

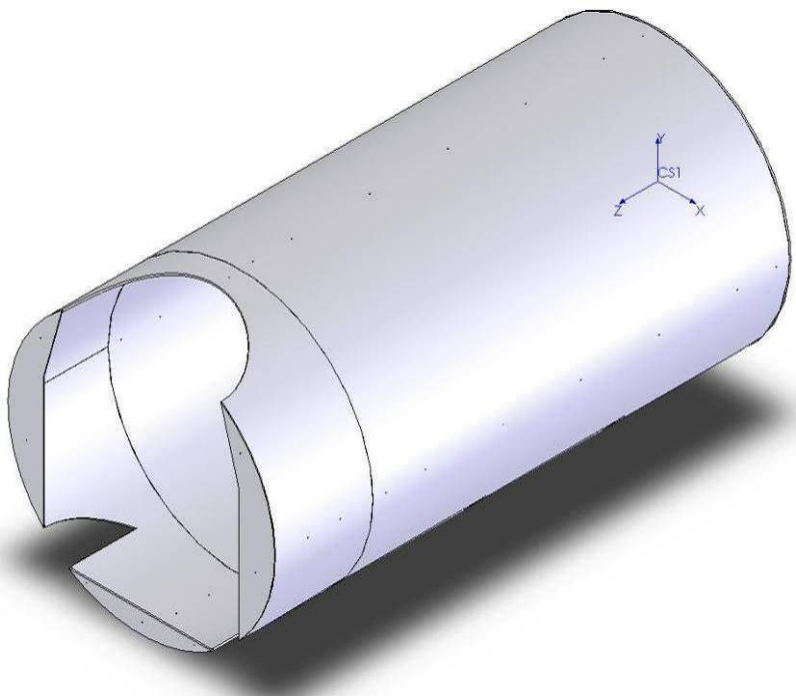

Figure 14 Penlight shroud and extension – isometric view

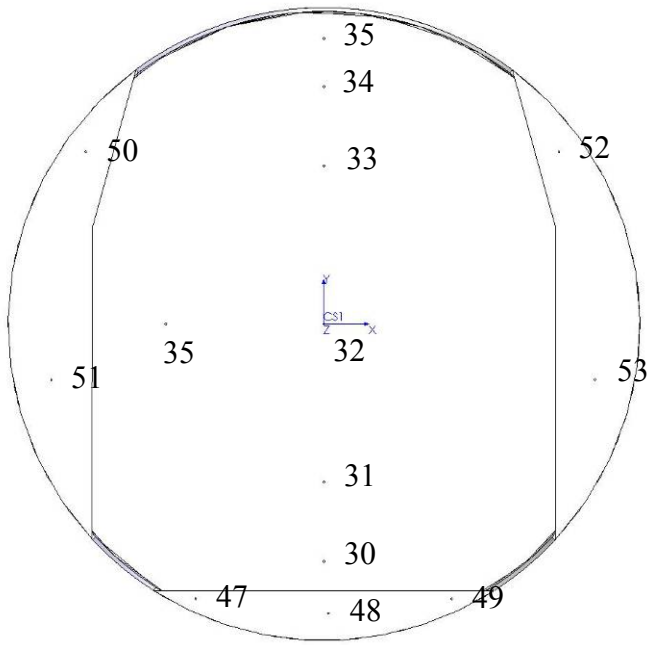

Figure 15 Penlight shroud and extension – front view

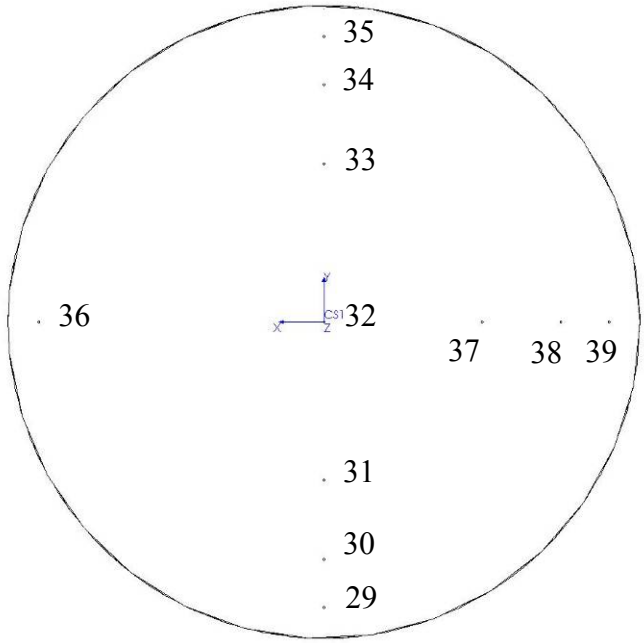

Figure 16 Penlight shroud and extension – back view

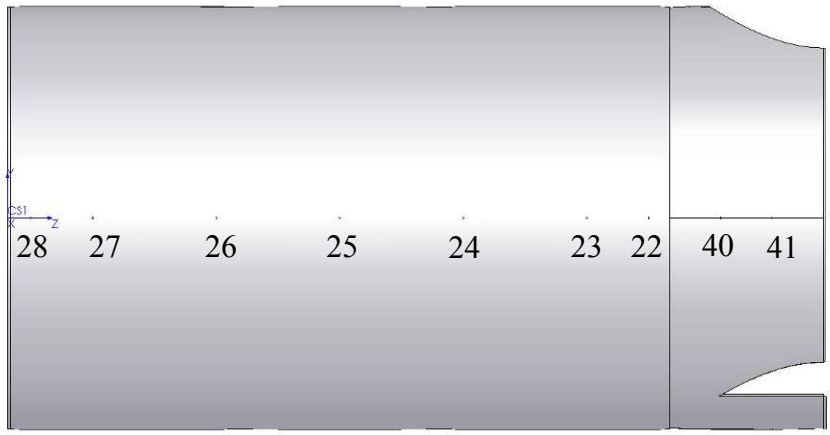

Figure 17 Penlight shroud and extension – left view

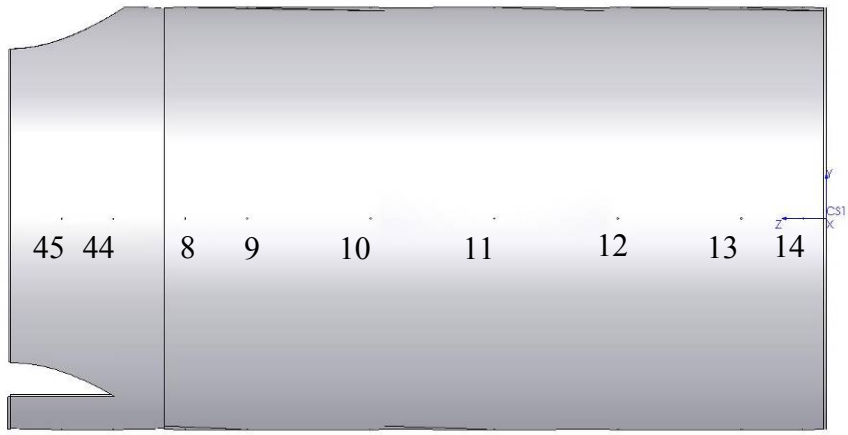

Figure 18 Penlight shroud and extension – right view

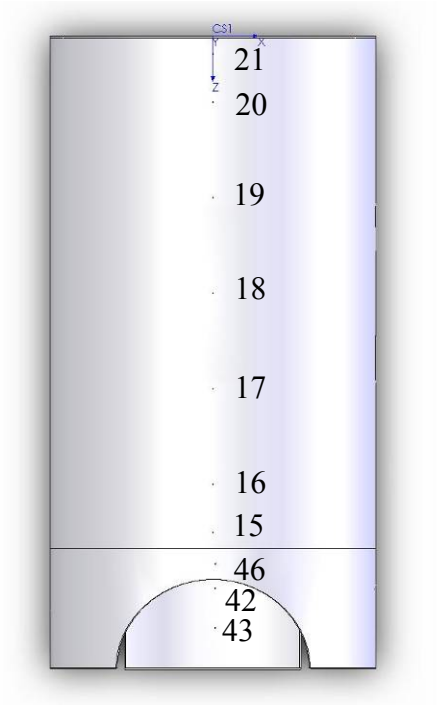

Figure 19 Penlight shroud and extension – top view

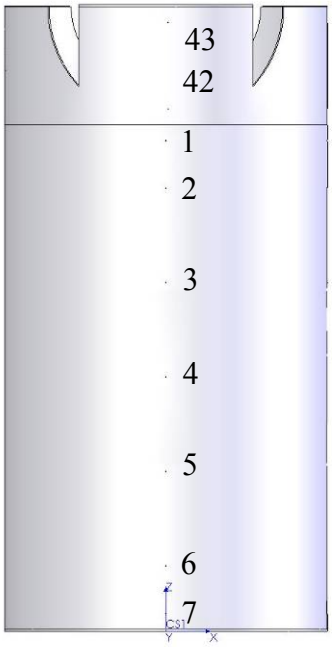

Figure 20 Penlight shroud and extension – bottom view

Table 1 Penlight Shroud and Extension Thermocouple Locations

X solidworks (inches)	Y solidworks (inches)	Z solidworks (inches)	name
0	-10.25	31	Cyl Shroud 1
0	-10.25	28	Cyl Shroud 2
0	-10.25	22	Cyl Shroud 3
0	-10.25	16	Cyl Shroud 4
0	-10.25	10	Cyl Shroud 5
0	-10.25	4	Cyl Shroud 6
0	-10.25	1	Cyl Shroud 7
10.25	0	31	Cyl Shroud 8
10.25	0	28	Cyl Shroud 9
10.25	0	22	Cyl Shroud 10
10.25	0	16	Cyl Shroud 11
10.25	0	10	Cyl Shroud 12
10.25	0	4	Cyl Shroud 13
10.25	0	1	Cyl Shroud 14
0	10.25	31	Cyl Shroud 15
0	10.25	28	Cyl Shroud 16
0	10.25	22	Cyl Shroud 17
0	10.25	16	Cyl Shroud 18
0	10.25	10	Cyl Shroud 19
0	10.25	4	Cyl Shroud 20
0	10.25	1	Cyl Shroud 21
-10.25	0	31	Cyl Shroud 22
-10.25	0	28	Cyl Shroud 23
-10.25	0	22	Cyl Shroud 24
-10.25	0	16	Cyl Shroud 25
-10.25	0	10	Cyl Shroud 26
-10.25	0	4	Cyl Shroud 27
-10.25	0	1	Cyl Shroud 28
0	-9.25	0	Back Shroud 29
0	-7.69	0	Back Shroud 30

0	-5.125	0	Back Shroud 31
0	0	0	Back Shroud 32
0	5.125	0	Back Shroud 33
0	7.69	0	Back Shroud 34
0	9.25	0	Back Shroud 35
9.25	0	0	Back Shroud 36
-5.125	0	0	Back Shroud 37
-7.69	0	0	Back Shroud 38
-9.25	0	0	Back Shroud 39
-10.25	0	33.15	Ext Shroud 40
-10.25	0	38.65	Ext Shroud 41
0	-10.25	33.15	Ext Shroud 42
0	-10.25	38.65	Ext Shroud 43
10.25	0	33.15	Ext Shroud 44
10.25	0	38.65	Ext Shroud 45
0	10.25	33.55	Ext Shroud 46
-4.386	-8.765	39.65	Ext Shroud 47
0	-9.265	39.65	Ext Shroud 48
4.386	-8.765	39.65	Ext Shroud 49
-7.73	5.58	39.65	Ext Shroud 50
-8.83	-1.8	39.65	Ext Shroud 51
7.73	5.58	39.65	Ext Shroud 52
8.83	-1.8	39.65	Ext Shroud 53

3.2 Penlight Characterization

The Penlight apparatus was characterized using IR emission spectroscopy (Kearney, 2002) in the configuration shown in Figure 12. Penlight is a large cavity with a small hole (diameter ratio = 21.5), so its emissivity was expected to be nearly 1. It is believed that the surprisingly low value 0.85-0.86 of the measured emissivity is largely due to the temperature gradient along the back plate portion of the shroud.

The shroud thermocouple data acquired during calibration experiments showed that there are significant temperature gradients along the surface of the Penlight shroud. These temperature gradients along with the much lower temperature of the front insulation-board cap (shown in Figure 12) can cause the effective radiation temperature of the Penlight cavity to be lower than the set point temperature. Axial temperature variations as large as several hundred Kelvin exist on the surface of the shroud. The back plate exhibits an approximately 90 K temperature gradient. The impact of the very large temperature gradients along the lateral portion of the shroud is likely mitigated because the view factor from the region of highest temperature gradient to the cavity opening is likely to be very small. The smaller gradient along the back plate portion of the shroud is likely to have a much greater impact because the view factor associated with this region is much larger.

3.3 Penlight Testing Overview

The entire complex calorimeter could not fit into the Penlight cavity. The complex calorimeter has a cylindrical-conical shape, with a support post normal to the axis through which thermocouple wires run to an exterior data acquisition system. Because of the post, only part of the calorimeter can be inserted into the Penlight cavity. The portions that will enter the cavity are the rear cylindrical end of the calorimeter up to the post, and the front conical end up to the post.

Testing was performed in three orientations: 1) a “nose in” orientation, 2) a “rear in” orientation, and 3) a “nose up” orientation (shown in Figure 22). In both the nose in (shown in Figure 21) and rear in (not shown) orientations, the calorimeter is inserted (up to the support arm) and centered in Penlight. In both orientations, the support arm exits at the 90° side.

The main purpose of the nose in and the rear in tests was in-situ function tests of the attached thermocouples. The data from the nose up tests were used to validate the CALORE heat transfer modeling of the complex calorimeter. Due to the additional rigor required for the data, the Penlight shroud was extended to cover the front half of the complex calorimeter (as discussed in detail in the previous section).

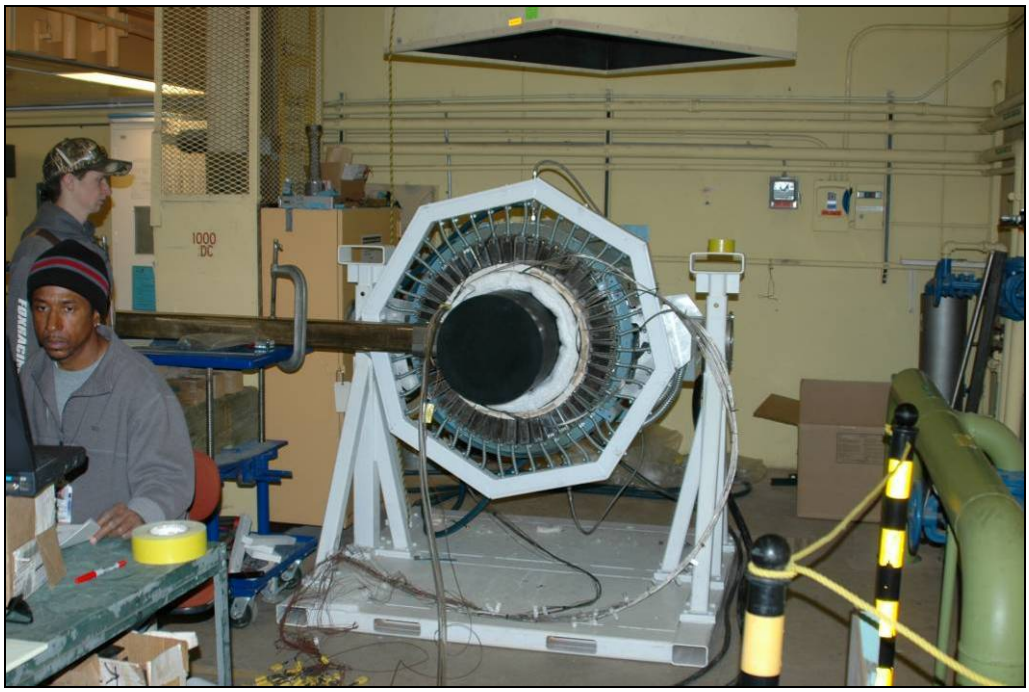

Figure 21 The complex calorimeter in the "nose in" orientation.

Figure 22 The nose up test utilizing the Penlight shroud extension.

The penlight and complex calorimeter geometry define the orientation for three sets of checks: 1) with the nose section inserted into the cavity, 2) with the aft end inserted into the cavity, and 3) with the middle section facing the open cavity. For the nose and aft end tests, the shroud temperature was increased to 300°C, 600°C, and 900°C, with a hold of approximately 5-10 minutes at these temperature levels to characterize response of the calorimeter in different temperature regimes.

In order to obtain a significant temperature response from the center blivet, the insulation strip between the inner and outer shell needed to be removed for the third test series (with the middle section facing the open cavity). Hold times of 30-60 minutes were used to obtain a significant response from the blivet (~60ºC increase). Note that the center insulation strip (between the inner and outer cylinders, opposite the blivet) was not in place for any of the penlight tests to minimize assembly/disassembly.

To accurately measure the temperature distribution and obtain post-test CALORE simulation boundary conditions, many thermocouples were attached to the cylindrical shroud (28) and back plate (13) for a total of 41 thermocouples. Instrumented and insulated shroud extensions were fabricated to close off all gaps to minimize air flow into the radiant cavity for the nose up configuration.

The data collected could be used to perform CALORE simulations of the experiments to validate the calorimeter thermal model (prediction of conductive, radiative, and convective heat transfer within the calorimeter). Boundary conditions for the thermal model are derived from a combination of thermocouple temperature measurement on the calorimeter surface, and from heat flux conditions at the surface derived from 1-D inverse heat transfer calculations (see [Figueroa et al., 2005]) augmented with predictions from a CALORE model of the shroud/insulated-extensions and presiding convective conditions. Before each test it was important to achieve a relatively uniform starting temperature throughout the calorimeter because this is the only type of initial condition (uniform temperature) presently allowed by CALORE.

Table 2 presents the list of experiments. Separate data files were needed to record both the penlight data and the complex calorimeter data. In addition, the status of the fume hood located above penlight (see Figure 21) is listed. There was a possibility that running the fume hood might affect the results of the “nose up” tests, where part of the calorimeter extends out of the shroud extension.

Table 2 List of penlight experiments.

Test	Complex Calorimeter Data File Name	Penlight Data File Name	Date:	Fume Hood	Notes:
1	nose-in-cc-1	nose-in-cal-pl-1	2/10/2005	on	Stick to left side
2	nose-in-cc-2	nose-in-pl-2	2/16/2005	on	Stick to left side.
3	rear-in-cc-1	rear-cc-pl-1	2/23/2005	on	Stick to left side
4	nose-up-cc-1	nose-up-pen-1	3/9/2005	on	Stick at 0 degrees
5	nose-up-cc-2	nose-up-pen-2	3/14/2005	off	Stick at 0 degrees
6	nose-up-cc-3	nose-up-pen-3	3/16/2005	off	Stick at 0 degrees
7	nose-up-cc-4	nose-up-pen-4	3/18/2005	off	Stick at 45 degrees, to left side
8	nose-up-cc-5	nose-up-pen-5	3/22/2005	off	Stick at 45 degrees, to right side

Results are presented for the three configurations; Test 1 presents a nose in response, Test 3 provides the rear in response, and Test 6 gives the nose up response. Note that all of the penlight data are included on the DVD. A snapshot from the animation of the time-dependant temperature response is also shown for each test.

3.4 Test 1 – Nose In 1

Test 1 (Penlight Test on February 10, 2005 (nose-in-cc-1)) was performed as an in-situ tests of the thermocouples attached to the cone section (both outer and inner shells). Figure 23 shows the orientation of the calorimeter in Penlight for Test 1.

Figure 23 The nose in configuration for Test 1.

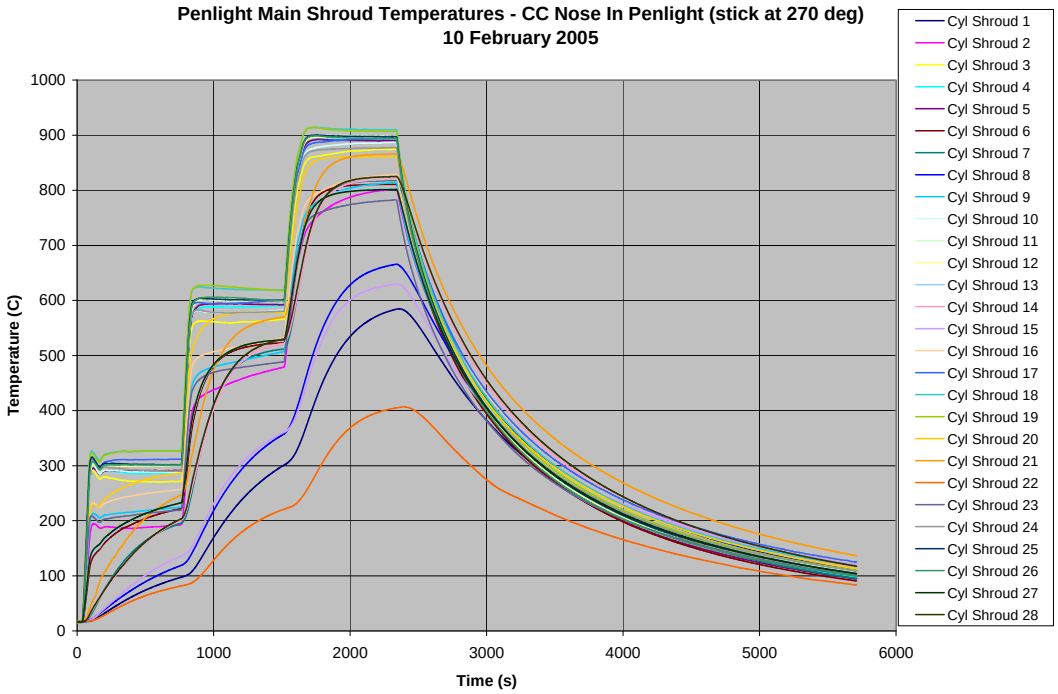

Figure 24 Penlight Main Shroud – 2/10/05

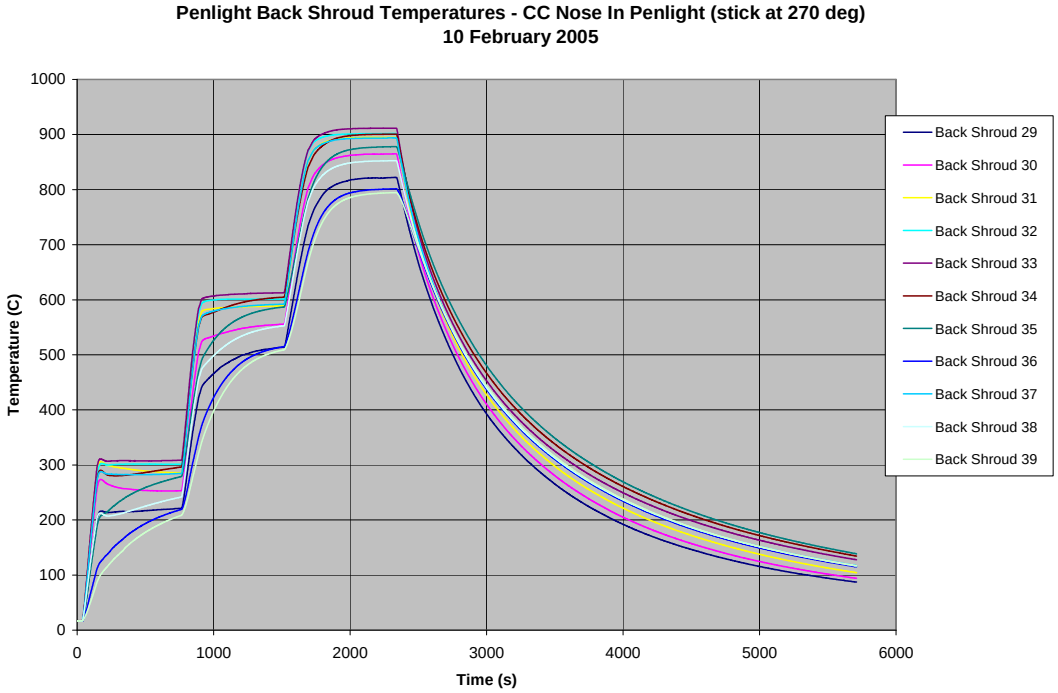

Figure 25 Penlight Back Shroud - 2/10/05

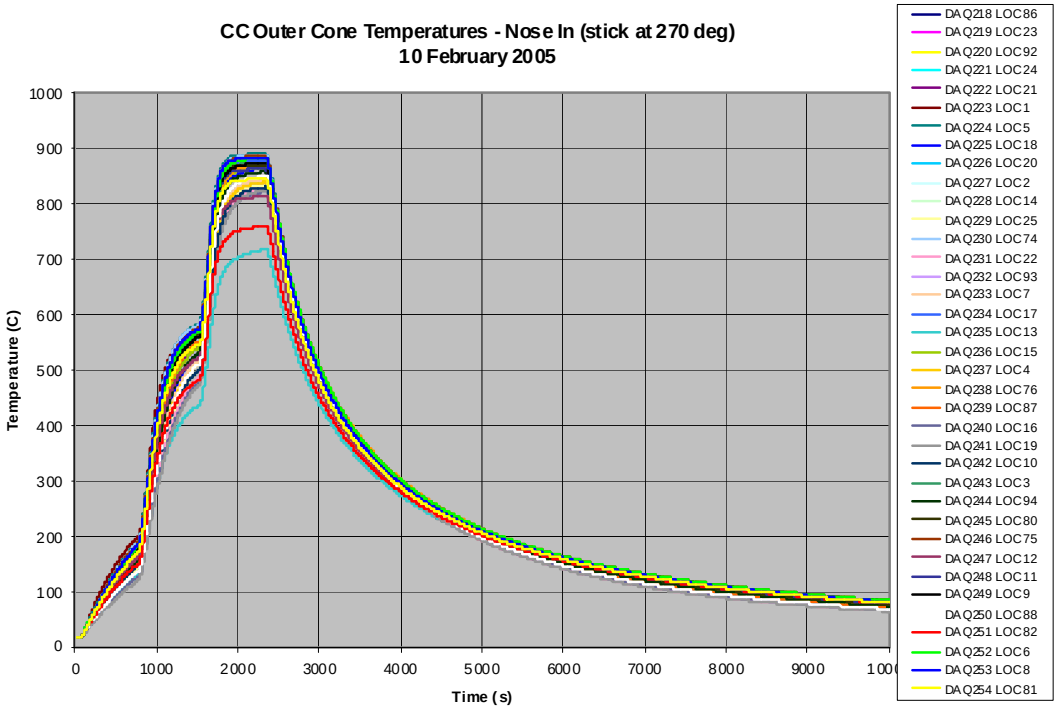

Figure 26 Outer Cone – 2/10/05

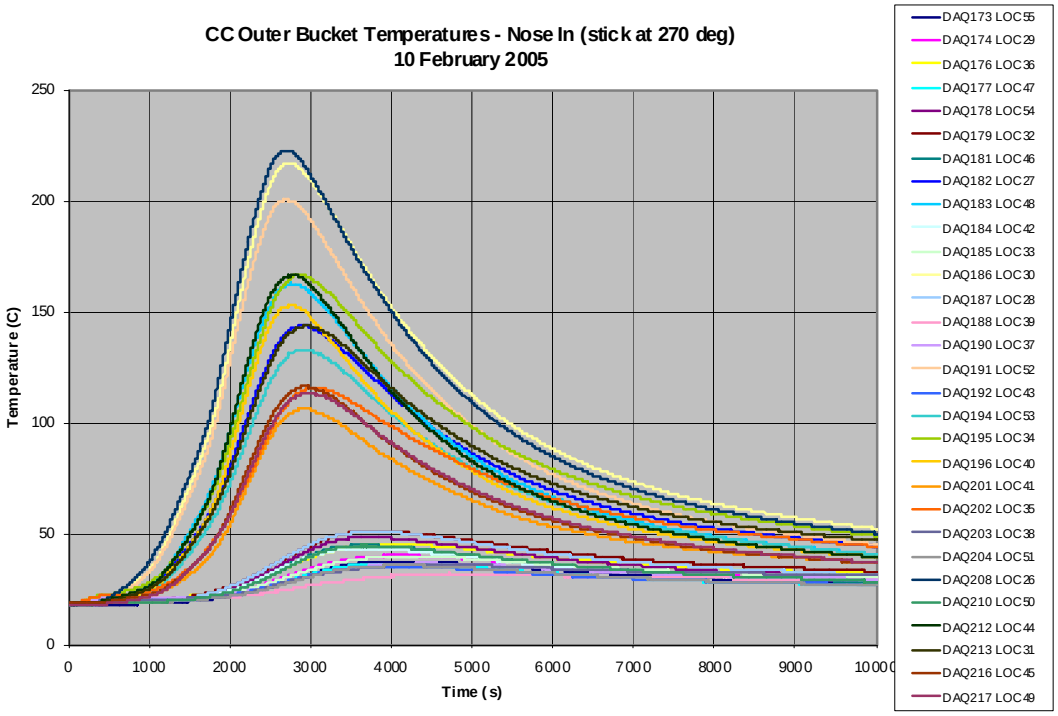

Figure 27 Outer Bucket - 2/10/05

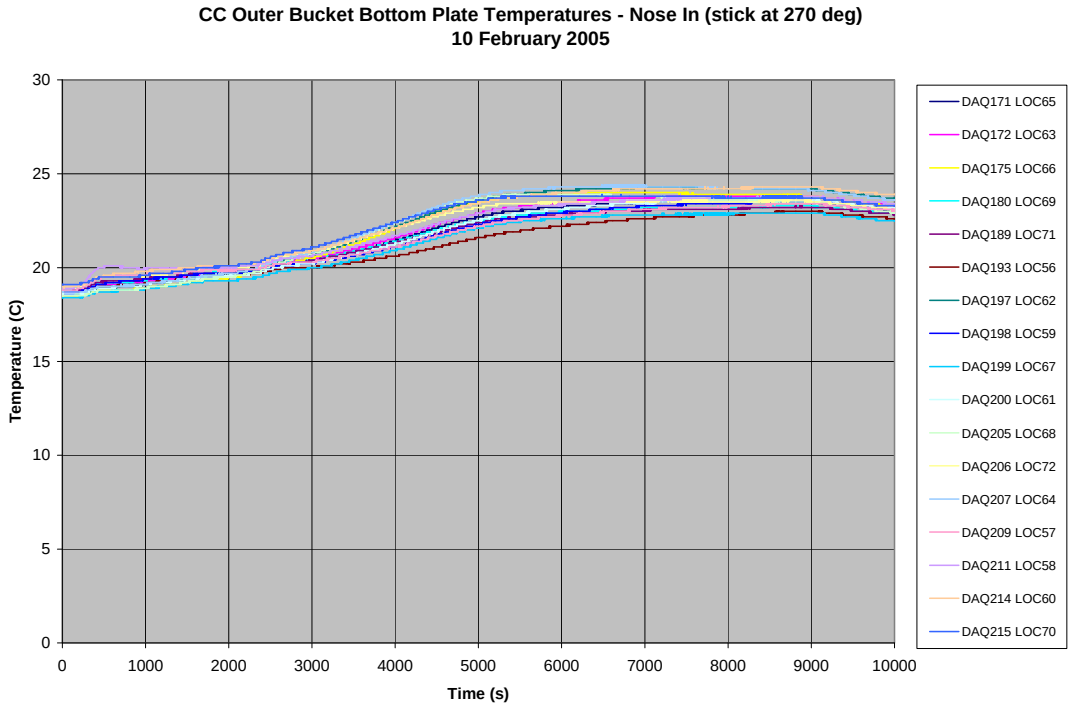

Figure 28 Outer Bucket Bottom Plate – 2/10/05

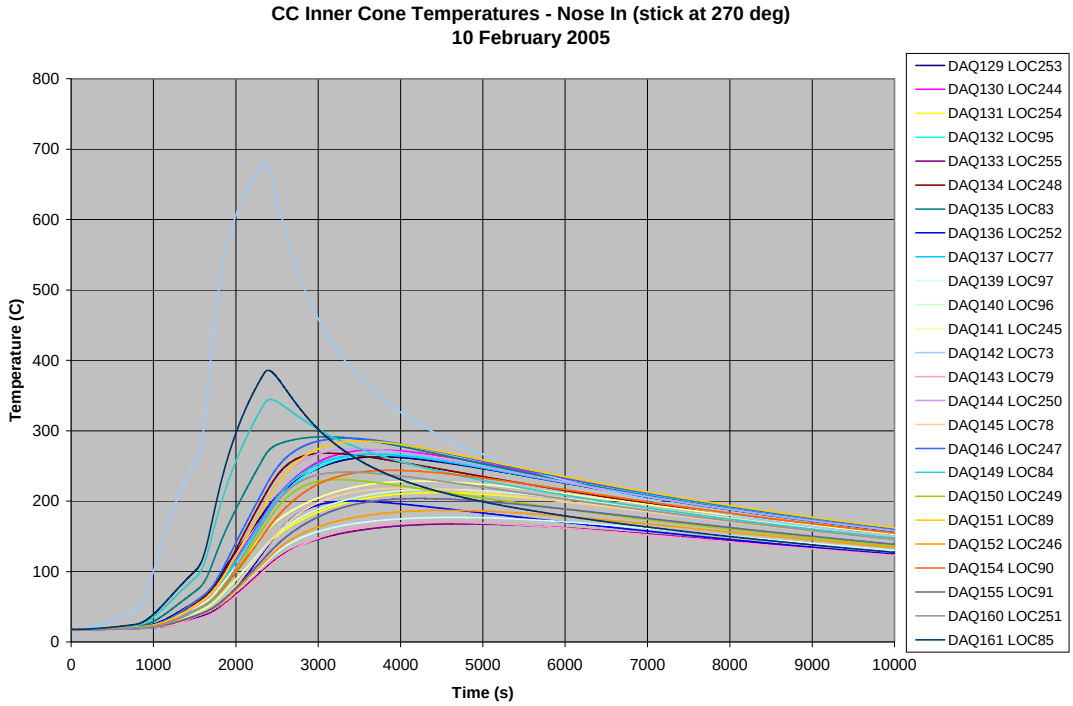

Figure 29 Inner Cone - 2/10/05

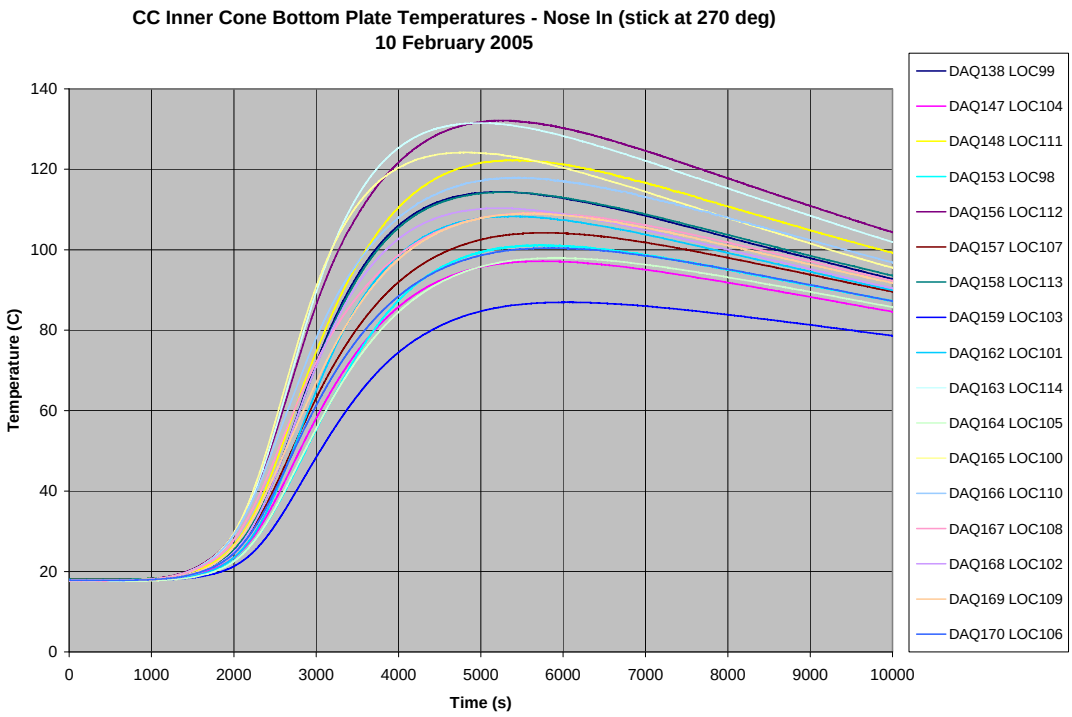

Figure 30 Inner Cone Bottom Plate – 2/10/05

Figure 31 Inner Bucket Outer Edge - 2/10/05

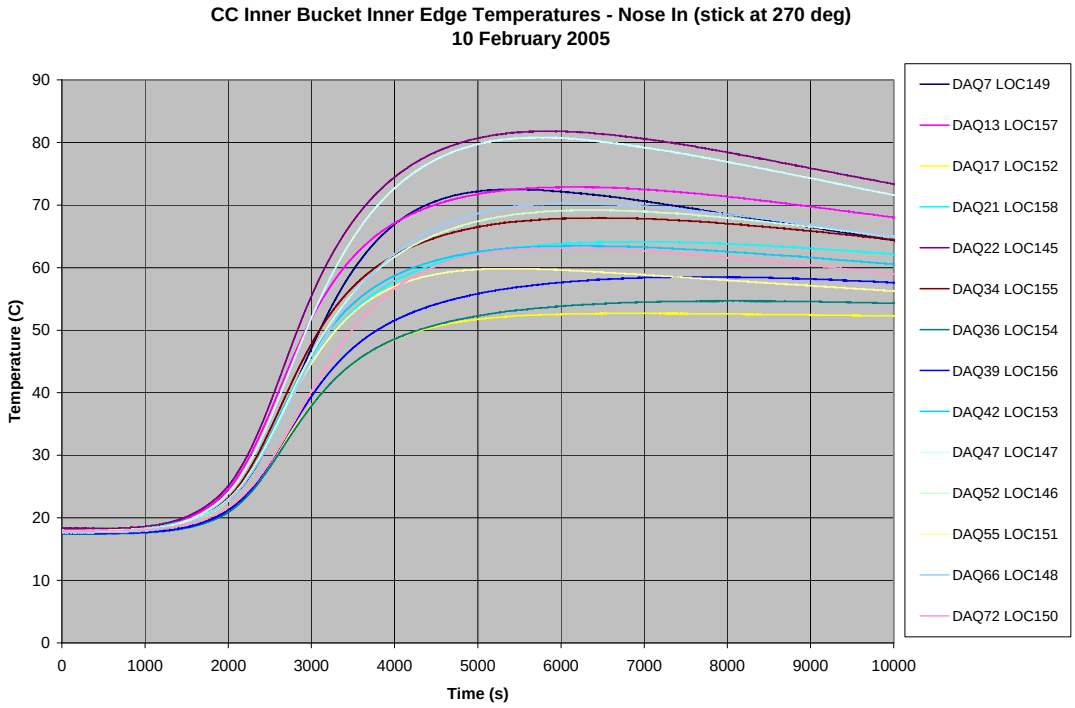

Figure 32 Inner Bucket Inner Edge – 2/10/05

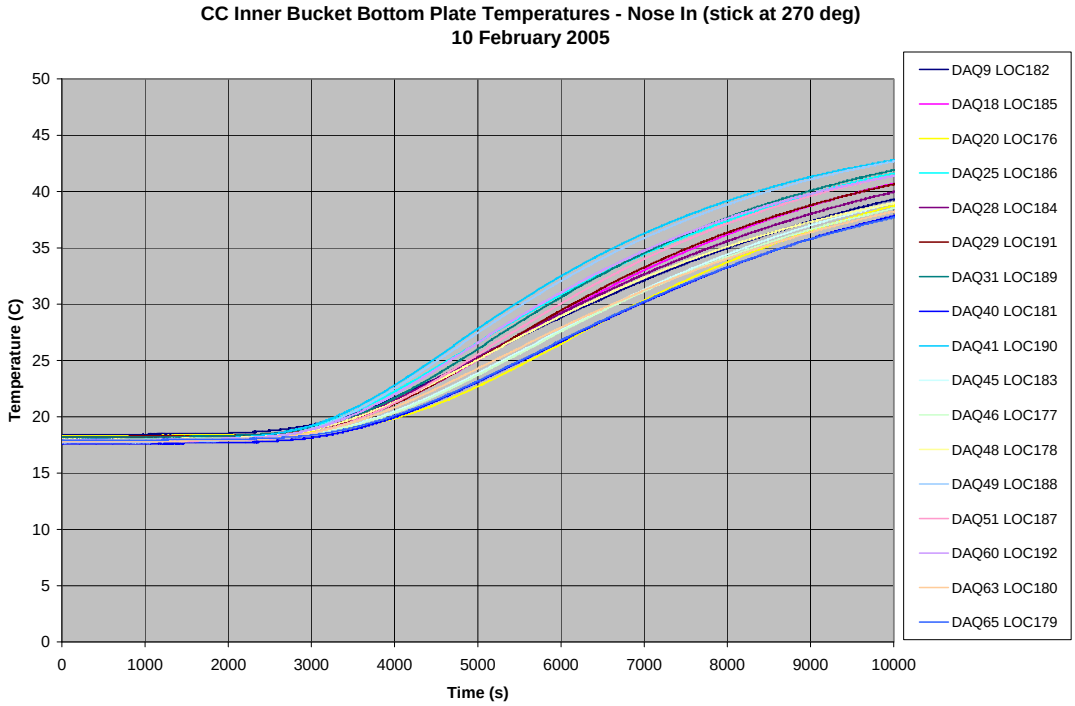

Figure 33 Inner Bucket Bottom Plate - 2/10/05

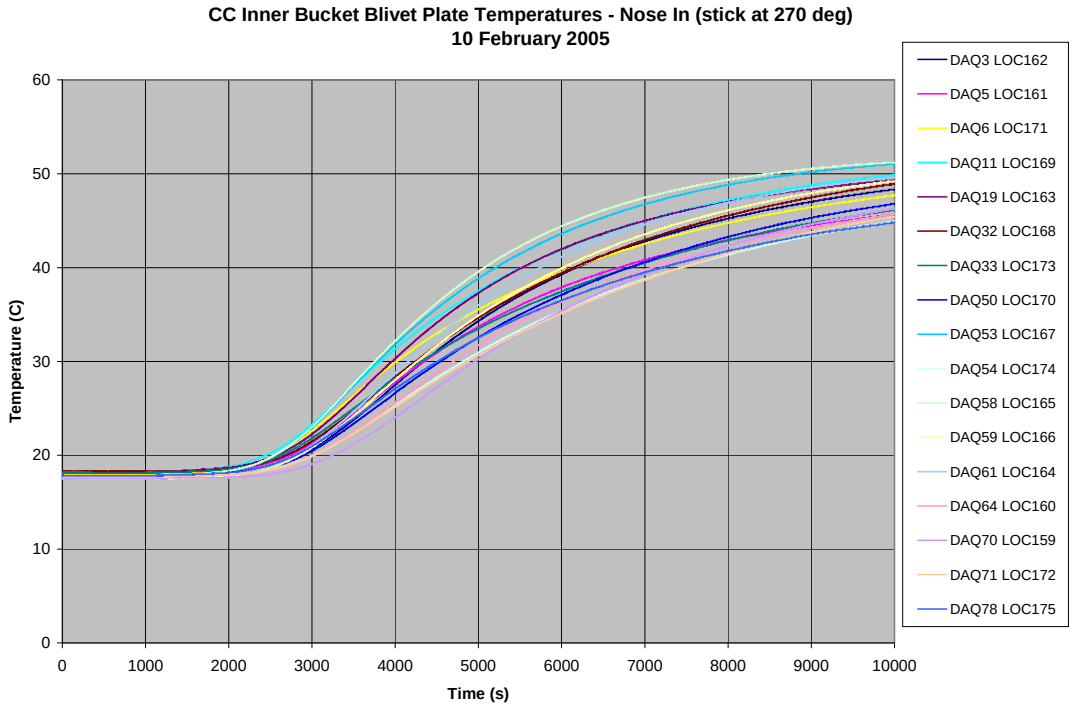

Figure 34 Inner Bucket Blivet Plate – 2/10/05

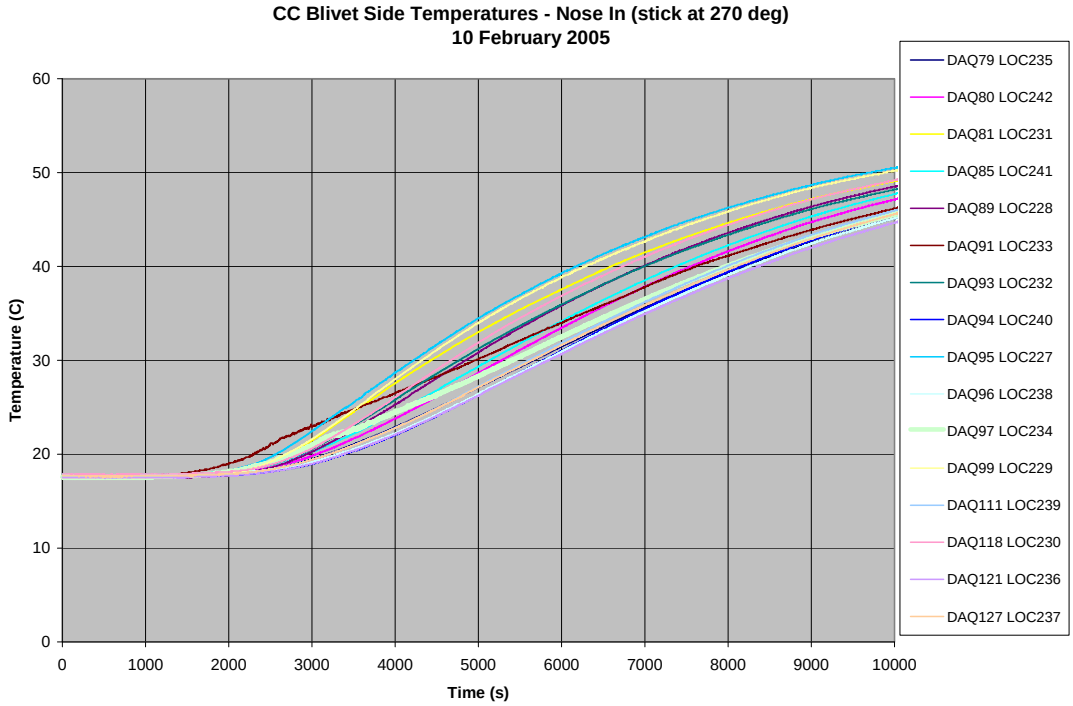

Figure 35 Blivet Side - 2/10/05

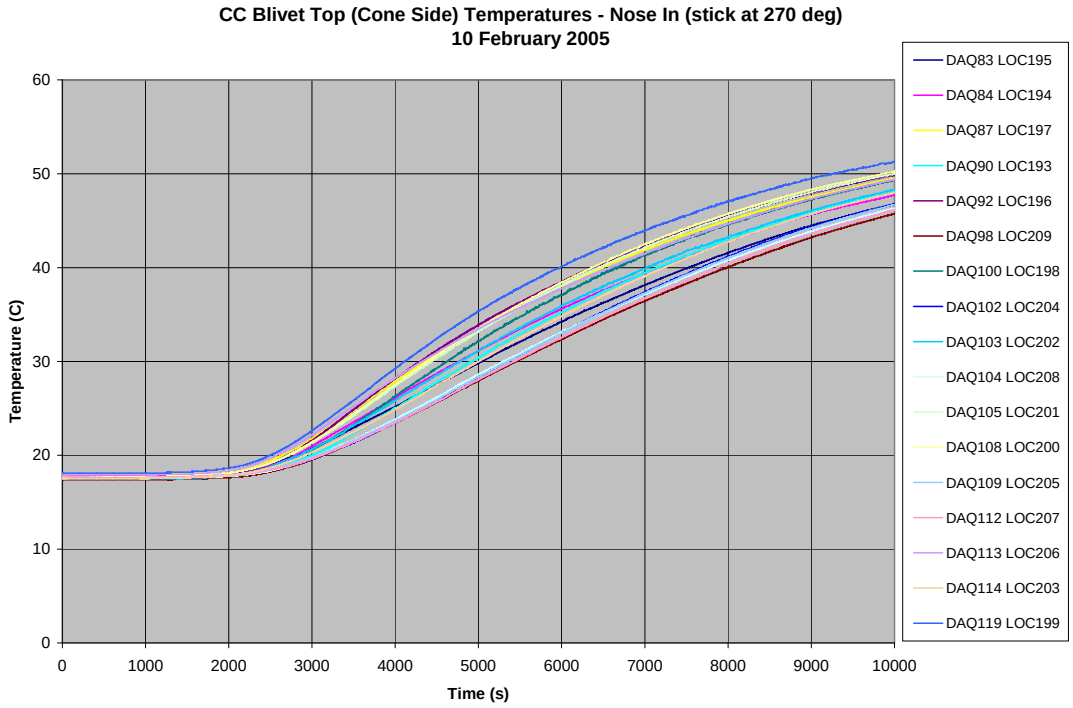

Figure 36 Blivet Top (Cone Side) – 2/10/05

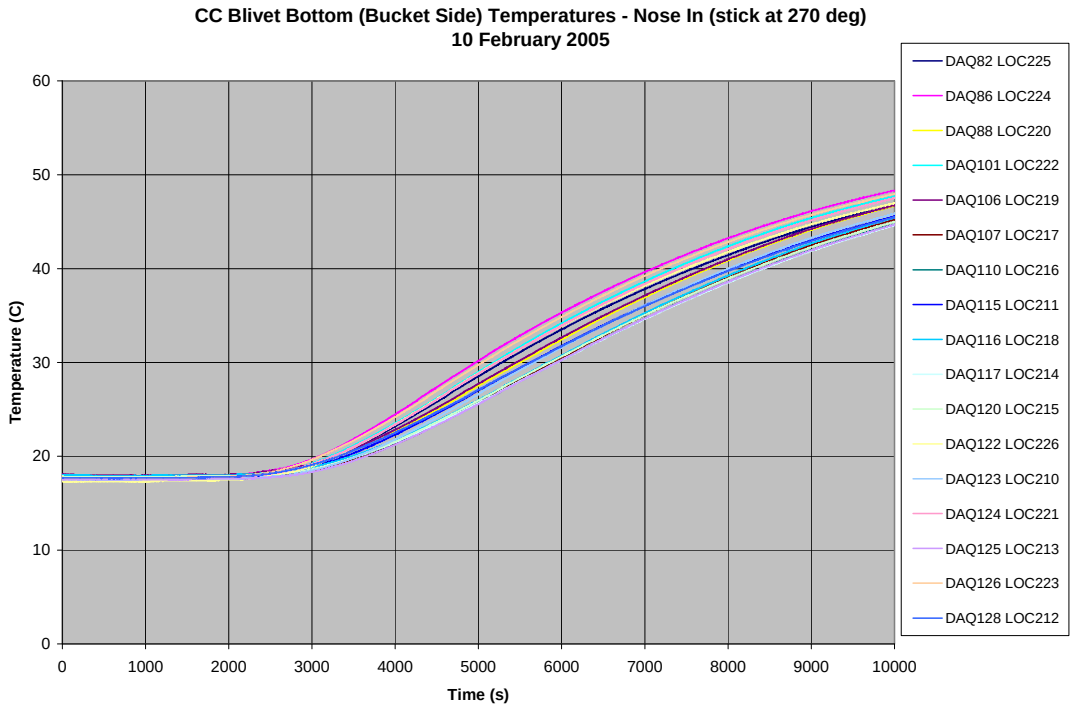

Figure 37 Blivet Bottom (Bucket Side) - 2/10/05

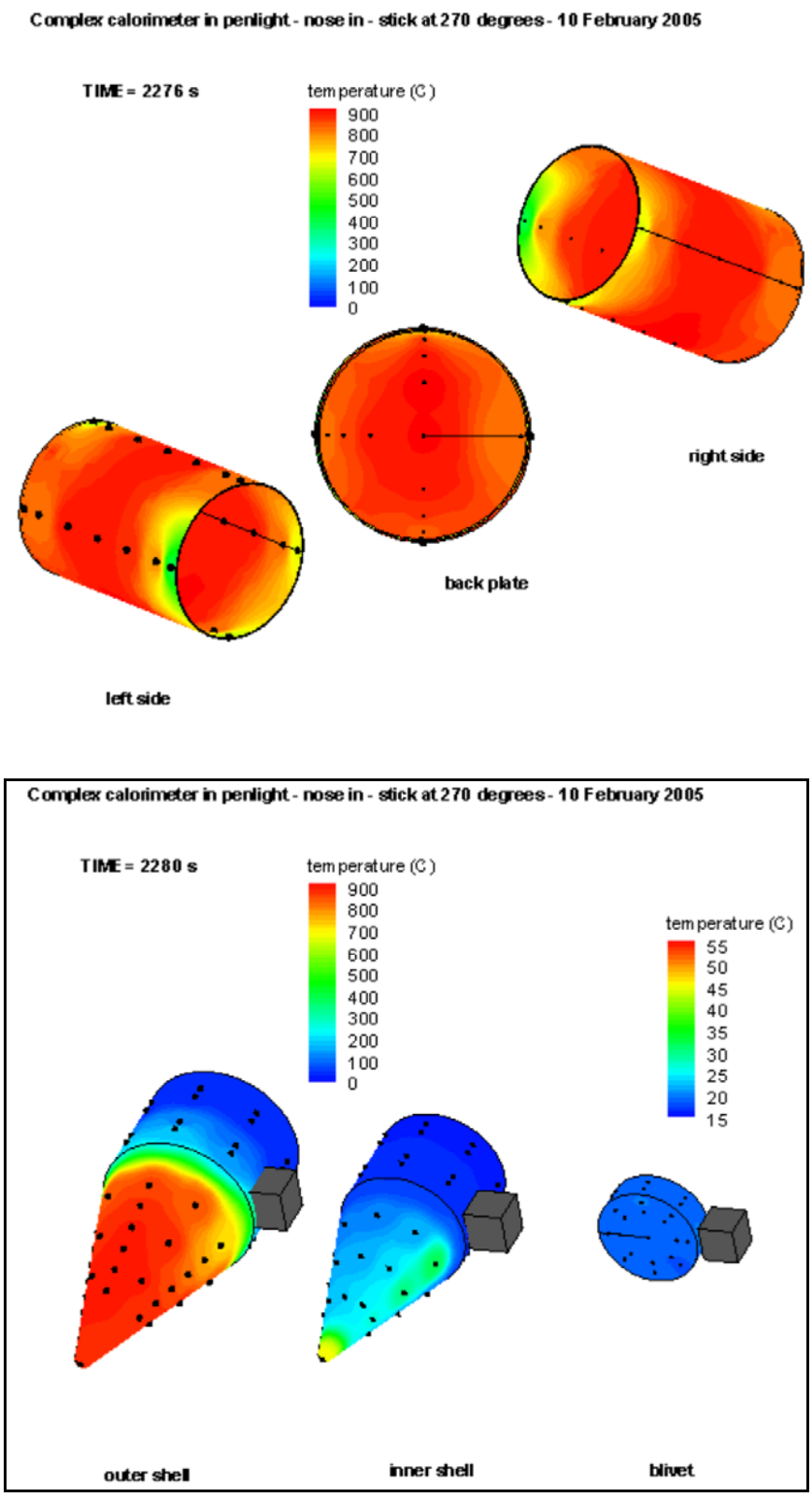

Figure 38 Penlight and calorimeter response (2280 s) in Test 1.

3.5 Test 3 – Rear In 1

Test 3 (Penlight Test on February 23, 2005 (rear-in-cc-1)) was performed for the in-situ checks of the thermocouples attached to the rear section (both outer and inner shells).

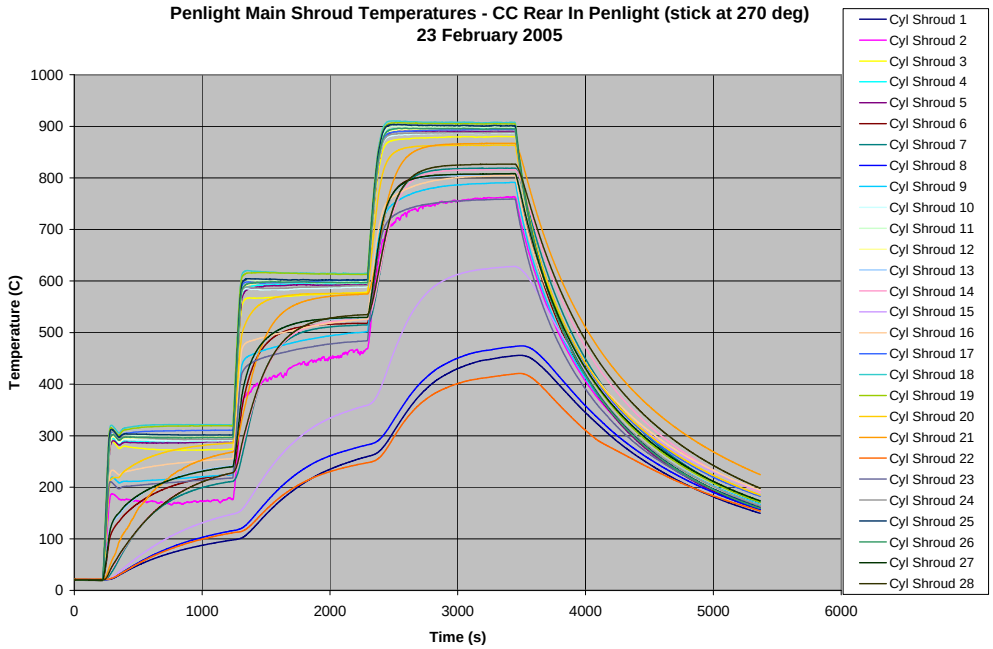

Figure 39 Penlight Main Shroud – 2/23/05

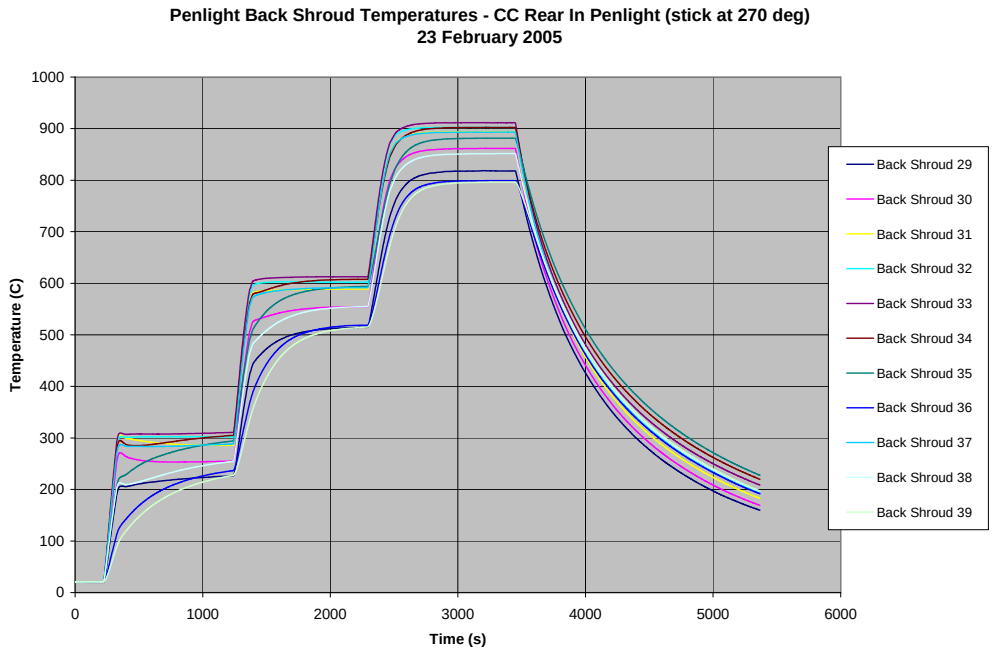

Figure 40 Penlight Back Shroud - 2/23/05

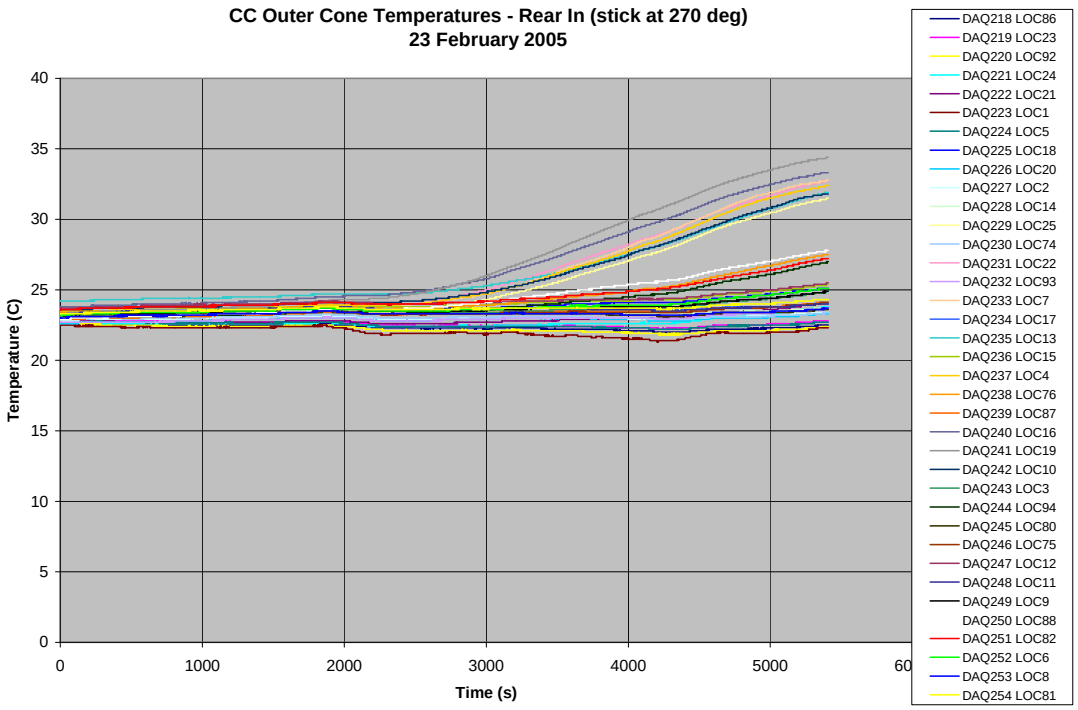

Figure 41 Outer Cone – 2/23/05

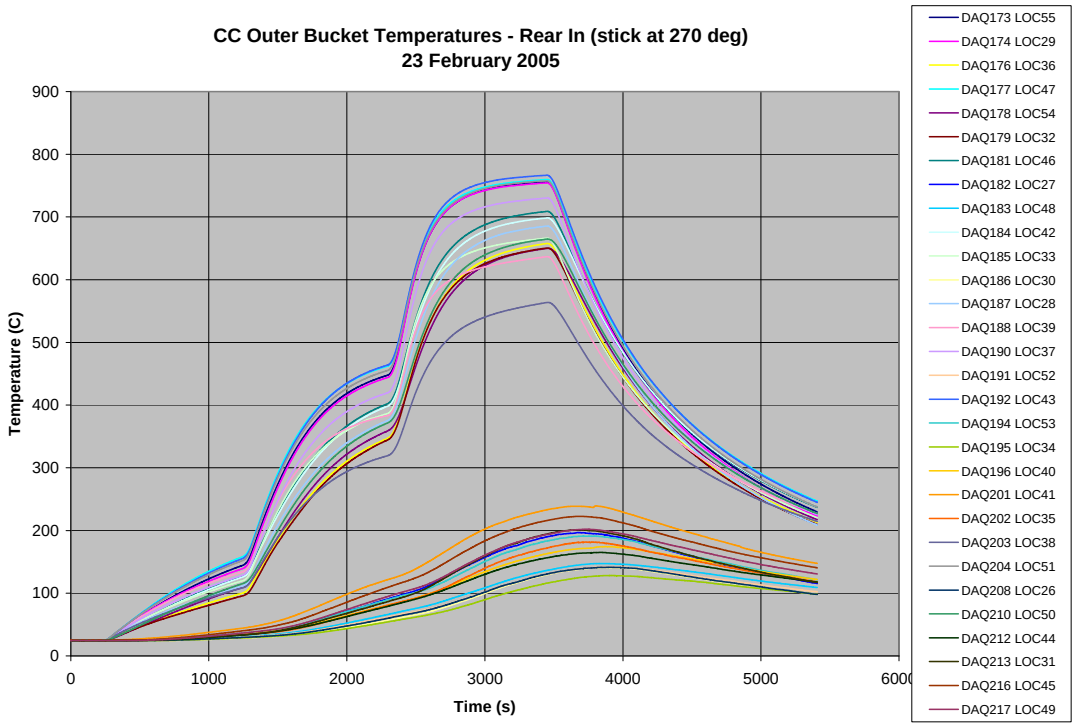

Figure 42 Outer Bucket - 2/23/05

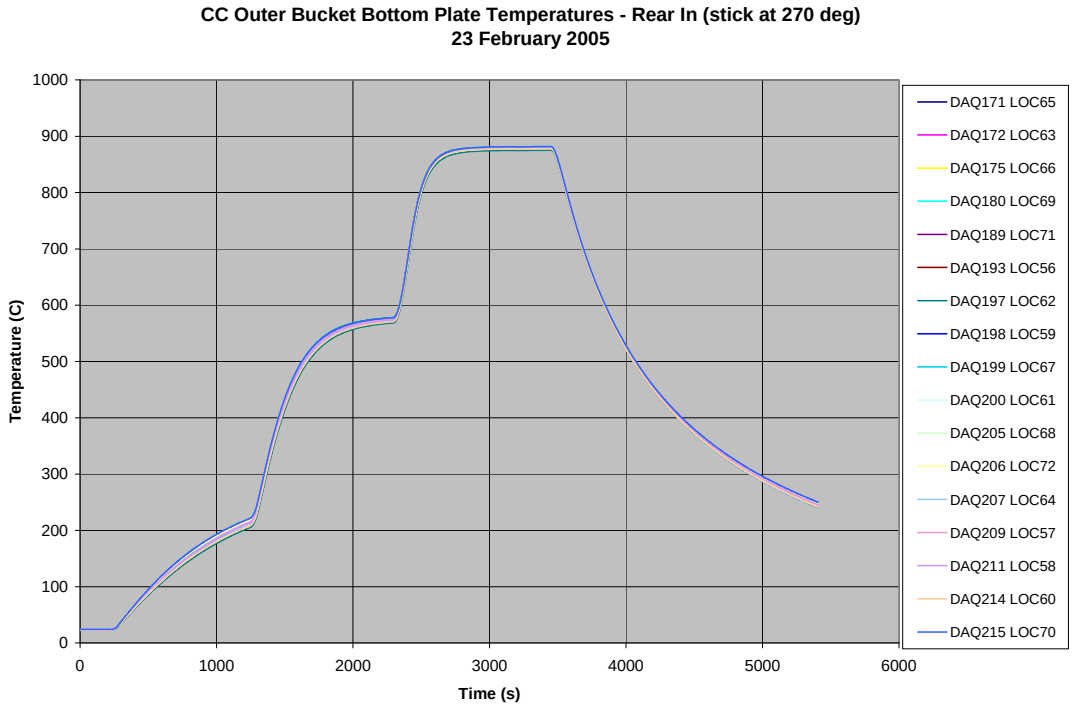

Figure 43 Outer Bucket Bottom Plate – 2/23/05

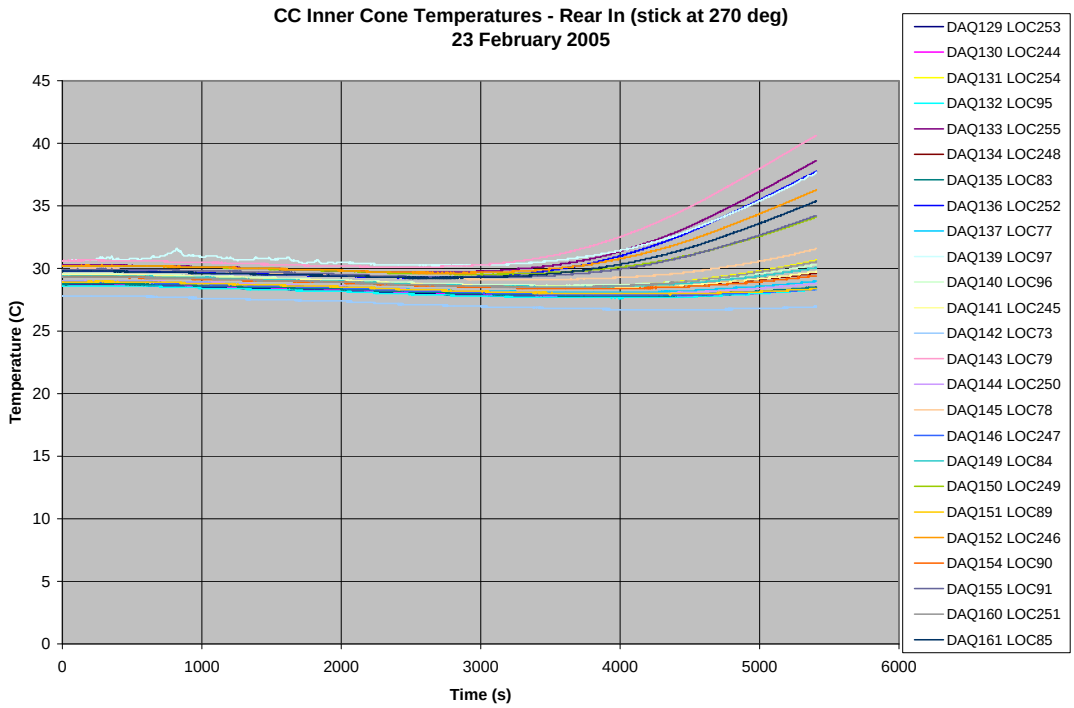

Figure 44 Inner Cone - 2/23/05

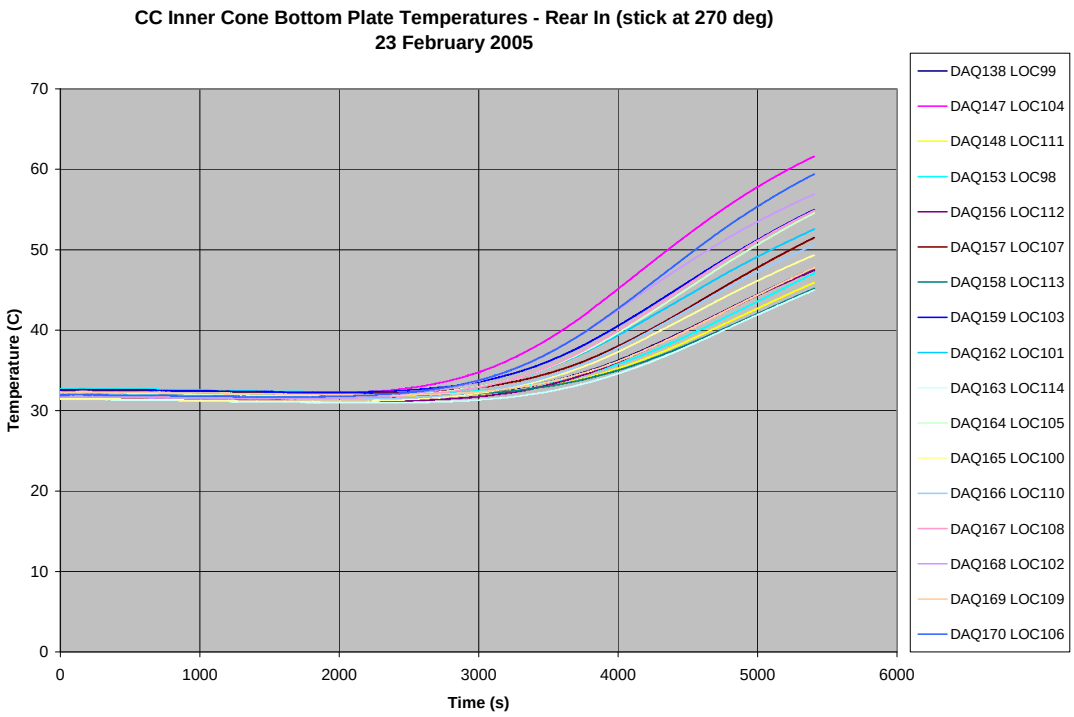

Figure 45 Inner Cone Bottom Plate – 2/23/05

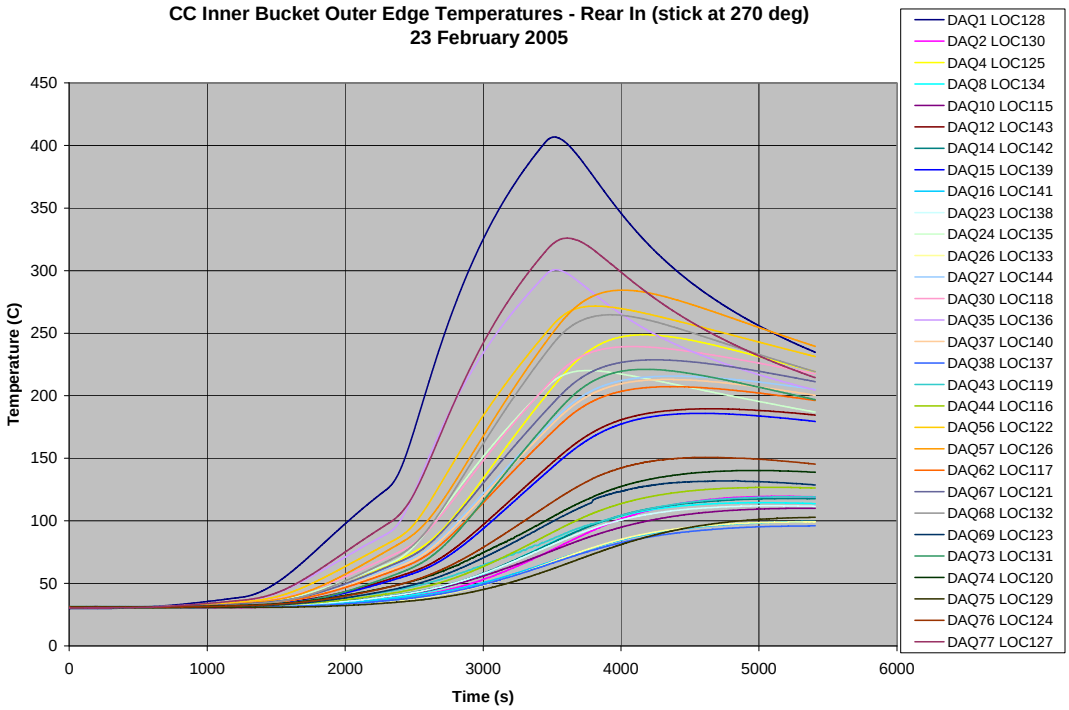

Figure 46 Inner Bucket Outer Edge - 2/23/05

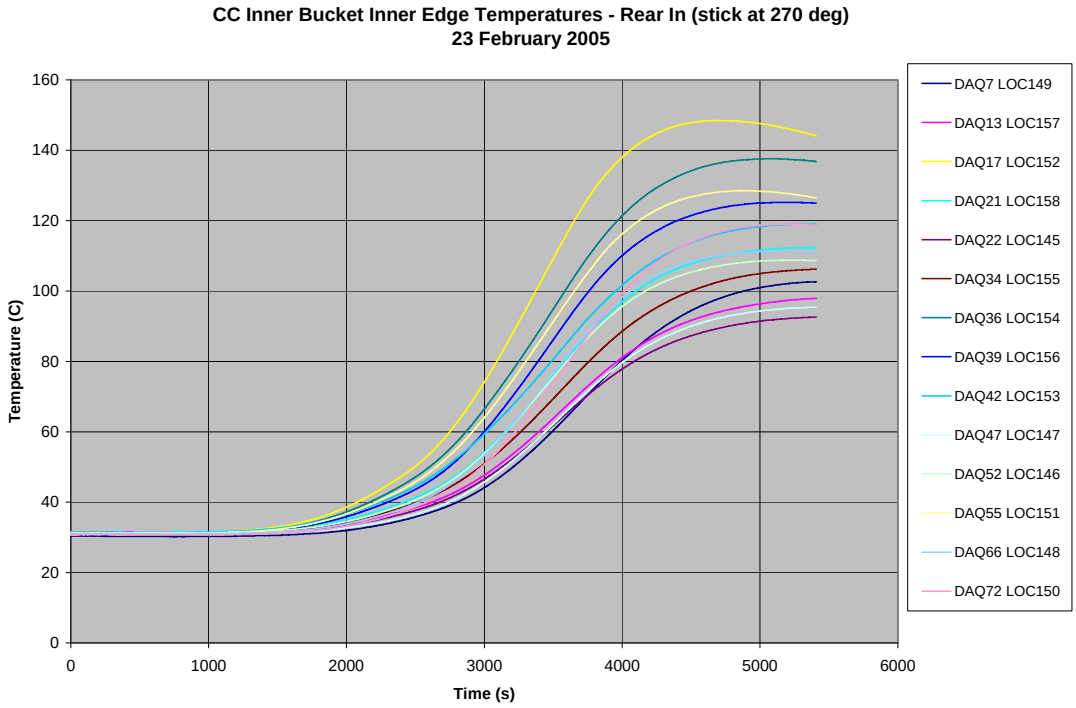

Figure 47 Inner Bucket Inner Edge – 2/23/05

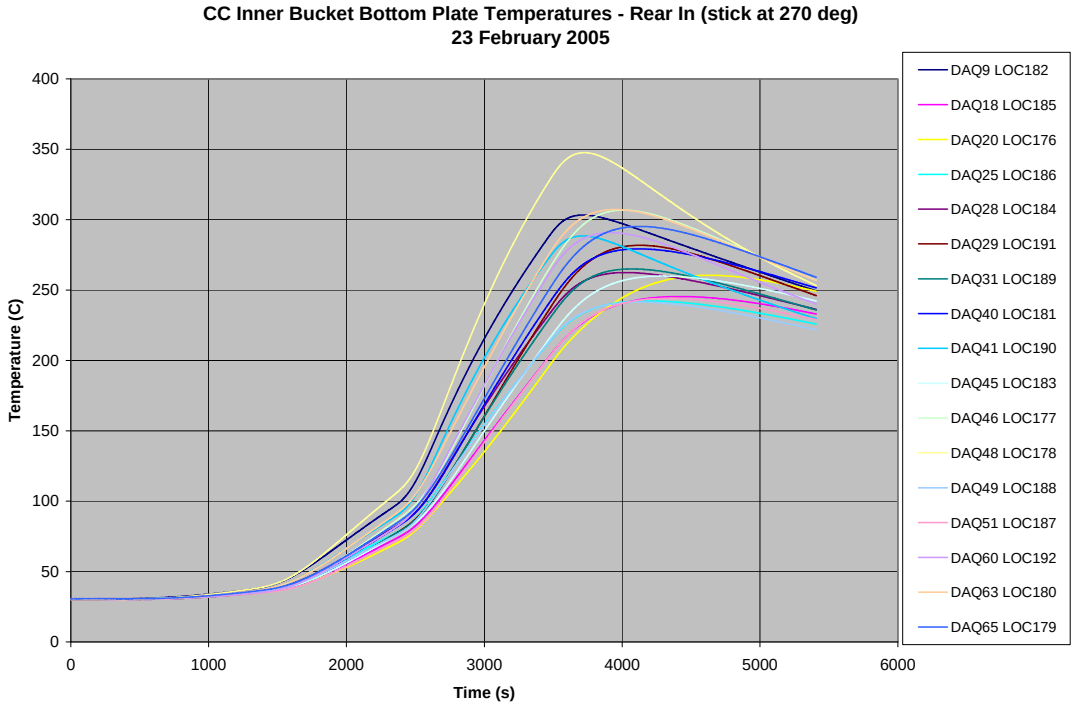

Figure 48 Inner Bucket Bottom Plate - 2/23/05

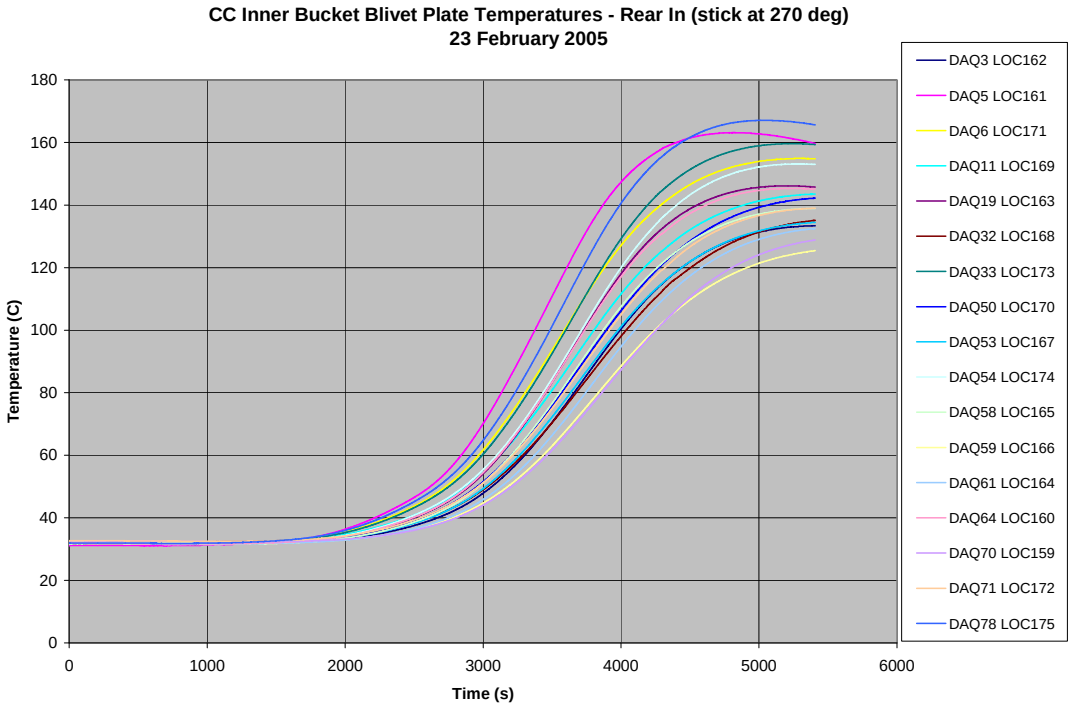

Figure 49 Inner Bucket Blivet Plate – 2/23/05

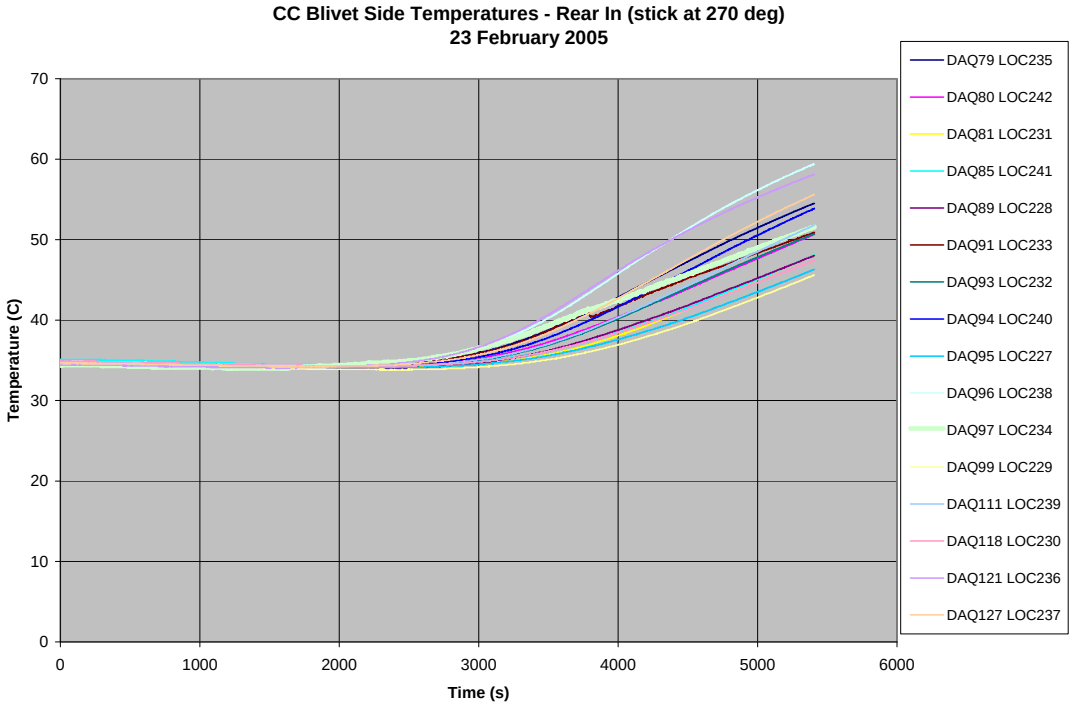

Figure 50 Blivet Side - 2/23/05

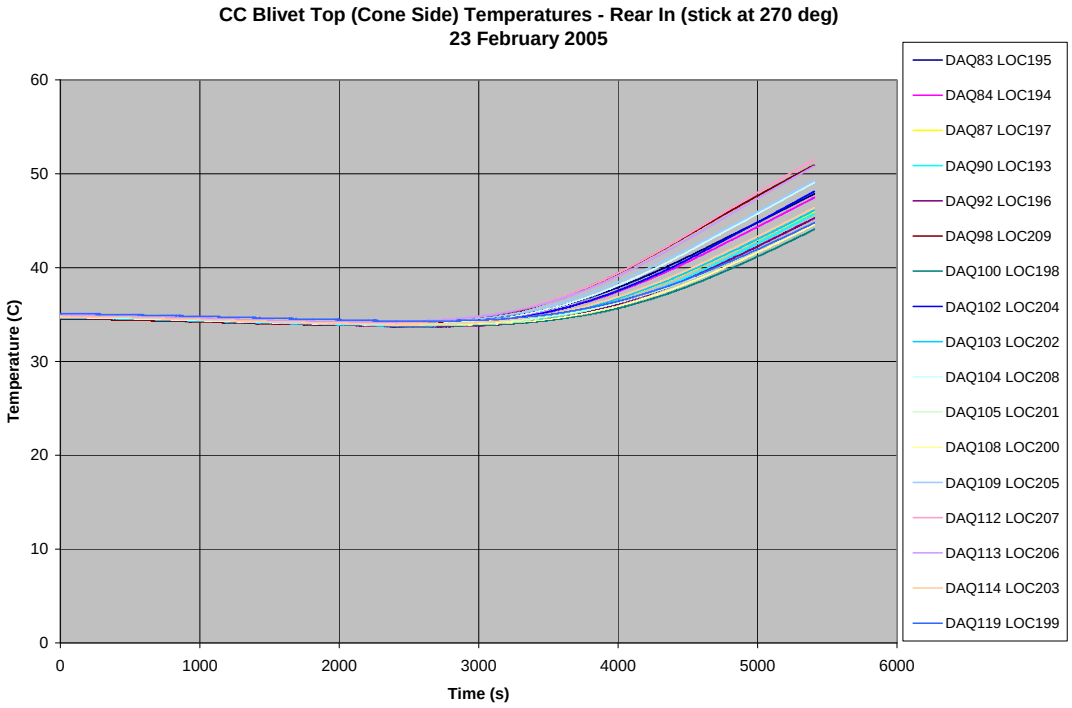

Figure 51 Blivet Top (Cone Side) – 2/23/05

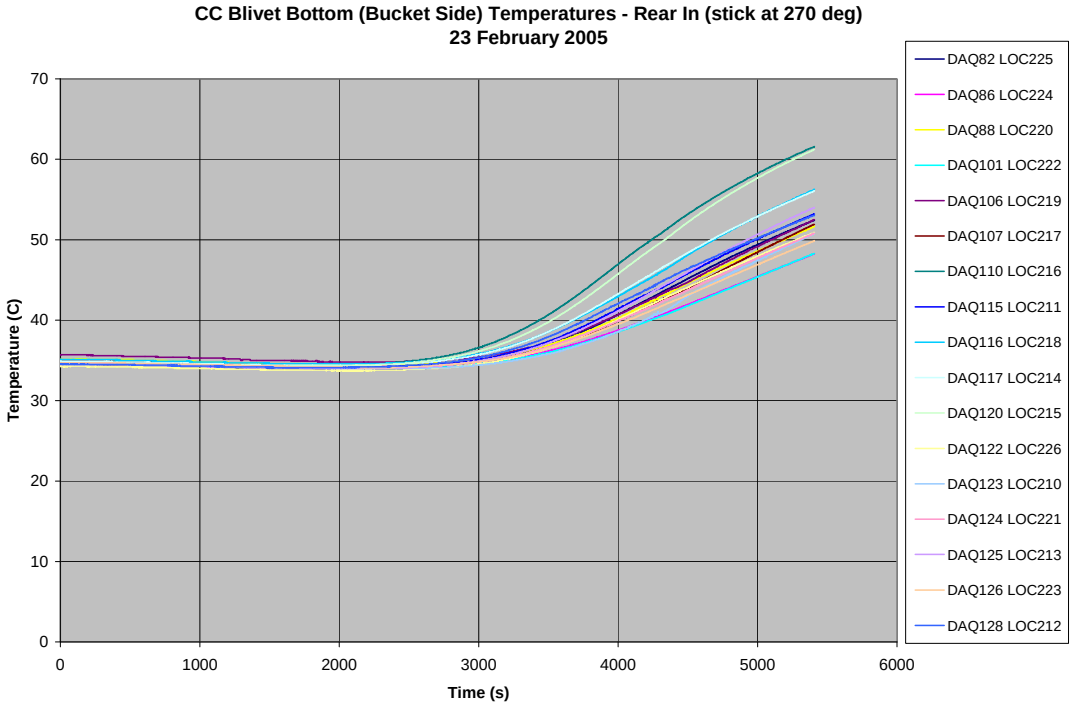

Figure 52 Blivet Bottom (Bucket Side) - 2/23/05

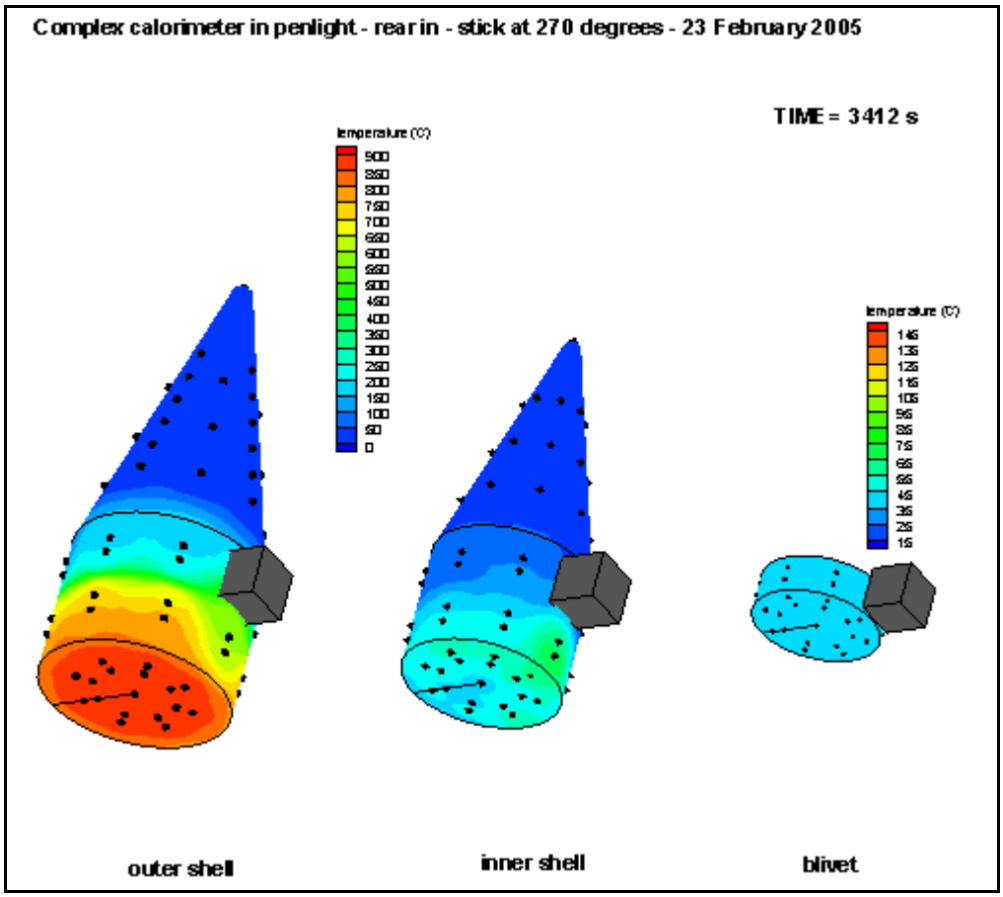

Figure 53 Calorimeter response (3400 s) in Test 3.

3.6 Test 6 – Nose Up 3

Test 6 (Penlight Test on March 16, 2005 (nose-up-cc-3)) was performed essentially to heat the blivet (see Figure 54 for orientation). The data from the nose up tests were used to validate the CALORE heat transfer modeling of the complex calorimeter.

Figure 54 The nose up configuration for Test 6.

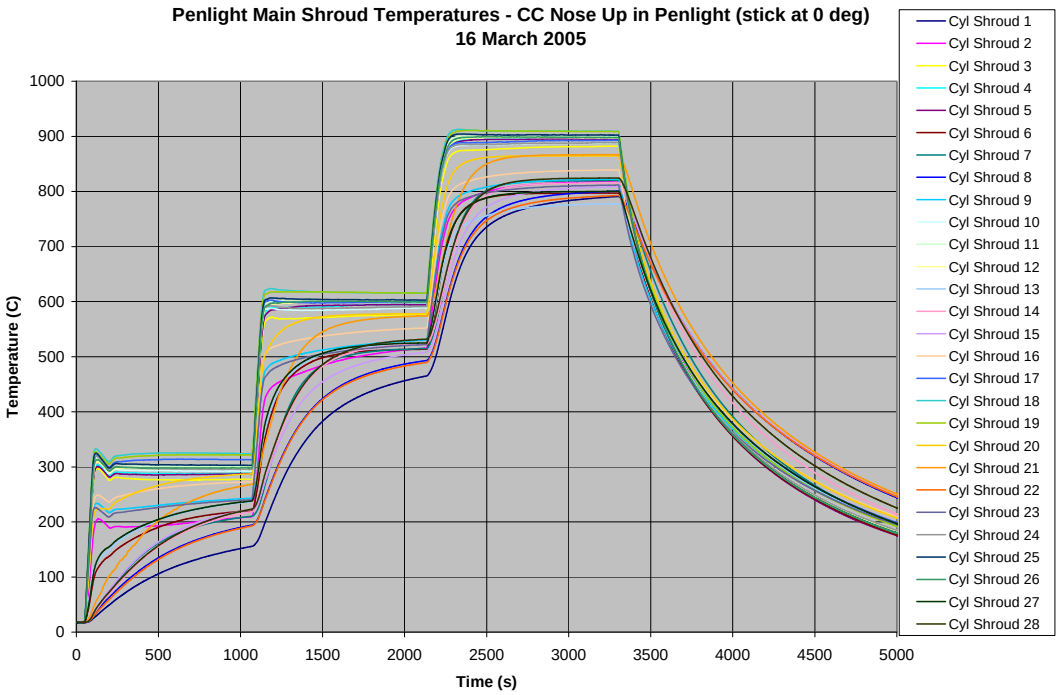

Figure 55 Penlight Main Shroud – 3/16/05

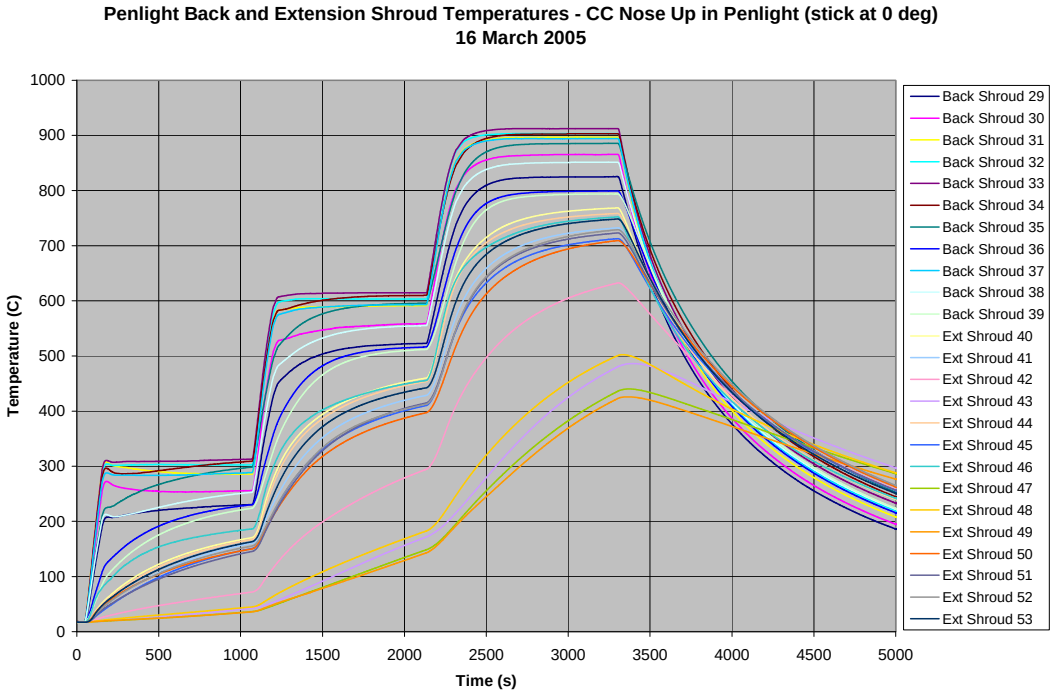

Figure 56 Penlight Back Shroud - 3/16/05

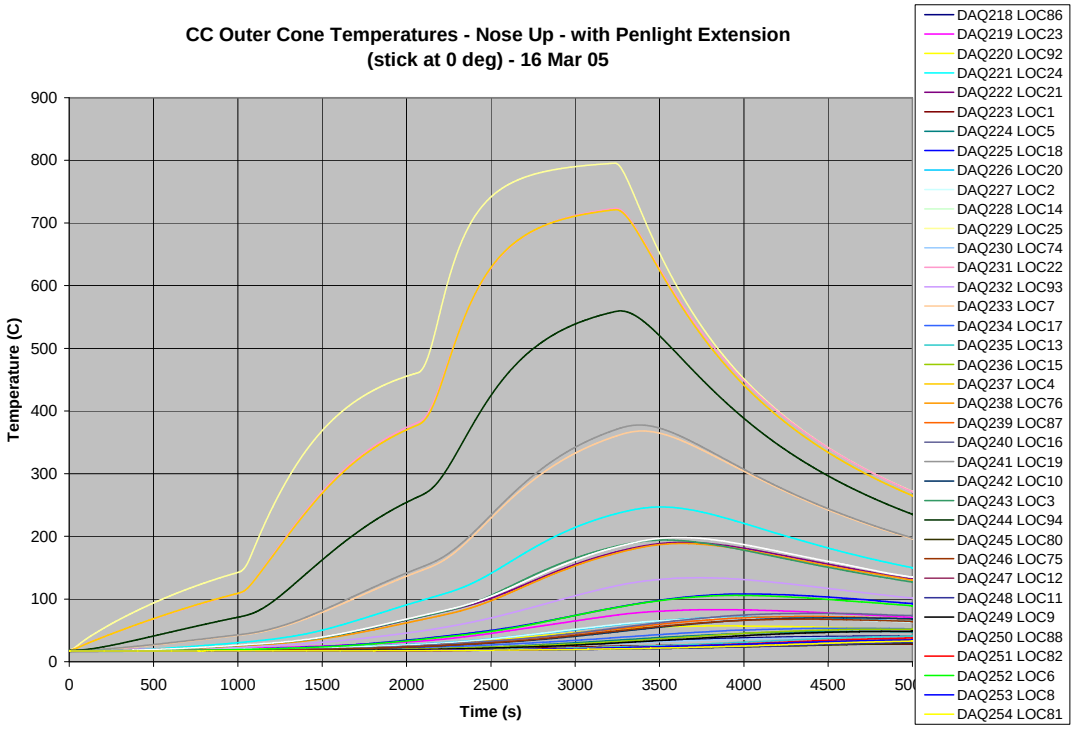

Figure 57 Outer Cone – 3/16/05

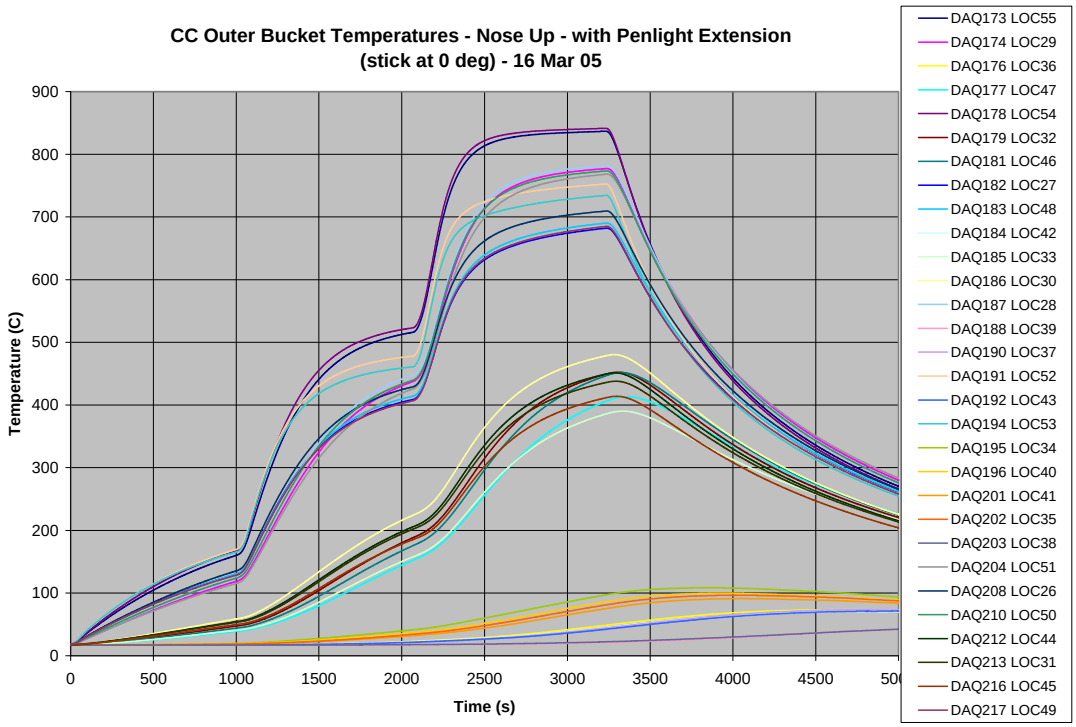

Figure 58 Outer Bucket - 3/16/05

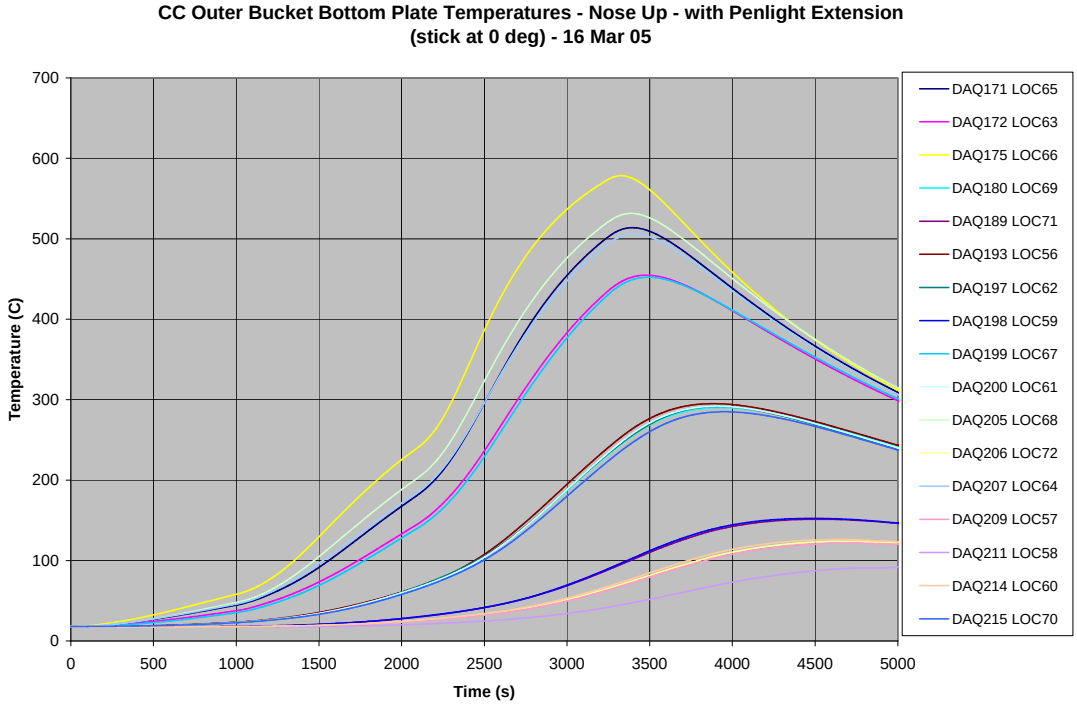

Figure 59 Outer Bucket Bottom Plate – 3/16/05

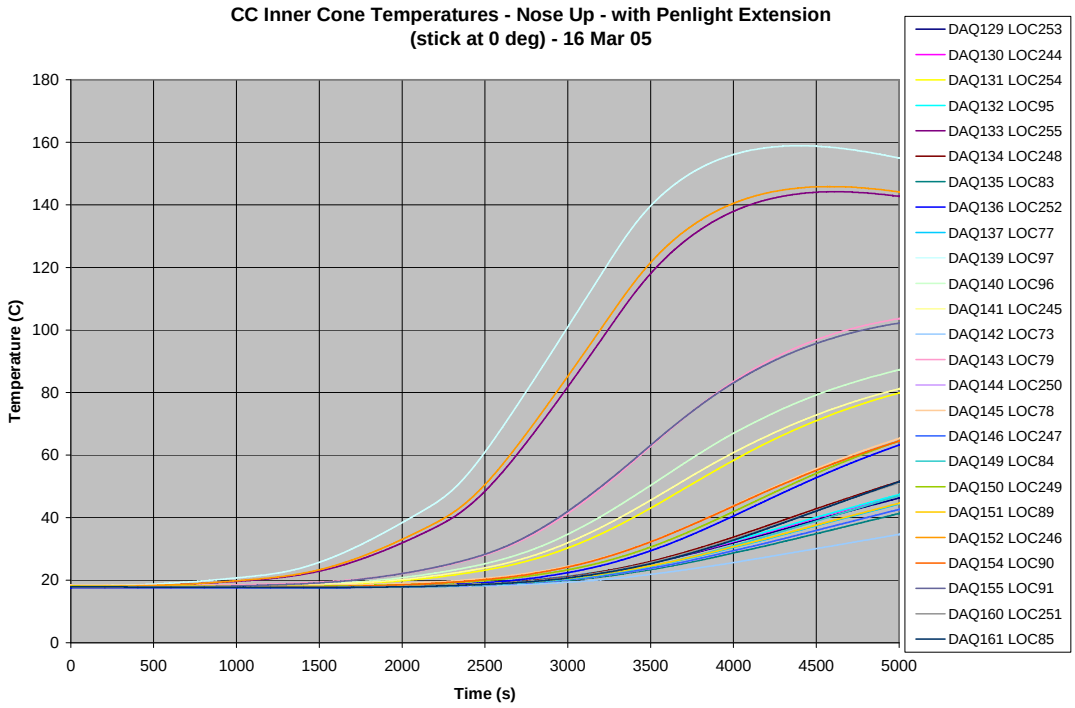

Figure 60 Inner Cone - 3/16/05

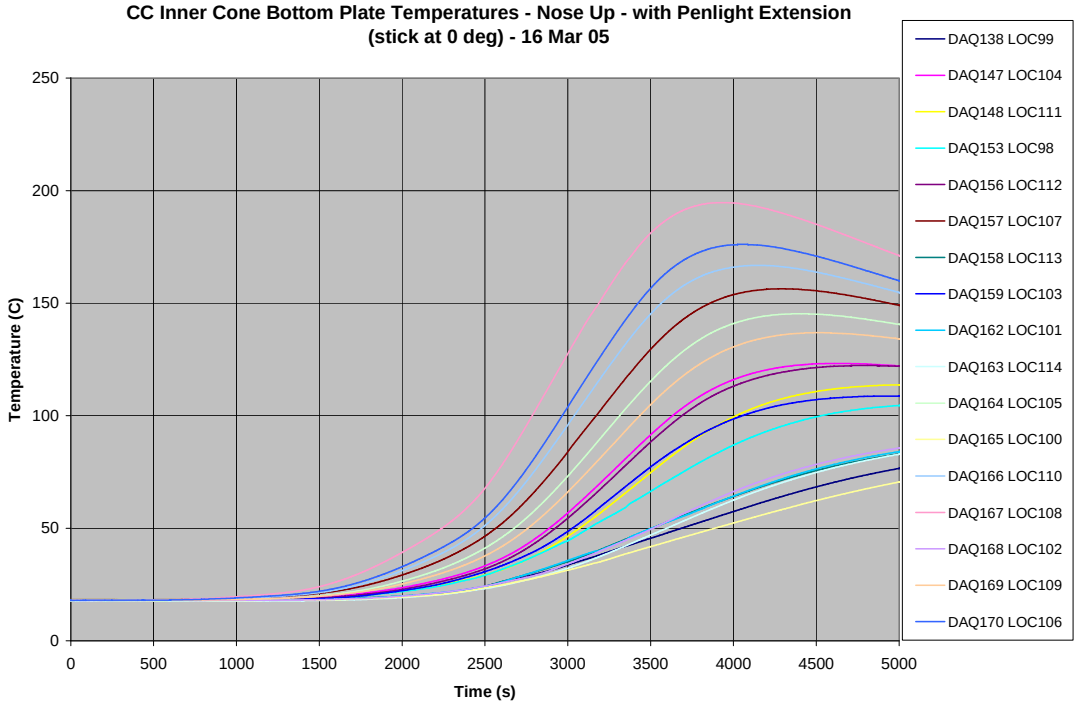

Figure 61 Inner Cone Bottom Plate – 3/16/05

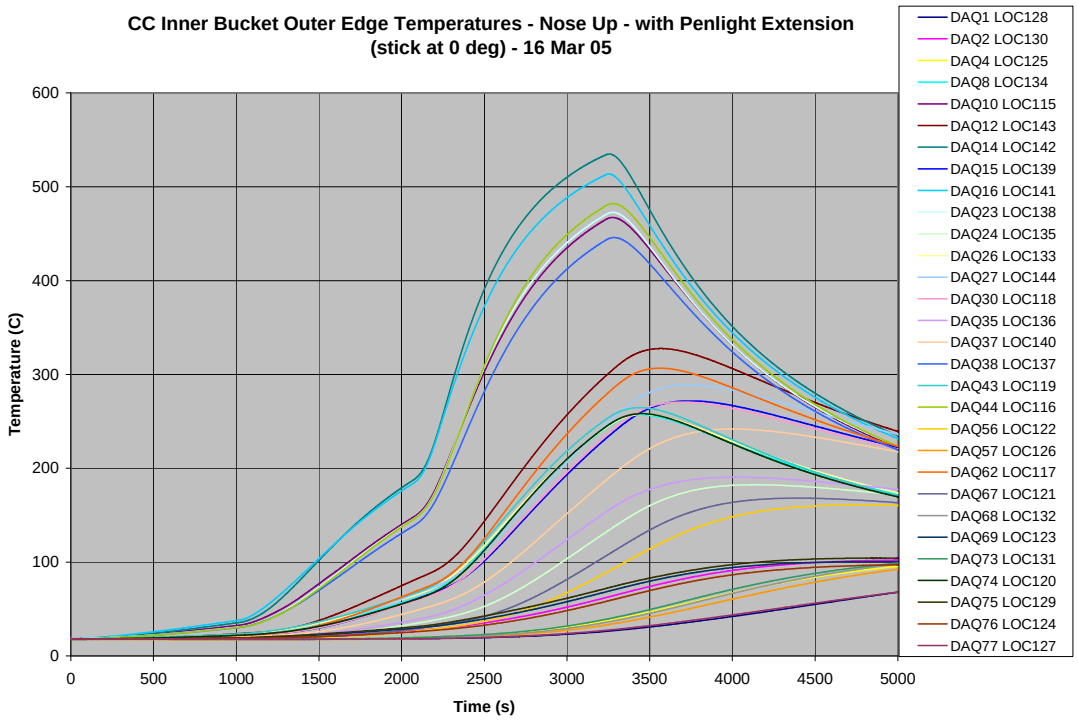

Figure 62 Inner Bucket Outer Edge - 3/16/05

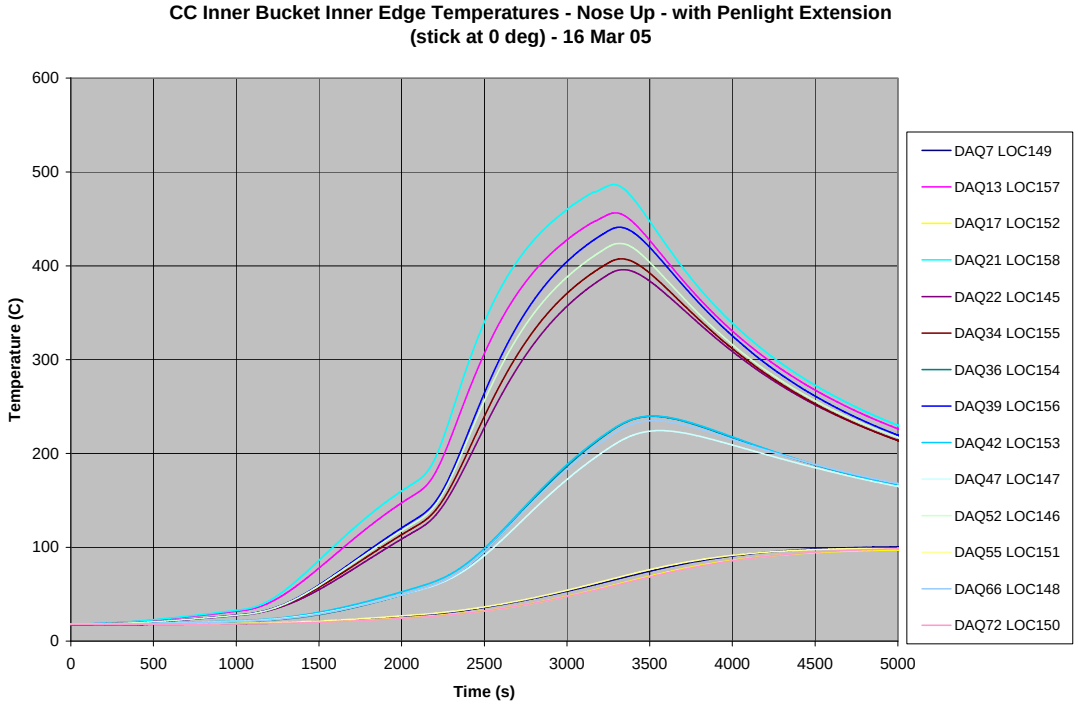

Figure 63 Inner Bucket Inner Edge – 3/16/05

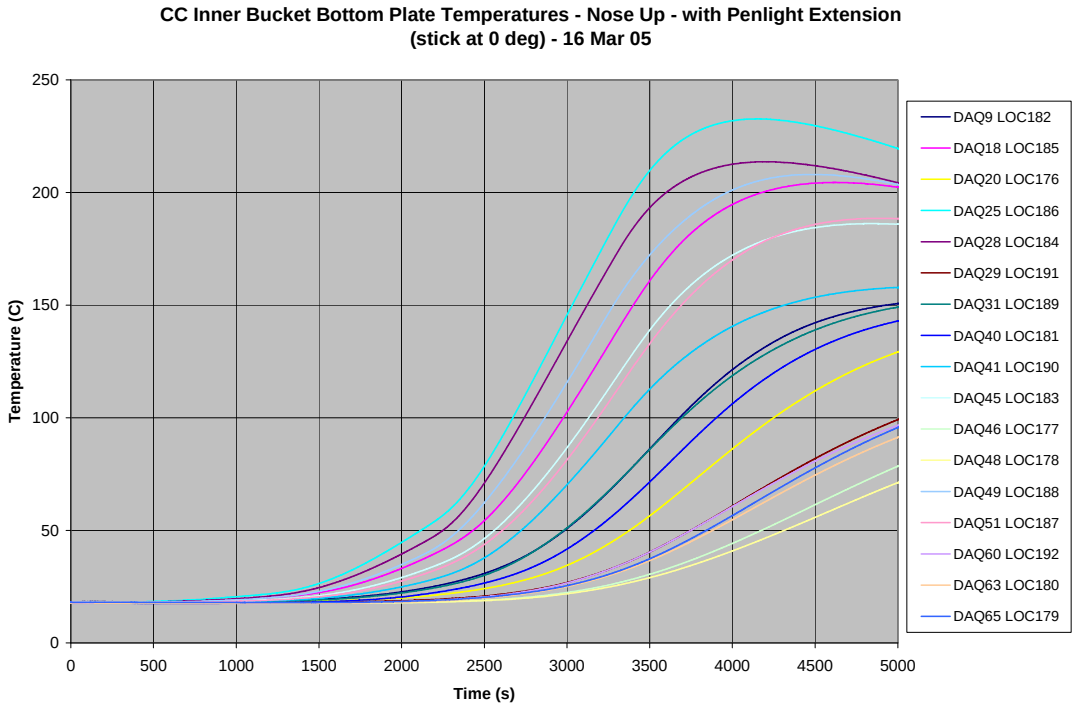

Figure 64 Inner Bucket Bottom Plate - 3/16/05

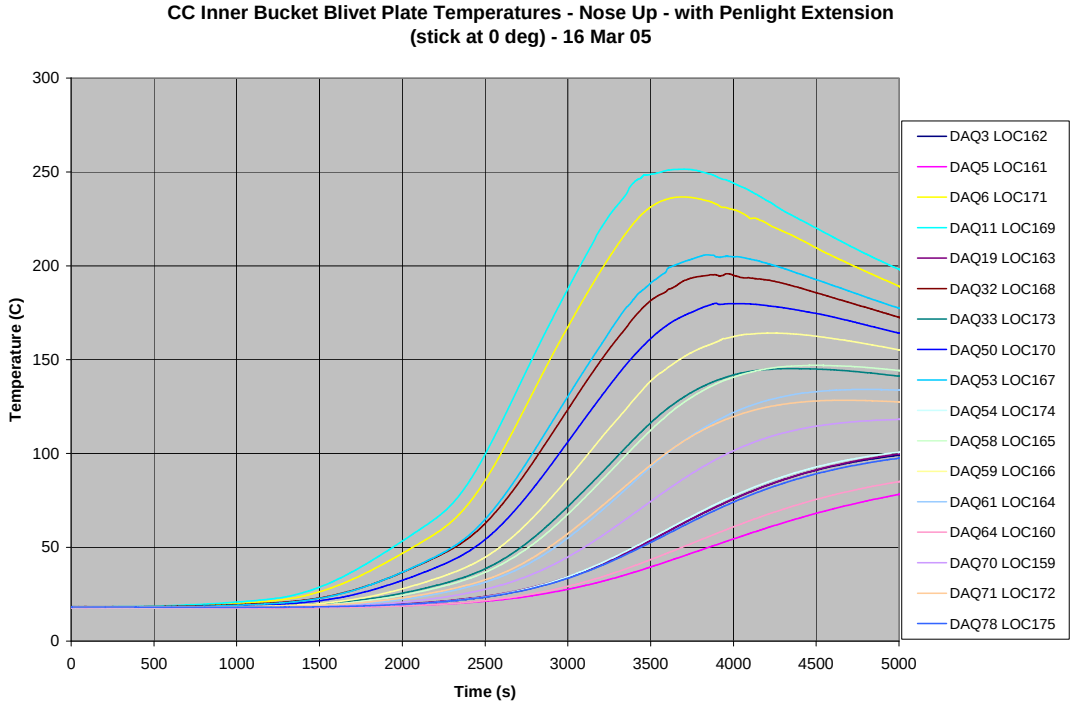

Figure 65 Inner Bucket Blivet Plate – 3/16/05

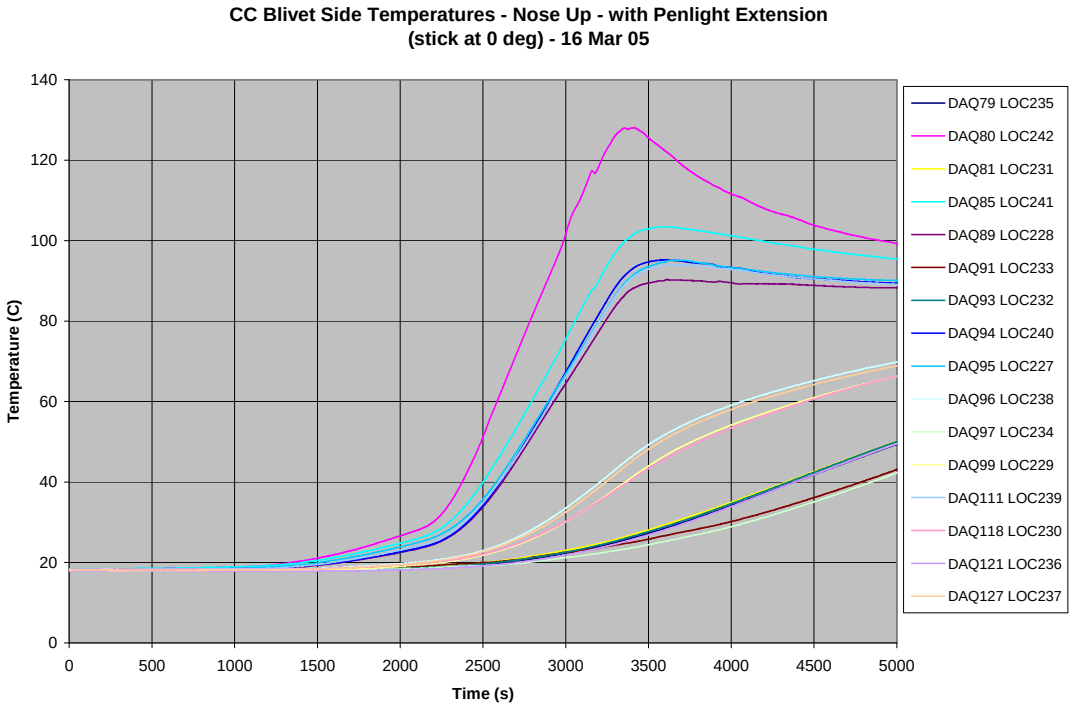

Figure 66 Blivet Side - 3/16/05

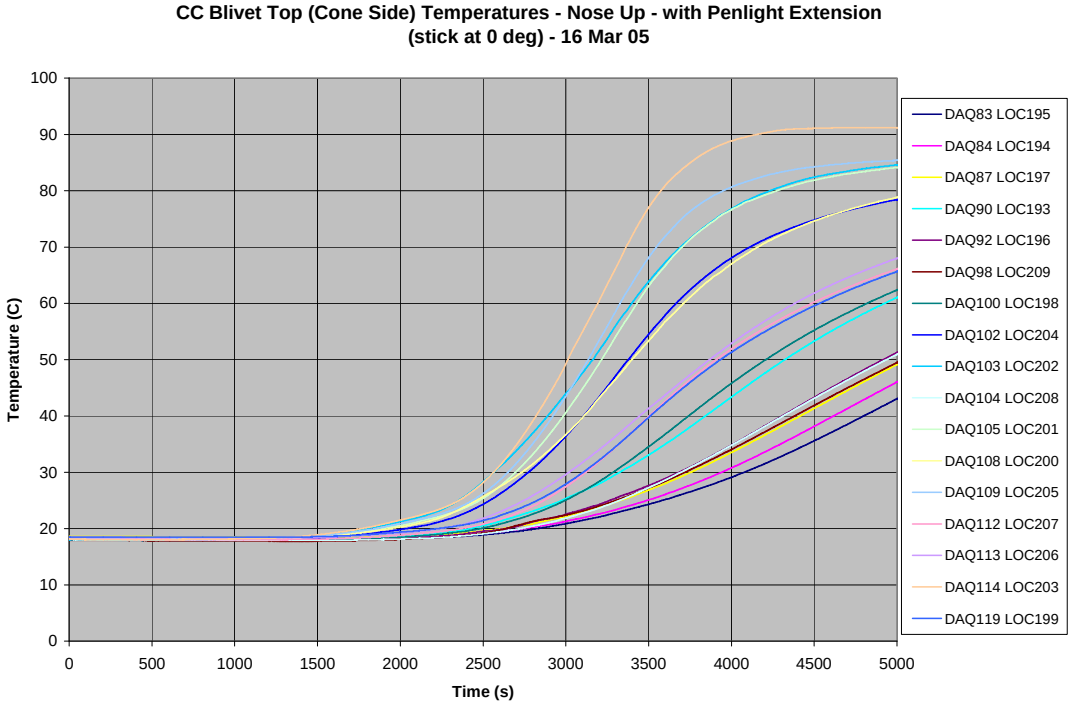

Figure 67 Blivet Top (Cone Side) – 3/16/05

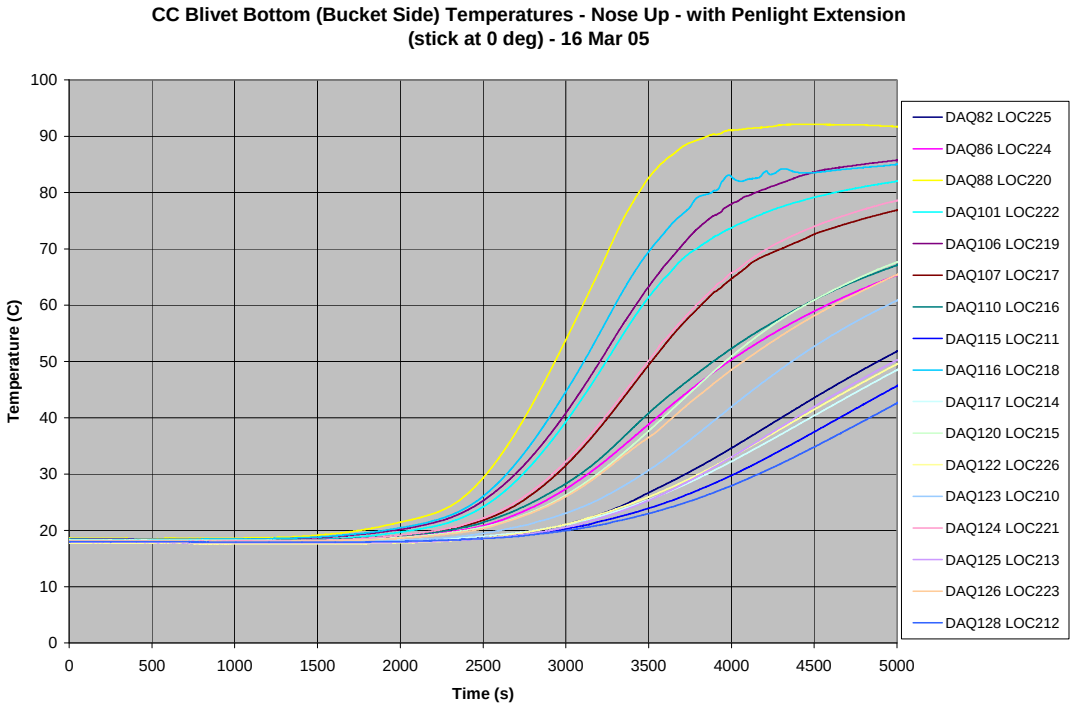

Figure 68 Blivet Bottom (Bucket Side) - 3/16/05

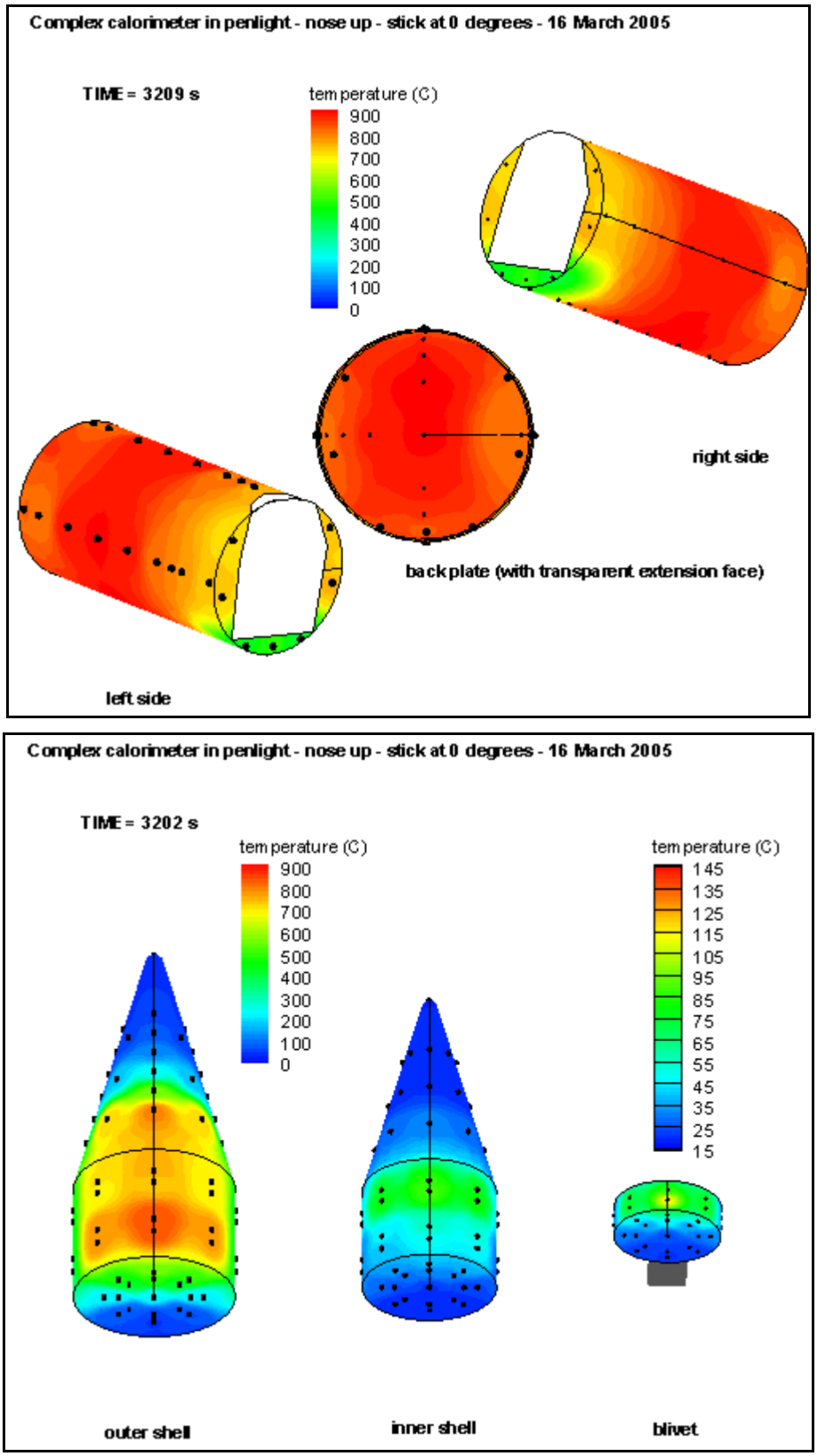

Figure 69 Penlight and calorimeter response (3200 s) in Test 6.

3.7 Summary of the Penlight Tests

Tests 4 (on March 9), 5 (on March 14), and 6 (on March 16) (identical nose-up tests) were used to determine data repeatability. Figure 70 shows temperature plots of two shroud locations (cylindrical shroud top centerline and back shroud center). The time-dependent standard error (standard deviation/average) at both locations is <1% during the steady portion of the curves, with increase to about 5% during the ramps.

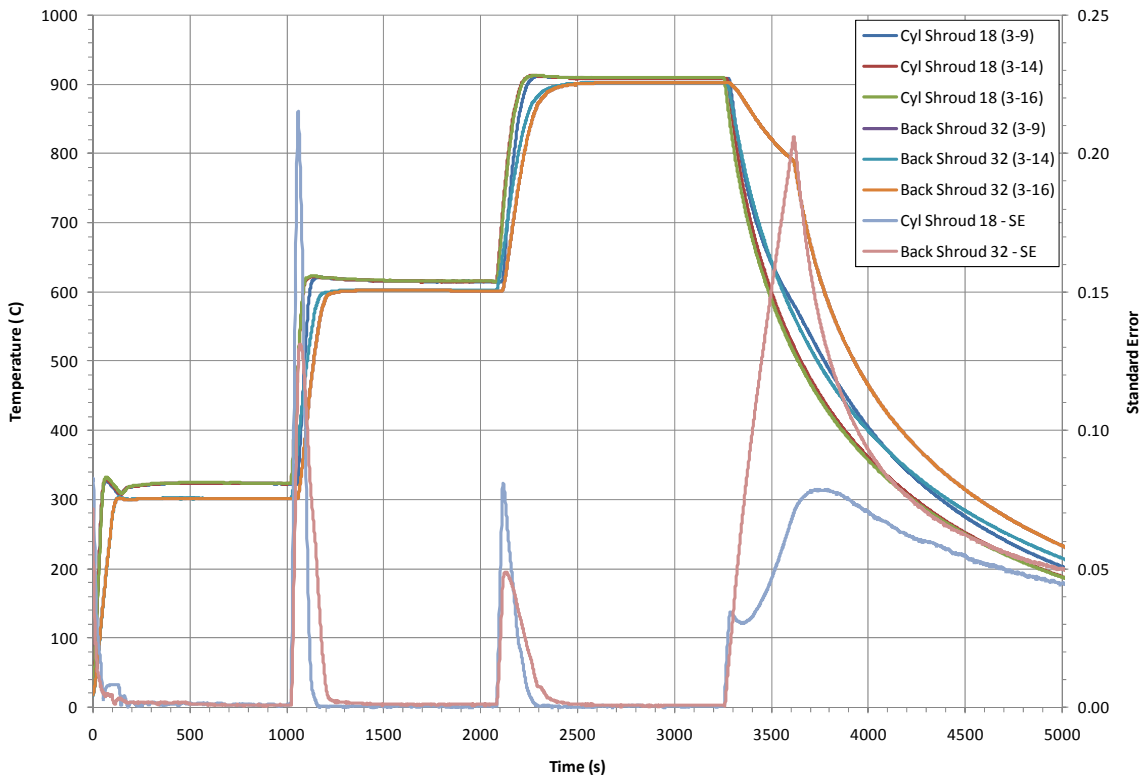

Figure 70 Repeatability of penlight shroud temperatures.

Figure 71 shows a plot of the time-dependent standard error for all of the thermocouples attached to the outer bucket. The standard error ranges from 6% at the start of the test to about 3% at test completion. Some of the difference is due to starting the heat ramp steps at slightly different time (~10 s, with manual control) and slightly different initial conditions (~3°C). Similar results were obtained for the repeatability of the blivet temperature measurements.

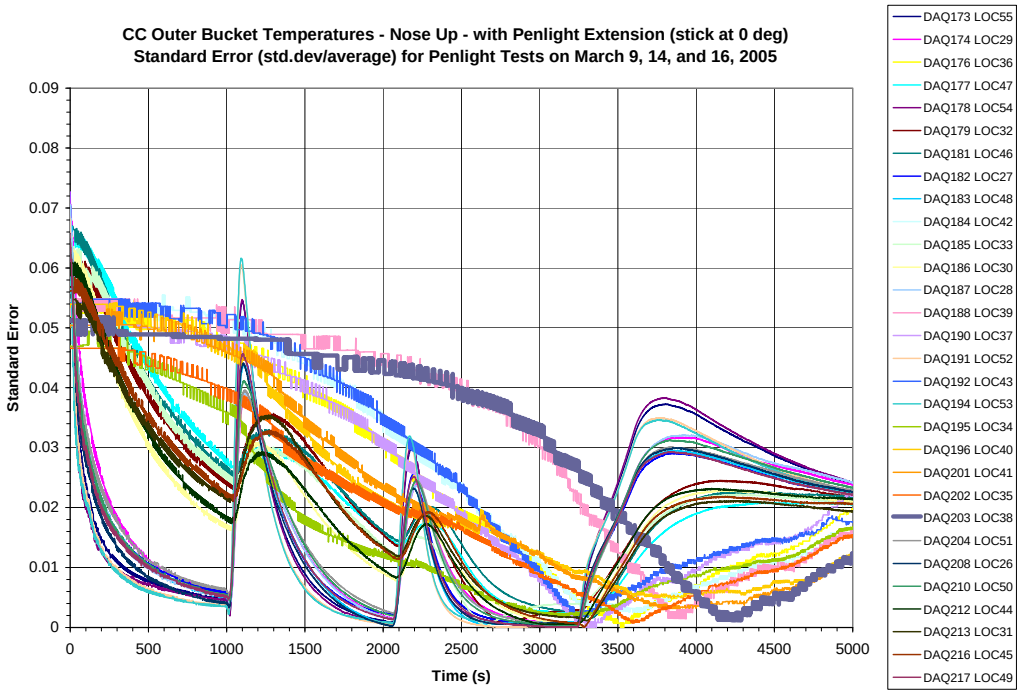

Figure 71 Computed standard error for the outer bucket over 3 penlight tests.

The penlight tests were extremely useful in that they provided a means of verifying the thermocouple attachment and operation "in-situ". In addition, data sets for future thermal conduction and radiation simulations for the Calore code were produced as the calorimeter outer surfaces provided known temperature boundary conditions for various configurations.

4. FLAME TESTING

4.1 Experimental Facility Description

The experiments were performed at FLAME using a 2-m pool filled with JP-8 jet fuel (shown in Figure 72). The dimensions of the facility (Figure 73) are approximately 6 m x 6 m x 10 m. The inlet air, conditioned by honeycomb and controllable by adjusting fan speed, enters through a ring on the floor. The fuel pan is located approximately 2.5 m from the floor allowing the air to be entrained radially at the base of the fire. The walls of the facility are water-filled for passive cooling temperature moderation. The water-cooled doors open to the south and are closed during testing.

While the air ring is centered in the facility, the pedestal and fuel pan are slightly offset from centerline, 7.5 inches to the west and 1 inch to the north.

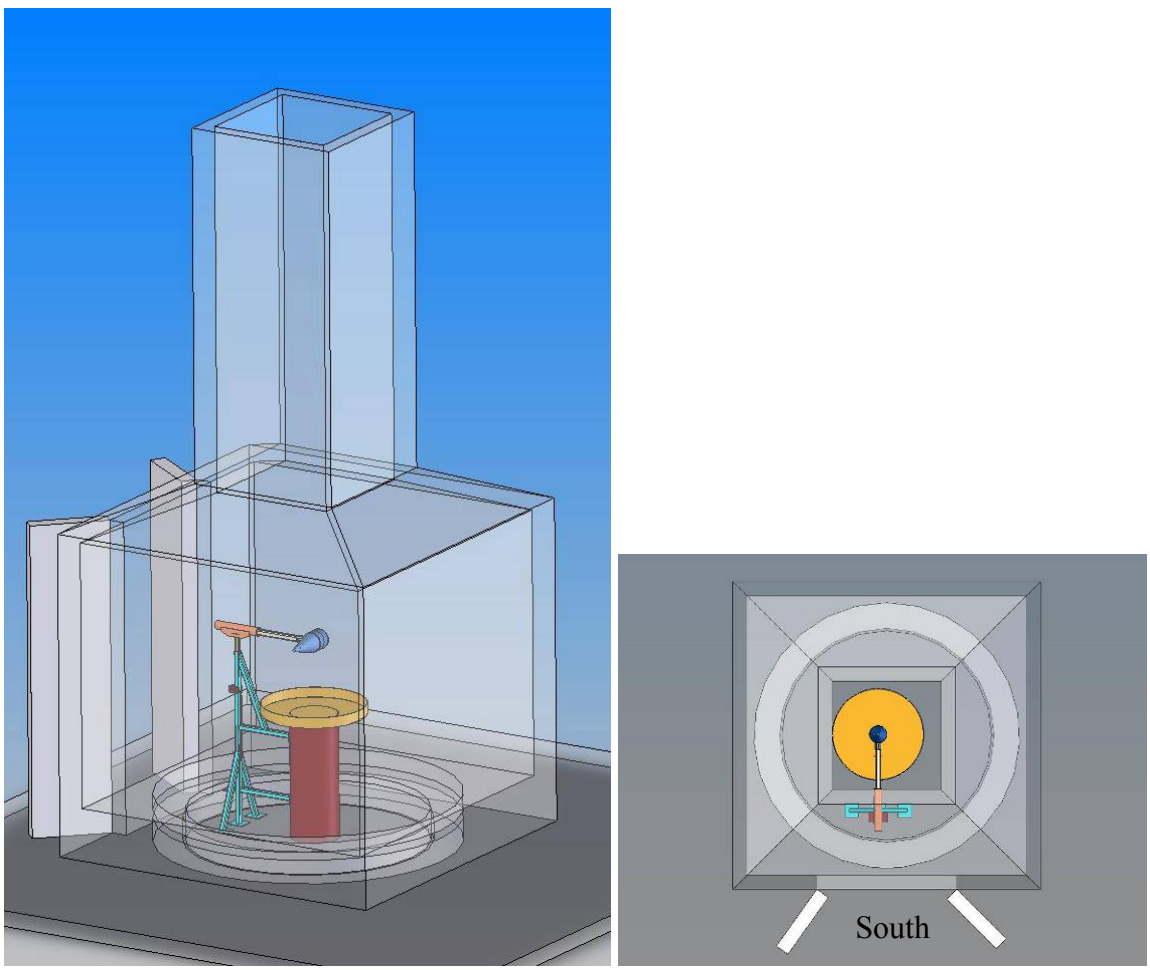

Figure 72 Complex calorimeter on support stand in FLAME.

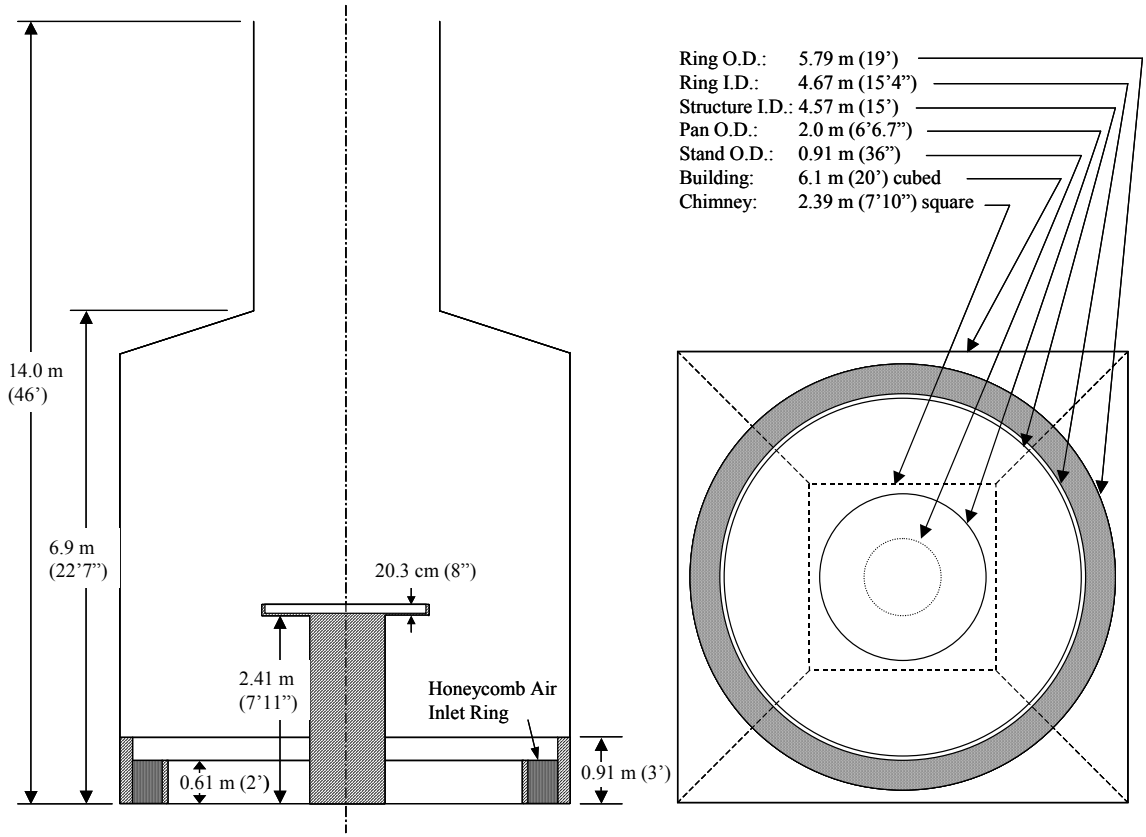

Figure 73 Side and top views of the flame facility with major dimensions.

Previous experiments [Brown and Blanchat, 2003] using a 2-m pan with 35 gallons of JP-8 determined that there is about a 200 s start up to steady-state conditions and about a 200 s fire termination period with water/fuel interactions, with a total burn time of about 1200 s. Also, the fuel recession ranged between 2-4 mm/minute, with an average recession of 2.6 mm/min during the steady burn period. Note: for a 2-m diameter pan, 1 mm of fuel corresponds to about 0.83 gallons.

The experiment duration required a minimum steady-state period of about 10 minutes. Note that the heat flux data obtained during first few minutes after ignition (while the fire is not fully developed) are typically not used for validation purposes; likewise, nor are the data during the last few minutes while the fuel is nearly exhausted and the fire is burning out.

In all tests, 35 gallons of JP8 fuel was floated on 4 inches of water (yielding a fuel height of 1 5/8 inches.

4.2 Experiment Measurements and Instrumentation

The boundary and initial condition measurements for all tests included:

- ambient air temperature

- ambient air pressure
- ambient wind speed
- ambient wind direction
- blower speed (4)
- duct flow rate (4)
- hot-wire anemometer measurements at air source exit (4)
- water depth
- fuel depth
- fuel amount
- fuel specific gravity
- fuel temperature/recession by thermocouple array
- fuel recession by differential pressure
- wall temperature (6)
- wall heat flux (8)
- heat flux to the pool surface (just outside the pool lip) (4)
- video coverage with time/date stamp (2)
- calorimeter temperature
- calorimeter surface emissivity

Where more than one instrument is required, that number is indicated in parenthesis. Locations of all instruments was determined and recorded prior to performing the experiments.

4.2.1 Facility Air Flow

In support of the gas burner particle image velocimetry (PIV) experiments [Tieszen et al., 1998], the duct FLAME facility flow and inlet air ring source was characterized using hot-wire anemometry [Blanchat, 2001]. It was determined that the standard error in velocity in the four inlet ducts feeding the air source was quite small (about 5%) for each speed and each blower. A curve was determined that yielded the volumetric flow rate as a function of the voltage measured by the permanently installed Kurz anemometer for each blower and associated duct. These curves were installed in the LabView blower operation program at FLAME, enabling accurate and stable flow rates from each blower.

The air source (sixteen connected trapezoidal panels in Figure 74 fed by four blowers and attached ductwork) was fully characterized using an automated data collection process (672 measurements taken about 1 inch above the honeycomb, using an automated measurement process based on a LabView software program controlling a 2-m by 2-m x-y translator table). Velocity data was taken at five different blower flow rates. A

standard deviation and the standard error were computed for each measurement point. The data was used to compute average velocity for each panel and then for the entire ring. A first order regression showed that the air source velocity in FLAME was a linear function of the ganged (all 4 operating at the same flow rate) blower flow rates and the velocity across a ring panel was found to be fairly uniform at different speeds and relatively independent of height (between 1 and 4 inches above the honeycomb).

The standard error for the average velocity of the air source ranged between 12-25% over the five blower flows. Fabrication tolerances caused small "hot spots" (small-scale features on the order of square centimeters around joints and edges of the 3-mm cell diameter, 5-cm deep honeycomb panels at the exit of the air ducts).

Table 3 shows that discarding the "hot spot" data yielded a spatial velocity distribution within about +/-10% of the air source ring average for the five flows.

Table 3 Average Air Source Velocity as a function of the ganged blower speed.

(without "hot spots" at the panel ID and OD and side edges)

Blower Speed (scfm)	**Average Velocity (standard m/s)**	**Standard Deviation (m/s)**	**Standard Error**
600	0.123	0.008	0.065
1000	0.184	0.016	0.084
1500	0.266	0.024	0.088
2000	0.339	0.032	0.095
4000	0.679	0.084	0.124
Re-characterization after rebuild, May 23 2002			
4000	**0.678**	**0.089**	**0.132**

The air source ring in FLAME was rebuilt in late 2001 to include stainless steel screen and moveable baffle plates placed at the air inlets (blower ductwork exhausts) in the four corners. The air source ring plenum was designed using rolled steel bar stock (19-foot OD and a 15.33-foot ID). To further smooth and evenly distribute the airflow, layers of stainless steel screen were placed at the inlet to the ring (opening at the bottom of the OD ring plenum). Finally, a layer of steel baffle plate, stainless steel screen (80x80 mesh, 0.007 inch wire diameter, 19.4 % opening), and 8-inch tall aluminum honeycomb at the ring outlet completed the air source modifications. The completed air source ring is shown in Figure 72, along with the fuel pan and pedestal.

Figure 74 The air source ring, fuel pan, and pedestal in FLAME.

The inlet air ring source was re-characterized at ganged blower speeds of 4000 standard cubic feet per minute (scfm) and 7000 scfm using hot-wire anemometry with the same methodology as described in [Blanchat, 2001]. Figure 75 compares the air ring velocity before and after the rebuild with ganged blowers operating at 4000 scfm. Table 3 shows that the average air velocity post-rebuild (May 2002) is essentially identical to the 2001 characterization (discarding the outer 'cold spot' ring of data at the source outer edge, similar to the data reduction performed with the 2001 data).

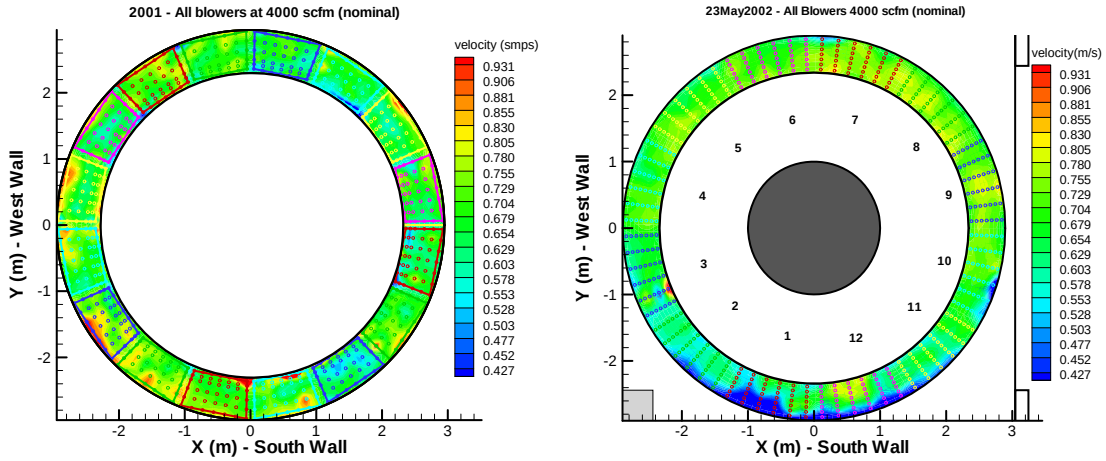

Figure 75 The air source ring, fuel pan, and pedestal in FLAME.

The inlet air ring source was monitored at four locations using TSI hot-wires shown in Figure 76.

Figure 76 TSI hot-wire velocity probes at the NE and SW locations.

4.2.2 Fuel Recession

Fuel regression rate was determined using a Setra model 239 differential pressure (DP) gauge positioned below the fuel pan with the high pressure tap connected to the base of the pan, and the low pressure tap just above the lip (to counteract fluctuations caused by the fire 'puffing'). Liquid level in the pan was monitored through a simple hydrostatic correlation (based on the measured fuel's specific gravity) between the pressure and height of fuel. The fuel was poured on top of an underlying water layer to aid in fuel leveling and to prevent pan distortion (note that water boiling has been observed to affect the recession rate near the end of a test).

Figure 77 presents the fuel differential pressure (inches JP-8), regression rate (mm/min), and pool mass loss rate (kg/m^{2}s, regression x fuel density, 802 kg/m^3) for two recent tests in a 2-m pan in FLAME. After adding water to the pool and zeroing the gauge, about 0.45 inches of fuel were added (10 gallons). The fuel recession and mass loss rate were determined for the quasi-static period between 100 and 200 s into the burn. The average pool recession and the average mass loss rate were very similar for both tests, at about 1.8 mm/min and about 0.024 kg/m^{2}s, respectively. Note that fuel recession increased during the burn. Average regression rates of 2.55 mm/min were reported for similar tests in FLAME, with the difference being longer duration tests that utilized 35 gallons of JP-8 [Brown et al., 2003].

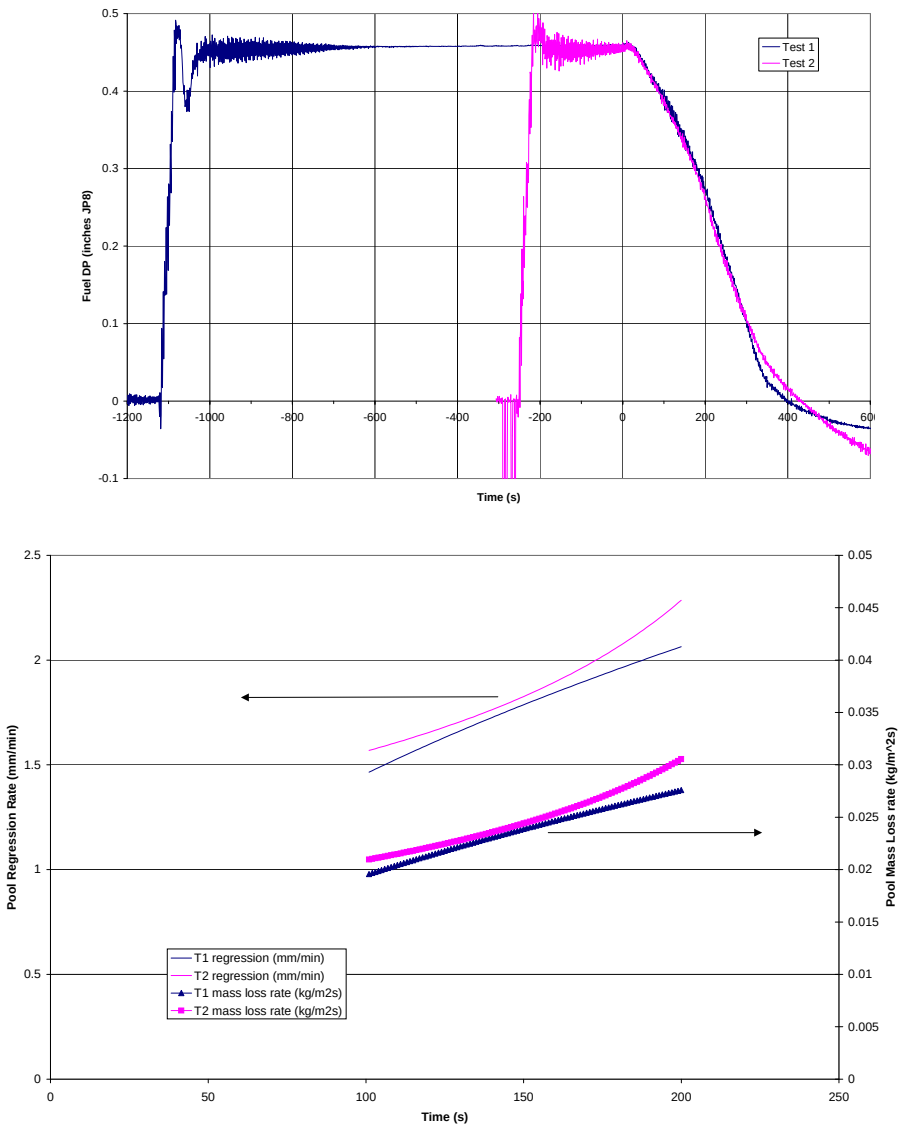

Figure 77 Fuel differential pressure, regression rate, and pool mass loss rate.

4.2.3 Fuel Temperature Measurements

Thermocouple arrays monitor the local fuel temperature and can also be used to verify the fuel recession rate. Correlation between the measured fuel temperature, recession rate, heat flux to the fuel surface, and the energy needed to gasify the fuel (as given by the sensible and latent heat requirements) provide a basis for understanding the thermal and mass transport within the fuel. Relevant transport includes heat transfer within the fuel, heat transfer to the underlying substrate (pan), convective mixing of the fuel, and horizontal transport of the fuel from regions of high to low heat flux (note that these transport mechanisms are not being measured in this work). This information would enhance the understanding of the fire-induced vaporization of the fuel, and is essential in

developing a realistic fuel recession sub-model for fire models. Given an understanding of the mechanisms, significant progress can be achieved toward defining fire environments where fuels are spilled or form pools on other substrates. Results from previous test series show that heating of the fuel is limited to the 0.5 inch layer near the top of the fuel surface.

Figure 78 shows the fuel temperature/recession thermocouple rake array (10 type-K, 1/16-inch diameter, inconel sheathed thermocouples are mounted on a steel pedestal 0.5 cm spacing). The recession measurement is based on isotherms between adjacent thermocouples on the fuel rake. The fuel thermocouples span part of the water layer, the entire fuel width (top to bottom), and extend into the flame zone. Immediately prior to a given test, the exact elevations of the thermocouples with respect to the fuel level are measured.

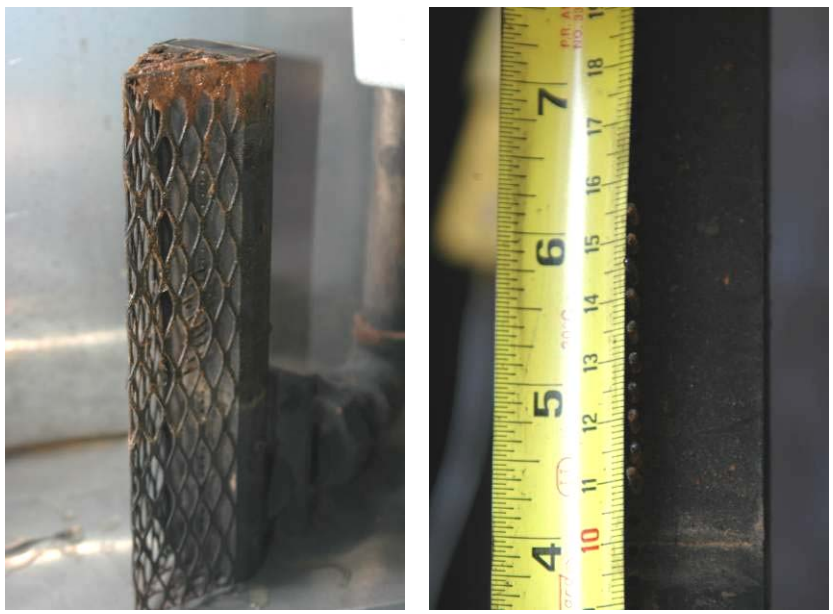

Figure 78 Thermocouple array for fuel recession.

4.2.4 FLAME Wall Temperature

The magnitude and distribution of heat flux and temperature on the FLAME interior surfaces is a principle measurement for the boundary condition. Re-radiation from the walls is not expected to be a major contributor, due to the low wall temperature (<373 K). Note that the walls of FLAME are heavily oxidized and blackened from years of experiments using JP-8 fuel.

The inside surface temperature of the water-cooled walls is monitored by a vertical array of six thermocouples attached the west wall (elevations of -1.1 m, -0.4 m, 0.6 m, 1.6 m, 2.6 m, and 3.6 m, all referenced to the fuel pan lip). In addition, two thermocouples measure water temperature near the bottom and near the top of one of the rectangular water tubes that comprise the walls of FLAME. Figure 79 shows the wall thermocouples, each covered with a thin stainless steel foil radiation shield.

Figure 79 Thermocouples on the FLAME West Wall.

4.2.5 FLAME Wall Heat Flux and Fire Plume Heat Flux

Incident heat flux to the inside surface is measured with a vertical array of four heat flux gauges attached to the east wall of FLAME (elevations of 0.1 m, 1.2 m, 2.2 m, and 3 m, all referenced to the pool surface). At each elevation resides a calibrated water cooled Schmidt-Boelter thermopile total hemispherical (180°) heat flux gauge.

In addition, a calibrated water-cooled Schmidt-Boelter thermopile narrow view (5°) radiometer was located on the east wall of FLAME (elevation of 1.2 m, referenced to the pool surface). With the narrow view angle, a spot size of ~0.27 m (10.5 inches) provided a surface emissive power of the flame. Figure 80 shows the thermopile array. Note one of the water cooled enclosures for a camera is shown mounted above the radiometer at the 1.2 m elevation.

Figure 80 FLAME East wall heat flux array.

4.2.6 Heat Flux to the Pool Surface

Four SNL heat flux gauges were attached outside and near the pool outer edge (facing upward, 90 degrees apart, vertically oriented) to measure the incident heat flux returning to the pool surface. Figure 81 shows the HFGs. Note the two horizontal rails welded on the pan south side (open door) and the north side. These rails (used in a previous experiment) and the HFGs were removed (Figure 82) after the first two tests were performed, as they appeared to be a source for flame attachment and would potentially hinder modeling of the data with the fire codes.

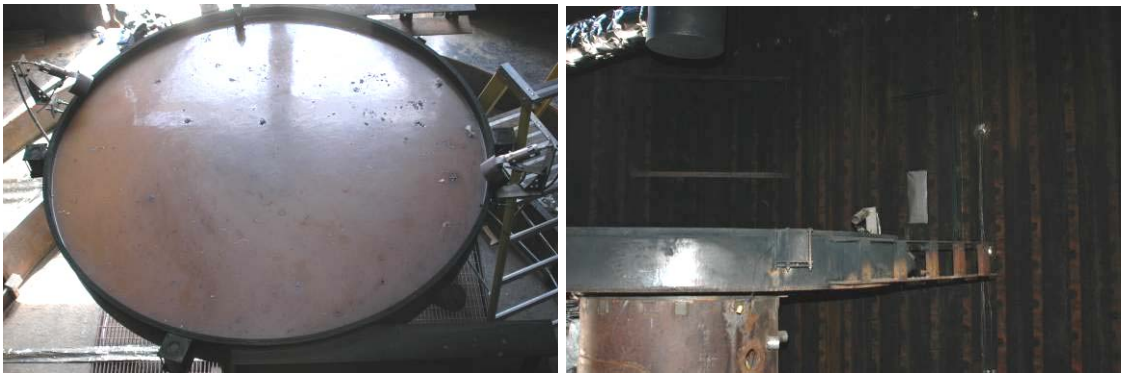

Figure 81 Fuel pan showing SNL HFGs, igniters, and rails.

Figure 82 Fuel pan rails, HFGs, and igniter shields removed.

The SNL HFG (Figure 83), showing a dual-sided gauge, is primarily a thin metal plate with one side facing the fire environment and the other side insulated. The metal plate (sensor surface) responds to the heat flux from the half space in front of the exposed face. If it is assumed the plate is in thermal equilibrium with a radiation-dominated environment, the plate temperature can 1) be converted to an incident flux characteristic of the half space, or 2) be interpreted as an effective temperature of the half space. The plate temperature is measured using a thermocouple attached to the insulated face of the metal plate. All HFG temperature data were processed post-test to provide an estimate of the instantaneous incident heat flux. A description of the gauge construction, the thermal response model used to reduce the HFG data, and the uncertainty analysis of the thermal response model is given in [Blanchat et al., 2000].

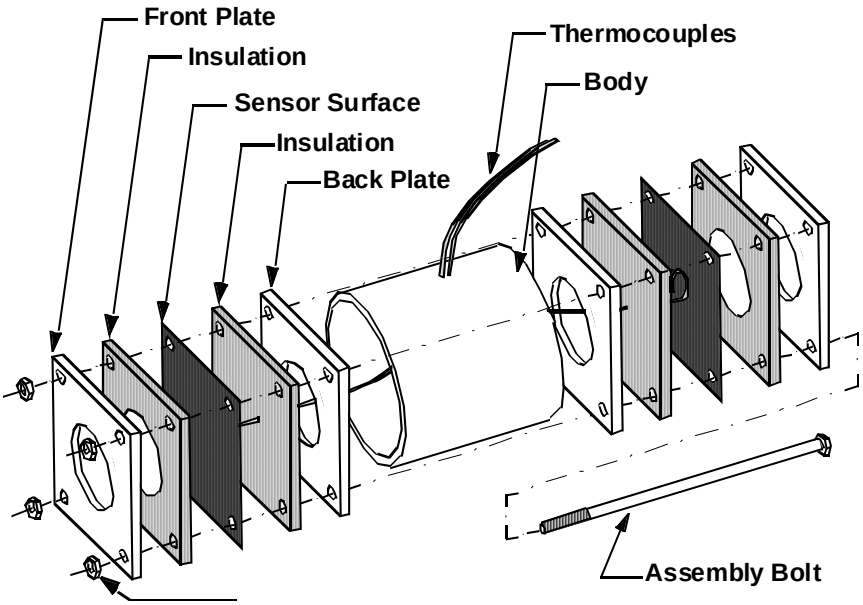

Figure 83 The Sandia HFG.

4.2.7 Photometric Fire Coverage

Two video cameras (in water-cooled enclosures) were attached to the FLAME north and east walls at the centerline position 1-m above the pool. The cameras recorded a normal view of the calorimeter. The vertical field of view of all the cameras was adjusted prior to the test to encompass the entire height of the continuous flame zone. A stadia indicator was used to calibrate camera field-of-view. Still photos were taken to record the instrumentation setup. Two additional video cameras (in water-cooled enclosures, Figure 84) were attached to the FLAME north and east walls at the wall-to-roof transition looking down at the fuel pan.

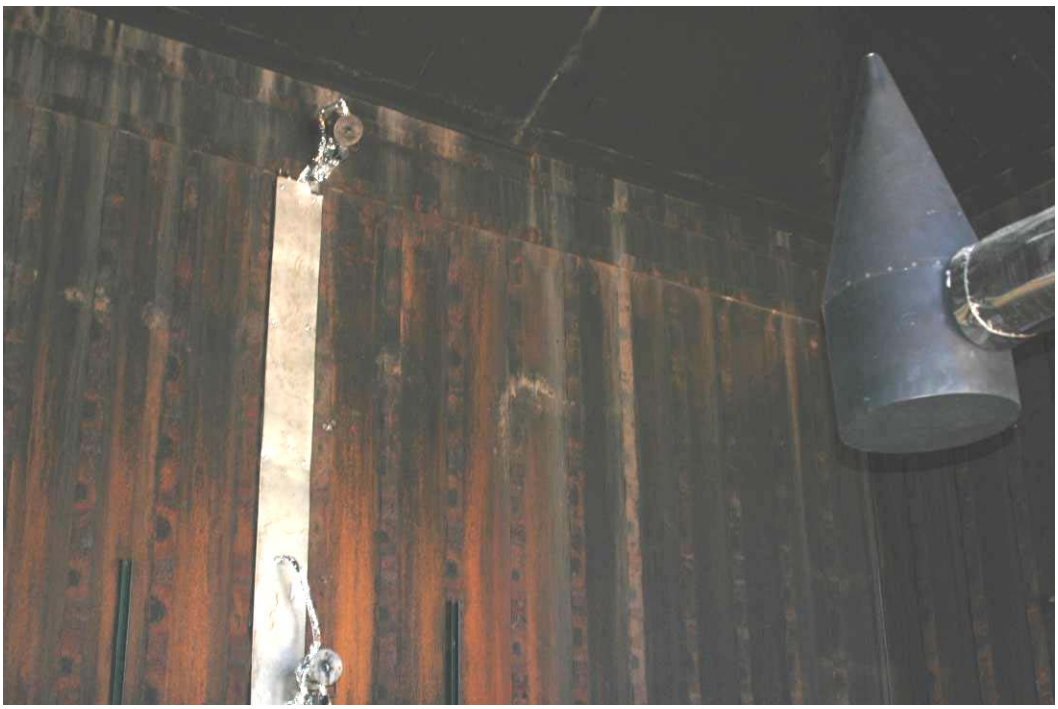

Figure 84 Video cameras on the North Wall.

4.2.8 Wind Speed and Direction Measurement

Even though enclosed, wind could affect FLAME boundary conditions as it blows across the chimney. Wind speed and direction are measured sufficiently far from FLAME in order to reduce the influence of the surrounding environment. Wind measurements are obtained with a YOUNG 81000 Ultrasonic Anemometer. The 81000 measures wind velocity based on the transit time of ultrasonic signals sent between the transducers. Depending on its orientation and magnitude, airflow alters the sonic signal transit time. By measuring the transit time in each direction along all three paths, the three dimensional wind velocity and speed of sound may be calculated.

4.2.9 Fuel Ignition

Ignition of the fuel is accomplished using two propane torches attached to the east and west sides of the pan. The torch consists of a standard propane "BBQ" gas cylinder, a spray nozzle, electrically-heated furnace coil, and a flame deflector plate. A fire set controls both the fuel and the coil heater. The propane fuel gas exiting the nozzle is ignited by the hot glowing coil and sprayed onto the fuel surface. Using dual igniters, the entire fuel surface is ignited quite rapidly and uniformly. Figure 85 shows the setup. Note the deflector plates attached to the nozzle exits were deemed unnecessary and removed after the 2nd test when the HFGs and the horizontal rails were removed.

Figure 85 Fuel igniter setup

4.2.10 Summary of Instrumentation

Table 4 summarizes the instrumentation for the complex calorimeter experiments.

Table 4 Instrumentation List

Measurement/Sensor Type	**No. of Locations**	**Sensors per location**	**No. of Sensors or TCs or Flux Gauges**
CC Outer Shell Temperature	84	1	84 TC
CC Inner Shell Temperature	86	1	86 TC
CC Blivet Temperature	50	1	50 TC
CC Blivet Face Environment Temperature	34	1	34 TC
FLAME Wall Temperature	6	1	6 TC
FLAME Wall Heat Flux	4	2	4 S-B thermopiles
Near Pan Heat Flux	4	1	4 SNL HFGs
Wind (vane gauge)(Speed/Direction)	1	1	1
FLAME Blower Flow rate	4	1	4 Anemometers
FLAME Blower RPM	4	1	4 Voltage
FLAME Ring Air Velocity	4	4	4 Anemometers
Ambient Pressure	1	1	AP
Ambient Temperature	1	1	1 TC
Fuel Recession (DP)	1	1	1 DP
Fuel Temperature	10	1	10 TC
Video	4	1	4 camera
Misc. Temperature (telltales, equipment, ambient, etc.)	10-20	1	10-20 TC
TOTALS			
Thermocouples (Type K)			~300
SNL Heat Flux Gauges			4
Schmidt-Boelter Heat Flux Gauges			4
Wind (speed, direction)			1
Absolute Pressure			1
Differential Pressure			1
Video Cameras			2

4.3 Data Acquisition (DAQ)

The Burn Site data acquisition systems is installed in a Mobile Instrumentation Trailer (MIU) (Figure 86) located on site between the large open pool facility and the FLAME facility. This greatly expands capabilities and provides rapid turnaround of experiments.

Figure 86 The mobile instrumentation trailer.

The Burn Site data acquisition system consists of a master control computer located in the MIU and a mobile slave system located either in the FLAME facility or at the Large Pool area. The slave system controls the FLAME blowers and monitors the permanent instrumentation (thermocouples, etc.) in FLAME. The master system controls the test, acquires some additional test data, and provides data conversion and user interface. The systems are linked by a local area network (LAN). The master system consists of a dual processor PC with a 4-monitor display and at least 512 Mbytes memory. The test data can be displayed in real time. The slave system consists of a PC with a 16-bit data acquisition card connected to a SCXI chassis. The slave system collects test data and transfers it to the master system.

The DAQ system has twelve 1102 cards with 1303 blocks for TCs and four 1104 cards with 1300 blocks for analog signals. This system provides flexibility in the number of analog signals or TC signals that can be recorded. Note that the SCXI-1001 presently holds 12 cards, yielding a total channel count of 384 channels if all slots are used for data acquisition. The system is upgradeable simply by adding an additional SCXI-1001 DAQ card and more multiplexer units (MUXs).

The data acquisition system can acquire temperature, heat flux, pressure, and wind vane data. The integrity of all thermocouple channels is evaluated prior to each experiment with an Ectron thermocouple simulator which inputs a controlled signal into each channel at the thermocouple device connection point and provides a check on the integrity of the channel hardware and software from that point to the final magnetic storage location.

The thermocouple simulators are calibrated yearly in the Sandia National Laboratories (SNL) Primary Standards Lab that is traceable to a National Institute of Standards Technology (NIST) standard.

Data are sampled simultaneously for all channels, typically at 1000 Hz with a running average recorded at a rate of at least one sample per second, starting approximately two minutes (+/- 1 min.) prior to ignition of the fuel, and continuing until two minutes (+/- 1 min.) after all the fuel is consumed, or longer if cool down data is desired.

Data acquisition systems are protected from power failure by an uninterruptible power supply (UPS) capable of sustaining data acquisition for up to 24 hours without commercial power. Temperatures are provided in Kelvin, pressures in Pascal, wind speed in m/s, and wind direction in degrees relative to the facility orientation. Following any test, all data (temperature, wind, and video) are normalized to include a common timing (e.g., time of fuel ignition) and backed up immediately.

Three general forms of data are required: 1) pre-test data which describes the organization information related to each test; 2) data collected during the test event; and 3) post-test data describing overall results or consequences. Pre-test data includes general information such as test number, configuration, ambient conditions, critical instrument settings, and the like. Post-test data describes any damage that might have occurred and provides an anecdotal summary of the test event. Pre- and post-test information are recorded on the Test Data Sheet.

A formal checklist for conducting the test is created and used to record actions during the test event. Test event data includes both actions taken during the test (i.e., a completed checklist) and data gathered electronically from the instrumentation. The data from the instrumentation is organized via a Data Channel Summary Sheet and with sketches showing instrumentation location. This summary sheet contains a channel-by-channel listing of the instrumentation with details such as expected range, sampling rate, calibration date and source, instrument location, and the data sample rate. Post-test, all data is collected and converted to electronic format for purposes of archiving and dissemination via PC multimedia (i.e., CD or equivalent) and also is logged into the Area III Data Management System.

4.4 Data Validation

A data validation process was instituted to confirm the validity of the data. The integrity of all channels were evaluated before the first experiment and checks made between subsequent experiments. An “end-to-end” calibration (thermocouple plug board to the output of the DAQ system) was made on each channel with a calibrated Ectron at 300°C and 900°C (a thermocouple simulator that inputs a known value into the TC plug-board). The acceptance criteria for the channles was ±2°C.

Data validity checks include checking for thermocouple shunting and obvious failures.

Additionally, upon receipt, each new TC was checked against a calibrated thermometer with stirred baths using ice-water and boiling-water.

All channels had an uncertainty to within ± 1.7 K. Data validity checks such as checking for thermocouple shunting[1] and obvious failures were performed on all channels. Obvious faults (e.g., physically impossible values, non-readings, readings inconsistent with other similar readings) were used to eliminate faulty channels.

Additionally, each calorimeter TC was heated with a heat gun after attachment to ensure each channel was properly identified and to assess the homogeneity of the exposed portions of the TC.

4.5 Experiment Configuration and Matrix of Experiments in FLAME

The complex calorimeter was mounted to a rigid support, only allowing movement between fires, shown in Figure 72. Several repeat experiments were performed for each calorimeter location and fire size and type. Table 5 presents the experimental matrix.

Table 5 Experiment Matrix for FLAME Tests

	Facility Air Flow					
	4000 SCFM/blower			**3000 SCFM/blower**		
Calorimeter	**Location**			**Location**		
Orientation	*CENTER LINE*	*½ R*	*R*	*CENTER LINE*	*½ R*	*R*
Up	WO 1,2,3,13, 14,15,16, 17,18					
Up	W 19,20					
Horizontal	WO 4,6	WO 8,12	WO 9,10,11	WO 5,7		
Horizontal	W 21, 22					
Down						

Notes:

[1] Shunting is a phenomena that occurs when the magnesium oxide insulation inside the TC reaches a high enough temperature so that its electrical resistivity decreases significantly. When this occurs "virtual" junctions for so the TC shorts or "shunts" and incorrect readings occur.

1. Three calorimeter locations: pan centerline, pan ½ radius, and at R (pan edge)
2. All test at one height above pool (1-m from JP8 surface to calorimeter bottom surface for any orientation)
3. Two calorimeter orientations: nose up and nose horizontal (nose down was not performed). In the horizontal tests, the nose was pointed to the FLAME West wall.
4. W - with insulation ring at center blivet location
5. WO - without insulation ring at center blivet location
6. All WO tests were performed prior to W tests

While horizontal orientation tests are deemed the most relevant to weapon in a fire scenario, the vertical (up) orientation tests are assumed to provide the best candidate data sets to yield good simulation comparisons. The W (with insulation surrounding the blivet) tests should reduce the uncertainty on the heat flux to the surface over the blivet region when using 1D inverse heat conduction analyses to reduce the thermocouple data.

Test numbers highlighted in red denote problems that occurred in those tests. In test #5, the fuel recession data by the DP transducer was bad (note that fuel recession could still be determined using the fuel thermocouple rake). There was an abnormally slow burn rate near the end of the fire (after t = 700 s) in tests 13 and 14 (it was determined later that the most likely cause was there was a thick fuel/water interface (water or rust or some other contaminant at the interface due to insufficient time for the fuel to separate from the water after adding to the pan). In test #9, the automatic control of the blowers was set shortly after the fuel was ignited (not before as in all other tests). In test #16, all thermocouples on the complex calorimeter read low due to a grounding problem (the data was kept for the fuel recession and plume heat flux).

Table 6 Boundary Conditions for the FLAME experiments.

Test	Test Date	Cal Position Radial From Center Line	Cal Orientation	center strip insulation	Pressure inHG	RH (%)	Ambient Temp (C)	JP8 SGx100 @ Temp (F)	Burn Rate (mm/min)	Blower Speed (cfm)
CC 1	6/28/2005	Centered	1m ver	without	23.98	31	25	800	2.81	4000
CC 2	6/30/2005	centered	1m ver	without	23.93	8	32	790 @ 92	2.95	4000
CC 3	7/6/2005	Centered	1m ver	without	23.94	9	36	792 @ 92	2.91	4000
CC 4	7/8/2005	Centered	1m hor	without	23.99	20	26	795 @ 89	2.85	4000
CC 5	7/12/2005	Centered	1m hor	without	24.08	23	29	797@ 85	2.75	3000
CC 6	7/14/2005	Centered	1m hor	without	23.97	17	31	800 @ 78	2.93	4000
CC 7	7/18/2005	Centered	1m hor	without	24.06	26	31	794 @ 92	3.17	3000
CC 8	7/20/2005	1/2 R	1m hor	without	23.96	18	35	794 @ 97	3.09	4000
CC 9	7/22/2005	1R	1m hor	without	24.08	45	26	800 @ 79	2.99	4000
CC 10	7/26/2005	1R	1m hor	without	23.95	37	28	794 @ 90	3.13	4000
CC 11	7/28/2005	1R	1m hor	without	24.06	55	18	805 @ 66	2.96	4000

CC 12	8/9/2005	1/2 R	1m hor	without	23.98		22	Not measured	2.92	4000
CC 13	8/15/2005	Centered	1m ver	without	23.99	66	22	801 @ 75	2.85	4000
CC 14	8/17/2005	Centered	1m ver	without	23.95	37	27	796 @ 89	3.01	4000
CC 15	8/19/2005	Centered	1m ver	without	23.94	56	21	804 @ 74	2.82	4000
CC 16	8/24/2005	Centered	1m ver	without	23.9	59	23	805 @ 70	2.82	4000
CC 17	8/29/2005	Centered	1m ver	without	23.9	51	26	799 @ 87	2.94	4000
CC 18	8/31/2005	Centered	1m ver	without	23.9	20	27	800 @ 85	3.00	4000
CC 19	9/16/2005	Centered	1m ver	with	24	58	29	808 @ 62	2.87	4000
CC 20	9/19/2005	Centered	1m ver	with	24.07	30	26	804 @ 74	2.99	4000
CC 21	9/26/2005	Centered	1m hor	with	24.01	11	29	794 @ 96	3.16	4000
CC 22	9/28/2005	Centered	1m hor	\with	23.92	50	19	805 @ 71	2.95	4000

Due to the vast amount of data, only Test 15 data will be presented in full. Note that the data from Tests 15, 17, and 18 (pan centerline, vertical orientation, without insulation at blivet) were used for the FUEGO ASC code data validation exercise (Black et al., 2007). All of the experimental datasets are archived on the DVD.

4.6 Presentation of FLAME Facility Data from Test 15 – Nose Up

Test 15 (FLAME Test on March 16, 2005 (nose-up-cc-3)) was performed to determine the calorimeter response due to an engulfing JP-8 fire. The calorimeter was oriented in a vertical configuration at pan centerline. The base of the calorimeter was positioned 1 m above the fuel surface. The top of the fuel was ~2 inches below the pan lip at the start of the test. The insulation strip surrounding the blivet (between the inner and outer shell) was removed to maximize the blivet response.

Two separate, independent data acquisitions systems (DAS) were used to conduct each experiment. One was dedicated to the thermocouples on the complex calorimeter. The other DAS recorded the FLAME facility support instrumentation. As such, two separate Excel files are included on the DVD for each experiment archiving the data from each DAS.

The FLAME DAS recorded the data:

1. Monitor temperatures. Unshielded thermocouple measuring ambient temperature, one placed near a TSI hot-wire anemometer probe, one placed inside the pan cylindrical pedestal stand, and one placed near the radiometer on the wall at the 1m height.
2. Fuel temperatures. The thermocouple rake monitoring fuel temperature and regression.
3. Pan HFGs. The thermocouples attached to the four Sandia HFGs. Note the data is only valid for tests 1 and 2 (the HFGS were removed and dummy TCs were installed in the DAS slots).

4. Support arm temperatures. Seven thermocouples were attached to the complex calorimeter support arm. The four TCs labeled 0", 12", 24", and 36" were attached to the top of the horizontal square tube (4 inch) supporting the calorimeter (0" is at the calorimeter-to-arm transition). The arm was then insulated with 2 layers: 1 inch of high temperature blanket insulation covered with a stainless steel foil, then an additional 1 inch blanket with a final foil wrap. Three thermocouples were placed inside the square tube monitoring the temperature of the complex calorimeter thermocouple bundles. One was placed ~2 inches inside the calorimeter, one at the calorimeter-to-arm transition, and one was placed at the mid arm location.
5. Fiducial and ignition. To allow time synchronization of each DAS, a 5 volt fiducial signal was sent to each DAS immediately prior to fuel ignition. In addition, a thermocouple was placed directly in front of one of the igniters that showed the start of the fuel ignition.
6. Wall temperatures. In addition to the six thermocouples attached to the West wall, four thermocouples monitor the temperature of the water inside the walls. Internal top and bottom monitor inside one of the rectangular tubes in the vertical section, and transition supply and return monitor the water feeding the water-cooled transition between the vertical walls and the roof.
7. TSI velocity probes. The velocity of the air exiting the air ring using four TSI hot-wire anemometers are recorded. This is essentially a check that the four blowers are operating nominally. Note that the readings slightly decrease during the fire, as the probes are affected by the radiant heat from the fire.
8. Ultrasonic wind probe. The raw voltage for the U, V, and W wind components and the sonic gas temperature from the Young ultrasonic (US) anemometer located near the FLAME chimney exit.
9. Wind. The reduced wind data (azimuthal direction and speed) from the Young anemometer in addition to two standard wind (whirl vane) anemometers.
10. Laser. The voltage output from the instrument monitoring the smoke exiting the chimney. The reduction in the laser signal is used with a soot extinction parameter to allow data reduction to a soot concentration measurement.
11. DP. The differential pressure signal from the transducer monitoring the liquid level in the fuel pan.
12. Wall Medtherms. The calibrated output from the heat flux gauges (total and radiometer) mounted on the East wall of FLAME.

Figures 87-98 present the data from the Excel spreadsheet (CC 15 FLAME 081905.xls) for the CC 15 test performed on August 19, 2005.

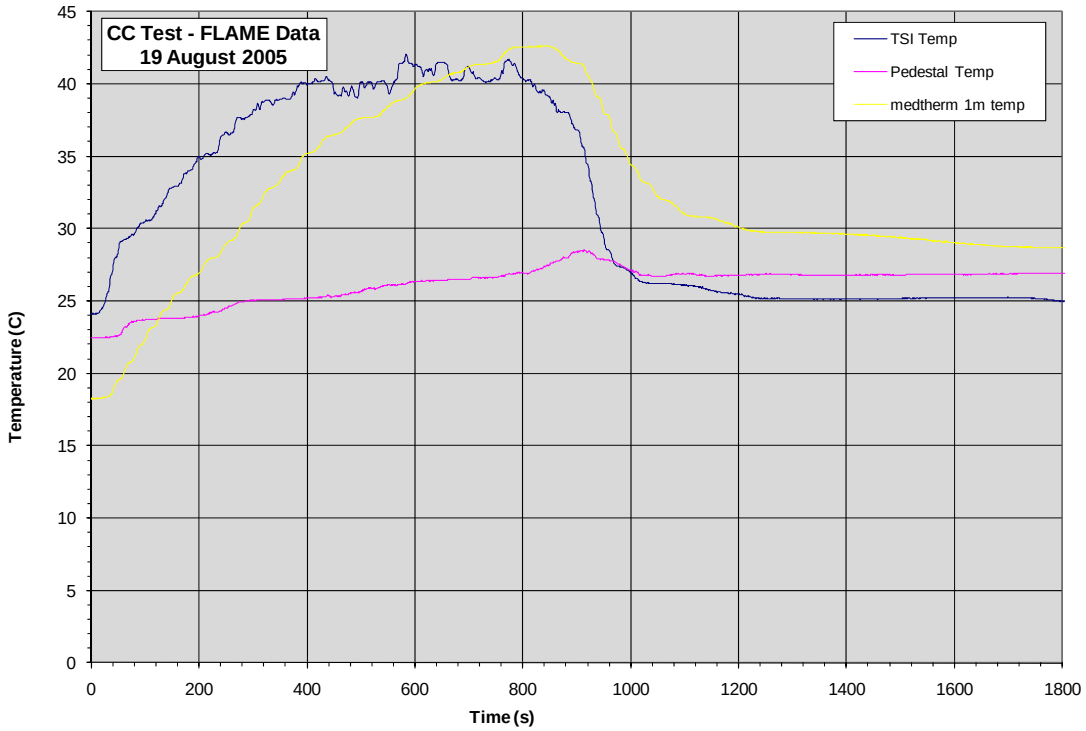

Figure 87 Ambient air monitor temperatures.

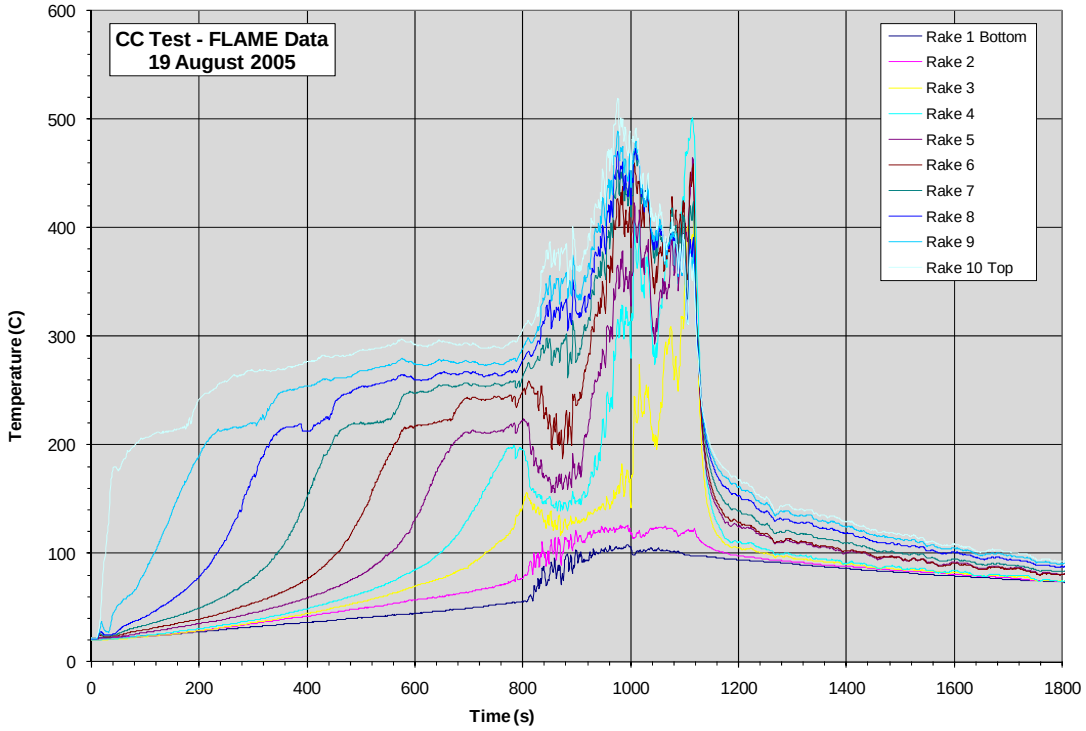

Figure 88 Fuel pan array temperatures.

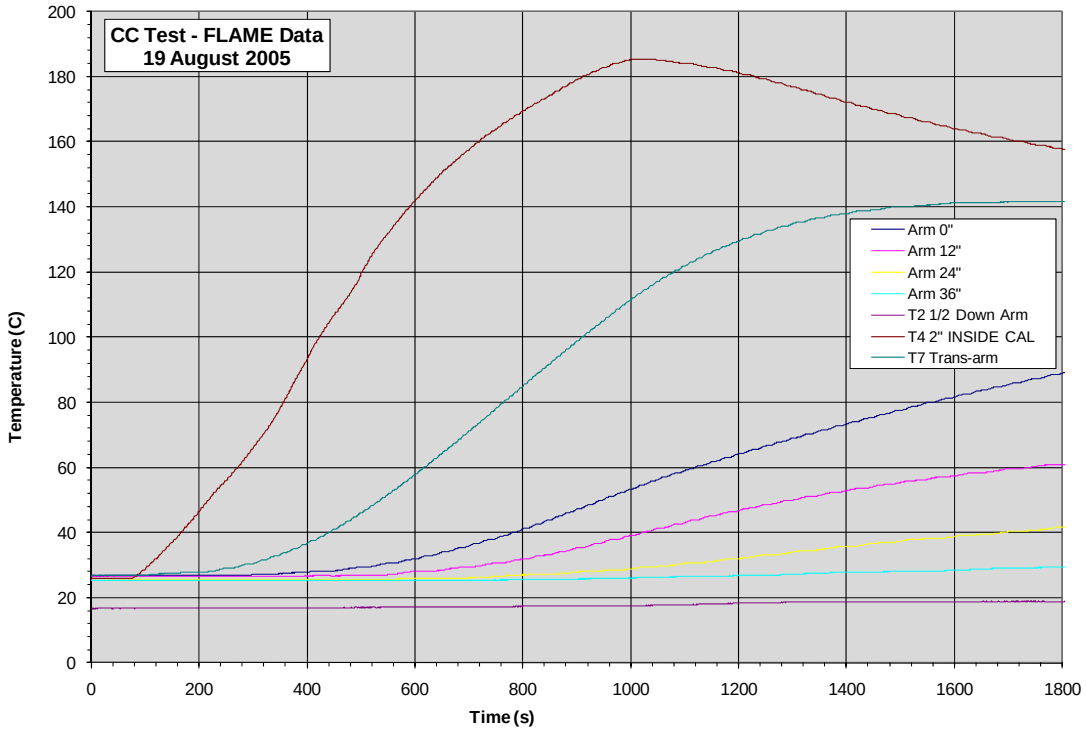

Figure 89 Monitor temperatures for the CC support arm.

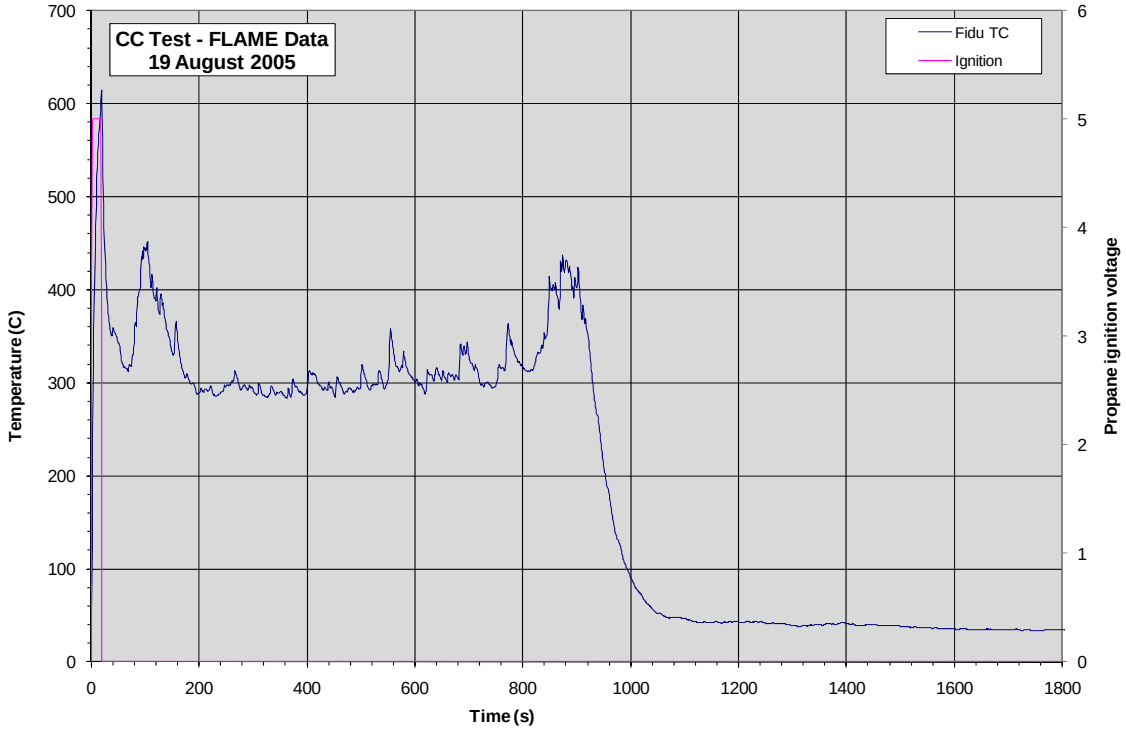

Figure 90 Fiducial signal for igniter.

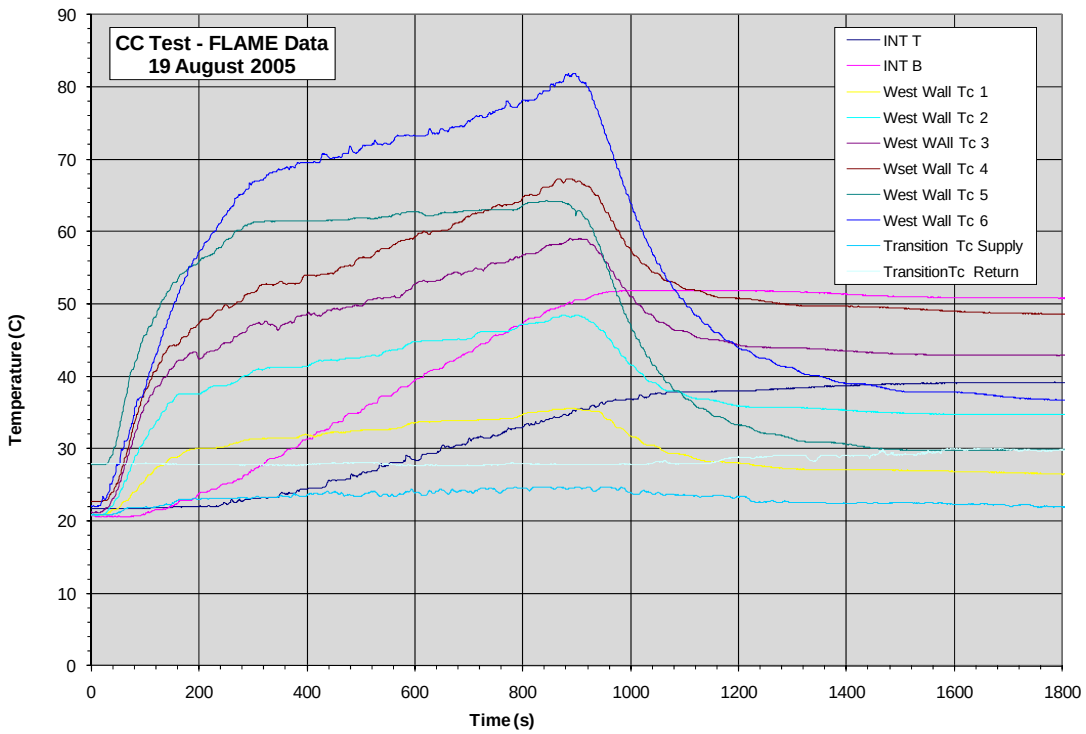

Figure 91 FLAME wall and coolant temperatures.

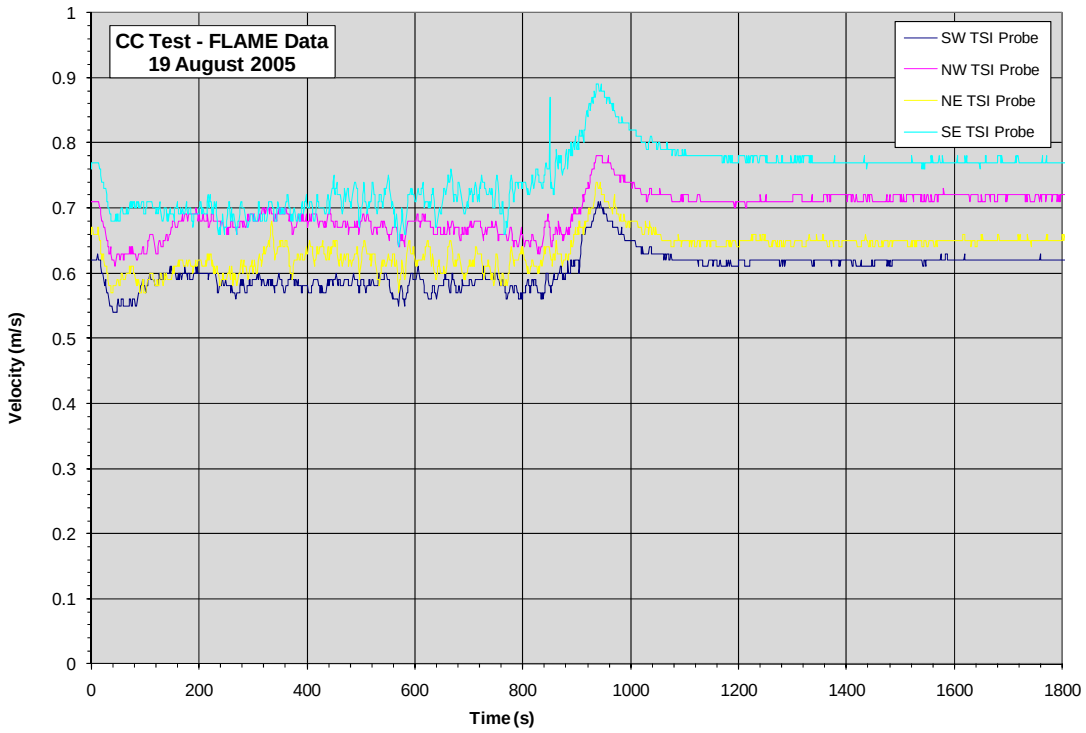

Figure 92 Air ring velocity from the TSI anemometers.

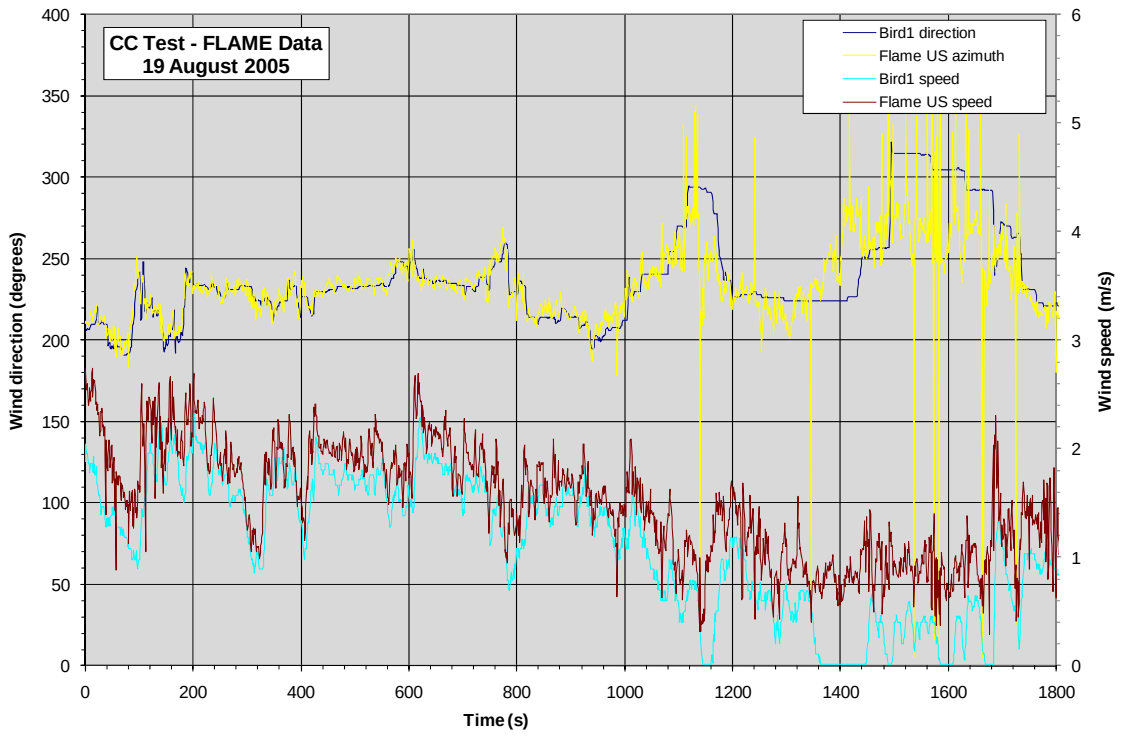

Figure 93 Wind Speed and Direction near FLAME chimney.

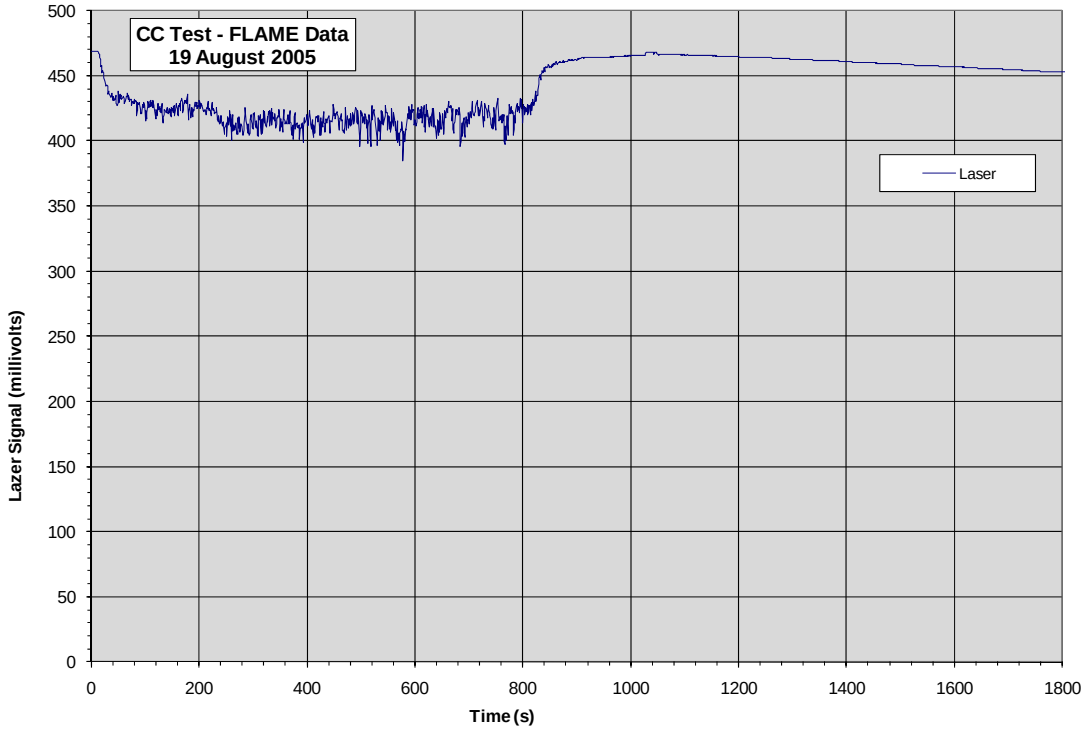

Figure 94 Laser signal for soot concentration analysis.

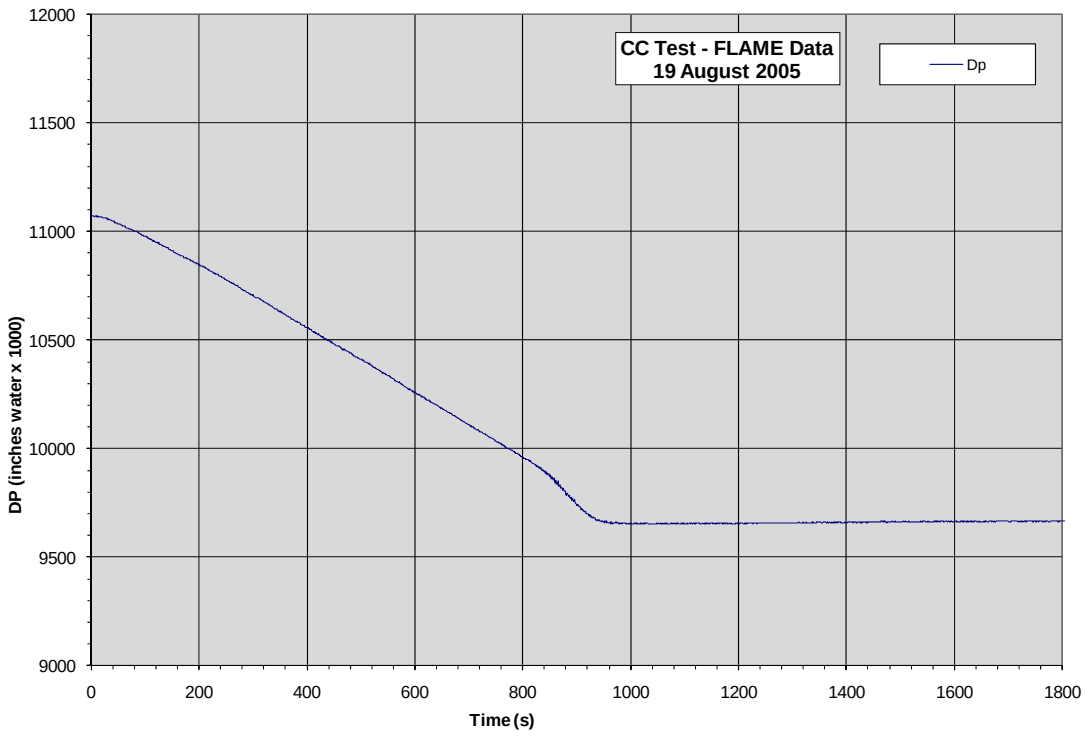

Figure 95 Fuel pan differential pressure measurement.

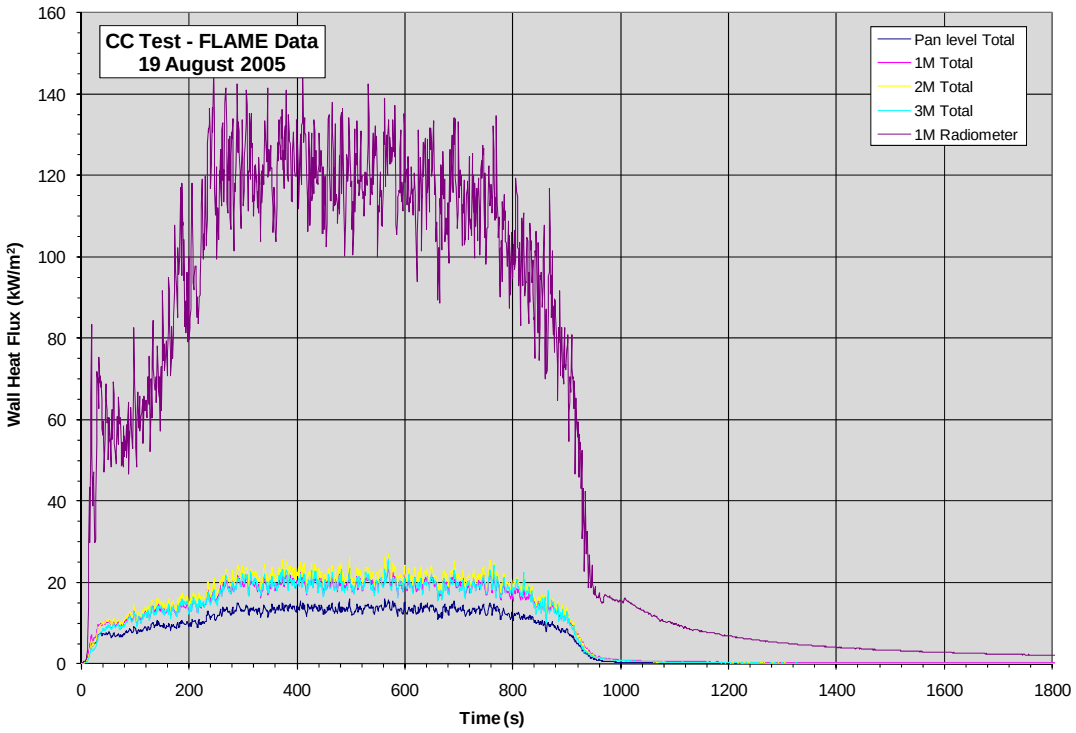

Figure 96 Heat flux measurements from the wall-mounted gauges.

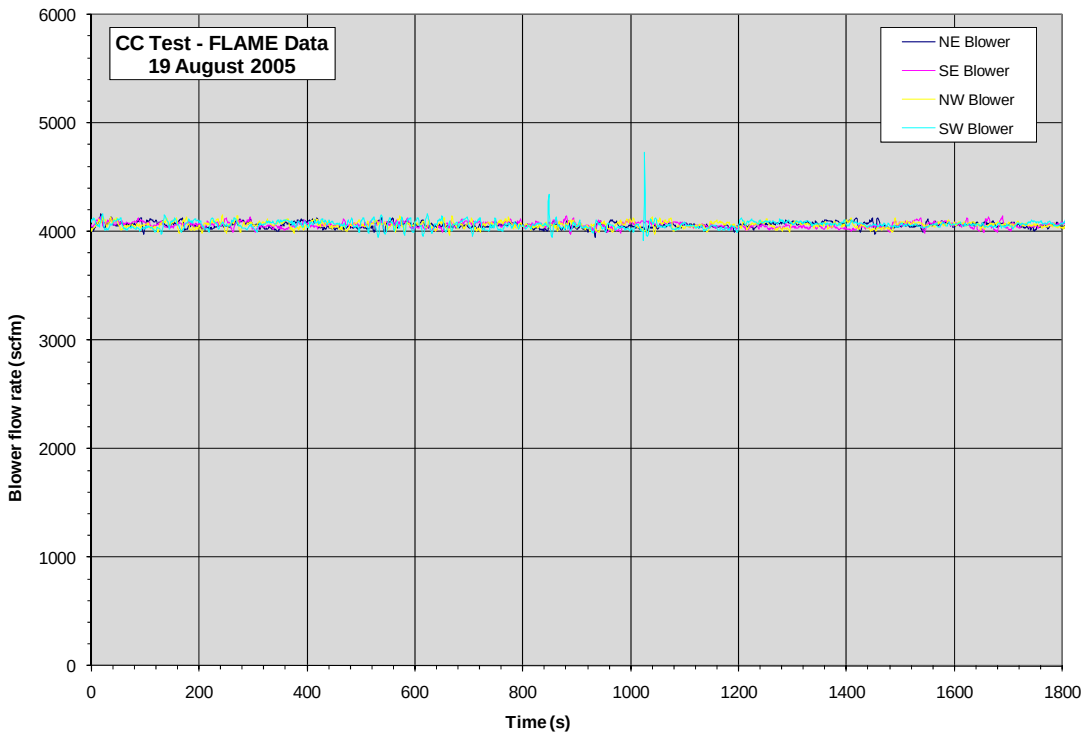

Figure 97 Flow rate from the four blowers supplying the air ring.

4.7 Presentation of Complex Calorimeter Data from Test 15 – Nose Up

As previously mentioned, a dedicated DAS monitored and recorded those thermocouples that were only on the complex calorimeter. Figures 98-109 present the data from the Excel spreadsheet (CC 15 081905.xls) for the CC 15 test performed on August 19, 2005.

Each figure presents the data with a grouping based on the location of TCs on each separate CC part. Refer to Appendix B for the section and the TC location on that section. The data in the plots are grouped by:

1. Outer cone
2. Outer bucket (also referred to as cylinder)
3. Outer bucket bottom plate
4. Inner cone
5. Inner cone bottom plate
6. Inner bucket outer edge (or surface)
7. Inner bucket inner edge (or surface)
8. Inner bucket bottom plate
9. Inner bucket blivet plate
10. Blivet side

11. Blivet top (inner cone side)
12. Blivet bottom (bucket blivet plate side)
13. Fiducial signal and igniter temperature (same instrumentation as recorded by the facility DAS).

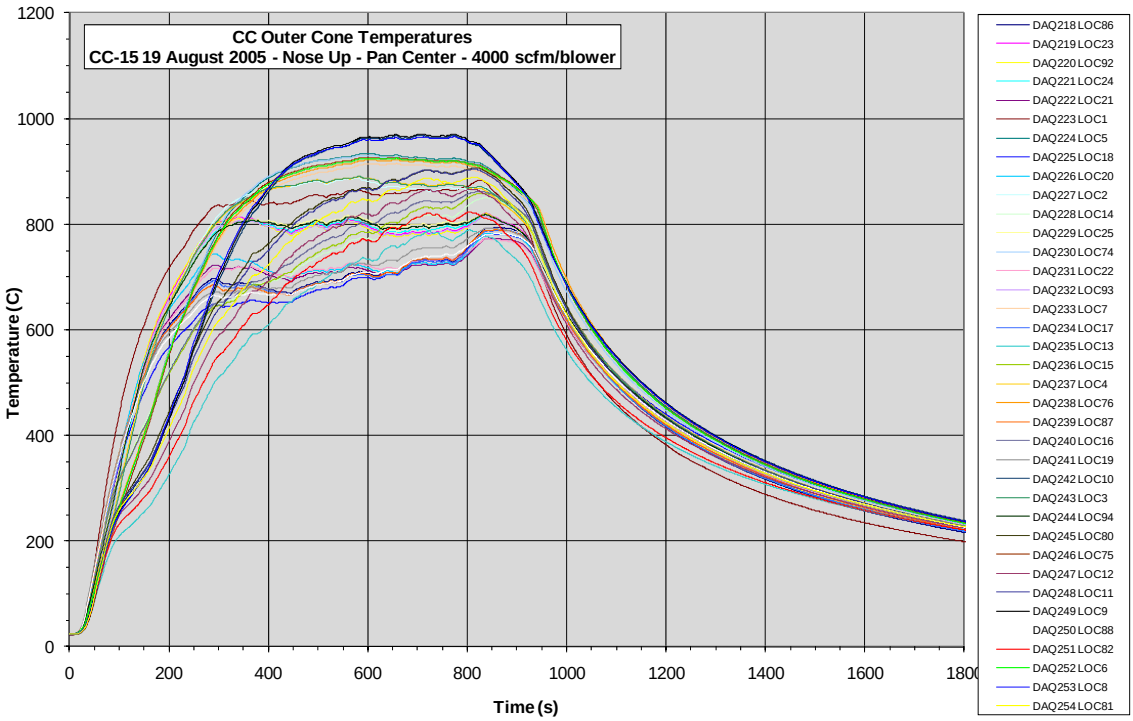

Figure 98 CC-15 outer cone temperatures.

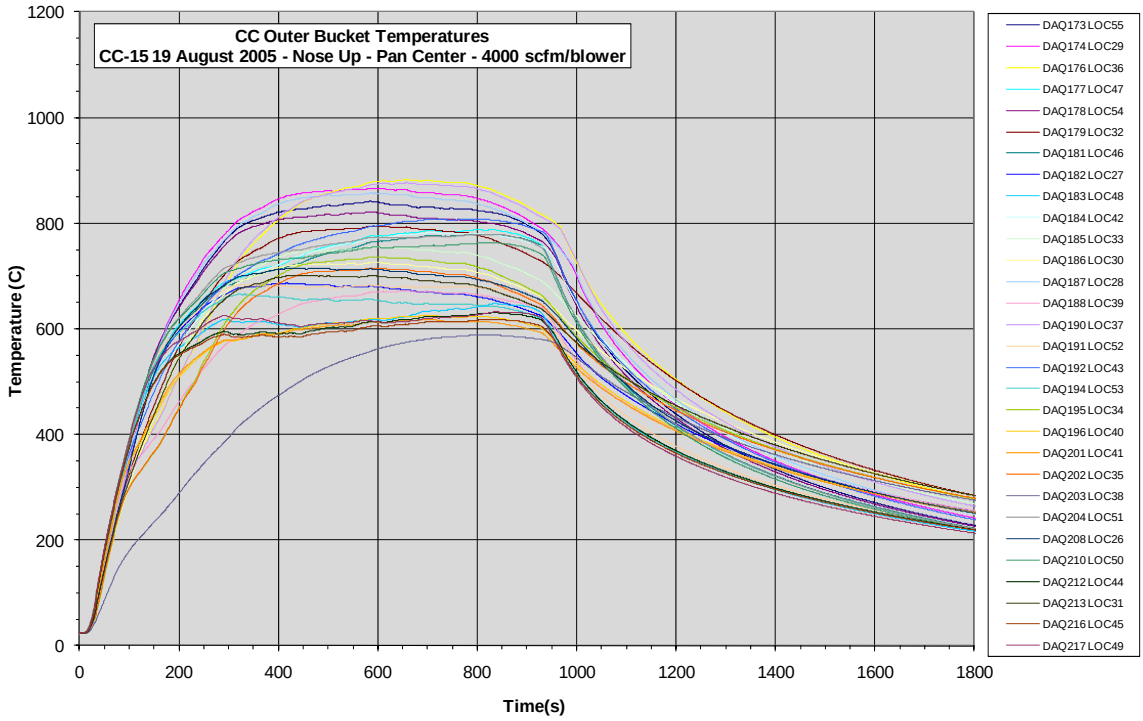

Figure 99 CC-15 outer bucket temperatures.

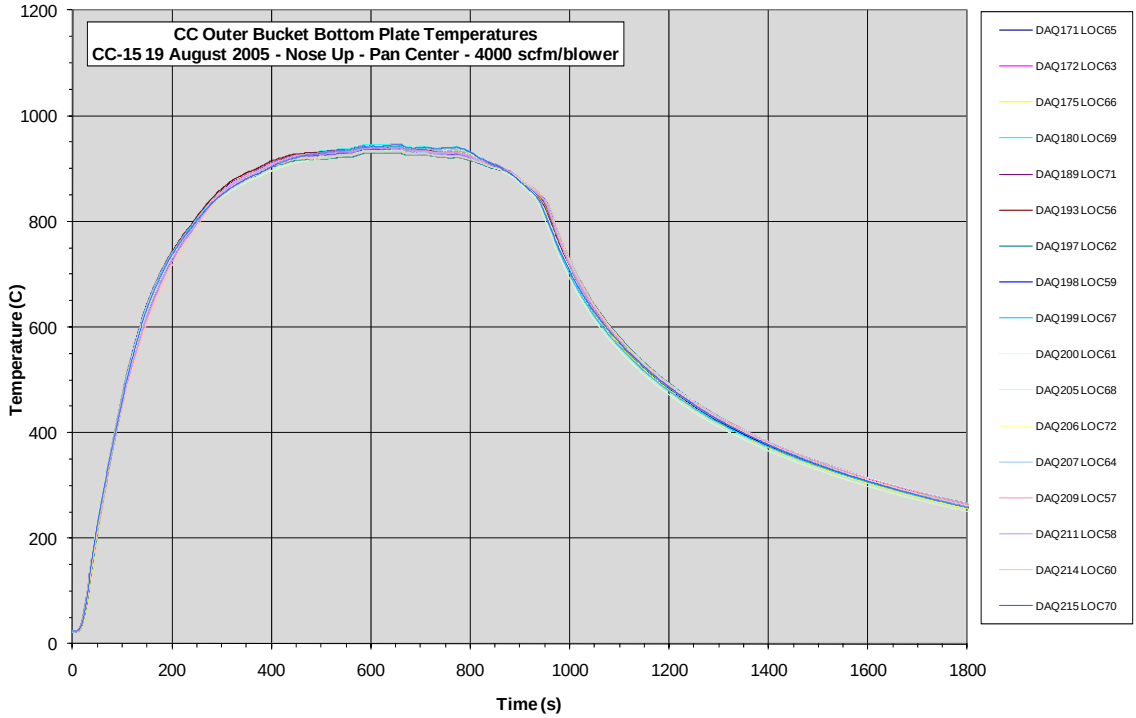

Figure 100 CC-15 outer bucket bottom plate temperatures.

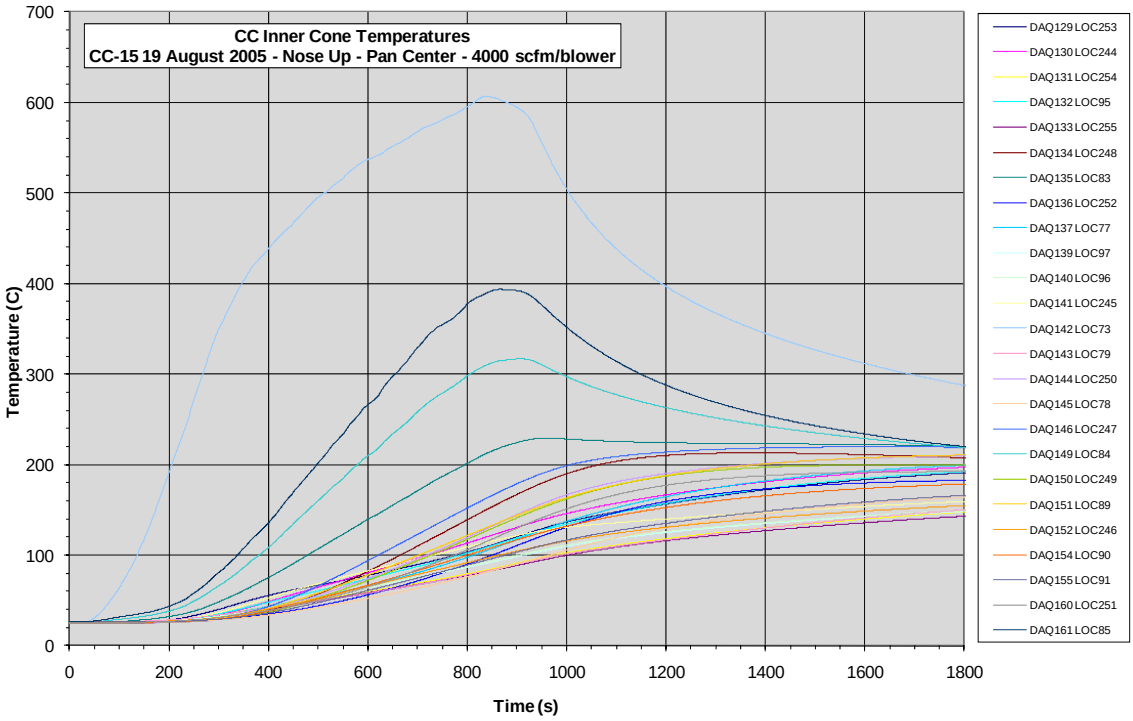

Figure 101 CC-15 inner cone temperatures.

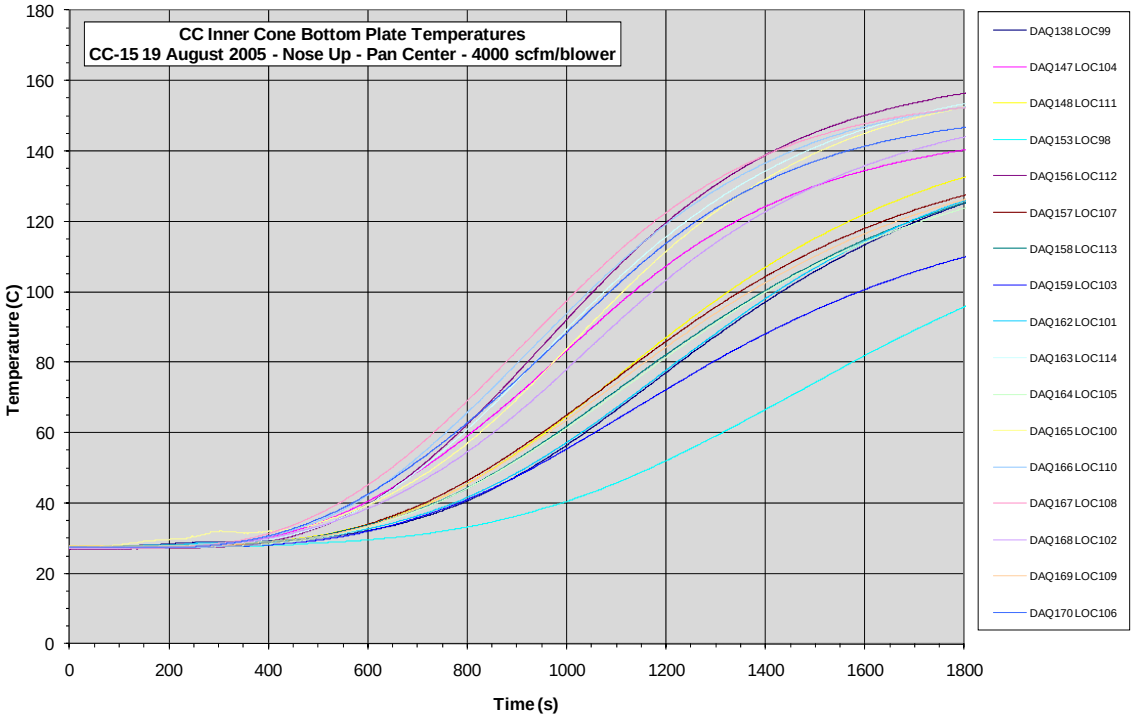

Figure 102 CC-15 inner cone bottom plate temperatures.

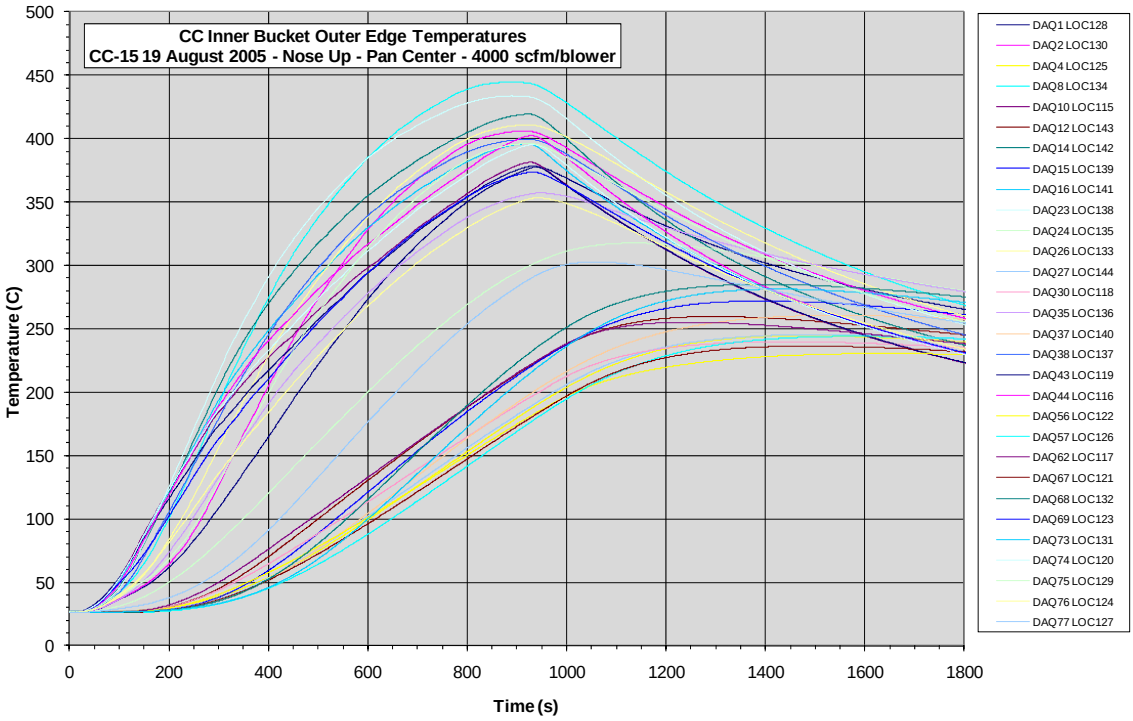

Figure 103 CC-15 inner bucket outer edge temperatures.

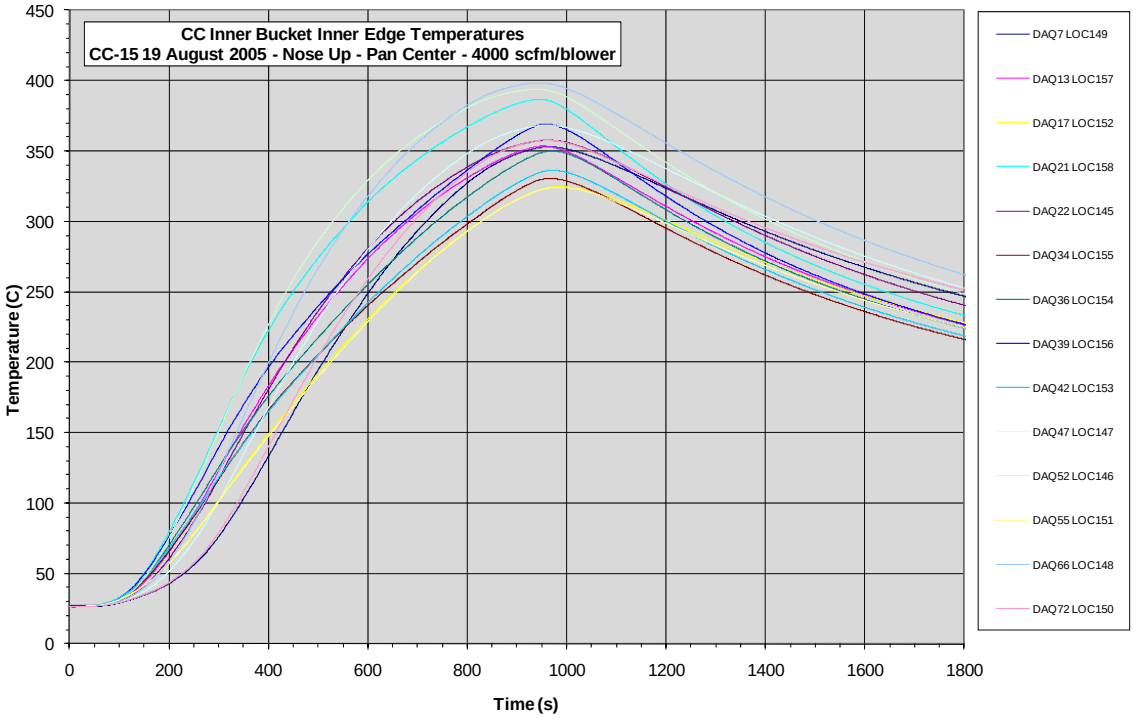

Figure 104 CC-15 inner bucket inner edge temperatures.

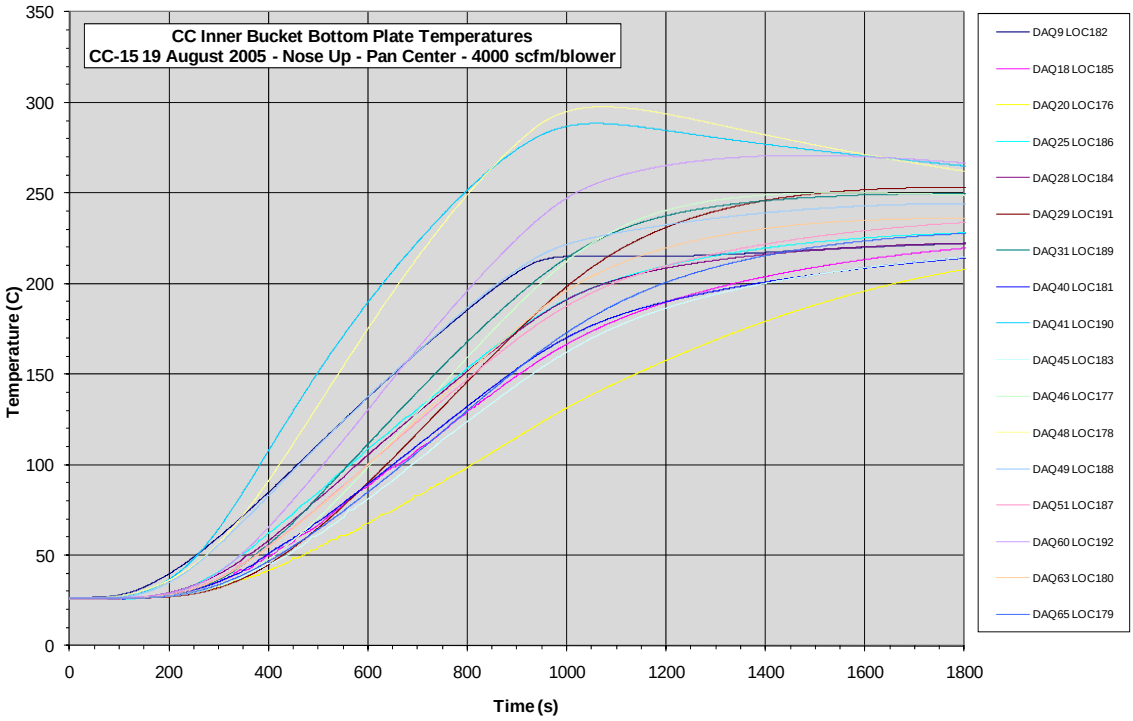

Figure 105 CC-15 inner bucket bottom plate temperatures.

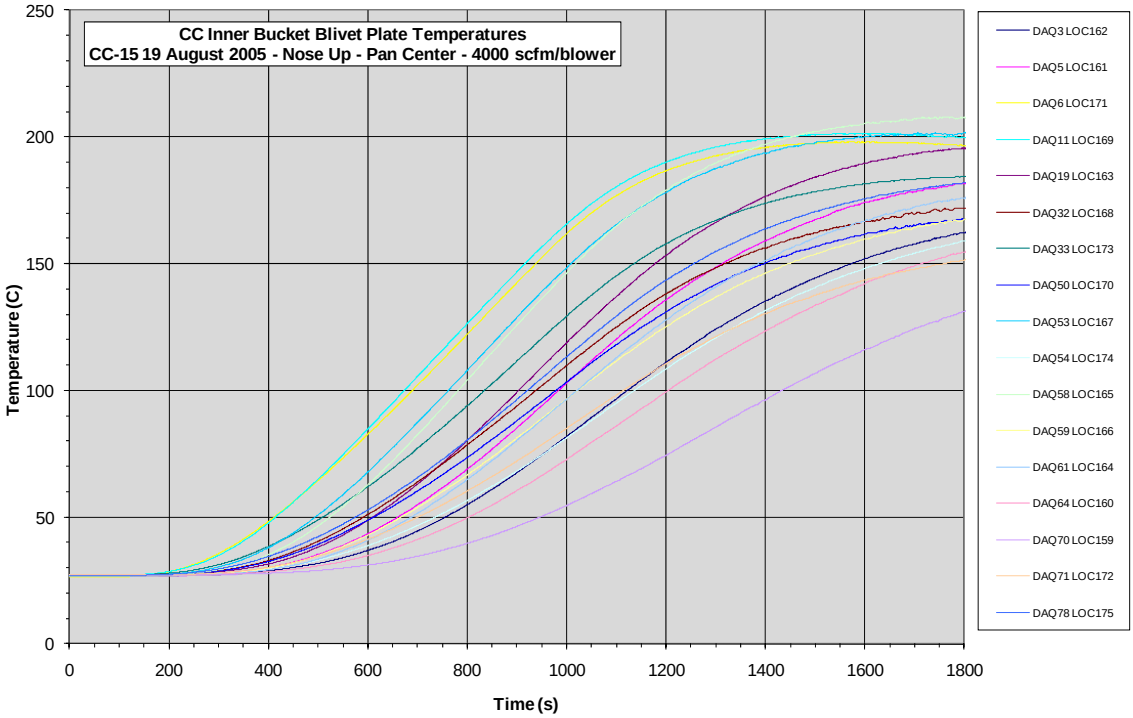

Figure 106 CC-15 inner bucket blivet plate temperatures.

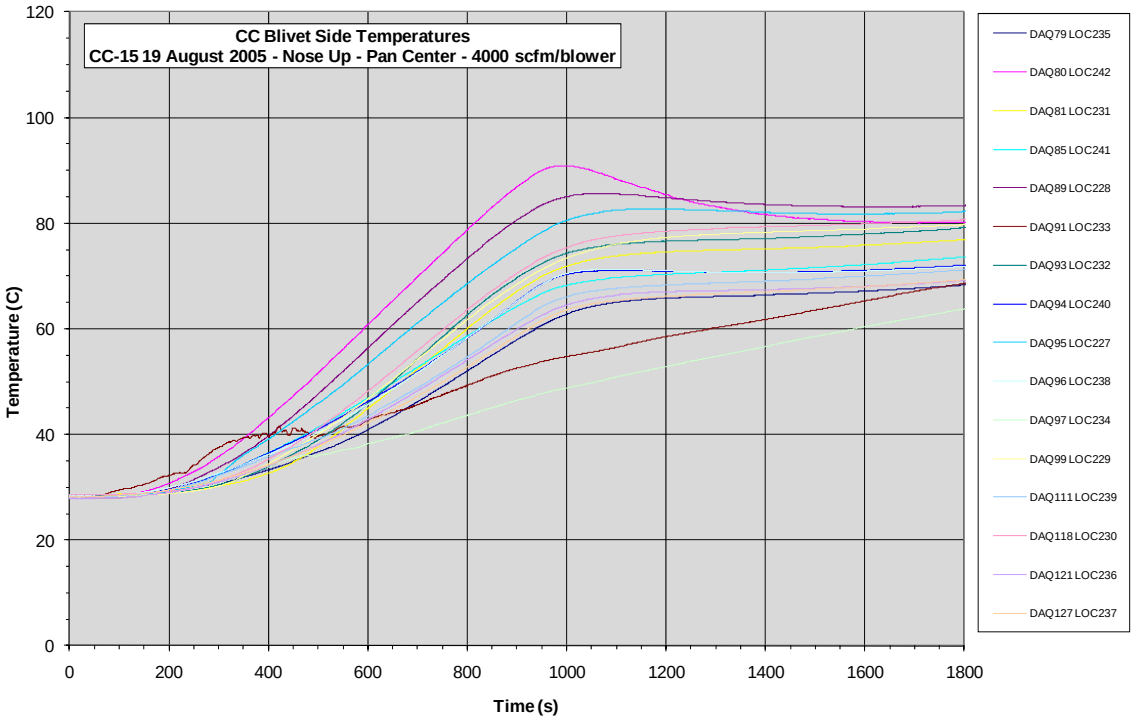

Figure 107 CC-15 blivet side temperatures.

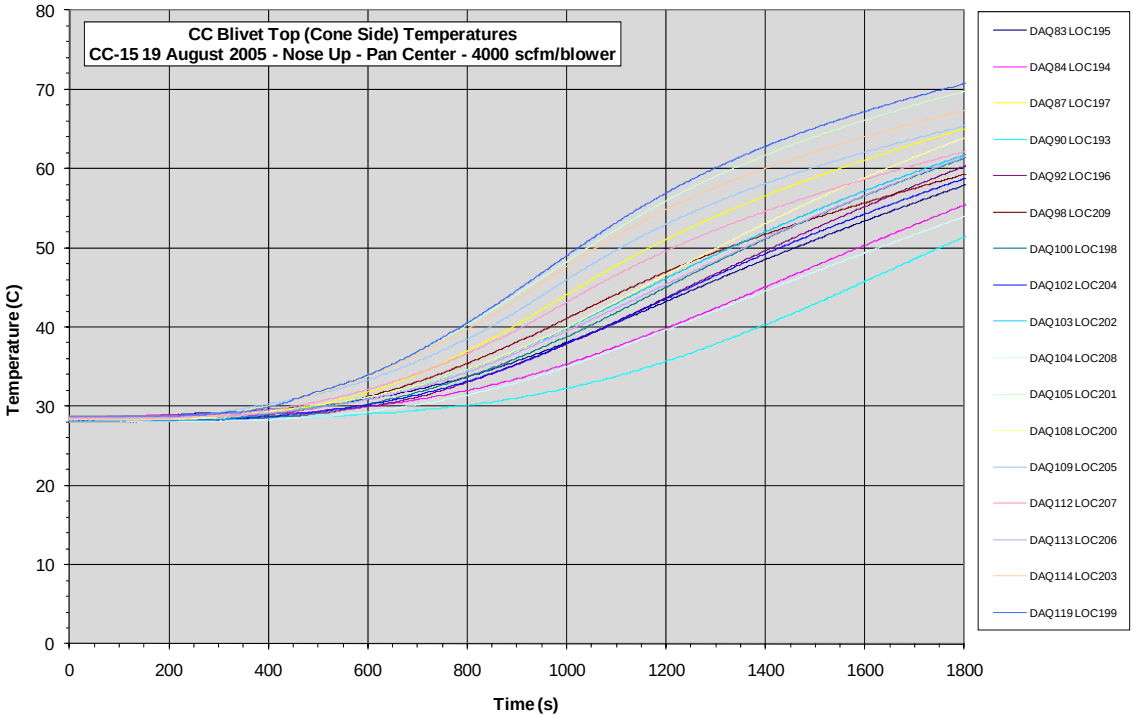

Figure 108 CC-15 blivet top (cone side) temperatures.

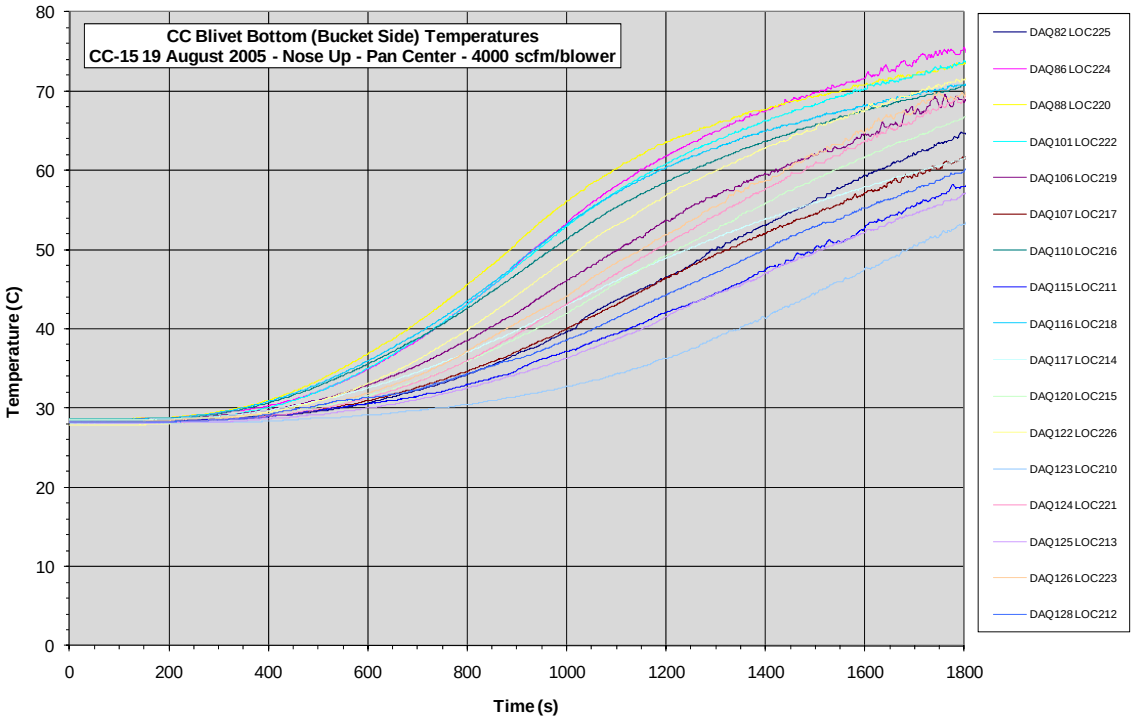

Figure 109 CC-15 blivet bottom (bucket side) temperatures.

As previously mentioned, while the pan is centered on the pedestal, the pedestal and fuel pan are slightly offset from centerline, 7.5 inches to the west and 1 inch to the north.

The fire tends to center itself in the facility and the chimney (i.e. leans slightly to the east). Figure 98 shows that the thermocouple locations 8, 9, and 10 (on the southeast side) yielded the highest temperature response.

A few thermocouples yielded unusual responses. Thermocouple location 38 on the outer bucket (Figure 99) yielded a low temperature response because it was covered by insulation wrapping the support arm, shown in Figure 110 (2 wraps of 1 inch thick high temperature blanket with a layer of stainless steel foil on top of each insulation layer). The support arm (and/or the support arm insulation) likely contributed to low temperature response on the two thermocouples on the blivet (locations 233 and 234) that directly faced the arm.

On the inner cone (Figure 101), high temperatures were seen at thermocouple location 73 (tip) and locations 83, 84, and 85 due to the method for installing the insulation between the inner and outer cone. The insulation was cut and wrapped around the inner cone with a seam running along the inside (arm side) edge (see Figure 11, Final assembly).

Figure 110 Insulation wrapping the support arm.

4.8 Animation of the CC-15 Test Temperature Data – Nose Up

Selected snapshots at 200 s intervals in time from the animation of the time-dependant temperature response are provided below.

As discussed previously, the calorimeter is positioned slightly offset toward the west wall results in higher heating to the calorimeter side that is facing the east wall. For reference, refer to the outer shell contour at lower left in Figure 111 (with the support arm toward the viewer). The side facing the east wall is on the right side. In the figures that follow, it is readily apparent that the east side heats faster. Note that the inner shell also responds faster in the region that covers the blivet due to the removal of the insulation between the inner and outer shells in that area. Note the delayed response in the blivet, and that the blivet continues to heat after the fire is out (due to the heat from the outer and inner shell, even though they are cooling down, they are still at a much higher temperature). Lastly, the hot spots on the inner cone are readily apparent on the tip and where the seam of the insulation occurs.

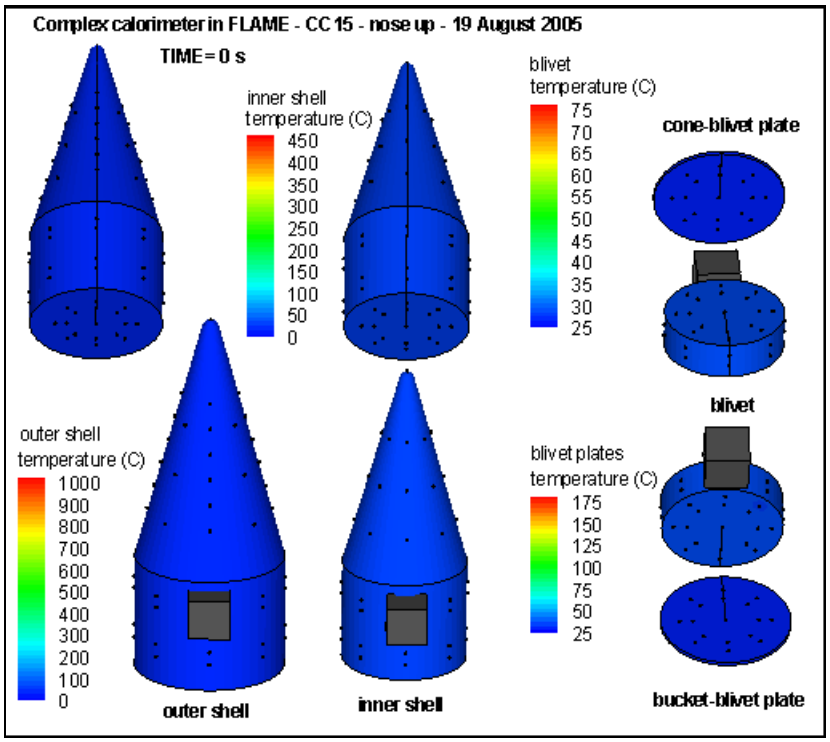

Figure 111 CC-15 surface temperature contours at 0 s.

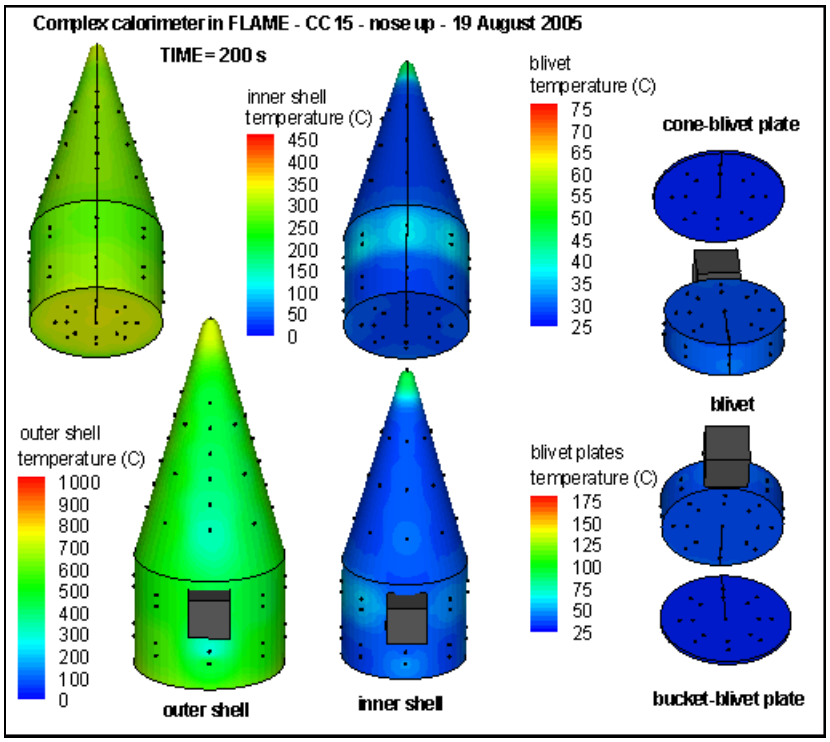

Figure 112 CC-15 surface temperature contours at 200 s.

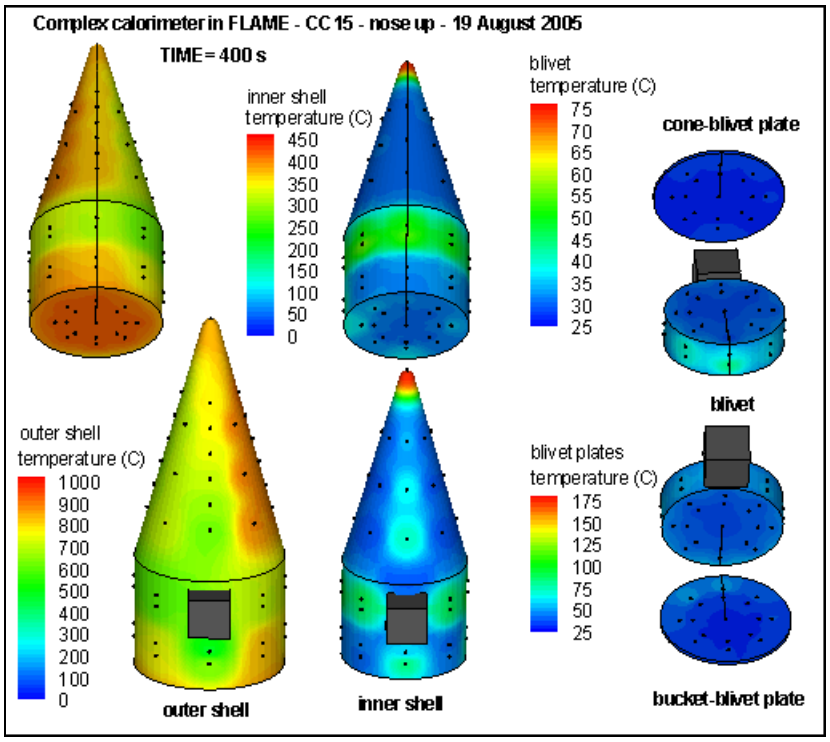

Figure 113 CC-15 surface temperature contours at 400 s.

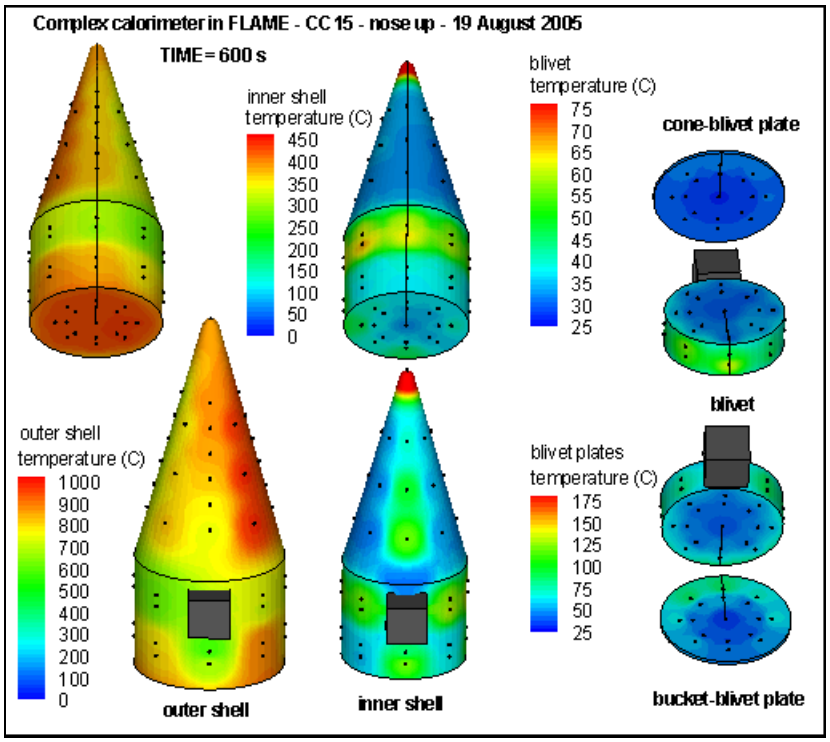

Figure 114 CC-15 surface temperature contours at 600 s.

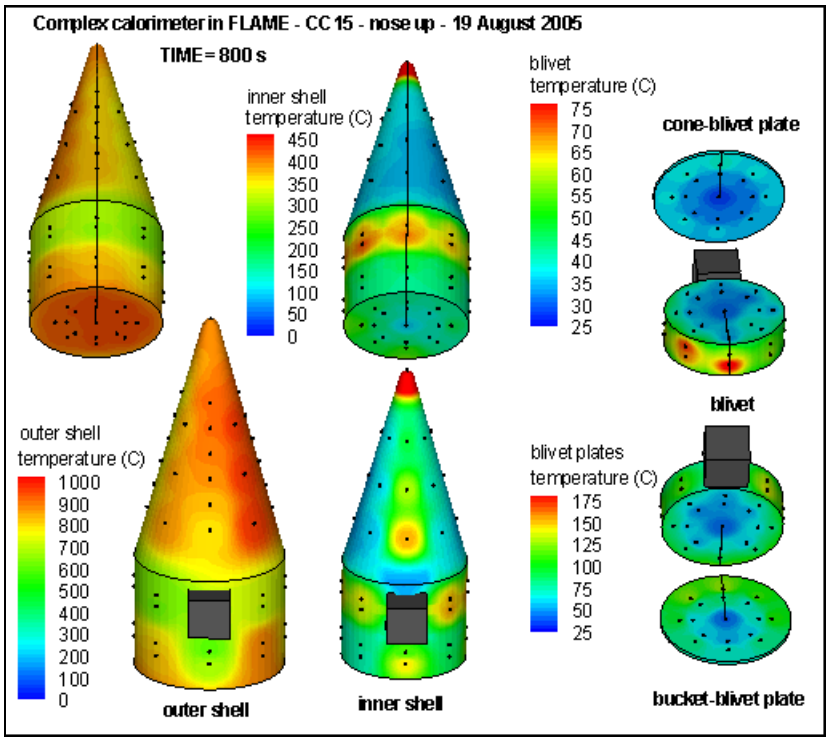

Figure 115 CC-15 surface temperature contours at 800 s.

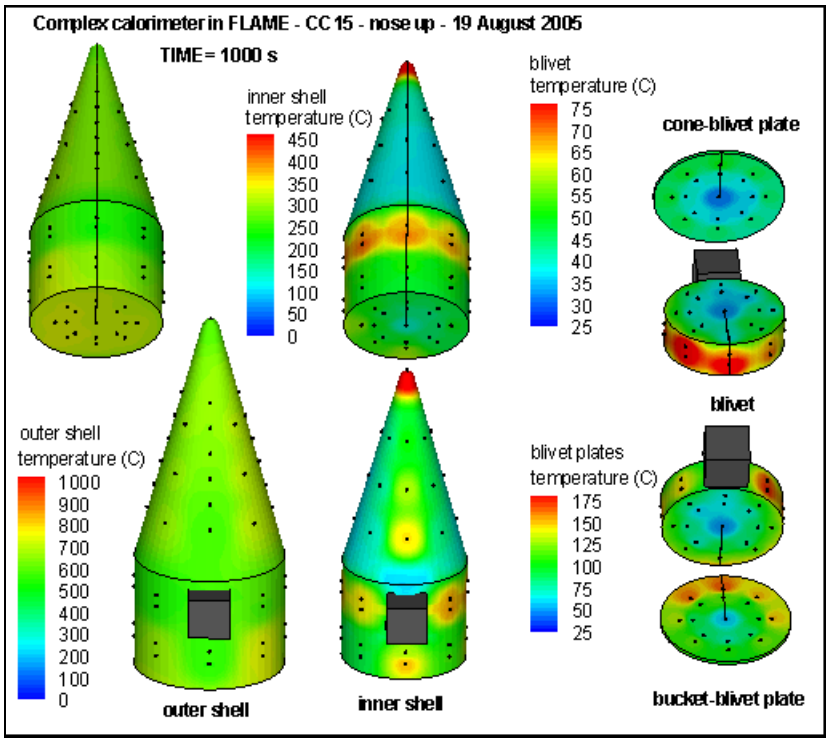

Figure 116 CC-15 surface temperature contours at 1000 s.

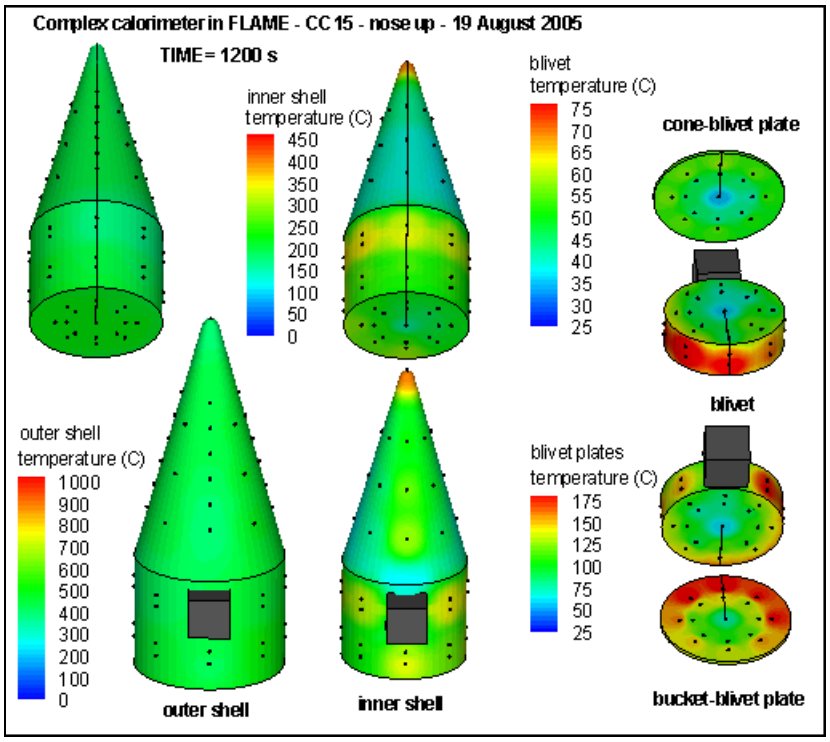

Figure 117 CC-15 surface temperature contours at 1200 s.

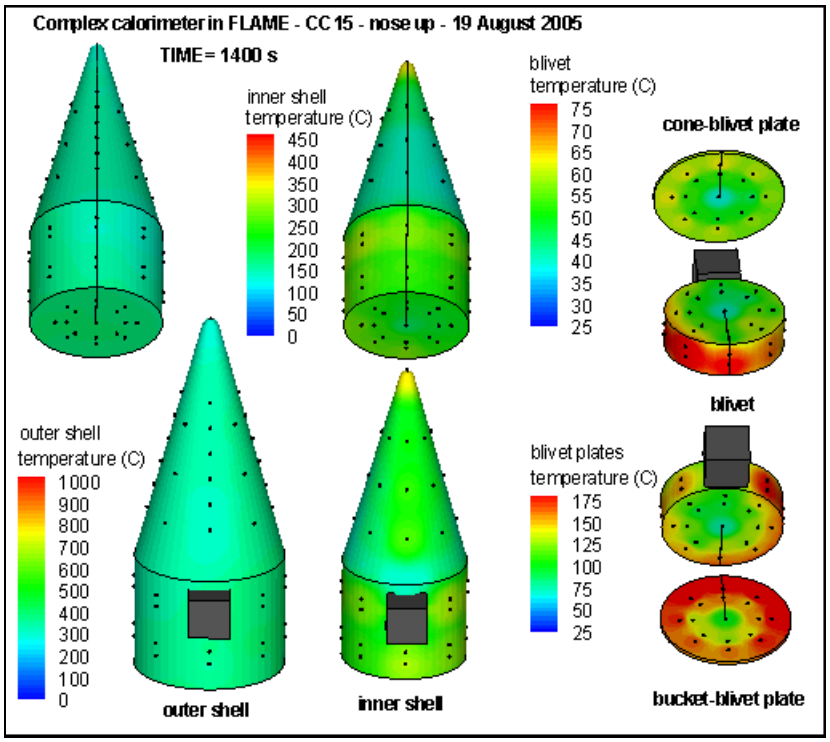

Figure 118 CC-15 surface temperature contours at 1400 s.

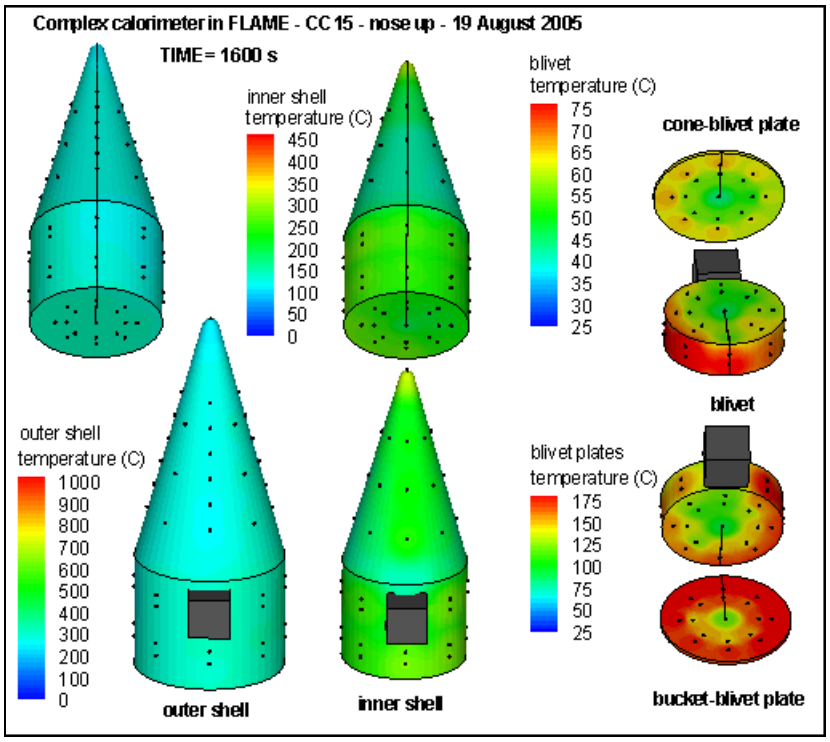

Figure 119 CC-15 surface temperature contours at 1600 s.

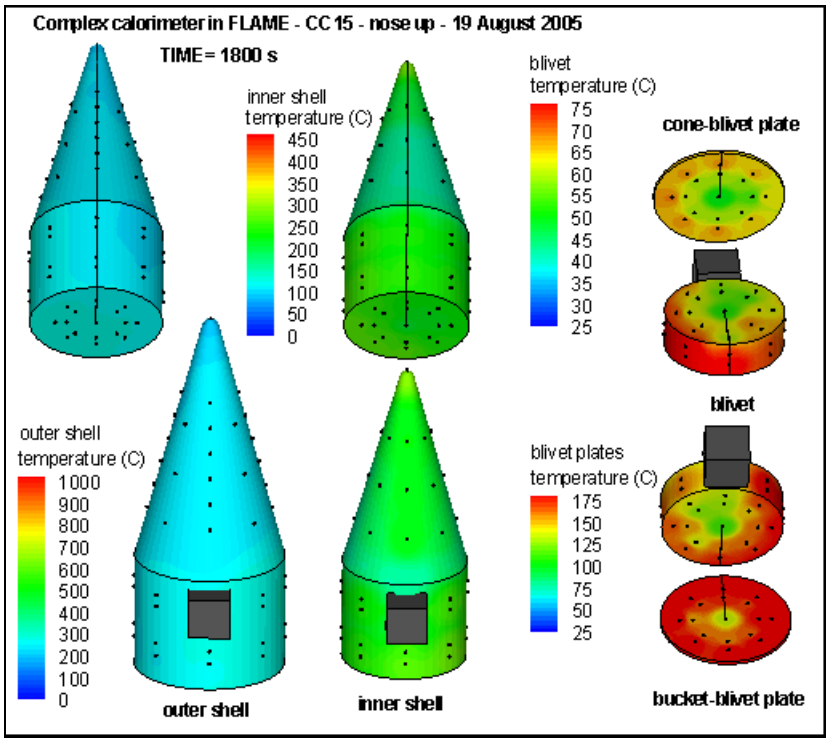

Figure 120 CC-15 surface temperature contours at 1800 s.

4.9 Animation of the CC-15 Test Surface Heat Flux Data – Nose Up

The Sandia HFG Analyzer [Blanchat, Humphries, and Gill, 2000] and the temperature-dependent material property data (provided in the following section) was used to reduce the calorimeter surface temperature data to an incident heat flux at on the calorimeter surface. Selected snapshots at 50 s intervals in time from the animation of the time-dependant surface heat flux response are provided below.

As discussed previously, the calorimeter is positioned slightly offset toward the west wall that results in higher heating to the calorimeter side that is facing the east wall.

The heat flux data from the locations on the bottom cylinder covering the blivet are unrealistic and should be discounted, as the insulation was removed (Figure 121) to maximize the heat input and thermal response of the blivet (the analyzer assumes all surfaces are in contact with insulation).

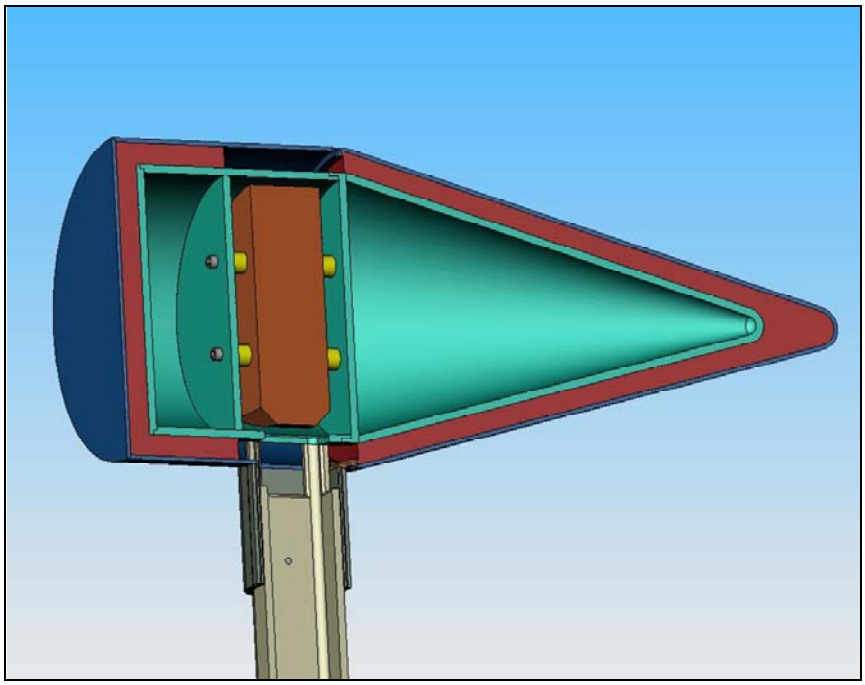

Figure 121 Calorimeter cutaway showing blivet supports and no mid insulation.

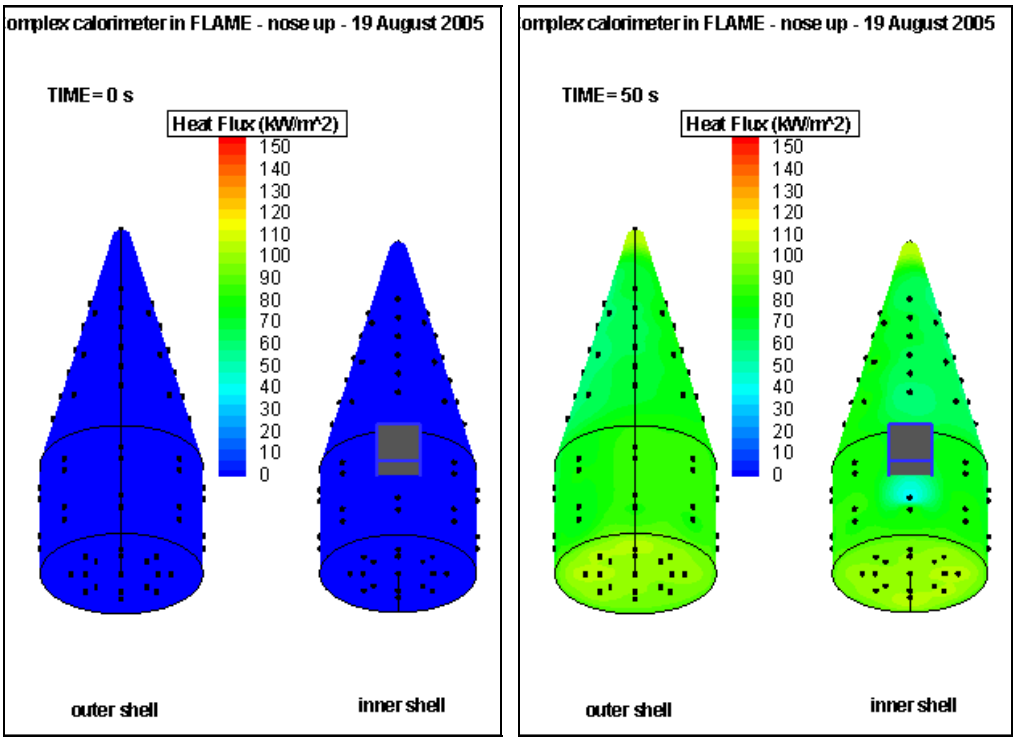

Figure 122 CC-15 surface incident heat flux contours at 0 s and 50 s.

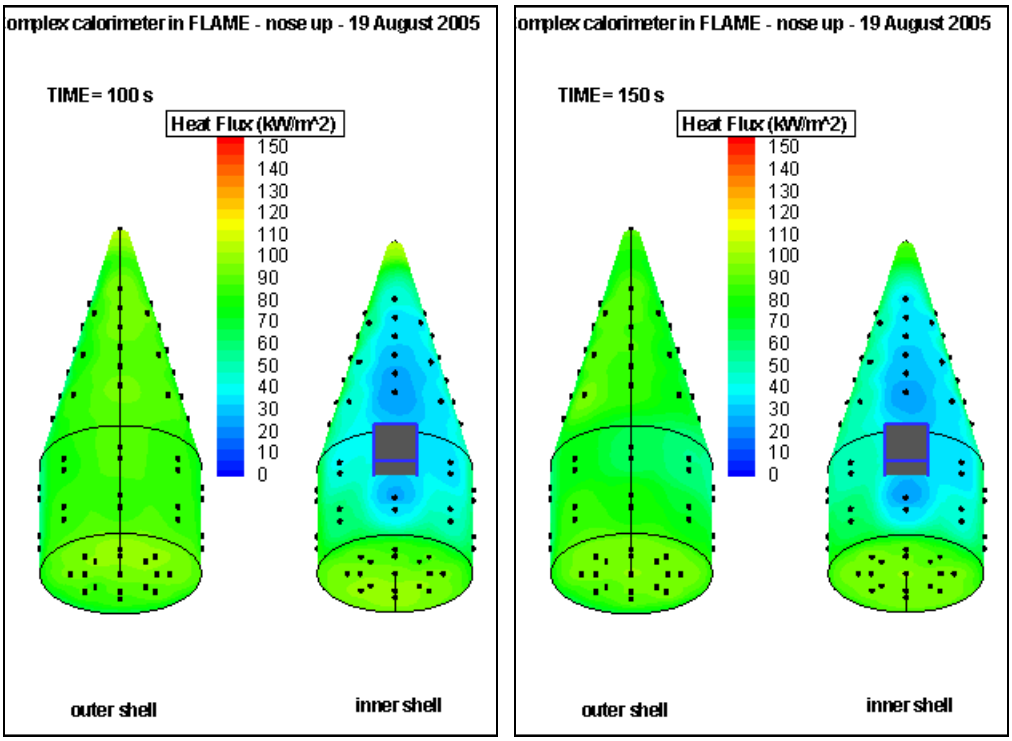

Figure 123 CC-15 surface incident heat flux contours at 100 s and 150 s.

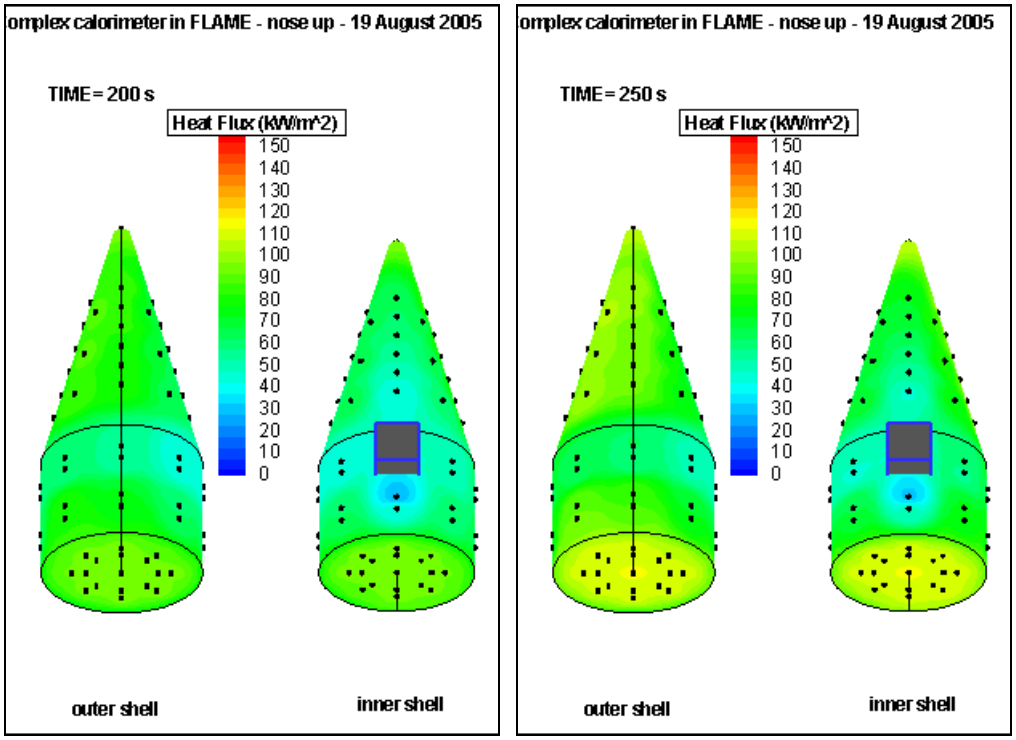

Figure 124 CC-15 surface incident heat flux contours at 200 s and 250 s.

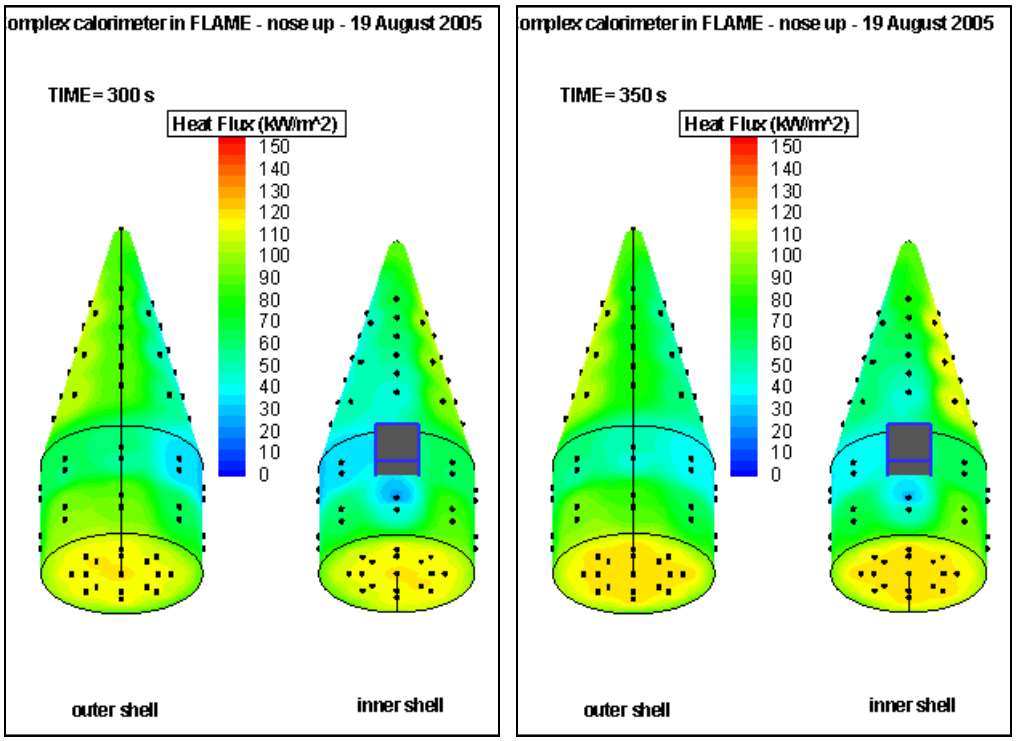

Figure 125 CC-15 surface incident heat flux contours at 300 s and 350 s.

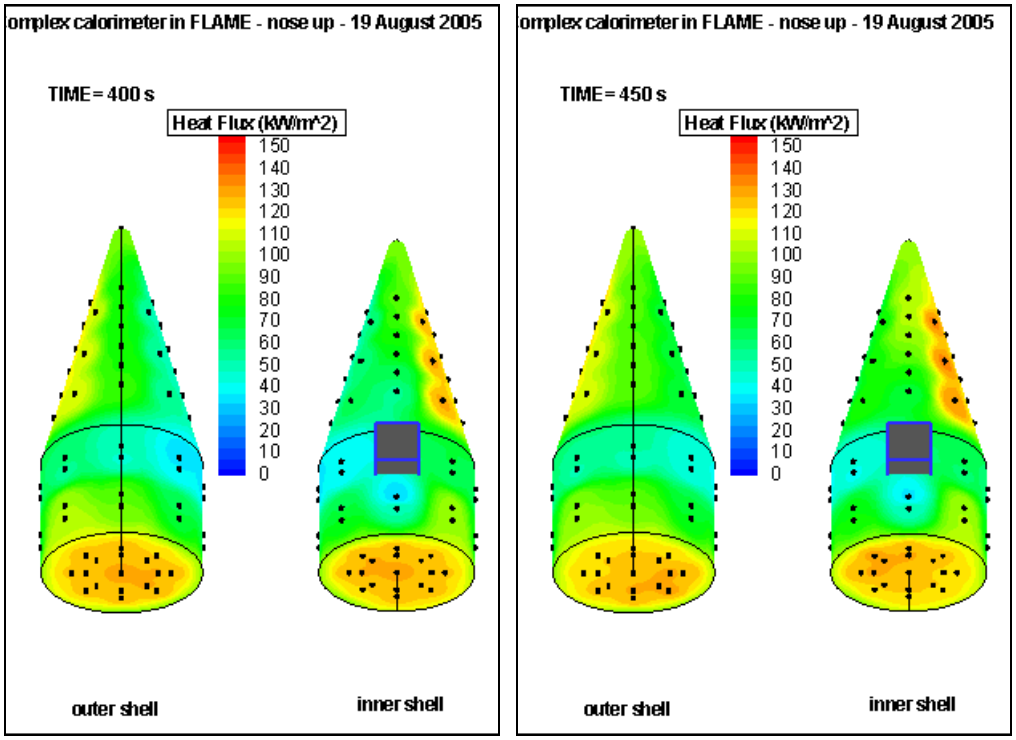

Figure 126 CC-15 surface incident heat flux contours at 400 s and 450 s.

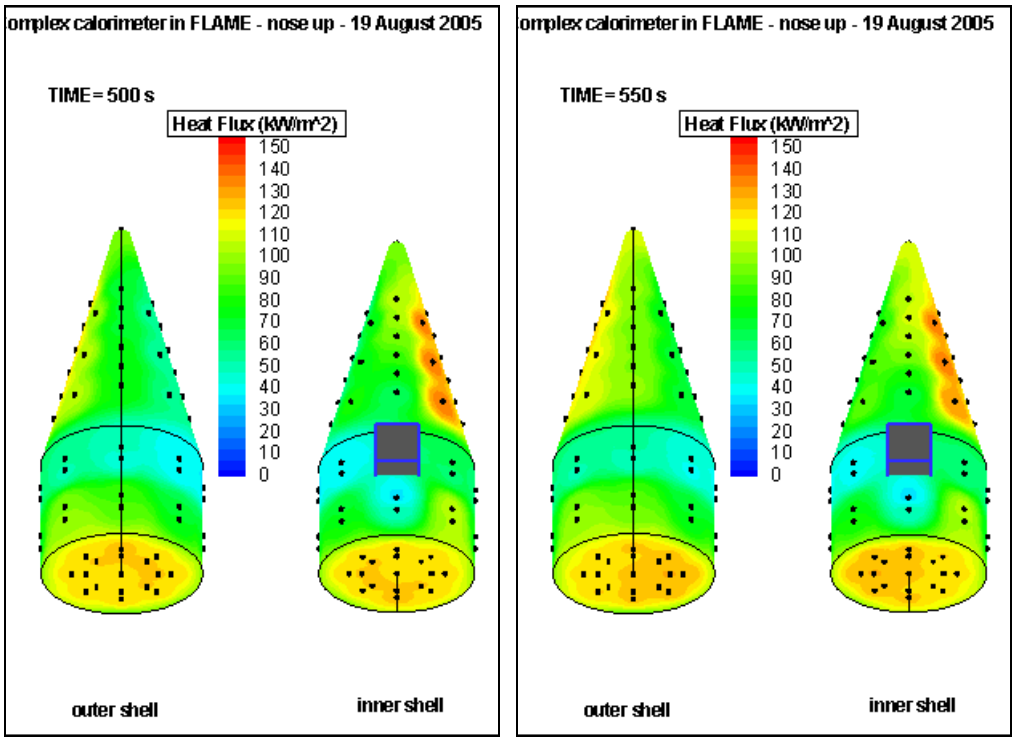

Figure 127 CC-15 surface incident heat flux contours at 500 s and 550 s.

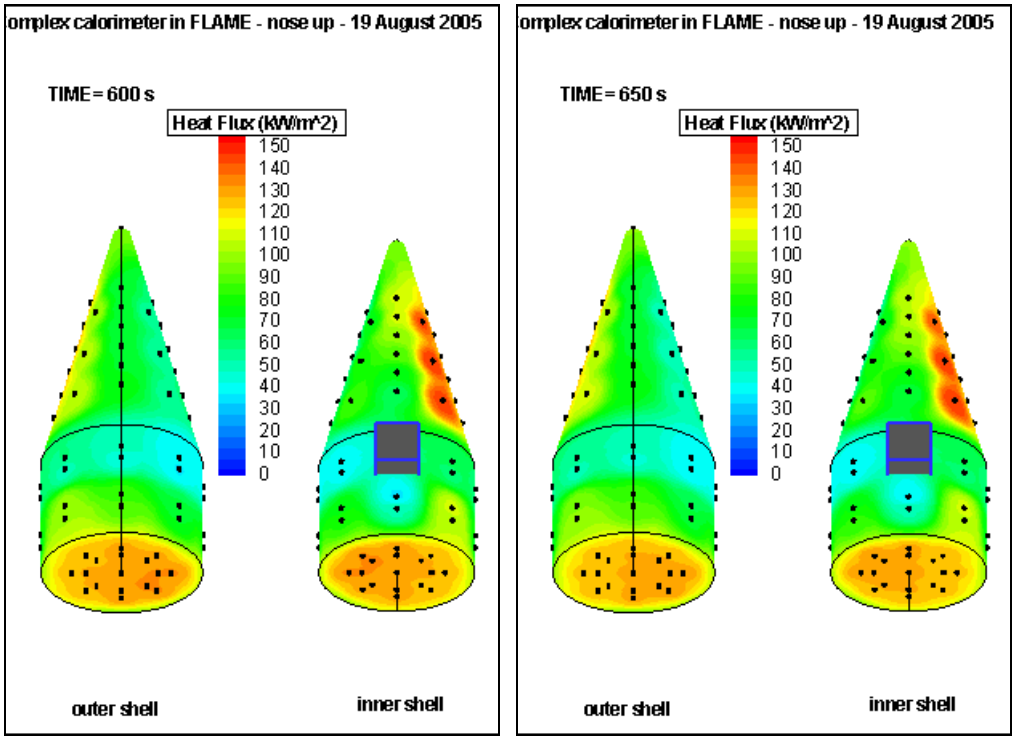

Figure 128 CC-15 surface temperature contours at 600 s and 650 s.

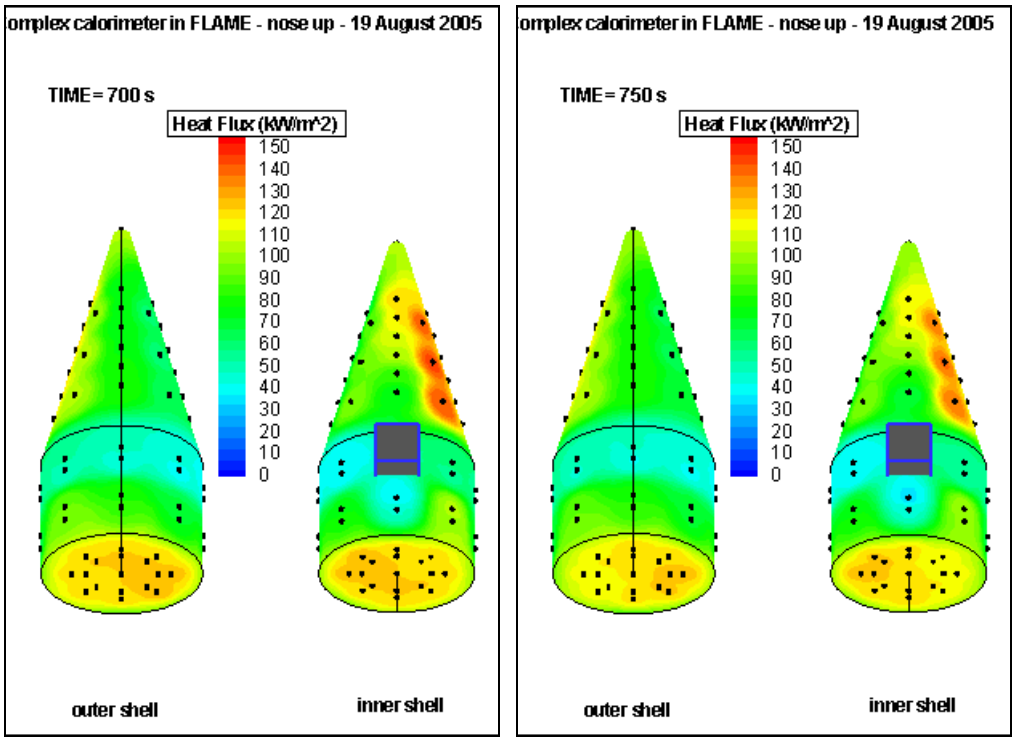

Figure 129 CC-15 surface incident heat flux contours at 700 s and 750 s.

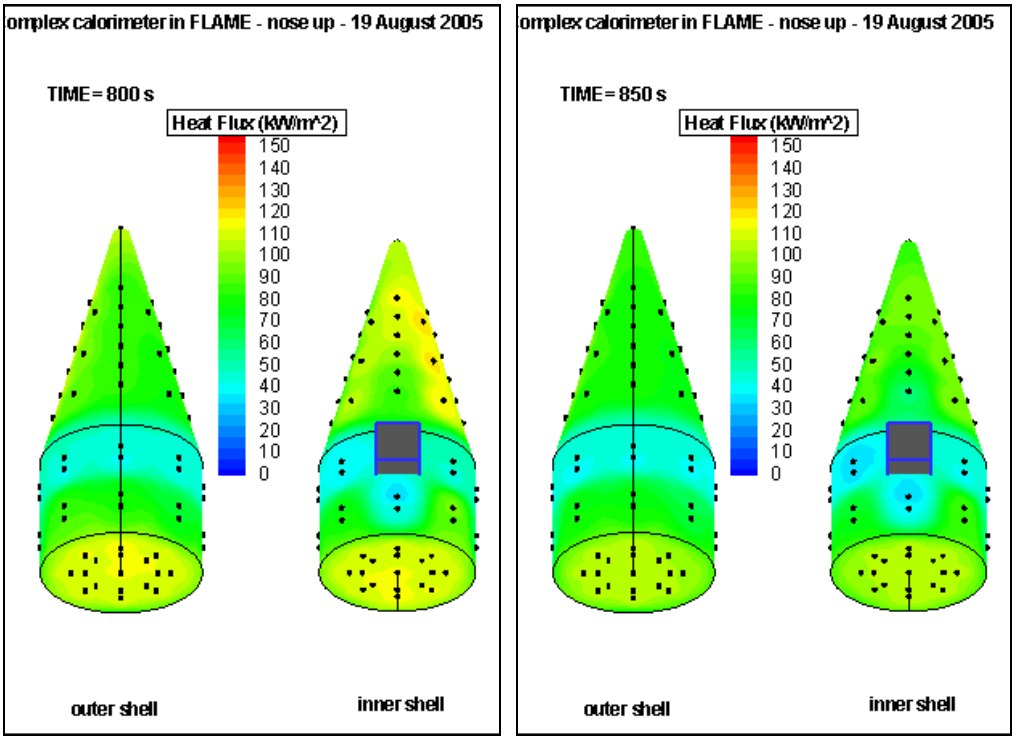

Figure 130 CC-15 surface incident heat flux contours at 800 s and 850 s.

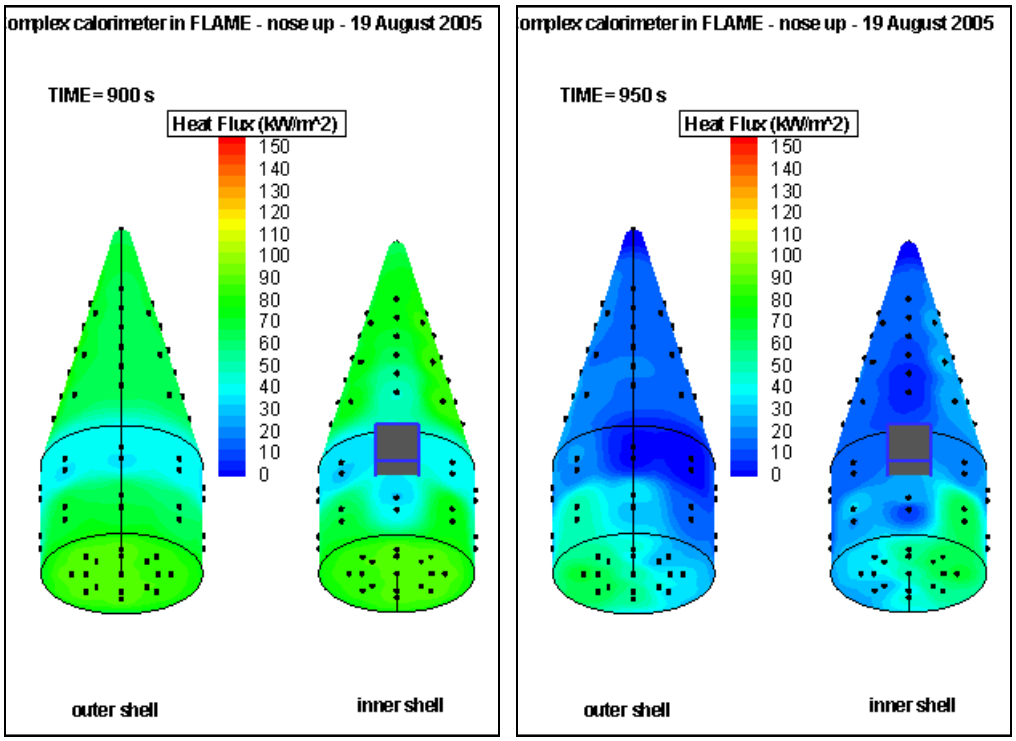

Figure 131 CC-15 surface incident heat flux contours at 900 s and 950 s.

Figure 132 provides four views from the lower north wall camera (the 1-minute "time-exposure" was at 4-5 minutes). Note the flame offset (tilts toward the east wall, due to the slight offset of the pan toward the west wall), so that the CC would be occasionally seen in the video.

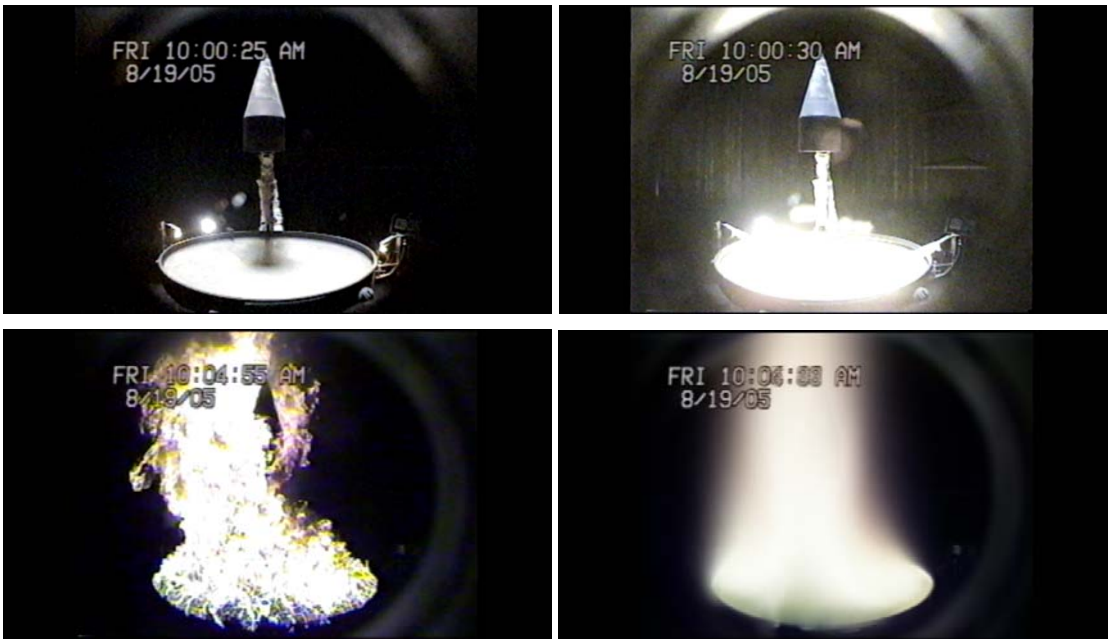

Figure 132 Lower north wall camera: prestart, ignition, 4 minutes, 1 min average.

5. MEASUREMENTS OF BOUNDARY CONDITIONS AND MATERIAL PROPERTIES

5.1 Pan Heat Flux

Heat flux from the fire back to the pan outer edge was measured in the 1st two tests by SNL HFGs. Figures 133 and 134 present the temperature and reduced heat flux data from CC-1; respectively. Results were similar for test CC-2. With the pedestal and pan slightly offset to the west and north side, the fire tended to lean to the east and south, as indicated by the higher heat fluxes on those sides of the pan.

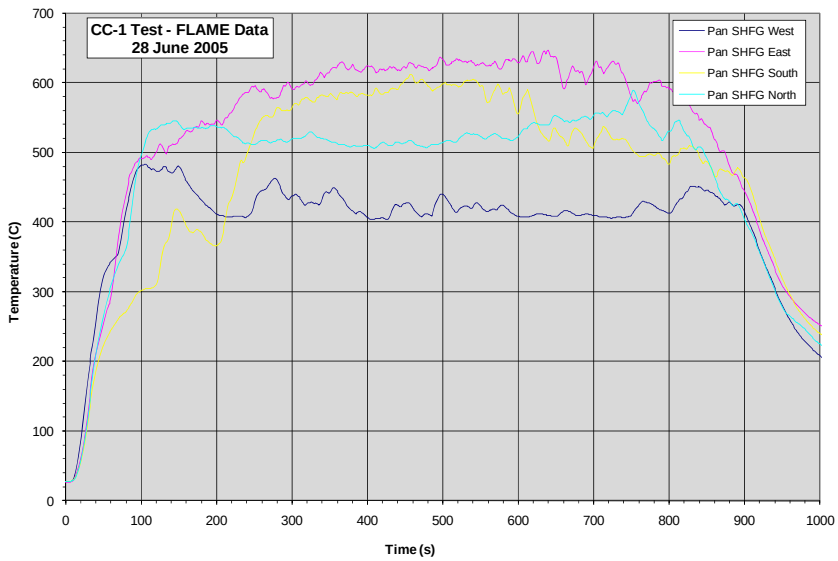

Figure 133 Temperature from pan SNL HFGs Pan in CC-1.

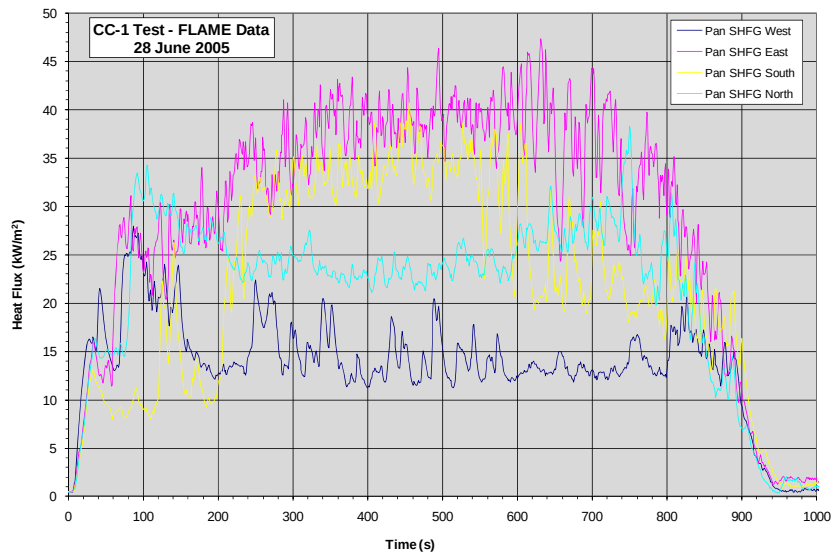

Figure 134 Incident heat flux from pan SNL HFGs Pan in CC-1.

5.2 Fuel Regression

Figure 135 shows the typical raw data as measured by the real-time Rosemount differential pressure gauge recording the liquid head (inches water x 1000) in the fuel pan. Thirty-five gallons typically produced ~1.3 inches of water head. Zeroing the data to the start of the test, and dividing by the measured specific gravity (measured during fueling prior to each test) yielded the fuel regression (mm/min).

Figure 136 shows the typical JP-8 regression profiles from the reduced data. Note the fire takes ~150 s before the regression approaches a steady-state condition, and is completely steady at ~300s. The peak at the end of each test is due to the somewhat violent interaction of the thin layer of fuel with the water layer. The minor "wiggle" in the steady-state portion is not real but caused by the curve fit routine.

The average fuel regression (with 1 std.dev.) at steady-state (300-700 s) for the 22 tests was 2.95 ± 0.11 mm/min. Table 6 present the fuel regression for each test. The measurement uncertainty is 0.6 % (contributors are pressure, time, and fuel SG). The average mass loss rate was 0.039 kg/m^{2}s (assuming an average specific gravity of 0.8). The average vapor velocity was 0.012 m/s (assuming a liquid density of 800 kg/m^3, an ambient pressure (in HG) of 23.98, a fuel boiling temperature of 500K, and a molecular weight (MW) of 167).

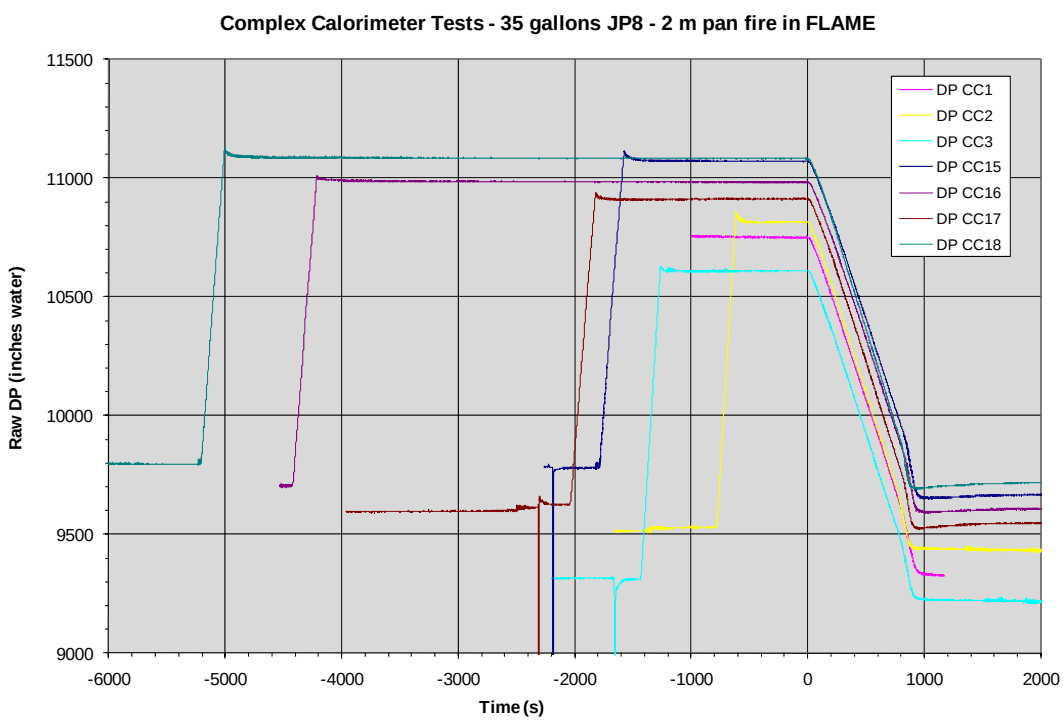

Figure 135 Fuel DP data.

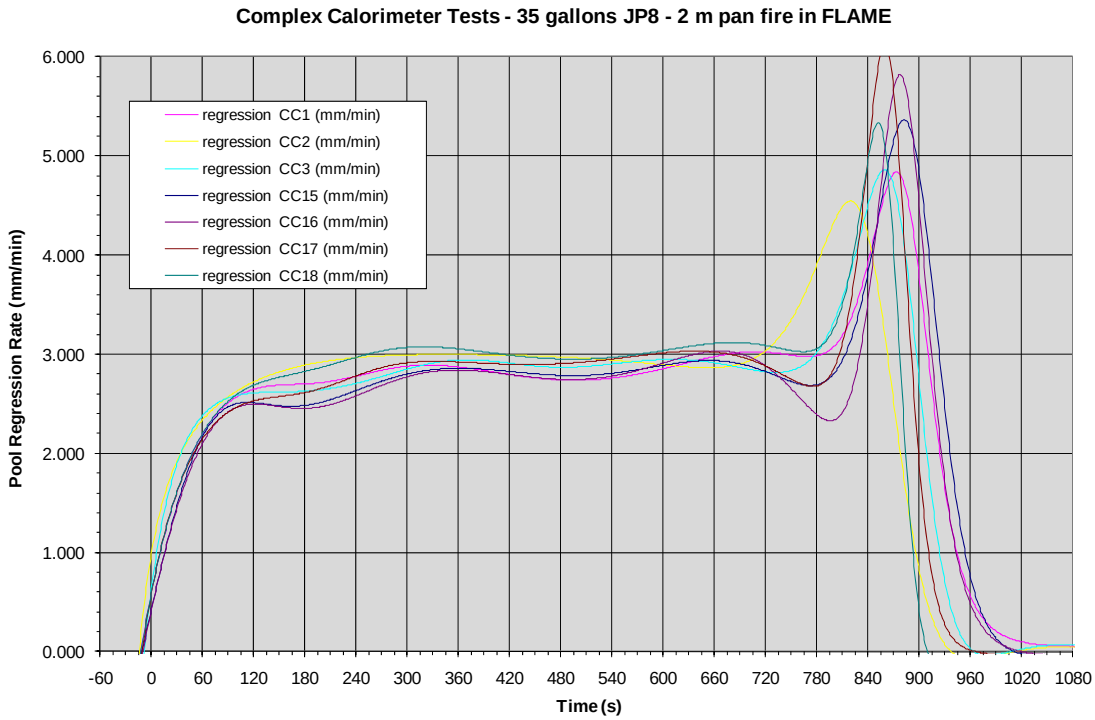

Figure 136 Fuel regression profiles.

5.3 Test-to-Test Variance in Calorimeter Surface Emissivity

As mentioned in Chapter 2, Pyromark® paint was applied to all exterior and accessible interior surfaces per manufacturer paint application and bake out schedules. Emissivity measurements using a calibrated Pyrofiber Model E10 were taken in the field to determine the extent of emissivity *change* over the course of the experiments.

A template (Figure 137) was fabricated that allowed probing the same 37 external surface locations in-situ after each test. The Pyrofiber Model E10 cup sensor fits in the holes, and the sample point is a 6 mm spot in the center of the circle.

After the test, a light layer of soot was found on the complex calorimeter (in many instances, the soot would have flaked off over large portions as the calorimeter cooled). When the calorimeter cooled to ambient temperature, measurements were taken twice; once before wiping it down (the "sooty" data) and after lightly wiping with a soft cloth. The measured spot emissivity (Figure 138) ranged from ~0.82-0.98. Note that the Pyrofiber Model E10 measured the emissivity at *single* wavelength of 0.95 μm and at a small angle, with a stated accuracy of ±0.01. This shows that the emissivity was not changing greatly from test to test. For analysis purposes, a mean emissivity 0.86 ± 0.09 should be used as a boundary condition, based on the *total* directional data for cured Pyromark on 304 stainless steel [Figueroa 2005].

The average surface emissivity over the course of the experiments is shown in Figure 139. The average surface emissivity for the entire series (both sooty and wiped) was 0.92. Note that the average surface emissivity before any of the tests was 0.96.

The FLAME internal wall emissivity may be of interest. The facility has been used for over 10 years, and the mild steel walls are heavily oxidized and sooted. One may assume an emissivity of 0.8 (never measured); however, this should not be a factor in radiation calculations as the walls are water-cooled and temperatures never exceed 100°C.

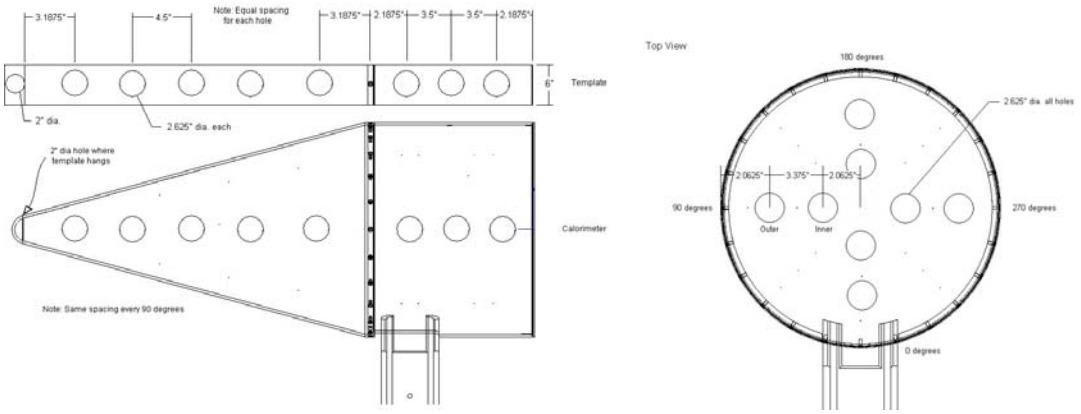

Figure 137 Templates for emissivity measurements.

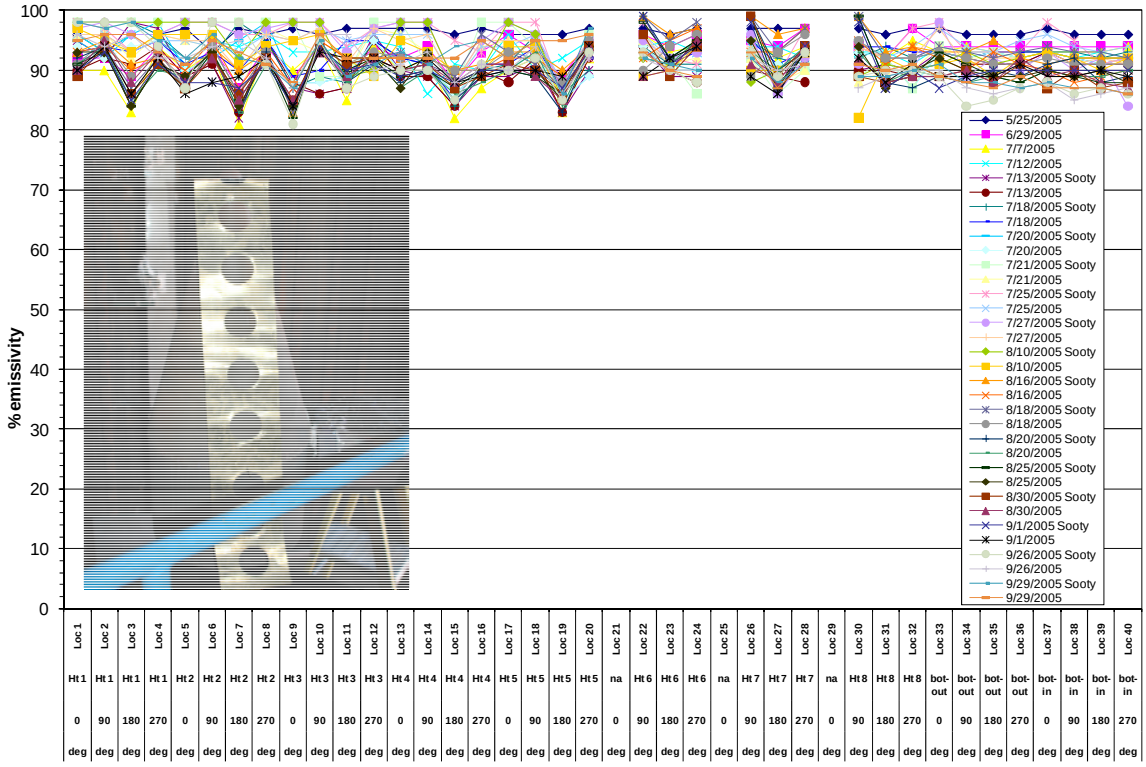

Figure 138 Complex Calorimeter surface spot emissivity.

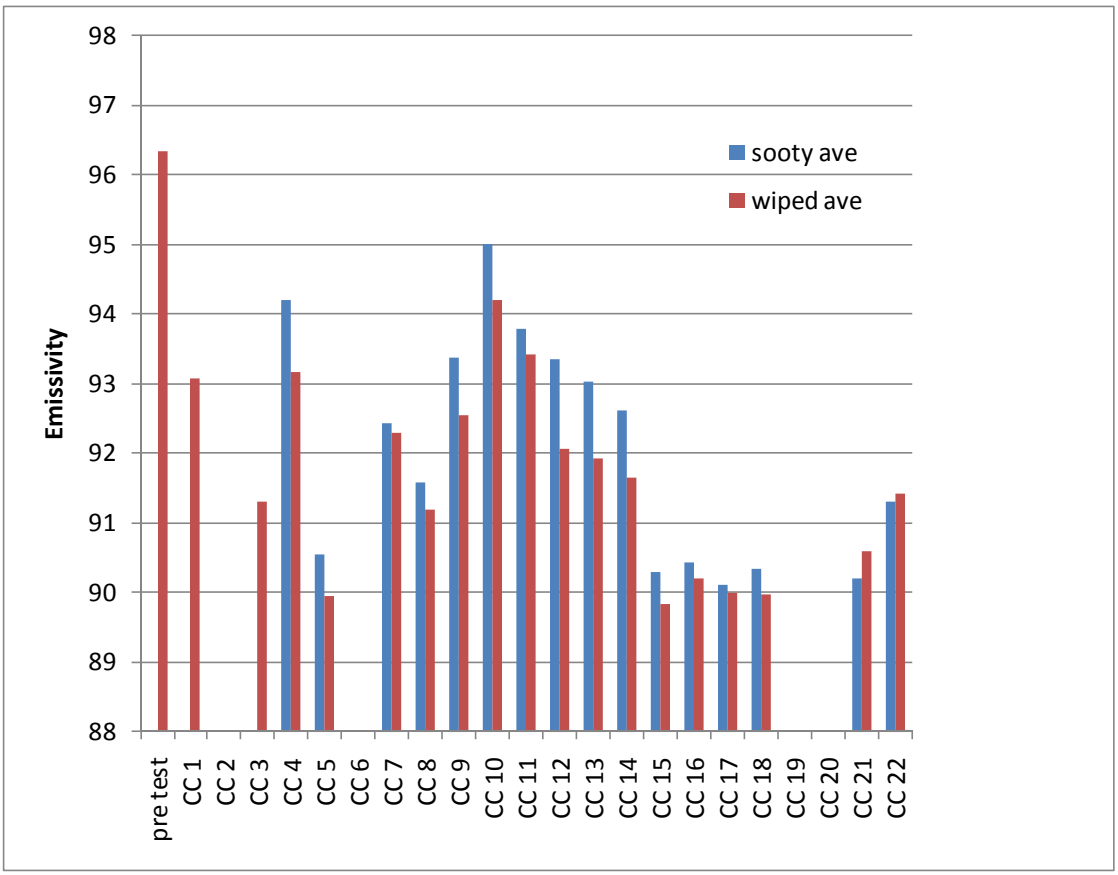

Figure 139 Average surface emissivity

5.4 Combustion Air Flow

As mentioned earlier, the FLAME air source was refurbished and characterized in 2001. During a test, the velocity is monitored with calibrated hot-wire anemometry (TSI Model 8455) at four points (Figure 92). Figure 140 shows the transient combined blower flow rate from seven tests (all blowers operating at a nominal 4000 scfm) that show a stable and consistent flow. Figure 141 plots the actual and standard velocity from the inlet air ring for all tests, based on

$$V_{\text{actual}} = V_{\text{standard}} \frac{P_{\text{standard}}}{P_{\text{actual}}} \frac{T_{\text{actual}}}{T_{\text{standard}}}$$

with P_{standard} = 14.7 psia and T_{standard} = 294 K. Table 7 tabulates the parameters used to reduce the blower flow rate data. Note the air ring flow area is 9.19 m^2 (98.95 ft^2).

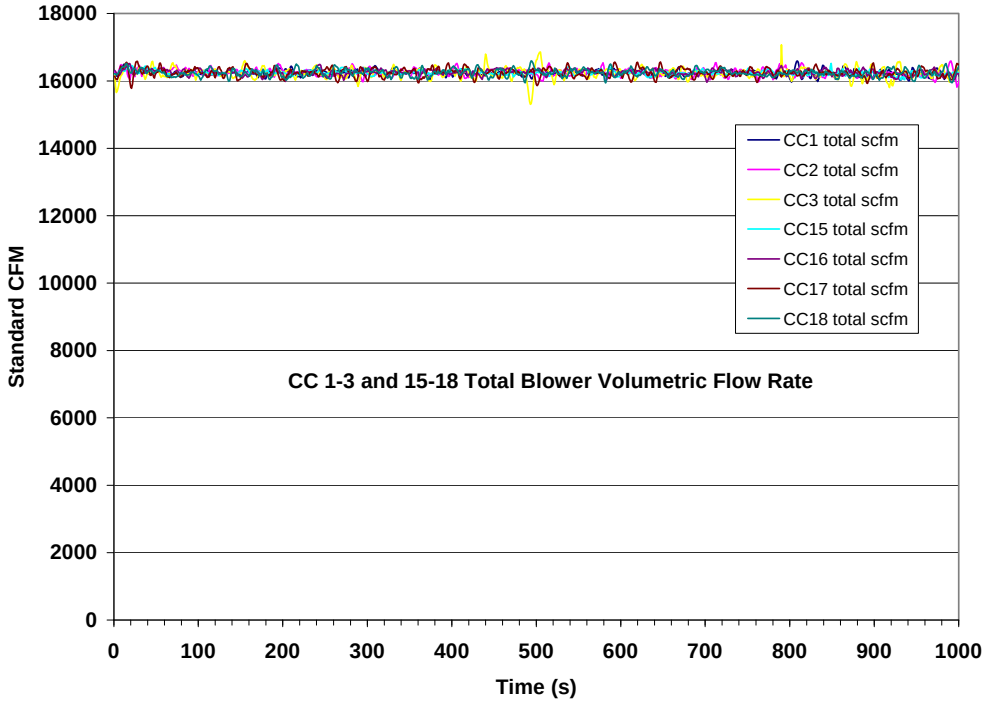

Figure 140 Combined transient blower flow rate.

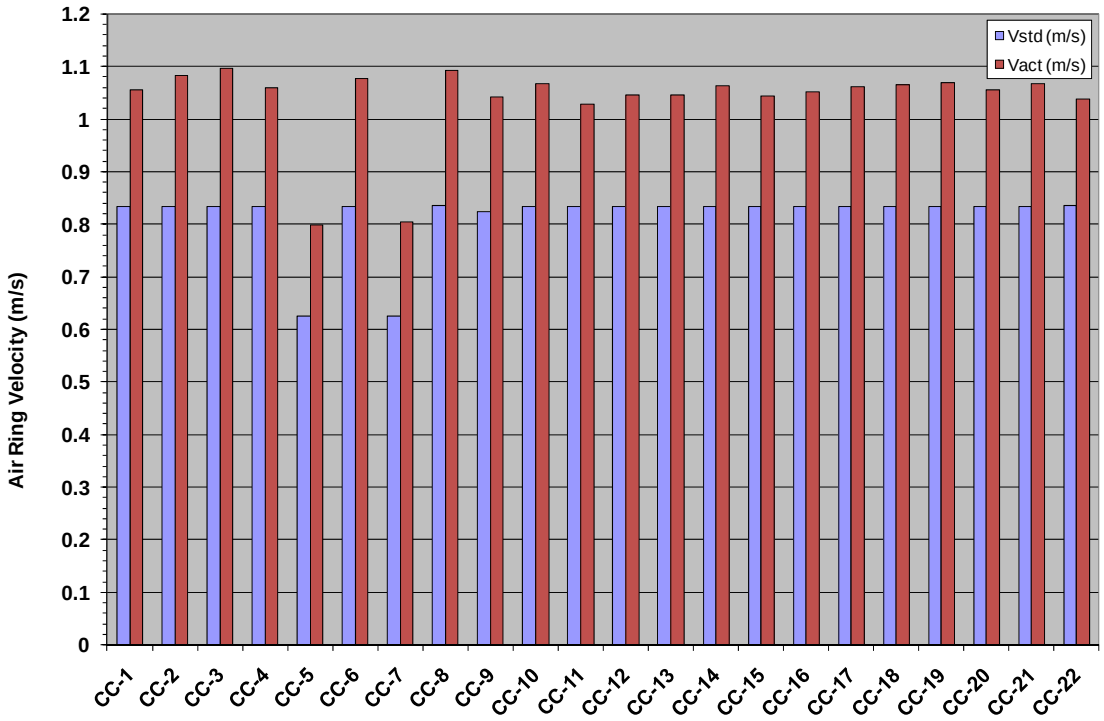

Figure 141 Air ring standard and actual air velocity (all tests).

Table 7 Air Ring Flow and Velocity

	Total Flow (scfm)	Pact (psia)	Tact (K)	Vstd (m/s)	Vact (m/s)
CC-1	16242	11.77	298	0.834	1.056
CC-2	16238	11.75	305	0.834	1.082
CC-3	16233	11.75	309	0.834	1.096
CC-4	16241	11.77	299	0.834	1.059
CC-5	12181	11.82	302	0.625	0.799
CC-6	16237	11.77	304	0.834	1.077
CC-7	12178	11.81	304	0.625	0.805
CC-8	16254	11.76	308	0.835	1.093
CC-9	16040	11.82	299	0.823	1.042
CC-10	16246	11.76	301	0.834	1.068
CC-11	16245	11.81	291	0.834	1.028
CC-12	16252	11.77	295	0.834	1.046
CC-13	16243	11.77	295	0.834	1.045
CC-14	16238	11.76	300	0.834	1.064
CC-15	16244	11.75	294	0.834	1.043
CC-16	16251	11.74	296	0.834	1.052
CC-17	16243	11.74	299	0.834	1.062
CC-18	16241	11.74	300	0.834	1.065
CC-19	16255	11.78	302	0.834	1.070
CC-20	16243	11.81	299	0.834	1.055
CC-21	16231	11.78	302	0.833	1.068
CC-22	16262	11.74	292	0.835	1.038
4000 scfm					
average	16234	11.767	299	0.834	1.060
std.dev.	46	0.024	5	0.003	0.018
3000 scfm					
average	12179	11.815	303	0.625	0.802
std.dev.	2	0.007	1	0.000	0.004

5.5 Insulation and Stainless Steel Thermal Properties

Reducing the temperature data to incident heat flux to the calorimeter surface requires knowing the insulation thermal properties. The values for the insulation thermal conductivity listed in the Thermal Ceramics product literature for 8 PCF Cerablanket is based on the test standard ASTM Method C201. This method uses three thermocouples in variable thickness samples and reports results in effective conductivity versus mean wall temperature and is consistent with industrial use of product, but inconsistent with SNL transient use. The effective values were converted to point (local temperature dependent) values [Oxford 2005]. The results are point values that are consistent with SNL use in thermal models. Note that the corrected values are higher by as much as 30%.

Figure 142 presents the thermal conductivity and the specific heat for the blanket insulation. The specific heat data is from bulk Kaolin; Kaolin is the raw, mineral material melted to form the fibers of the Cerablanket® insulation.

The body of the calorimeter was fabricated using 304 stainless steel. Figure 143 presents the temperature dependent thermal conductivity and the specific heat for the 304 SS.

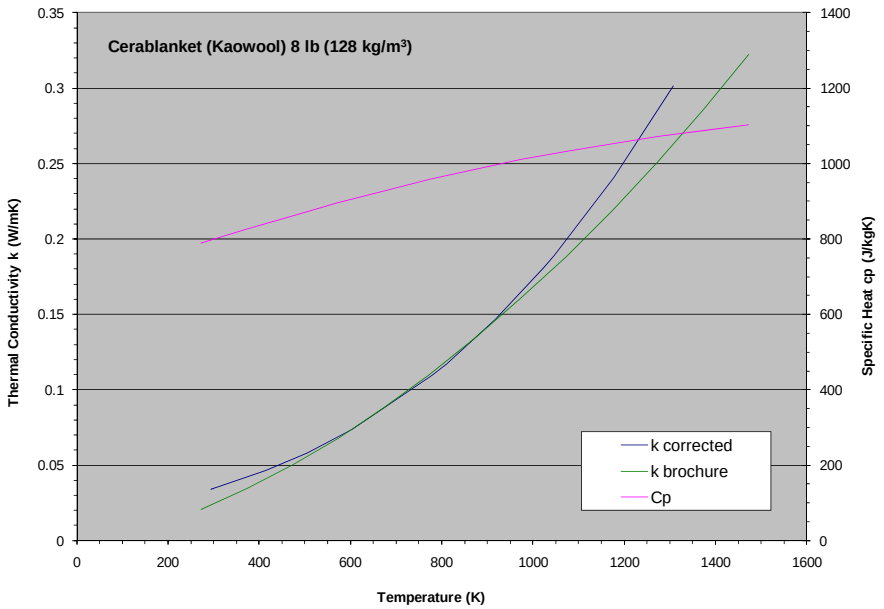

Figure 142 Thermal properties for 8 pcf Cerablanket.

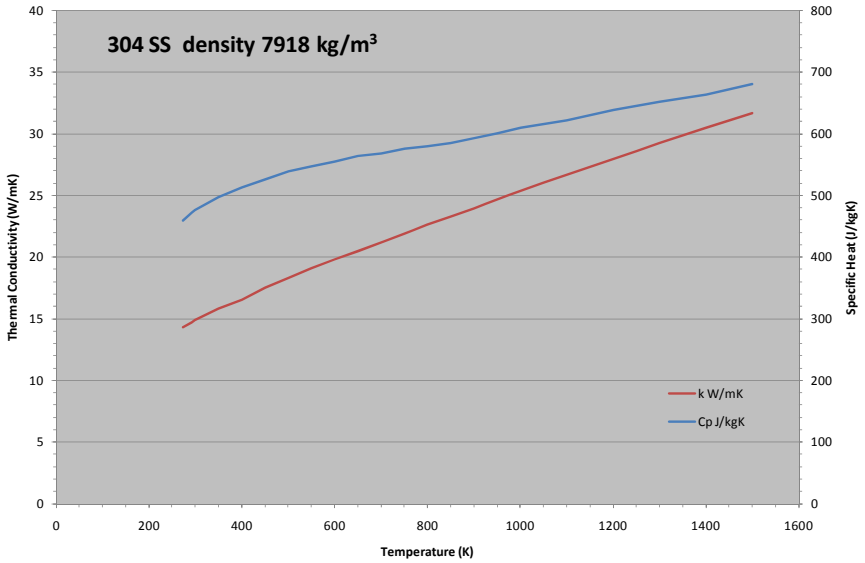

Figure 143 Thermal properties for 304 stainless steel.

5.6 Properties of JP-8 Jet Fuel

Table 8 presents fuel properties based on handbook and referenced data, laboratory measurements, and previous experiments with 2 m diameter fuel pans.

Table 8 Properties of JP-8 Jet Fuel

Properties	Properties	Units	JP8
Name	**Formula**	**-**	$C_{11.5}H_{22.8}$
molecular weight	MW	-	160.8
Boiling point handbook	T_b	C	215
smoke point	l_s	m	0.019
heat of vaporization	hv	kJ/kg	280.0
specific heat	c_p	kJ/kg K	2.01
heat of gasification	hg	kJ/kg	670
density	ρ	kg/m^3	808
heat of combustion	Δhc	kJ/kg	44100
heat of combustion (measured)	Δhc	kJ/kg	45854
carbon monoxide component	Δhc_{CO}	kJ/kg	12200
carbon dioxide component	Δhc_{CO2}	kJ/kg	14100
oxygen component	Δhc_{O2}	kJ/kg	12700
burning rate$_\infty$	max m"-dot	kg/m^2 s	0.04
HRR	Q_T	kW	5542
flame height		m	5.3
radiative flux	to wall (8.48 m)	kW/m^2	2.0
radiant fraction	χ_r	-	0.32
smoke yield	ψ_s	g/g	0.06

References:

Aviation Fuel Properties, Coordinating Research Council, Inc. 1988

Distillation Range 177-266 C

kerosene — 2m complex calorimeter data

SFPE ed. 3, Table 3-4.10

Galbraith Labs

6.

7. MEASUREMENT UNCERTAINTY

7.1 Uncertainty of Overall System

In order to qualify weapon systems performance or validate computer models, the uncertainty of the experimental data used for that purpose must be determined. The following summarizes the description and uncertainty estimates for TC data acquisition systems (DASs) for two of Sandia's experimental facilities that routinely gather data from normal and abnormal thermal environment experiments, the Radiant Heat Facility (RHF) and Lurance Canyon Burn Site (LCBS) [Nakos, 2004].

Figure 144 gives an example of a typical DAS used for thermal experimentation, separated into the following components:

1) Thermocouple (TC)
2) TC connectors
3) TC extension cable
4) TC plug board inside weatherproof steel box
5) National Instruments DAQ system including SCXI-1102 (Signal Conditioning extensions for Instrumentation)
6) Fiber-optic cable
7) Data reduction computer

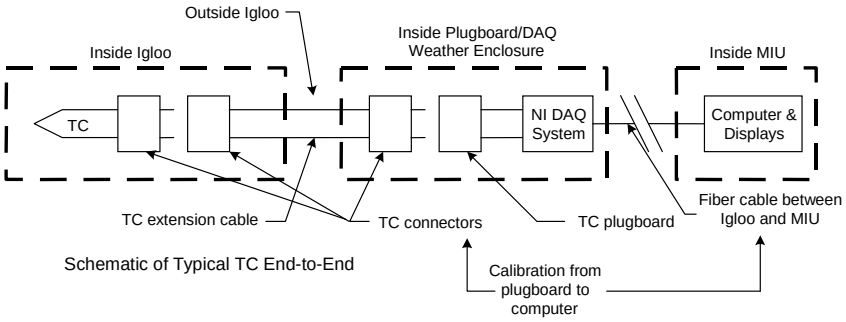

Figure 144 Schematic of a typical TC data acquisition system.

Nakos performed uncertainty analyses for several TC data acquisition systems used at the RHF and LCBS. These analyses apply to Type K, chromel-alumel thermocouples of various types: fiberglass sheathed TC wire; mineral-insulated metal-sheathed (MIMS) TC assemblies; and other types. Several DASs were analyzed, one Hewlett-Packard (HP) 3852A system, and several National Instrument (NI) systems. The uncertainty analyses were performed on the entire system from the TC to the DAS output file. Uncertainty sources include TC mounting errors, ANSI standard calibration uncertainty for Type K TC wire, potential errors due to temperature gradients inside connectors, extension wire effects, DAS hardware uncertainties including noise, common mode rejection ratio, digital voltmeter accuracy, mV to temperature conversion, analog to digital conversion, and other possible sources. Typical results for "normal" environments (e.g., maximum of

300-400K) showed the total uncertainty to be about ±1% of the reading in absolute temperature. In high temperature or high heat flux ("abnormal") thermal environments, total uncertainties range up to ±2-3% of the reading (maximum of 1300K). The higher uncertainties in abnormal thermal environments are caused by increased errors due to the effects of imperfect TC attachment to the test item.

The uncertainty of the entire TC DAS is determined by evaluating the individual uncertainties of each contribution, then adding them using the root-sum-square method (ASME PTC 19.1-1998, "Test Uncertainty, Instruments and Apparatus"). Any systematic bias errors that can be modeled, such as that due to thermocouple attachment imperfection, are algebraically subtracted from the TC reading, and any modeling uncertainty about the nominal mean estimate of the bias is included in the root-sum-square calculation [Romero et al., AIAA-2004].

7.2 Uncertainty of Calorimeter Sheathed Temperatures

In addition to the overall TC DAQ system, the systematic error associated with the TC measurements on the inside (unheated) surface of the calorimeter has to be included.

The TCs are 1/16" (1.6 mm) diameter, inconel sheathed, Type K and have a time response on the order of 1-5 seconds.

The TCs are sampled via an NI DAS system with a 2 Hz low pass filter at a maximum rate of about 1 sample/sec/channel (i.e., all channels are sampled at approximately 1000 Hz but averaged (and recorded) over 1 second). The TCs cannot respond fast enough to capture information at rates faster than about 1 Hz, so these transients cannot be measured with the DAS. The temperature measured is an average. One might capture some high and low temperatures, but likely not the highest or lowest. TCs of this size and type are used because smaller, less protected ones do not survive the fire – they melt and fail.

Uncertainties of the sheathed TCs inside the calorimeters are affected by the systematic uncertainty because the measuring junction inside the sheath is not the same temperature as the insulation blanket surrounding it (note that the insulation temperature changes relatively slowly). Assuming a relatively large value of ±2K, the error from this source is about 0.16% at 1273K and 0.54% at 373K, and is a systematic uncertainty. If this source is added to other systematic uncertainties the overall error at 1273K does not change significantly. The uncertainty at 373K increases slightly to 1.6% [Nakos, 2004].

In summary, an overall uncertainty of ± 2-3% of the reading of the TC data will be assumed. For the calorimeter tests, this yields values of ~30ºC for outer shell temperatures and ~3ºC for the blivet temperatures.

7.3 MIMS Thermocouple Bias Errors

Figueroa [2005] analyzed the potential for bias errors from mineral-insulated, metal-sheathed (MIMS) thermocouples. Surface temperature measurement errors can vary from 1.5% to 6% at 1300K (as compared to intrinsic thermocouple measurements). The large range is believed to be the results of significantly different radiation boundary

conditions seen by the thermocouple (1.5% for TCs with embedded surrounding insulation, 6% for TCs on a hot surface in an open cavity that has the potential to radiate to a cold surface.

7.4 Heat Flux Measurements made by Sandia HFG Analyzer

The Sandia HFG Analyzer has a feature that estimates the uncertainty or error in incident heat flux. As indicated in [Blanchat, Humphries, and Gill, 2000], HFGs are suitable for use during mostly steady environments. The gauge is less suitable for rapidly varying transient heat flux environments because of the slow response of the sheathed thermocouples mounted on the sensing plate. Therefore, the uncertainty of the heat flux measurements is much higher during periods of rapidly varying heat flux, and lower during periods where the flux is slowly varying or steady.

Average heat flux error with SNL HFGs is about 10-20% if the fire is fairly steady. During the time when the heat flux is high and fluctuating rapidly, the flux error can be high, about ± 50%. These results are a reality of heat flux measurements in fires; such measurements are very difficult to accomplish with low uncertainty due to the severe environment, soot deposition, limited material properties, etc.

7.5 Heat Flux Measurements made by Beck Engineering IHCP1D Code

Rugged and inexpensive calorimeters are fabricated to measure heat flux. These calorimeters employ thermocouples to measure temperature, and inverse heat-conduction methods to infer heat flux. Inverse heat-conduction methods estimate heat flux at specific material interfaces using temperature-boundary conditions, material properties, and usually an assumption of one-dimensional (1-D) heat flow. This method is in common use at Sandia's fire test facilities.

An uncertainty analysis was performed to better understand the effect of input parameter variation on calculated heat flux when using the inverse heat conduction method [Figueroa et al., 2005]. A typical calorimeter (a device used to infer heat flux) was examined. The calorimeter was a cylinder about 40.6 cm (16-in.) in diameter and 0.32-cm-thick (1/8-in.), made of 304 stainless-steel filled with 2.5-cm-thick (1-in.) ceramic fiber insulation. Parameter variations were examined to establish the effect on heat flux uncertainty. The parameters that varied were steel-wall thickness, thermal conductivity, and volumetric heat capacity; insulation thickness, thermal conductivity, and volumetric heat capacity; temperature uncertainty, type of cold side boundary condition, temperature sample rate, number of computational nodes per region, number of calculated per measured time steps, and the number of future time steps. One-dimensional heat transfer was assumed in all cases.

Results of the analysis show that at the maximum heat flux, the most important parameters were temperature uncertainty, and steel thickness and volumetric heat capacity. The use of a constant thermal conductivity rather than temperature-dependent values also made a significant difference in the resultant heat flux. As an example, several parameters were changed to predict a scenario with typical parameter

uncertainties. The resulting total uncertainty to 95% confidence estimation was approximately 15-19% at the highest flux, not counting 2- or 3-dimensional effects. Estimates of error that is introduced when 1-D inverse heat transfer techniques are applied to multidimensional problems was investigated by Lopez et al. [2000]. They determined maximum errors of 3%, 7%, and 18% for a non-uniform flux applied to a surface covering 360°, 180°, and 90° of a cylinder, respectively.

7.6 Fuel Regression Measurements

An uncertainty analysis was performed using the method described by Coleman and Steele [1999]. The uncertainty for fuel regression concentrates on the Type B uncertainty, or systematic uncertainty. Parameters contributing to the Type B uncertainty are primarily based on manufacturer's specifications. Contributions to the error include the pressure measurement uncertainty (0.4%), the time measurement uncertainty (0.03%), and the fuel specific gravity measurement uncertainty (0.5%). The calculated total uncertainty in the fuel regression measurement due to Type B uncertainty is 0.6%.

7.7 Measurement Uncertainty Summary

Table 9 summarizes the measurement uncertainties for these types of experiments. Due to the many approximations made, the calculated uncertainties are rounded up to add some conservatism.

Table 9 Measurement Uncertainty Summary

Measurement Type	**Maximum Total Uncertainty**	**Comments**
1) Generic TC measurements	± 2.6K at 373K or ± 5.5K at 1273K **Approximate by ±2% at all temperatures**	Does not include systematic errors due to mounting, etc.
2) Calorimeter temperatures	± 2.5K at 373K or ± 5.5K at 1273K **Approximate by ±2% at all temperatures**	
3) SNL HFG heat flux estimates	For periods of steady flux **±10-20% average errors**	±50% error during maximum fluctuations
4) IHCP1D heat flux estimates	For periods of steady flux, total uncertainty **~10-14%**	(to 95% confidence estimate)
5) Schmidt-Boelter HFGs	Accuracy: **±3%** rms	(Others report ±9% rms)
6) Fuel Regression	Uncertainty: **±1%**	0-15 inches WC
7) Wind Speed	Accuracy: **±1%** rms ±0.05 m/s	0 to 30 m/s
8) Wind Direction	Accuracy: **±2°** (1 to 30 m/s)	1 to 30 m/s
9) Wind Temperature	Accuracy: **±2°C**	0 to 30 m/s

8. QUANTIFY THE EXPERIMENTAL UNCERTAINTY – A POSTTEST VISIT WITH ANALYSTS

When the experiments were completed, coupled fire-environment/thermal-response models were validated using the above described data for the complex calorimeter engulfed in a JP8 hydrocarbon fuel fire. Fire model predictions of heat flux from FUEGO (shown in Figure 145) were coupled with thermal response model predictions from CALORE to predict the transient internal temperature distribution of the blivet. Three-dimensional, transient calculations were compared with the experimental data obtained in the FLAME facility. The measurement/prediction comparisons were quantified using appropriate validation metrics and parameter variations were used to assess output variability in support of uncertainty quantification [Black et al., 2005].

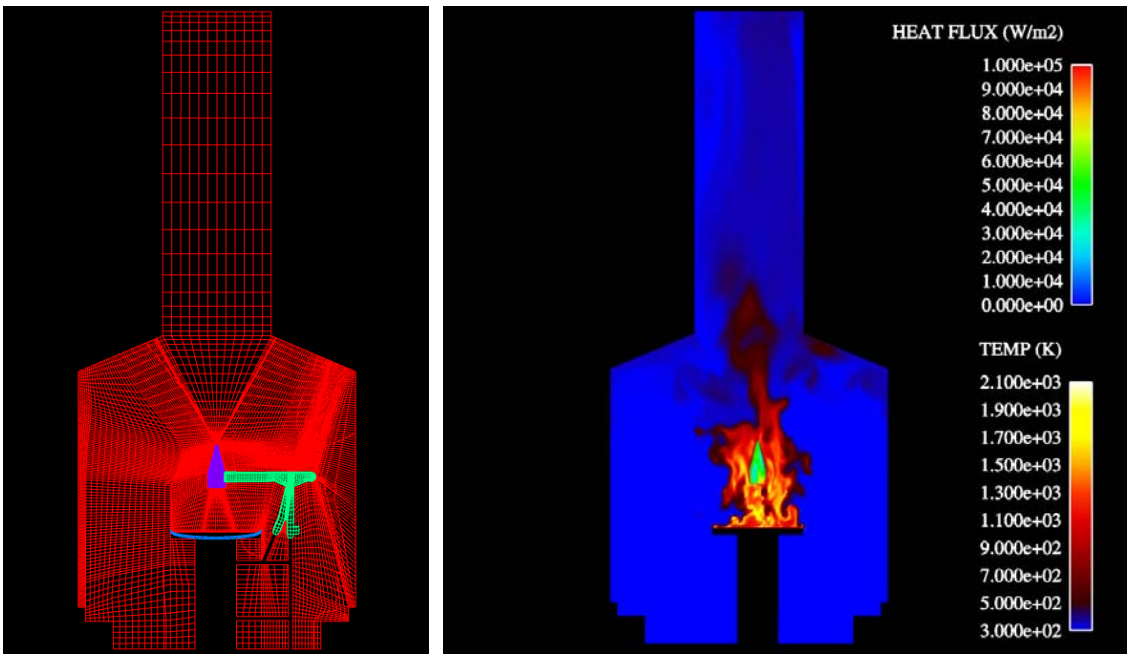

Figure 145 Cross section and fine mesh TFNS solution for the calorimeter in the FLAME facility.

Predictions of transient external shell temperatures as well as the surface temperatures of the embedded mass were averaged spatially and compared to an average of data from three experiments, CC-15, CC-17, and CC-18. The comparisons showed that the response variable was more sensitive to fire model parameters than to thermal model parameters. The observed relative difference in measurements and model predictions was also compared to the model uncertainty. The comparisons showed that the model plus uncertainty bounded the experimental data.

Over the course of the comparisons, the analysts revisited a number of thermal experimental parameters to fully understand their effect on the experiment uncertainty.

8.1 Insulation – Posttest Status and Variability in the Thermal Properties

After ~23 tests (including scoping) the calorimeter was disassembled. Figure 146 compares pretest conditions to posttest conditions. On the cone, where the seam was formed parallel to the arm, a large gap is seen near the base of the cone. In addition, a small cap of insulation placed on the cone tip was missing. The insulation appeared to shrink somewhat and also was susceptible to falling apart when handled. Inspection of insulation in the cylinder section showed the disk of insulation on the bottom of the "bucket" was fairly well intact; however, a tear was noted on one side of the cylinder wrap. It is unknown if this tear occurred during testing or during disassembly.

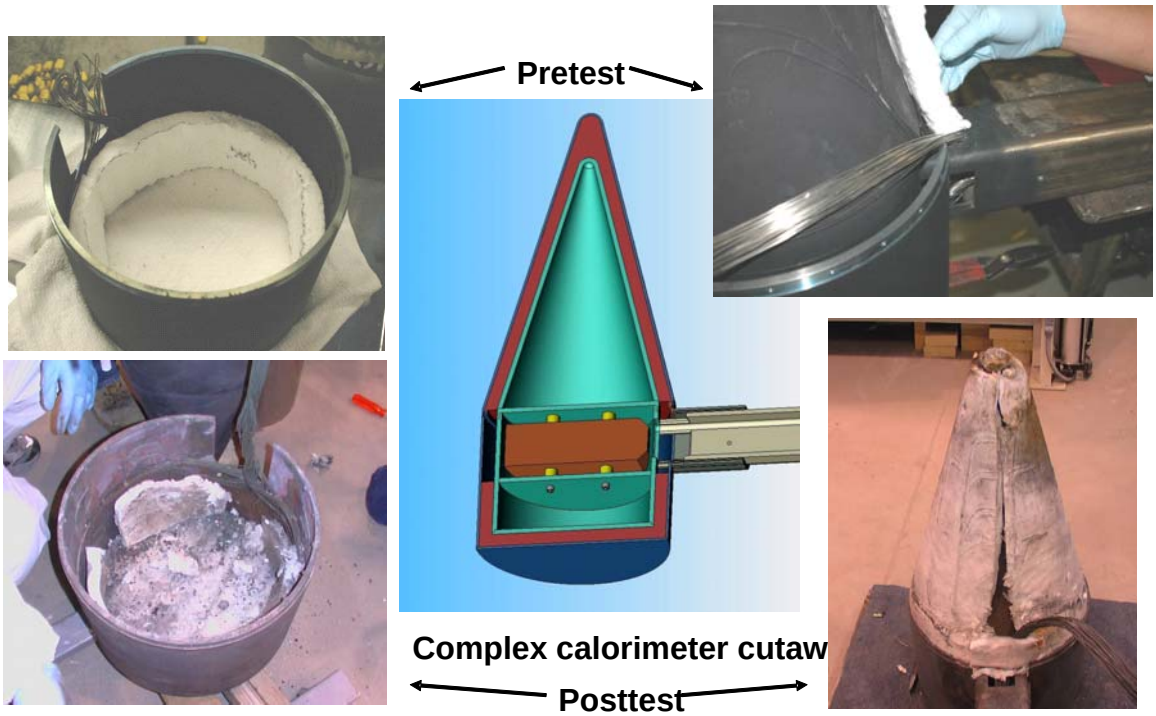

Figure 146 Post test status of insulation.

As noted earlier, the manufacturer's values for thermal conductivity properties was based on the ASTM C201 Test Standard. This method for measuring properties uses steep thermal gradients in 1" thick samples and reports results in terms of average temperature (a method consistent with industrial use of product, but inconsistent with SNL use). The ASTM C201 average values were corrected to point values for use in the model prediction. We noted that the corrected values are higher by as much as 30%.

A experimental effort was initiated to check the correction. Figure 147 shows some preliminary experimental results for thermal conductivity that indicates the correction may be too small. In addition, it was confirmed that the blanket insulation shrinks when heated. In the model predictions, the uncertainty on the thermal property values bounds the experimental data and the sensitivity studies show no impact.

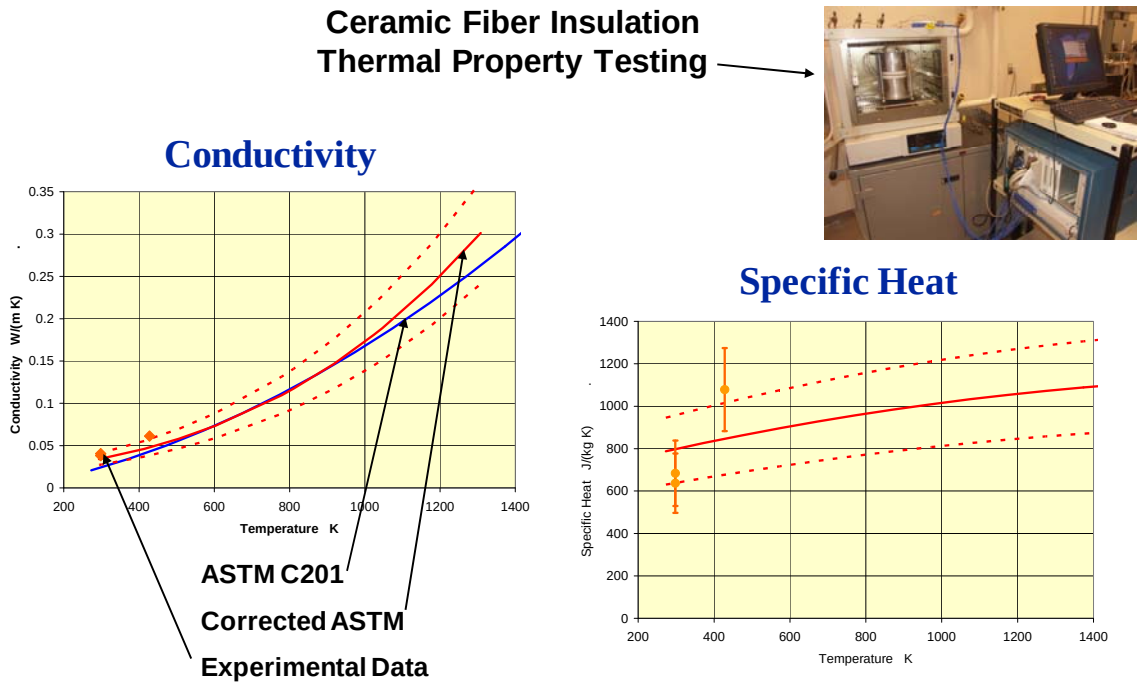

Figure 147 Testing of thermal properties of ceramic fiber insulation.

8.2 Pyromark® Paint Emissivity – Large Uncertainty

The analysts were given a mean total direction calorimeter surface emissivity of 0.86 ± 0.09 for use in model predictions. This drives large uncertainty in temperature predictions. They asked why such large uncertainty?

As part of a separate study, an experimental effort was initiated to obtain a set of emittance data for five commonly used materials in experiments: Inconel 600, 304 Stainless Steel, 7-4PH Stainless Steel, Aluminum 7075, and Mk 4 Aeroshell material [Figueroa 2005].

Two emissivity measurement devices (Figure 148) were used. The first was a Cary-Integrating Sphere (CIS) Reflectometer that measures emissivity at angles from 10° to 80° and at wavelengths from 0.3 to 2 microns (room temperature only). The 2nd device was a SOC-100 Hemispherical Directional Reflectometer that measures emissivity at angles from 10° to 80° and at wavelengths from 2 to 25 microns and at temperatures up to ~540°C.

The discussion here focuses on the 304 stainless steel samples painted with Pyromark 2500 cured at 1000° and a test suite of measurement angles of 10°, 40°, 60°, and 80°, all at room temperature and at 540°C. Figure 149 presents the directional spectral and total emissivity data for Pyromark 2500 on 304 stainless steel, clearly showing the effects angle, wavelength, and temperature. Note also the small angle, ambient temperature

emissivity value of ~0.95 at 1 micron, corresponding fairly well with the in-situ Pyrofiber Model E10 measurement average value of 0.92 over the course of the experiments.

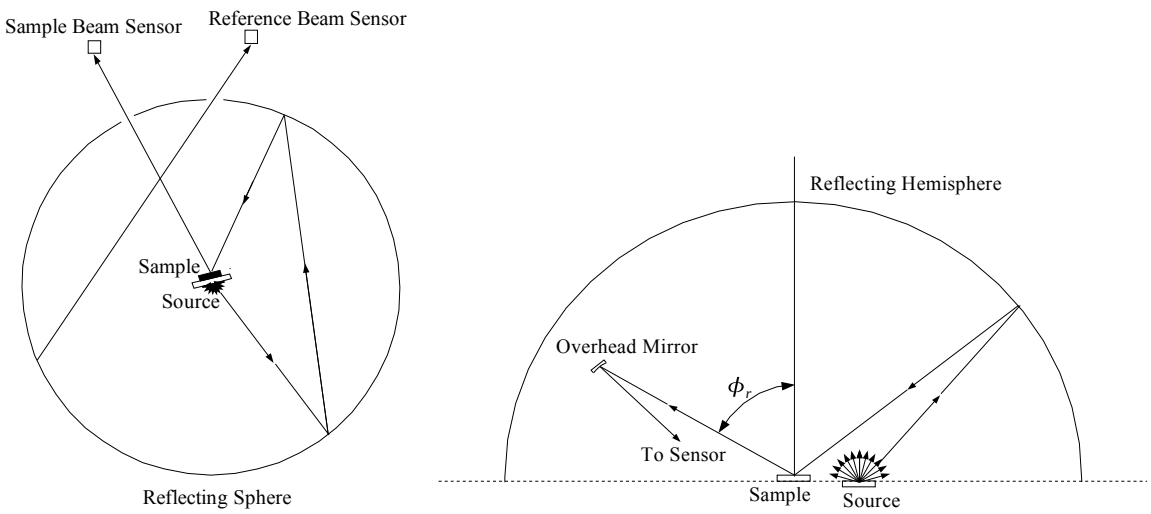

Figure 148 The Cary-Integrating Sphere and SOC-100 Hemispherical Directional Reflectometers.

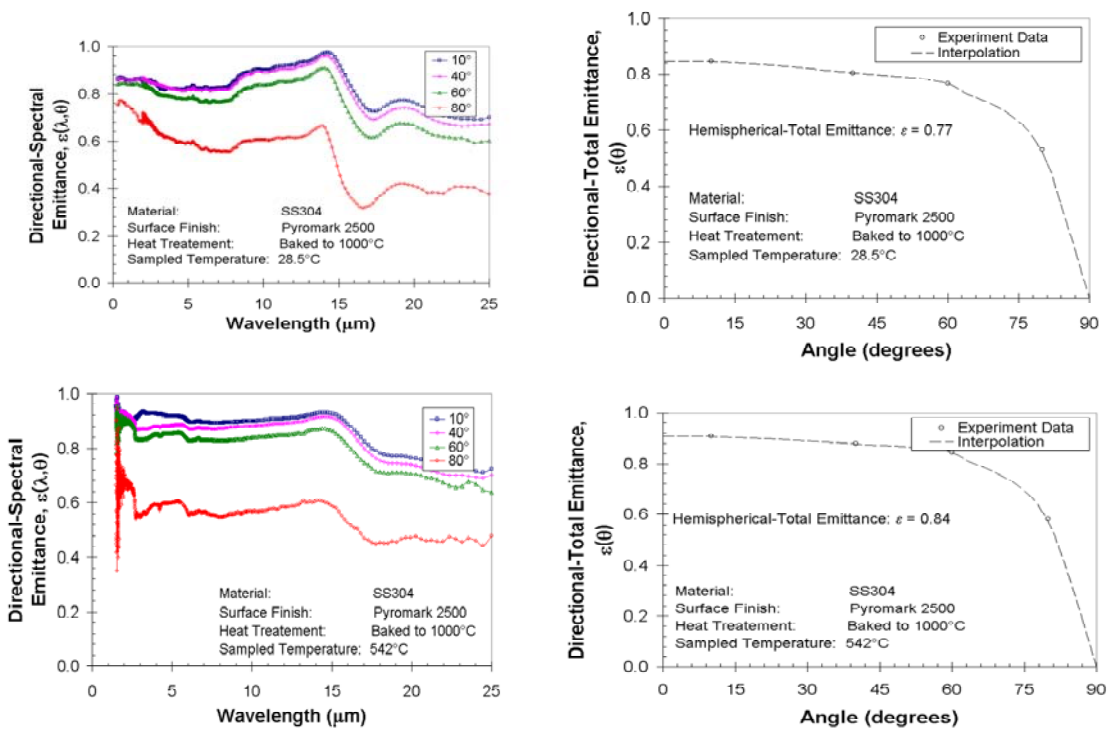

Figure 149 Emissivity data for 304SS with Pyromark paint.

In summary, baked Pyromark 2500 on 304 stainless steel has a hemispherical total emittance of ~0.77 at room temperature. The emittance increase with temperature to a value of 0.84 at 540ºC. Single wavelength (0.95 micron) and small angles yields ε ~ 0.9 – 1.0

Sources of uncertainty for emissivity include:

- Measurement
  - CIS: less than ±1.5%
  - SOC-100: ±1% in the angles between 0° and 70° and ±3% beyond 70°
- Integration of Data Points
  - Small for wavelength integration
  - Significant for angle integration
    - Few angle points ~ ±1-3%
- Temperature ~ ±5%

The combination of all sources yields a total uncertainty of ~ ±10%

8.3 Thermocouple Bias Errors

In order for a true comparison between model predictions and experimental data, the thermocouple (TC) measurements were bias corrected to account for differences between the temperature at the thermocouple junction or bead and the temperature at the attached surface or outer calorimeter shell. The surface temperature is higher than the thermocouple bead temperature when the thermocouple is mounted on a surface that faces away from the heat source as shown in Figure 150.

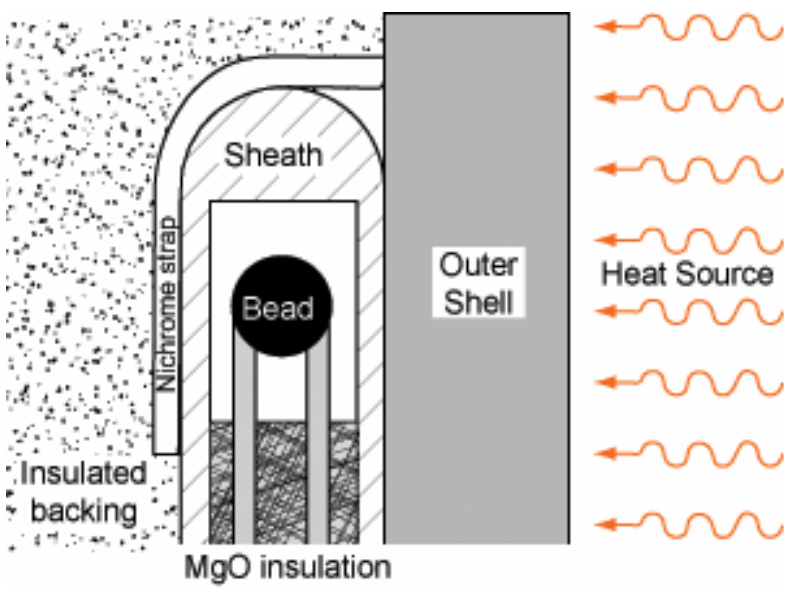

Figure 150 Schematic of thermocouple mounted on outer shell.

Figure 150 shows the thermocouple backed by insulation, which reduces bias error caused by heat loss. Without insulation the thermocouple acts like a fin and causes the bead temperature to be lower than the shell temperature. For 60 mil diameter thermocouples without insulated backing, the outer shell temperature is expected to be 1351 K when the bead is at 1273 K [Nakos et al., 2004b]. In other words, the inner surface of the outer shell is 6.1% higher (78° higher) than the thermocouple bead temperature. The temperature difference is smaller when the thermocouple is insulated. For thermocouples with insulated backing, the temperature of the inner surface of the outer shell is expected to be 1288 K when the bead is at 1273 K.[2] The outer shell temperature is 1.2% higher (15° higher) than the thermocouple bead.

The bias correction for the thermocouples on the inside of the outer shell of the complex calorimeter is expected to vary linearly with temperature. The correction is assumed to be zero at 300 K and 6.1% of the absolute temperature at 1273 K for thermocouples without insulated backing. For the thermocouples with insulated backing, the correction is assumed to be zero at 300 K and 1.2% of the absolute temperature at 1273 K. The temperature of the inner surface of the outer shell was determined as follows:

$$T = T_m\left[1 + 6.2 \times 10^{-5}\left(T_m - 300\right)\right], \qquad \text{for TC's without insulated backings and (1)}$$

$$T = T_m\left[1 + 1.2 \times 10^{-5}\left(T_m - 300\right)\right], \qquad \text{for TC's with insulated backings, (2)}$$

where T (K) and Tm (K) represent the temperature of the inner surface of the outer shell and the measure temperature of the thermocouple bead, respectively.

Table 10 shows the bias correction from Nakos [2004b] for TCs not backed by insulation as well as the bias correction from equation 1 and 2. Most of the correction occurs at higher temperatures as shown in Figure 151 which shows the measured temperature for flame experiment CC-15 at location 53. The thermocouple at location 53 is a thermocouple without insulation backing (on the outer cylindrical shell opposite the blivet)..

Table 10 Percent correction of absolute temperature for given plate temperatures.

Plate temp (K)	Ref. Nakos 2004b	6.2×10^{-5} ($T_m - 300$)	1.2×10^{-5} ($T_m - 300$)
1173	5.7	5.4	1.0
1273	6.1	6.1	1.2
1373	6.8	6.8	1.3

[2] Table obtained from Nakos et al., 2004b. The correction for insulation backed thermocouples is based on data from SNL HFG studies that used intrinsic, 20 and 63 mil TCs on insulated 10 mil plate [Blanchat et al., 2000]. The intrinsic error was assumed to be negligible.

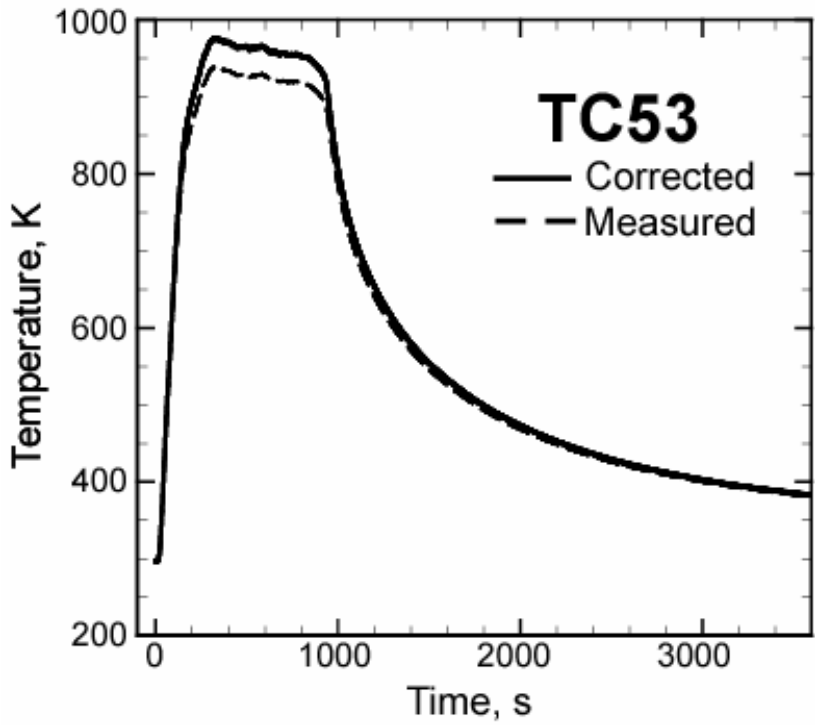

Figure 151 Measured and corrected temperatures at location 53 for CC-15.

8.4 Posttest Thermocouple Attachment and Survivability

One concern that arose following the completion of the test series was the robustness of the thermocouple attachments after being subjected to twenty-three engulfing fuel fires. Figure 152 shows pictures of pristine TC attachments and attachments posttest during disassembly.

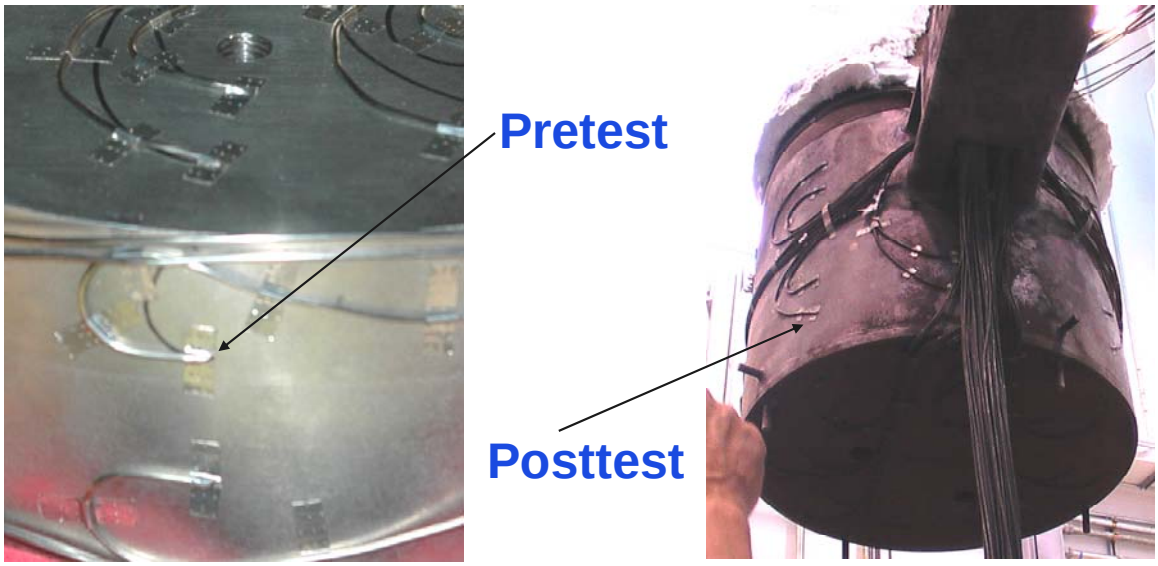

Figure 152 Pretest and posttest views of thermocouple attachments.

A unique experimental technique was developed to quantify attachment error. Each thermocouple was turned into a miniature heater by applying a known and fixed power profile and the resulting thermal response (temperature decay) was measured. Figure 153 illustrates the steps: 1) Take raw TC voltage check data during the temperature decay after applying the power, 2) Normalize with minimum and maximum values, and 3) Fit a lumped model to the normalized response.

$$\frac{1}{\tau} = {h_c A_s}/{\rho V C_p}$$

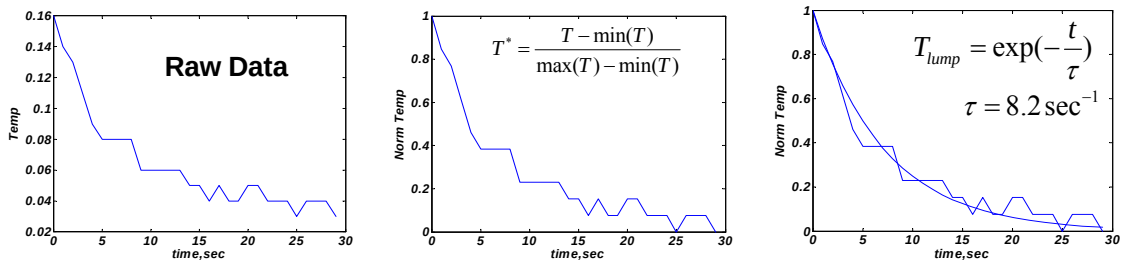

Figure 153 Procedure to analyze thermocouple attachment.

The final step was to determine if a TC is "significantly different (larger)" from other TCs by determining a τ -value such that

$$z = \frac{\tau_i - mean(\tau)}{std(\tau)} > 2$$

where mean(τ) and std(τ) (standard deviation) are calculated for a set of TCs. Note that z > 2 is an arbitrary cut-off value based on a standard normal distribution P(z > 2) = 2.5%.

An analysis of all TCs was performed. Figure 154 pictorially shows that data analysis from only the inner shell TCs.

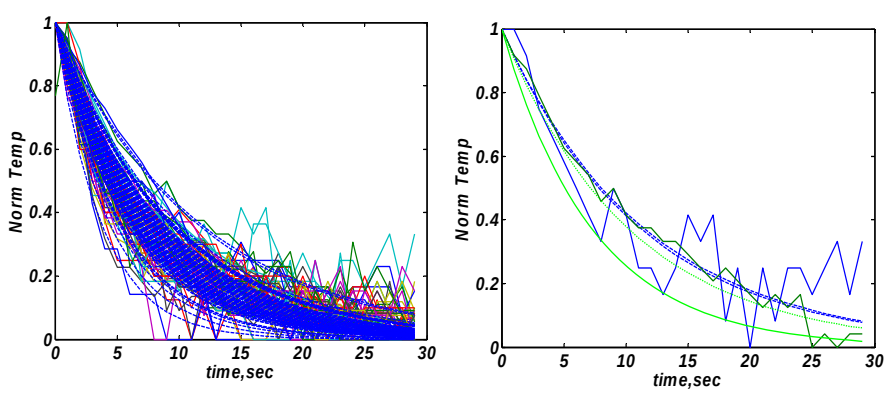

Figure 154 Inner shell thermocouple attachment analysis.

Table 11 lists eleven TCs (4% of the 254 total) that fall outside 2 standard deviations of the mean. Point-to-point comparisons with model predictions should not be performed at these locations.

Table 11 Thermocouples failing attachment criteria.

Region	Mean(τ) sec	Std(τ) sec	Identified TCs (z>2)
Blivet (all)	7.0	1.2	209, 210, 221
Outer Shell	7.8	1.5	21, 22, 82, 32, 39, 67
Inner Shell	7.3	1.5	91, 79

8.5 Experiment Repeatability

Data repeatability is an important factor when performing model prediction for validation purposes. The code predictions of the complex calorimeter focused on the three later "nose up" experiments performed at the pan centerline, CC-15, CC-17, and CC-18.

Slight variability in boundary conditions could affect the data, those are noted below. The CC-15 test was performed at ambient temperatures ~5ºC colder than CC-18. It also had a ~6% lower regression rate (from 300-700 s, as noted in Figure 155 by the smaller slope in fuel DP measurements) and a ~2% lower actual air velocity.

- CC-15, 2.82 mm/min regression rate, 1.043 m/s air velocity
- CC-17, 2.94 mm/min regression rate, 1.062 m/s air velocity
- CC-18, 3.00 mm/min regression rate, 1.063 m/s air velocity

We did note small differences in thermal response, as indicated in Figures 156 and 157 for the blivet and the cone/cylinder sections, respectively.

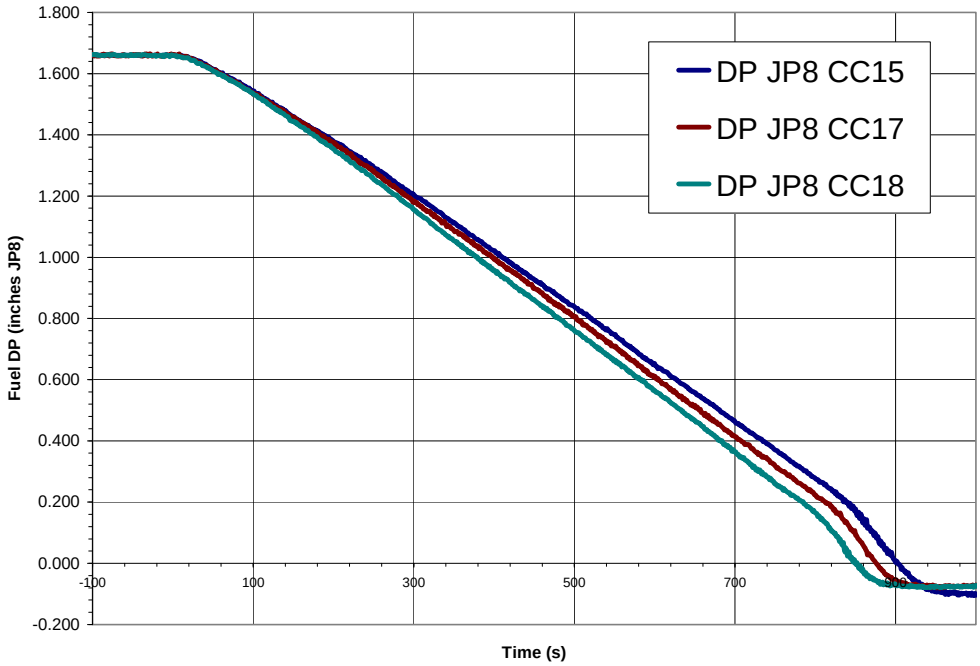

Figure 155 Comparison of fuel regression in CC-15, CC-17, and CC-18.

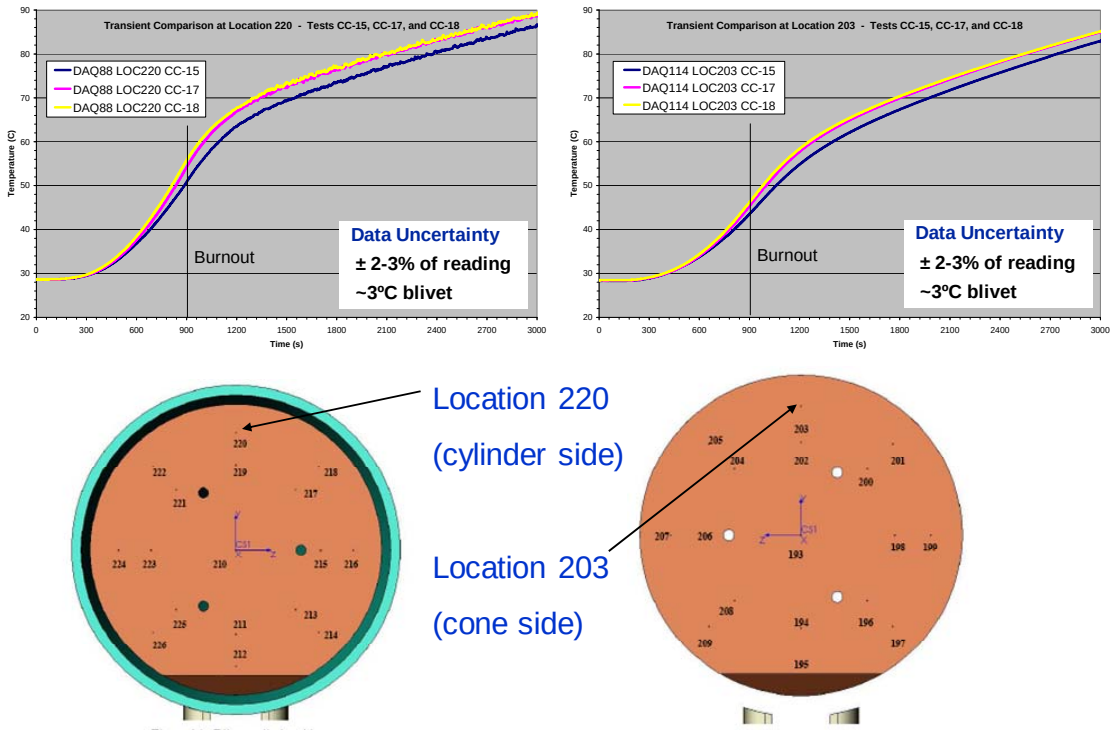

Figure 156 Blivet response repeatability.

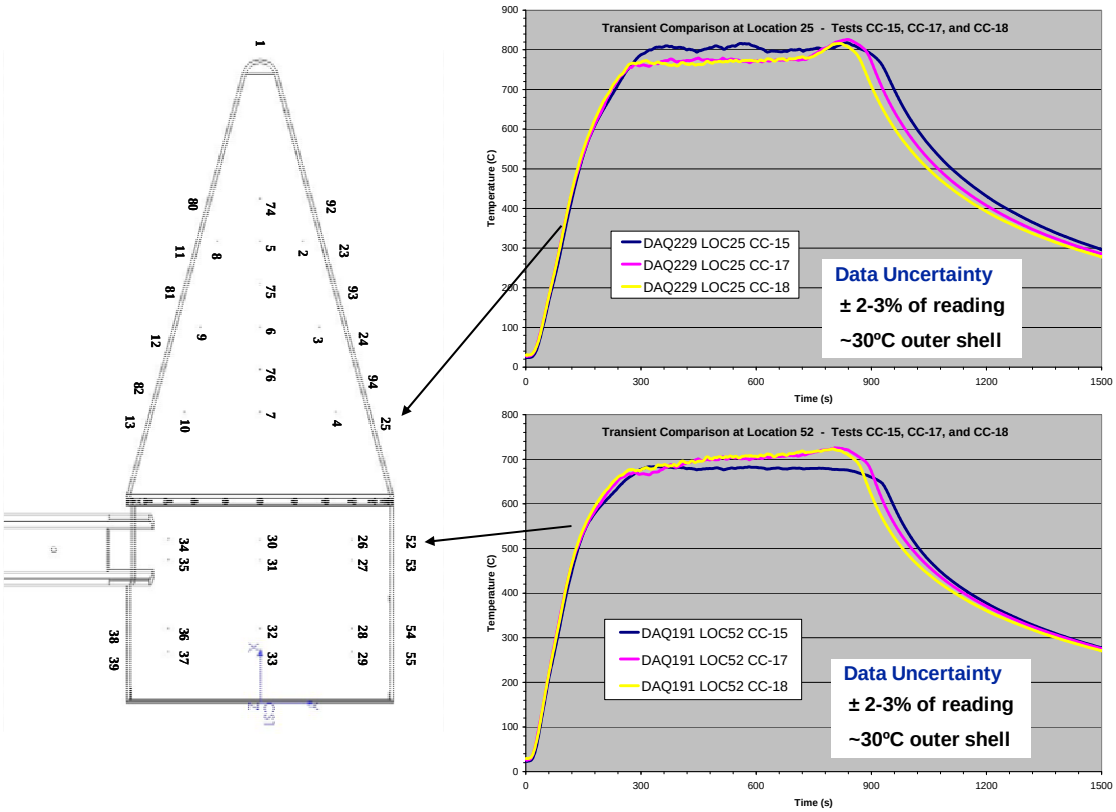

Figure 157 Cone and cylinder response repeatability.

In summary, three nominally identical experiments were conducted and the variability among the experiments was studied. The relative difference of each experiment from the mean and standard deviation in this difference was quantified. The bottom of the calorimeter had the least variation, ~ ± 5%. The cone and cylinder varied by ~ ± 10%. Finally, the average blivet temperature had the largest variance, ~ ± 19%. Figure 158 shows the relative difference (based on the difference of experiments from the mean) of the three experiments for different sections of the calorimeter at early (2.5 minutes) and late (5 minutes) times. The bars are 2 standard deviations of the three experiments.

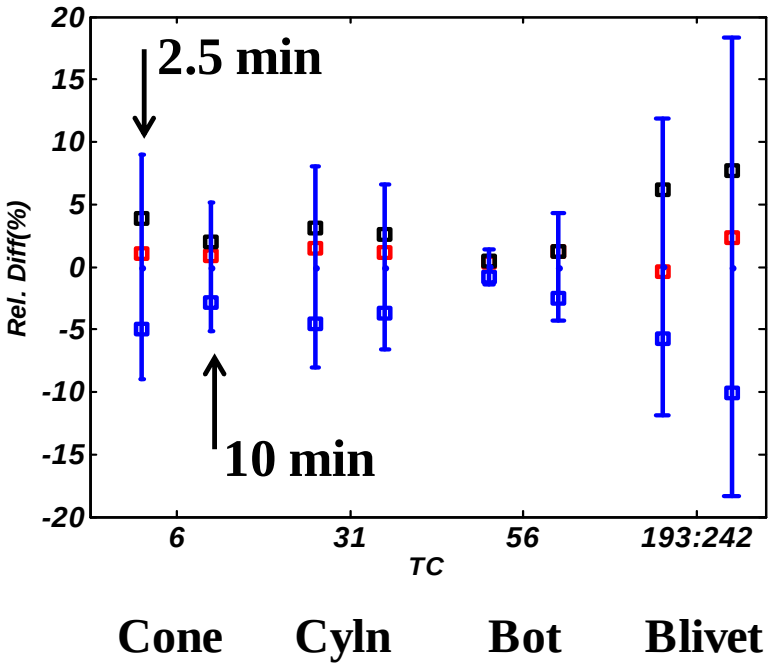

Figure 158 Relative difference of the experiments used for model prediction.

9. CONCLUSION

Validation quality data sets are the standard by which modeling and simulation uncertainty can be quantified. For the first time in 50 years of fire testing, heat flux to an object and its thermal response in a fire with well-controlled and well-characterized boundary conditions has been measured with archival datasets. A data loss rate of only 4% over 23 tests in notoriously harsh environments was achieved. These datasets include the most comprehensive experimental uncertainty of a fire to date. Emissivity of the object surface, determined pretest to be the source of the largest experimental uncertainty, was very well characterized.

This data set is the 6th data set funded by Campaign 6 and ESRF in support of fire model validation. The published datasets include:

- Study of a Turbulent Buoyant Helium Plume (O'Hern et al., 2005)
- Study of a 1 Meter Diameter Methane Fire (Tieszen et al., 2002)
- Study of Soot and Species in a JP8 Fire (Jensen et al., 2007)
- Study of Mixed Convection from a Horizontal Cylinder in Crossflow (Laskowskia et al., 2007)
- Study of Radiation/Convection Partitioning (Blanchat et al., 2009)

The authors appreciate management's continued support for diagnostics development and validation quality data sets. Finally, we note that Engineering Sciences has a clear commitment to science in support of our weapons programs and is committed to supporting the research community through publication of its data sets where appropriate.

10. REFERENCES

Black, A. R., Hobbs, M. L., Dowding, K. J., Blanchat, T. K., 2007, "Uncertainty Quantification and Model Validation of Fire/Thermal Response Predictions", 18th AIAA Computational Fluid Dynamics Conference, Miami, FL, June 25-28, AIAA 2007-4204.

Blanchat, T., Humphries, L., Gill, W., "Sandia Heat Flux Gauge Thermal Response and Uncertainty Models," Sandia Report SAND2000-1111, Sandia National Laboratories, Albuquerque, NM, May 2000.

Blanchat, T.K., July, 2001, "Characterization of the Air Source and the Plume Source at FLAME," Sandia Report SAND2001-2227.

Blanchat, T. K., Luketa-Hanlin, A., Romero, C., Tieszen, S., and Romero, V., "Plan to Develop Validation Data for Heat Flux to a Complex Object in a Fire Plume for the SYRINX/FUEGO/CALORE Fire and Thermal Response Codes," Sandia Report SAND2005-3912, Sandia National Laboratories, Albuquerque, NM, August 2005.

Blanchat, T., O'Hern, T., Kearney, S., Ricks, A., and Jernigan, D., "Validation Experiments to Determine Radiation Partitioning of Heat Flux to an Object in a Fully Turbulent Fire," Proceedings of the Combustion Institute 32 (2009) 2511–2518.

Bova, S.W., M.W. Glass, K.J. Dowding, R.R. Lober, R.J. Cochran, "CALORE, A Thermal Analysis Program: User Manual" Sandia National Laboratories, http://www.scico.sandia.gov/calore/doc/Calore12pr.pdf.

Brown, A. and Blanchat, T.K., "A Validation Quality Heat Flux Dataset for Large Pool Fires", Proceedings of HT2003: 2003 ASME Summer Heat Transfer Conference July 22-23, 2003, Las Vegas, NV, USA, HT2003-40249

Brown A.L., and Blanchat, T.K., "A Validation Quality Heat Flux Dataset for Large Pool Fires," HT2003-40249, Proceedings of HT2003: 2003 ASME Summer Heat Transfer Conference, July 22-23, 2003, Las Vegas, NV.

Coleman and Steele. *Experimentation and Uncertainty Analysis for Engineers*, Wiley & Sons, 1999.

Figueroa, V.G., Nakos, J.T., and Murphy, J., "Uncertainty Analysis of Heat Flux Measurements Estimated Using a One-Dimensional, Inverse Heat Conduction Program", Sand2005-0339, Sandia National Laboratories, Albuquerque, NM, February 2005.

Jensen, K., Suo-Anttila, J., and Blevins, L. "Measurement of Soot Morphology, Chemistry, and Optical Properties in the Visible and Near-Infrared Spectrum in the Flame Zone and Overfire Region of Large JP-8 Pool Fires" Combustion Science and Technology, 179: 12, 2453-2487, 2007.

Kearney, S., “Results of recent experiments at Penlight,” Sandia internal memo to T. Blanchat and Distribution, dated April 15, 2002.

Laskowski, G.M., Kearney, S.P., Evan, G., and Greif, R., “Mixed Convection Heat Transfer To and From a Horizontal Cylinder in Cross-flow with Heating from Below,” International Journal of Heat and Fluid Flow, Volume 28, Issue 3, June 2007, Pages 454-468, 2007.

Lopez, C., Koski, J. A., and Razani, A., “Estimates of Error Introduced when One-Dimensional Inverse Heat Transfer Techniques are Applied to Multi-Dimensional Problems,” SAND2000-0067C, December 1999. (Presented at the 2000 National Heat Transfer Conference, Pittsburgh, PA (US), 08/20/2000-08/22/2000)

Luketa-Hanlin, A. and Blanchat, T. “Validation and Uncertainty Analysis of Numerical Simulations of Heat Flux to a Calorimeter in a 2-Meter JP-8 Pool Fire”, Accepted for presentation at INTERFLAM 2004, 5-7th July 2004, Edinburgh, Scotland.

Nakos, J.T., “Uncertainty Analysis of Thermocouple Measurements Used in Normal and Abnormal Thermal Environment Experiments at Sandia’s Radiant Heat Facility and Lurance Canyon Burn Site,” Sand2004-1023, April 2004, Sandia National Laboratories, Albuquerque, NM.

Nakos, J. T., Suo-Anttila, and Gill, W., “Shroud boundary condition characterization experiments at the Radiant Heat Facility,” SAND2004-5080, October 2004b.

O'Hern, T. J., Weckman, E. J., Gerhart, A. L., Tieszen, S. R., and Schefer, R. W., “Experimental Study of a Turbulent Buoyant Helium Plume”, Journal of Fluid Mechanics, 544, pp 143-171, 2005.

Oxford, R. of Thermal Ceramics with J. Beck and N. Keltner, Personal Communication, 2005.

Romero, C., “Pretest Complex Calorimeter CALORE Simulations, Sandia internal memo to T. Blanchat, dated Sept. 10, 2004.

Romero, V.J., M.P. Sherman, J.F. Dempsey, L.R. Edwards, K.C. Chen, R.V. Baron, C.F. King, "Development and Illustration of Model Validation Concepts on a Component Failure Model," paper AIAA-2004-1991. 45th AIAA/ASME/ASCE/AHS/ASC Structures, Structural Dynamics, and Materials Conference, April 19-22, 2004, Palm Springs, CA.

Sherman, M.P., Sandia Internal Memorandum to V. J. Romero, T. Blanchat, A. R. Black, J. W. Shelton III, M. Pilch, “Matching Blanchat’s location of thermocouples on complex calorimeter outer shell,” February 2, 2005 (Revised 2/9/05 & 6/16/05)

Tieszen, Sheldon R., Timothy J. OHern, Robert W. Schefer, and Leroy D. Perea, Spatial and Temporal Resolution of Fluid Flows: LDRD Final Report, SAND98-0338, Sandia National Laboratories, February 1998.

Tieszen, S.R., O'Hern, T.J., Schefer, R.O., Weckman, E.J., and Blanchat, T.K., "Experimental Study of the Flow Field In and Around A One Meter Diameter Methane Fire," Combustion and Flame, 129:378-391, 2002

Tieszen, Sheldon R., Timothy J. OHern, Robert W. Schefer, and Leroy D. Perea, Spatial and Temporal Resolution of Fluid Flows: LDRD Final Report, SAND98-0338, Sandia National Laboratories, February 1998.

APPENDIX A ENGINEERING DRAWINGS OF THE COMPLEX CALORIMETER

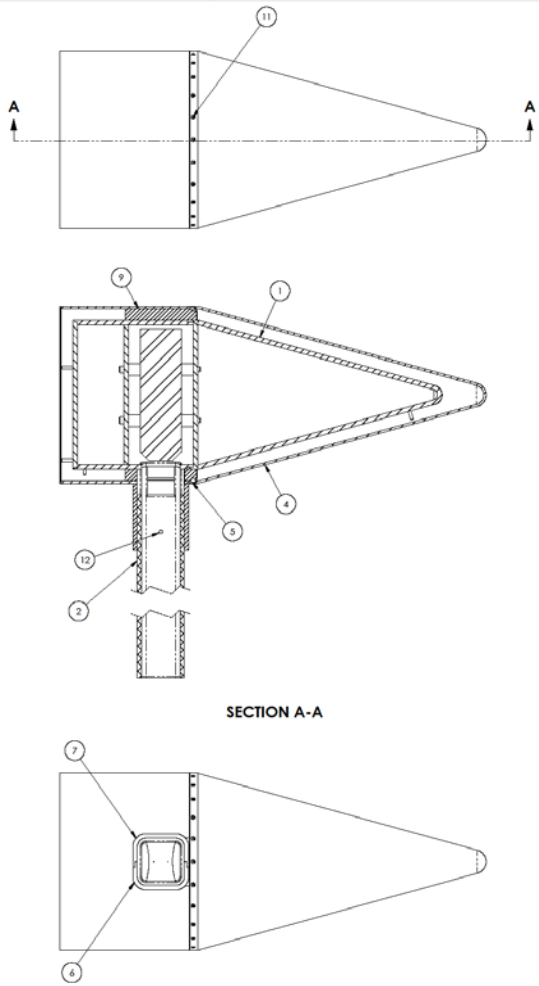

DESIGN AGENCY PART NUMBER	REVISION ISSUE	SHEET ZONE	PREPARED BY	DESCRIPTION	DATE	CHKD	APVD
R63033-000	A		D. SAMUEL, 2992/ P. H. HELMICK, 6871/T. BLANCHAT,9132		3/17/2004		PHH

QTY.	PART NO.	DESCRIPTION	NOTE	ZONE	ITEM
2		SCREW, MACH, FLAT, SOC, .313-18UNC, .75 LG			12
24		SCREW, MACH, FLAT, SOC, .164-32UNC-2A, .438 LG			11
1	R63046-000	INSULATION, MID SECTION			9
1	R63044-000	SUPPORT TUBE COLLAR, RIGHT			7
1	R63043-000	SUPPORT TUBE COLLAR, LEFT			6
1	R63042-000	OUTER SHELL INSERT			5
1	R63041-000	OUTER SHELL CONE			4
1	R63040-000	OUTER SHELL ASSEMBLY			3
1	R63039-000	SUPPORT TUBE			2
1	R63034-000	INNER SHELL ASSEMBLY			1
NA	9919100	MARKING, GENERAL METHODS			
NA	9900000	GENERAL REQUIREMENTS AND DRAWING INTERPRETATION			

ALT-ALTERNATE AR-AS REQ'D ARS-AS REQ'D PER ASSY EM-EXPENSE MATERIAL NA-DOCUMENT PM-PROCESS MATERIAL

SHEET	1 2 3 4 5 6
ISSUE	A
PART CLASSIFICATION	UNCLASSIFIED
DRAWING CLASSIFICATION	UNCLASSIFIED
TITLE	COMPLEX CALORIMETER ASSEMBLY
SIZE	D
DRAWING NUMBER	R63033
CAGE	14213
SCALE	1:4
SHEET	1 OF 1
STATUS	SA-REL-3/17/2004
ORIGIN	SolidWorks 2004

GEOMETRIC PRECISION = NA

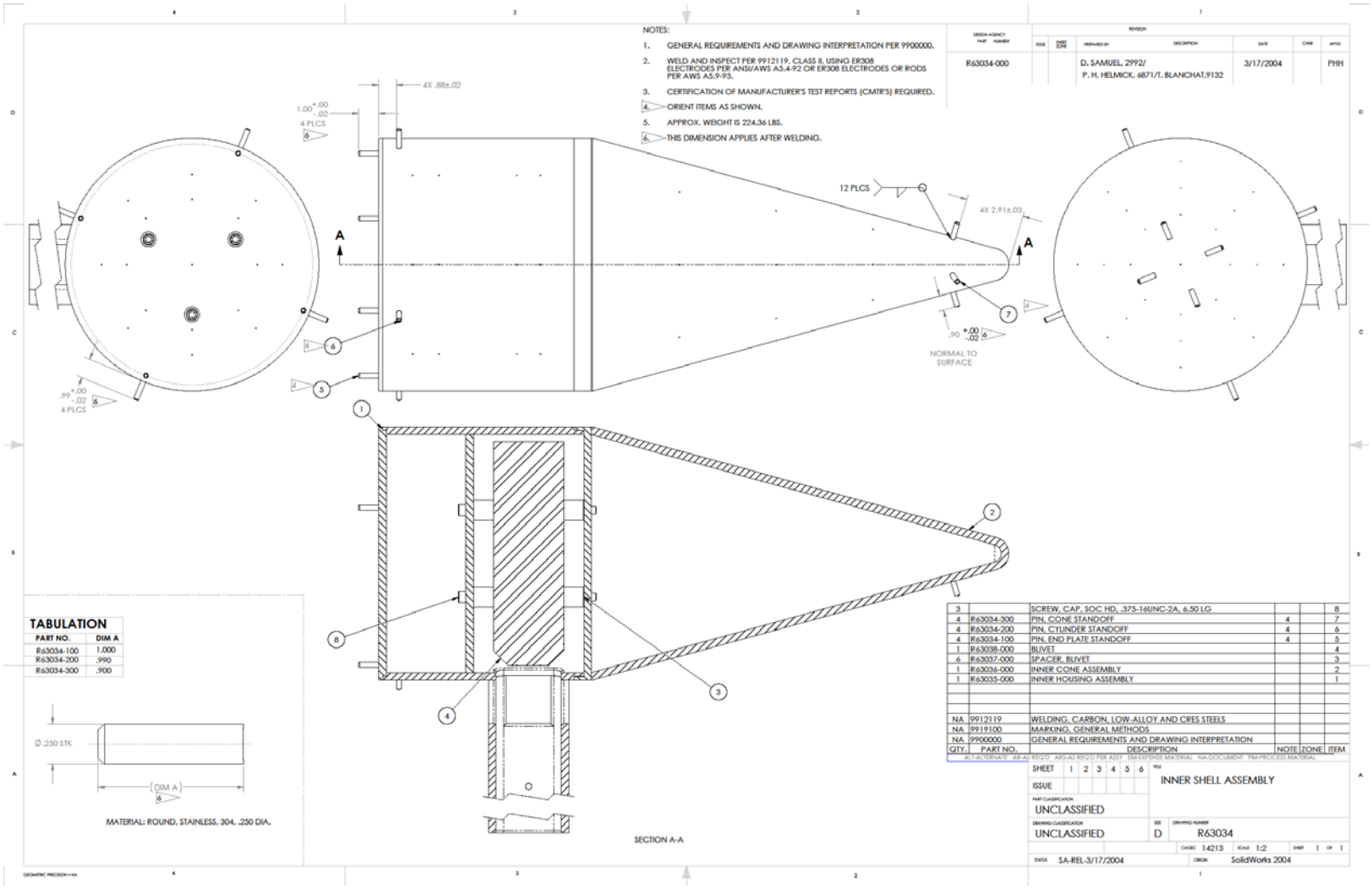
NOTES:
1. GENERAL REQUIREMENTS AND DRAWING INTERPRETATION PER 9900000.
2. WELD AND INSPECT PER 9912119. CLASS II, USING ER308 ELECTRODES PER ANSI/AWS A5.4-92 OR ER308 ELECTRODES OR RODS PER AWS A5.9-93.
3. CERTIFICATION OF MANUFACTURER'S TEST REPORTS (CMTR'S) REQUIRED.
4. ORIENT ITEMS AS SHOWN.
5. APPROX. WEIGHT IS 224.36 LBS.
6. THIS DIMENSION APPLIES AFTER WELDING.
DESIGN AGENCY PART NUMBER
R63034-000
REVISION
ISSUE
DATE CODE
PREPARED BY
DESCRIPTION
DATE
CHKR
APVD
D. SAMUEL, 2992/
P. H. HELMICK, 6871/T. BLANCHAT,9132
3/17/2004
PHH
4X .88±.02
1.00 +.00 -.02
4 PLCS
12 PLCS
4X 2.91±.03
A
A
.90 +.00 -.02
NORMAL TO SURFACE
.99 +.00 -.02
4 PLCS
SECTION A-A
TABULATION
PART NO. DIM A
R63034-100 1.000
R63034-200 .990
R63034-300 .900
Ø .250 STK
DIM A
MATERIAL: ROUND, STAINLESS, 304, .250 DIA.
3 SCREW, CAP, SOC HD, .375-16UNC-2A, 6.50 LG 8
4 R63034-300 PIN, CONE STANDOFF 4 7
4 R63034-200 PIN, CYLINDER STANDOFF 4 6
4 R63034-100 PIN, END PLATE STANDOFF 4 5
1 R63038-000 BLIVET 4
6 R63037-000 SPACER, BLIVET 3
1 R63036-000 INNER CONE ASSEMBLY 2
1 R63035-000 INNER HOUSING ASSEMBLY 1
NA 9912119 WELDING, CARBON, LOW-ALLOY AND CRES STEELS
NA 9919100 MARKING, GENERAL METHODS
NA 9900000 GENERAL REQUIREMENTS AND DRAWING INTERPRETATION
QTY. PART NO. DESCRIPTION NOTE ZONE ITEM
ALT-ALTERNATE AR-AS REQ'D AKS-AS REQ'D FOR ASSY EM-EXPENDED MATERIAL NA-DOCUMENT PM-PROCESS MATERIAL
SHEET 1 2 3 4 5 6
ISSUE
INNER SHELL ASSEMBLY
PART CLASSIFICATION
UNCLASSIFIED
DRAWING CLASSIFICATION
UNCLASSIFIED
SIZE D
DRAWING NUMBER R63034
CAGE/RC 14213
SCALE 1:2
SHEET 1 OF 1
STATE SA-REL-3/17/2004
ORIGIN SolidWorks 2004

NOTES:

1. GENERAL REQUIREMENTS AND DRAWING INTERPRETATION PER 9900000.
2. FIELD WELD AND INSPECT PER 9912119, CLASS II, USING ER308 ELECTRODES PER ANSI/AWS A5.4-92 OR ER308 ELECTRODES OR RODS PER AWS A5.9-93.
3. CERTIFICATION OF MANUFACTURER'S TEST REPORTS (CMTR'S) REQUIRED.
4. ORIENT ITEMS AS SHOWN.
5. APPROX. WEIGHT IS 63.1 LBS.
6. APPLIES AFTER WELDING.

DESIGN AGENCY PART NUMBER	REVISION: ISSUE	SHEET ZONE	PREPARED BY	DESCRIPTION	DATE	CHKR	APVD
R63035-000			D. SAMUEL, 2992/ P. H. HELMICK, 6871/T. BLANCHAT,9132		3/17/2004		PHH

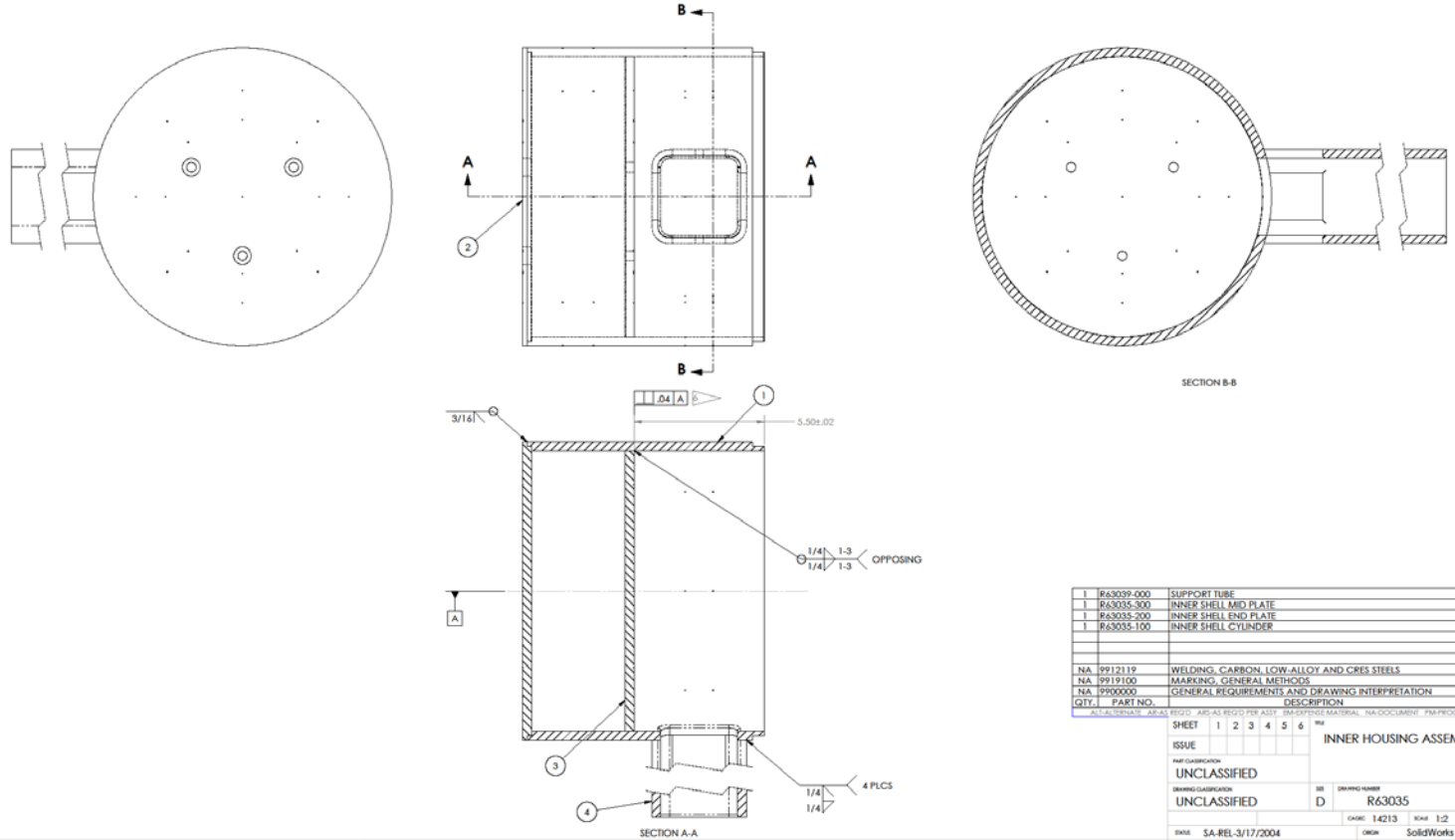

QTY.	PART NO.	DESCRIPTION	NOTE	ZONE	ITEM
1	R63039-000	SUPPORT TUBE			4
1	R63035-300	INNER SHELL MID PLATE			3
1	R63035-200	INNER SHELL END PLATE			2
1	R63035-100	INNER SHELL CYLINDER			1
NA	9912119	WELDING, CARBON, LOW-ALLOY AND CRES STEELS			
NA	9919100	MARKING, GENERAL METHODS			
NA	9900000	GENERAL REQUIREMENTS AND DRAWING INTERPRETATION			

AL-ALTERNATE AR-AS REQ'D ARS-AS REQ'D PER ASST DM-DEFINE MATERIAL NA-DOCUMENT PM-PROCESS MATERIAL

SHEET 1 2 3 4 5 6 TITLE INNER HOUSING ASSEMBLY

ISSUE

PART CLASSIFICATION UNCLASSIFIED

DRAWING CLASSIFICATION UNCLASSIFIED

SIZE D DRAWING NUMBER R63035

CAGE/RC 14213 SCALE 1:2 SHEET 1 OF 3

STATE SA-REL-3/17/2004 ORIGIN SolidWorks 2004

GEOMETRIC PRECISION = NA

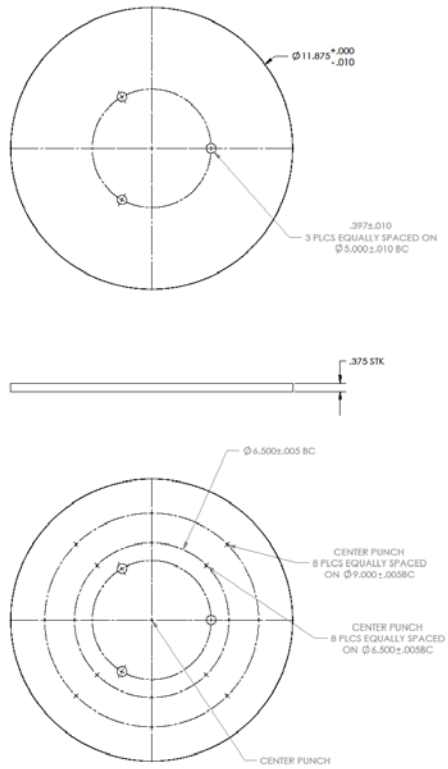

DETAIL: ITEM 3

MAT'L: STEEL, STAINLESS, 304, .375 THK

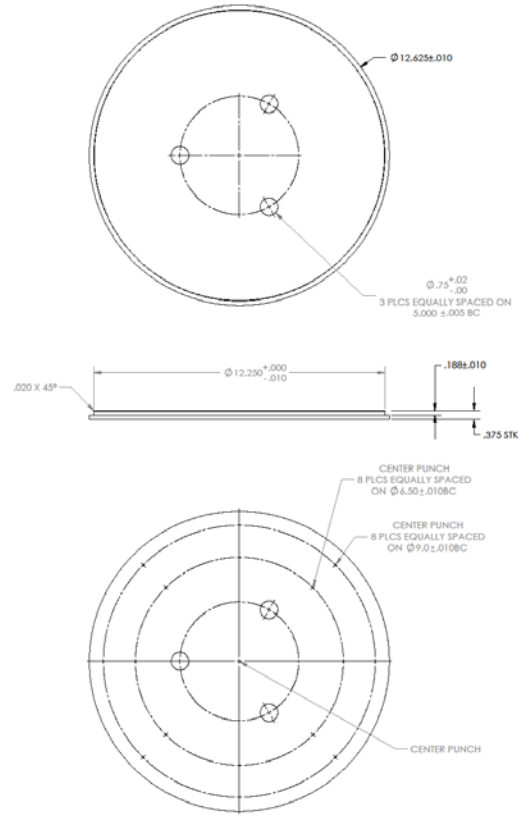

DETAIL: ITEM 2

MAT'L: STEEL, STAINLESS, 304, .375 THK

DRAWING NUMBER
R63035
DRAWING CLASSIFICATION
UNCLASSIFIED

SIZE	CAGE CODE	SCALE	
D	14213	1:2	
	SOLIDWORKS	SHEET	2 OF 3

STATUS SA-REL-3/17/2004

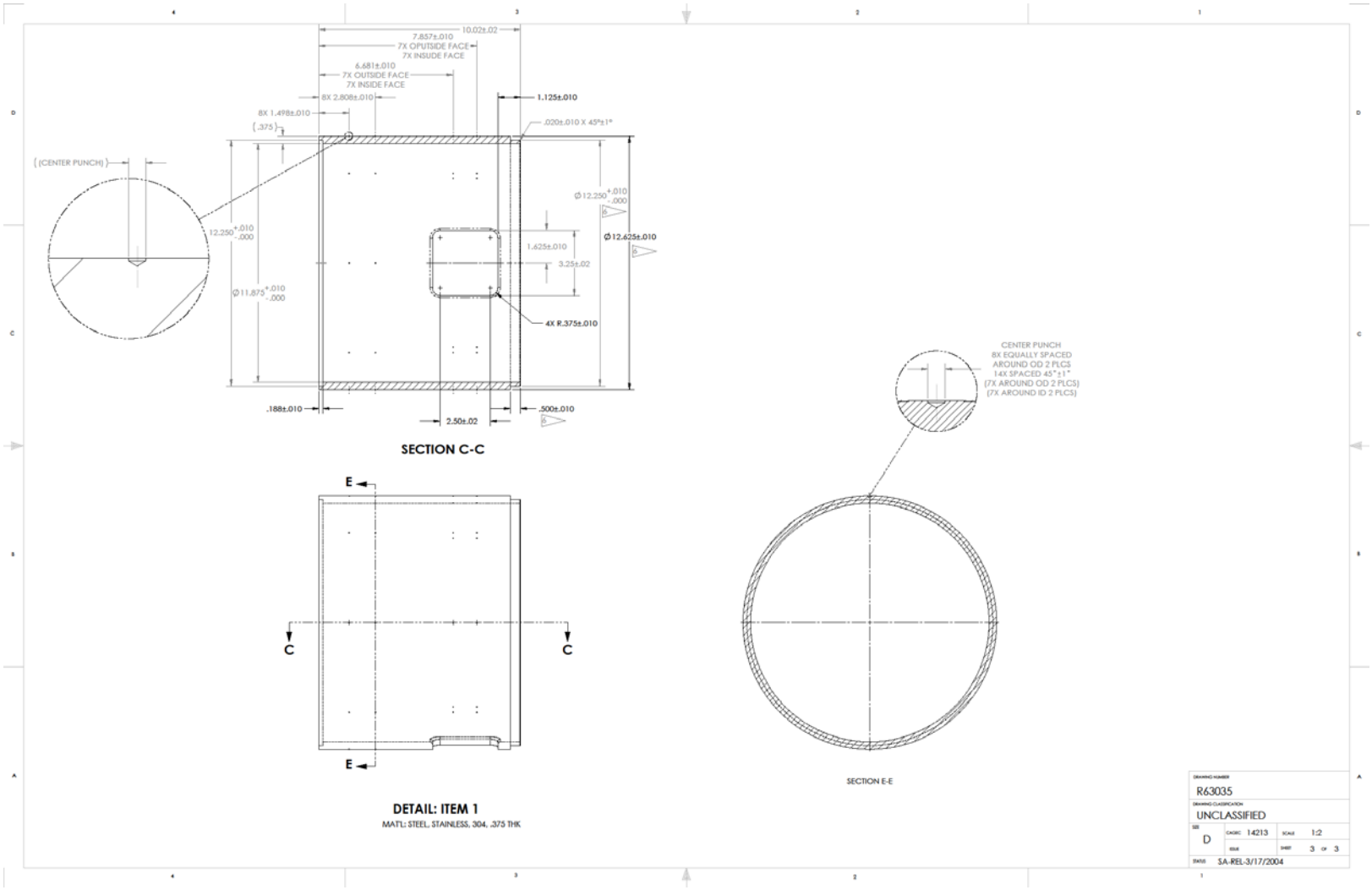
7.857±.010
10.02±.02
7X OPUTSIDE FACE
7X INSUDE FACE
6.681±.010
7X OUTSIDE FACE
7X INSIDE FACE
8X 2.808±.010
8X 1.498±.010
(.375)
1.125±.010
.020±.010 X 45°±1°
(CENTER PUNCH)
12.250 +.010 -.000
Ø11.875 +.010 -.000
Ø12.250 +.010 -.000
Ø12.625±.010
1.625±.010
3.25±.02
4X R.375±.010
.188±.010
2.50±.02
.500±.010
SECTION C-C
E
C
C
E
DETAIL: ITEM 1
MATL: STEEL, STAINLESS, 304, .375 THK
CENTER PUNCH
8X EQUALLY SPACED
AROUND OD 2 PLCS
14X SPACED 45°±1°
(7X AROUND OD 2 PLCS)
(7X AROUND ID 2 PLCS)
SECTION E-E
DRAWING NUMBER
R63035
DRAWING CLASSIFICATION
UNCLASSIFIED
SIZE
D
CAGE NO. 14213
SCALE 1:2
SHEET 3 OF 3
STATUS SA-REL-3/17/2004

NOTES:

1. GENERAL REQUIREMENTS AND DRAWING INTERPRETATION PER 9900000.
2. WELD AND INSPECT PER 9912119, CLASS II, USING ER308 ELECTRODES PER ANSI/AWS A5.4-92 OR ER308 ELECTRODES OR RODS PER AWS A5.9-93.
3. CERTIFICATION OF MANUFACTURER'S TEST REPORTS (CMTR'S) REQUIRED.
4. ORIENT ITEMS AS SHOWN.
5. APPROX. WEIGHT IS 61.63 LBS.
6. THIS AREA TO BE MACHINED AFTER WELDING.

DESIGN AGENCY PART NUMBER	REVISION						
	ISSUE	SHEET ZONE	PREPARED BY	DESCRIPTION	DATE	CHKR	APVD
R63036-000			D. SAMUEL, 2992/ P. H. HELMICK, 6871/T. BLANCHAT,9132		3/17/2004		PHH

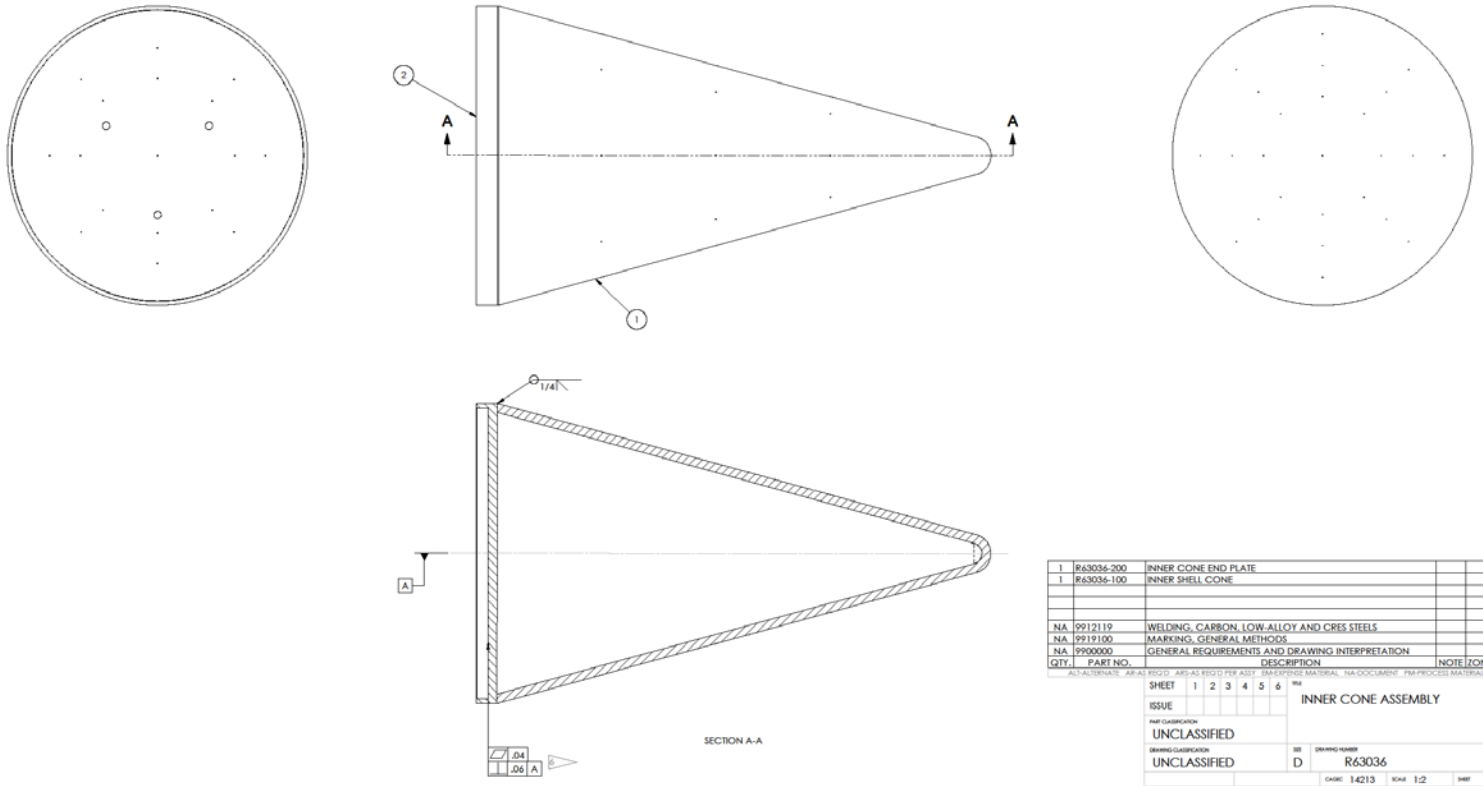

QTY.	PART NO.	DESCRIPTION	NOTE	ZONE	ITEM
1	R63036-200	INNER CONE END PLATE			2
1	R63036-100	INNER SHELL CONE			1
NA	9912119	WELDING, CARBON, LOW-ALLOY AND CRES STEELS			
NA	9919100	MARKING, GENERAL METHODS			
NA	9900000	GENERAL REQUIREMENTS AND DRAWING INTERPRETATION			

ALT-ALTERNATE AR-AS 8512/D AR3-AS 8512/D PER ASST DM-DEFINED MATERIAL NA-DOCUMENT PM-PROCESS MATERIAL

SHEET 1 2 3 4 5 6

ISSUE

TITLE INNER CONE ASSEMBLY

PART CLASSIFICATION UNCLASSIFIED

DRAWING CLASSIFICATION UNCLASSIFIED

SIZE D DRAWING NUMBER R63036

CAGE/RC 14213 SCALE 1:2 SHEET 1 OF 2

STATE SA-REL-3/17/2004 ORIGIN SolidWorks 2004

GEOMETRIC PRECISION = NA

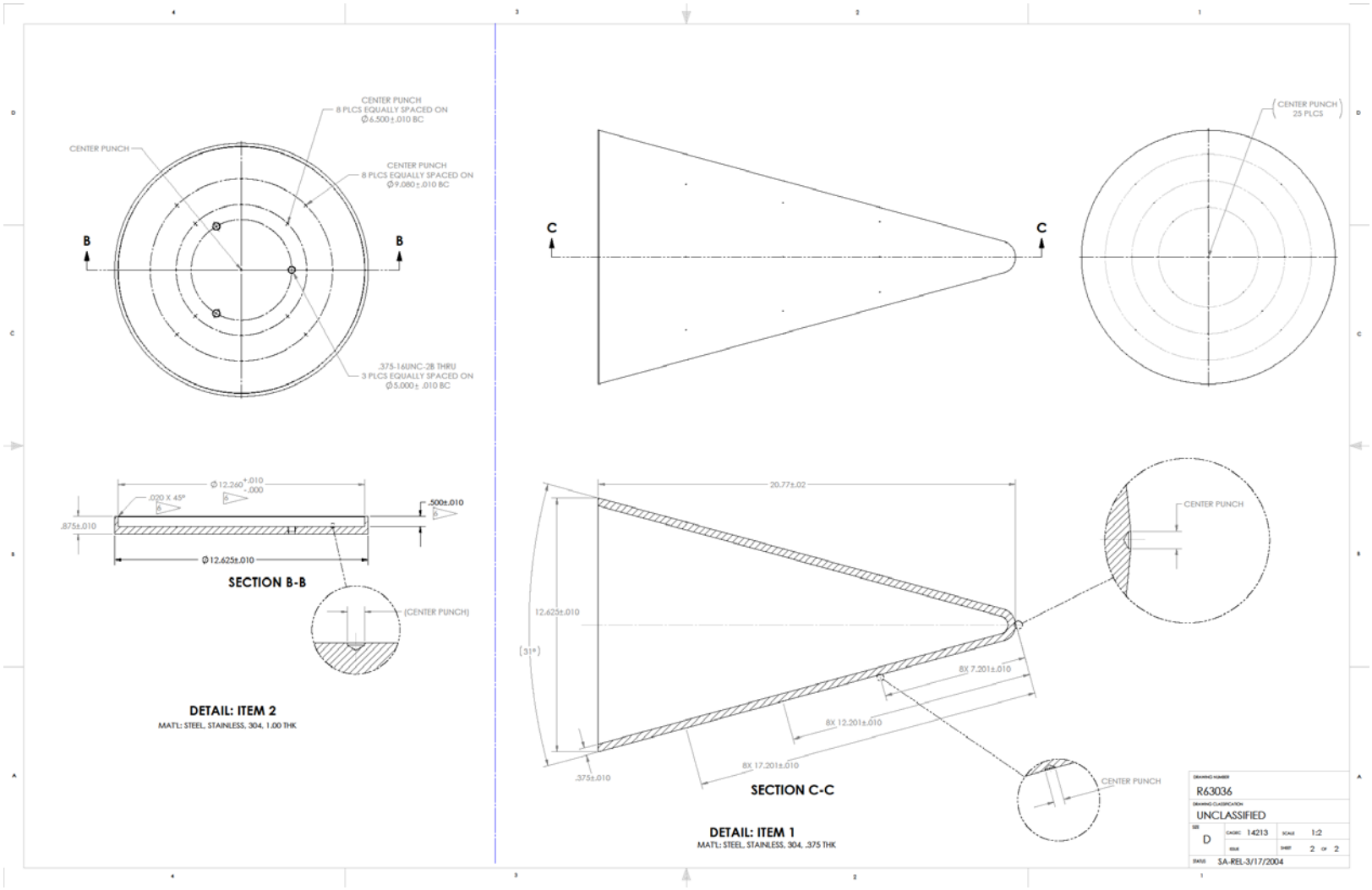
CENTER PUNCH
8 PLCS EQUALLY SPACED ON
Ø6.500±.010 BC
CENTER PUNCH
CENTER PUNCH
8 PLCS EQUALLY SPACED ON
Ø9.080±.010 BC
B
B
.375-16UNC-2B THRU
3 PLCS EQUALLY SPACED ON
Ø5.000± .010 BC
Ø12.260 +.010 -.000
.020 X 45°
.875±.010
.500±.010
Ø12.625±.010
SECTION B-B
(CENTER PUNCH)
DETAIL: ITEM 2
MAT'L: STEEL, STAINLESS, 304, 1.00 THK
C
C
CENTER PUNCH
25 PLCS
20.77±.02
CENTER PUNCH
12.625±.010
(31°)
8X 7.201±.010
8X 12.201±.010
8X 17.201±.010
.375±.010
SECTION C-C
CENTER PUNCH
DETAIL: ITEM 1
MAT'L: STEEL, STAINLESS, 304, .375 THK
DRAWING NUMBER
R63036
DRAWING CLASSIFICATION
UNCLASSIFIED
SIZE
D
CAGE NO. 14213
SCALE 1:2
SHEET 2 OF 2
STATUS SA-REL-3/17/2004

UNCLASSIFIED

NOTES:

1. GENERAL REQUIREMENTS AND DRAWING INTERPRETATION PER 9900000.
2. MATERIAL: ROUND, STAINLESS, 304.
3. CERTIFICATION OF MANUFACTURER'S TEST REPORTS (CMTR'S) REQUIRED.
4. APPROX. WEIGHT IS 0.19 LBS.

DESIGN AGENCY PART NUMBER	REVISIONS						
	ISSUE	SHEET ZONE	PREPARED BY	DESCRIPTION	DATE	CHKR	APVD
R63037-000			D. SAMUEL, 2992/ P. H. HELMICK, 6871/T. BLANCHAT,9132		3/17/2004		PHH

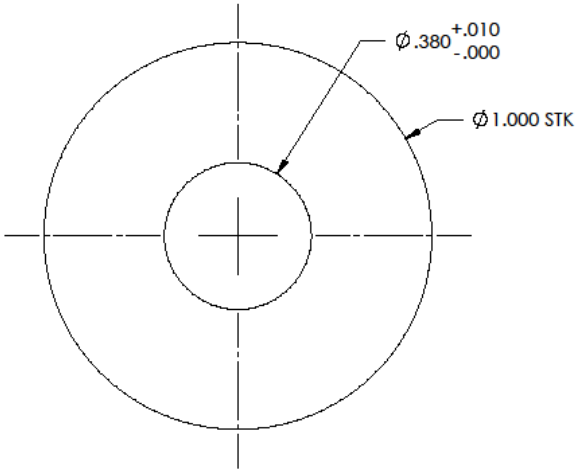

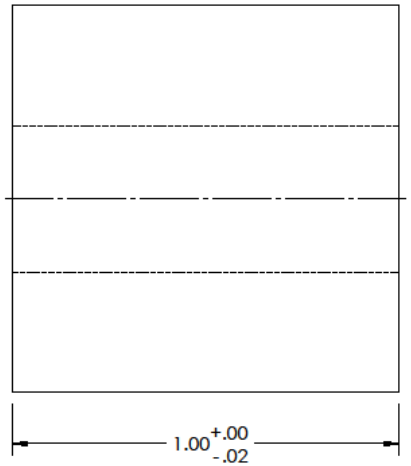

SHEET	1	2	3	4	5	6	TITLE SPACER. BLIVET
ISSUE							
PART CLASSIFICATION UNCLASSIFIED							
DRAWING CLASSIFICATION UNCLASSIFIED					SIZE B	DRAWING NUMBER R63037	
				CAGE: 14213	SCALE 4:1	SHEET 1 OF 1	
STATUS SA-REL-3/17/2004				ORIGIN SolidWorks 2004			

GEOMETRIC PRECISION = NA

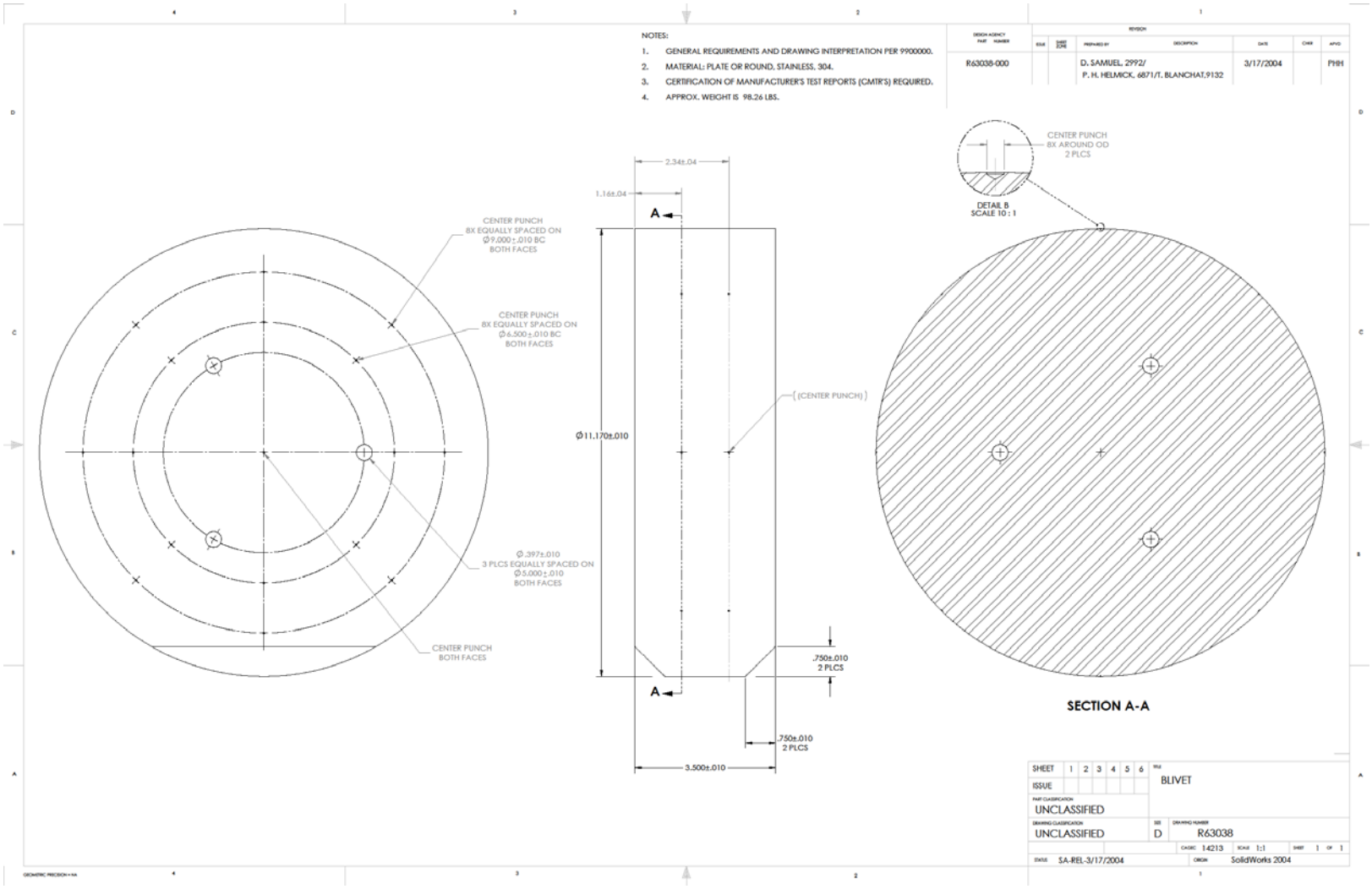
NOTES:
1. GENERAL REQUIREMENTS AND DRAWING INTERPRETATION PER 9900000.
2. MATERIAL: PLATE OR ROUND, STAINLESS, 304.
3. CERTIFICATION OF MANUFACTURER'S TEST REPORTS (CMTR'S) REQUIRED.
4. APPROX. WEIGHT IS 98.26 LBS.
R63038-000
D. SAMUEL, 2992/
P. H. HELMICK, 6871/T. BLANCHAT,9132
3/17/2004
PHH
CENTER PUNCH
8X EQUALLY SPACED ON
Ø9.000±.010 BC
BOTH FACES
CENTER PUNCH
8X EQUALLY SPACED ON
Ø6.500±.010 BC
BOTH FACES
Ø.397±.010
3 PLCS EQUALLY SPACED ON
Ø5.000±.010
BOTH FACES
CENTER PUNCH
BOTH FACES
2.34±.04
1.16±.04
A
Ø11.170±.010
(CENTER PUNCH)
.750±.010
2 PLCS
3.500±.010
CENTER PUNCH
8X AROUND OD
2 PLCS
DETAIL B
SCALE 10 : 1
SECTION A-A
SHEET 1 2 3 4 5 6
ISSUE
BLIVET
UNCLASSIFIED
UNCLASSIFIED
D
R63038
14213
1:1
1 OF 1
SA-REL-3/17/2004
SolidWorks 2004

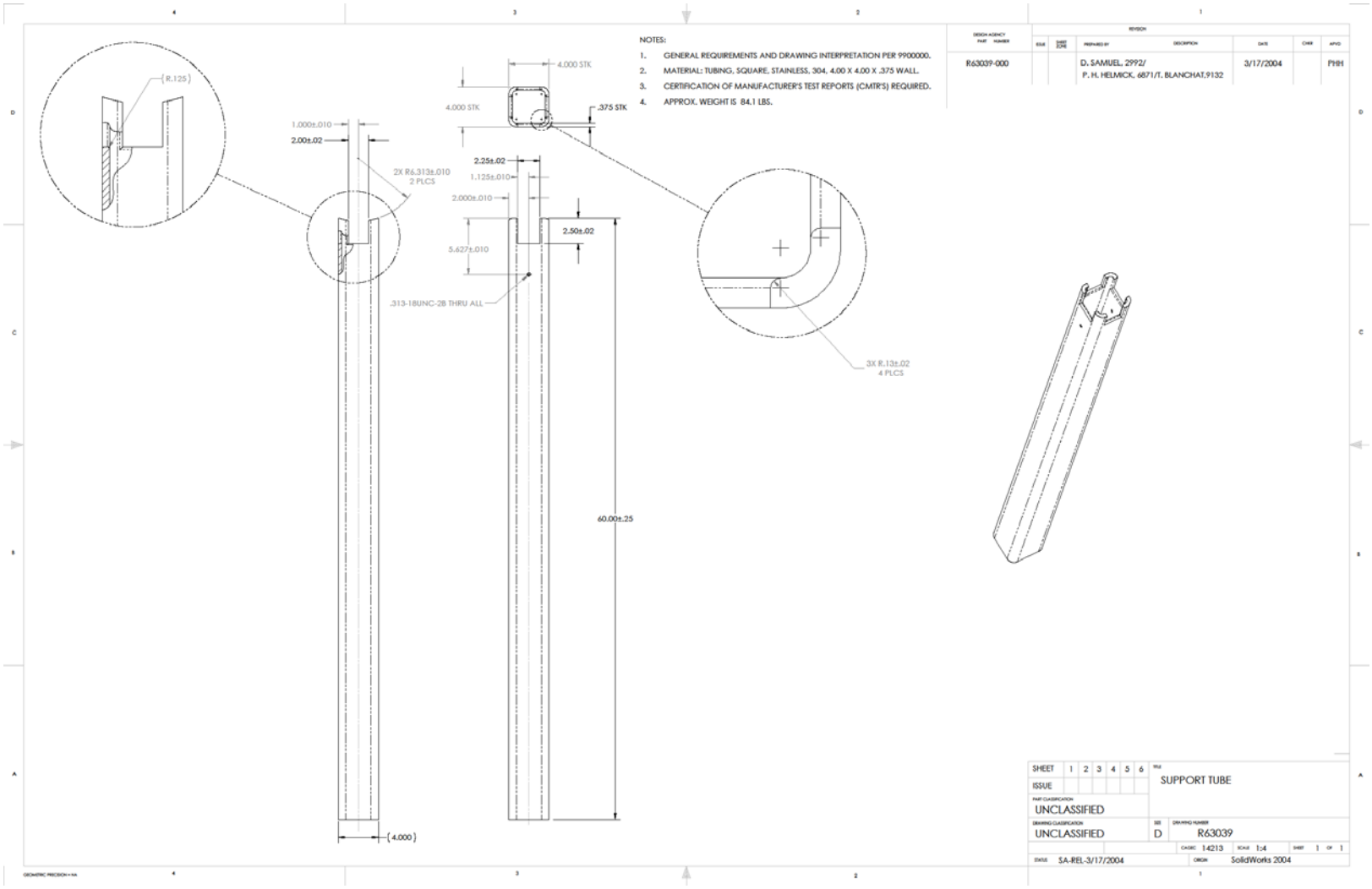
NOTES:
1. GENERAL REQUIREMENTS AND DRAWING INTERPRETATION PER 9900000.
2. MATERIAL: TUBING, SQUARE, STAINLESS, 304, 4.00 X 4.00 X .375 WALL.
3. CERTIFICATION OF MANUFACTURER'S TEST REPORTS (CMTR'S) REQUIRED.
4. APPROX. WEIGHT IS 84.1 LBS.
DESIGN AGENCY PART NUMBER
R63039-000
REVISION
ISSUE
DATE CODE
PREPARED BY
DESCRIPTION
DATE
CHKR
APVD
D. SAMUEL, 2992/
P. H. HELMICK, 6871/T. BLANCHAT,9132
3/17/2004
PHH
(R.125)
1.000±.010
2.00±.02
2X R6.313±.010
2 PLCS
4.000 STK
4.000 STK
.375 STK
2.25±.02
1.125±.010
2.000±.010
2.50±.02
5.627±.010
.313-18UNC-2B THRU ALL
3X R.13±.02
4 PLCS
60.00±.25
(4.000)
SHEET 1 2 3 4 5 6
ISSUE
PART CLASSIFICATION
UNCLASSIFIED
DRAWING CLASSIFICATION
UNCLASSIFIED
TITLE
SUPPORT TUBE
SIZE
D
DRAWING NUMBER
R63039
CAGE CODE 14213
SCALE 1:4
SHEET 1 OF 1
STATUS SA-REL-3/17/2004
ORIGIN SolidWorks 2004

NOTES:

1. GENERAL REQUIREMENTS AND DRAWING INTERPRETATION PER 9900000.
2. WELD AND INSPECT PER 9912119, CLASS II, USING ER308 ELECTRODES PER ANSI/AWS A5.4-92 OR ER308 ELECTRODES OR RODS PER AWS A5.9-93.
3. CERTIFICATION OF MANUFACTURER'S TEST REPORTS (CMTR'S) REQUIRED.
4. ORIENT ITEMS AS SHOWN.
5. APPROX. WEIGHT IS 37.05 LBS.

DESIGN AGENCY PART NUMBER	REVISION					
	ISSUE	ZONE	PREPARED BY / DESCRIPTION	DATE	CHKR	APVD
R63040-000	A		D. SAMUEL, 2992/ P. H. HELMICK, 6871.T. BLANCHAT, 9132	3/17/2004		PHH
	B	2A4	D. SAMUEL, 2992/ P. H. HELMICK, 6871/T. BLANCHAT,9132 CORRECTED DWG NO. & ISSUE DISPLAY CHANGED T/C BOLT CIRCLES	12/7/2004		PHH

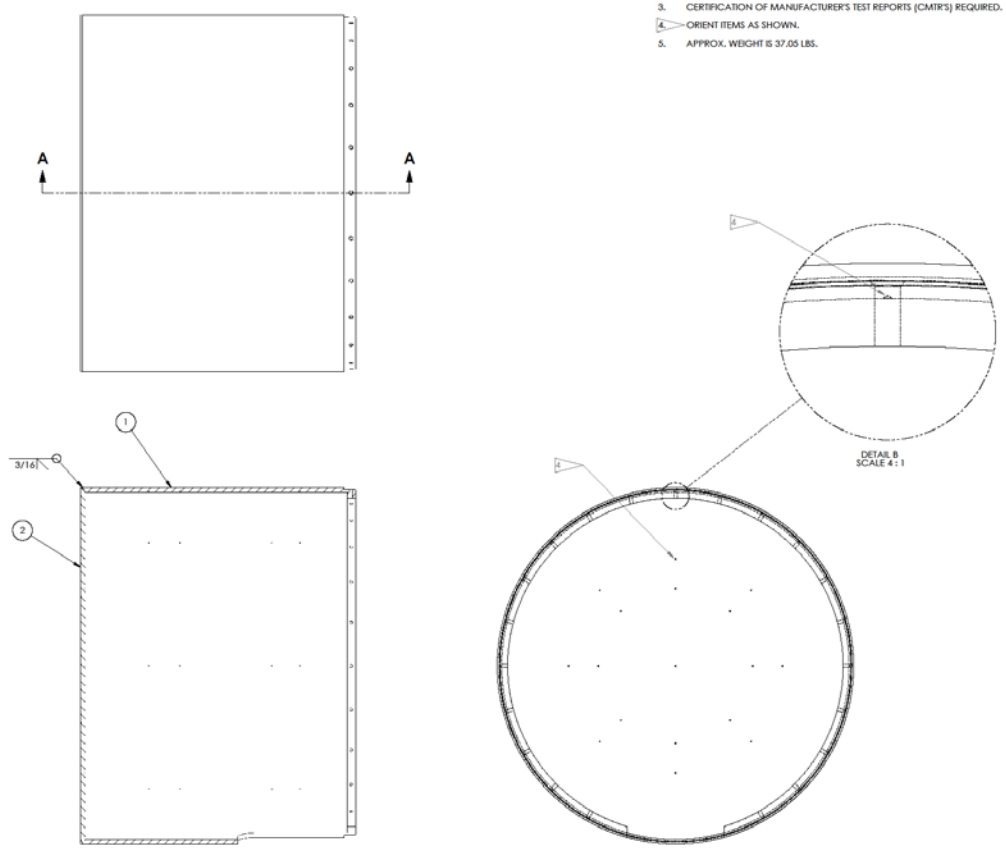

QTY.	PART NO.	DESCRIPTION	NOTE	ZONE	ITEM
1	R63040-200	OUTER SHELL END PLATE			2
1	R63040-100	OUTER SHELL			1
NA	9912119	WELDING, CARBON, LOW-ALLOY AND CRES STEELS			
NA	9919100	MARKING, GENERAL METHODS			
NA	9900000	GENERAL REQUIREMENTS AND DRAWING INTERPRETATION			

ALT-ALTERNATE AR-AS REQ'D AR5-AS REQ'D PER ASST EM-EXPENSE MATERIAL NA-DOCUMENT PM-PROCESS MATERIAL

SHEET	1	2	3	4	5	6
ISSUE	B	B				

TITLE: OUTER SHELL ASSEMBLY

PART CLASSIFICATION: UNCLASSIFIED

DRAWING CLASSIFICATION: UNCLASSIFIED

SIZE: D DRAWING NUMBER: R63040

CAGE: 14213 SCALE: 1:1 SHEET 1 OF 2

STATE: SA-CHK-12/7/2004 ORIGIN: SolidWorks 2004

C:\Data\maven\Fy04\COMPLEX_CALORIMETER\dsamuel\FROM_DAVID_S-05_13_2004\

GEOMETRIC PRECISION = NA

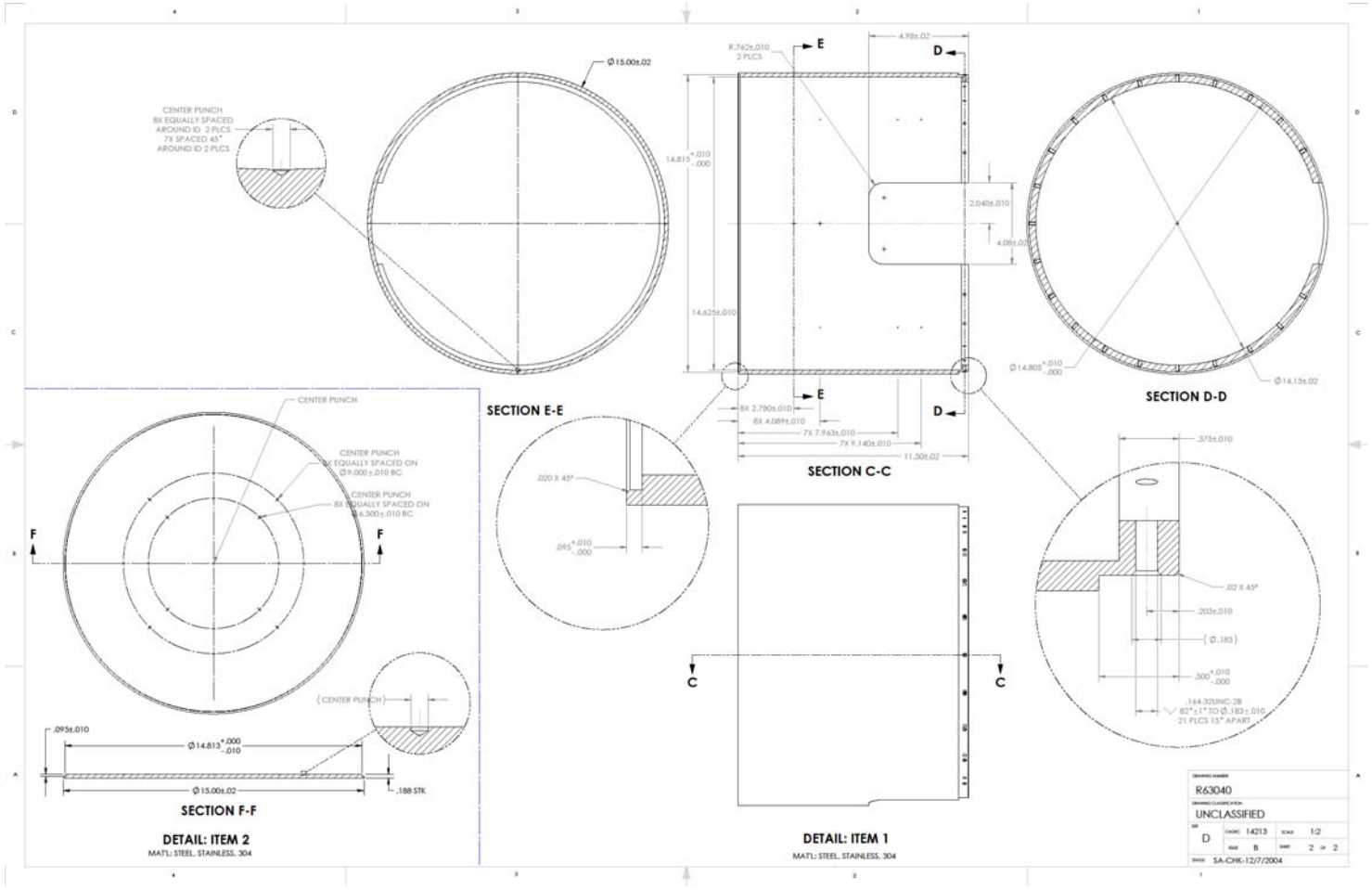
CENTER PUNCH
8X EQUALLY SPACED
AROUND ID 2 PLCS
7X SPACED 45°
AROUND ID 2 PLCS
Ø15.00±.02
R.762±.010
2 PLCS
E
D
4.98±.02
14.815 +.010 -.000
2.040±.010
4.08±.02
14.625±.010
Ø14.805 +.010 -.000
Ø14.13±.02
SECTION D-D
SECTION E-E
8X 2.780±.010
8X 4.089±.010
7X 7.963±.010
7X 9.140±.010
11.50±.02
SECTION C-C
.020 X 45°
.095 +.010 -.000
CENTER PUNCH
CENTER PUNCH
8X EQUALLY SPACED ON
Ø9.000±.010 BC
CENTER PUNCH
8X EQUALLY SPACED ON
Ø6.500±.010 BC
F
F
(CENTER PUNCH)
.095±.010
Ø14.813 +.000 -.010
Ø15.00±.02
.188 STK
SECTION F-F
DETAIL: ITEM 2
MAT'L: STEEL, STAINLESS, 304
C
C
DETAIL: ITEM 1
MAT'L: STEEL, STAINLESS, 304
.375±.010
.02 X 45°
.203±.010
(Ø.183)
.500 +.010 -.000
.164-32UNC-2B
82°±1° TO Ø.183±.010
21 PLCS 15° APART
R63040
UNCLASSIFIED
D
CAGE 14213
SCALE 1:2
SIZE B
SHEET 2 OF 2
SA-CHK-12/7/2004

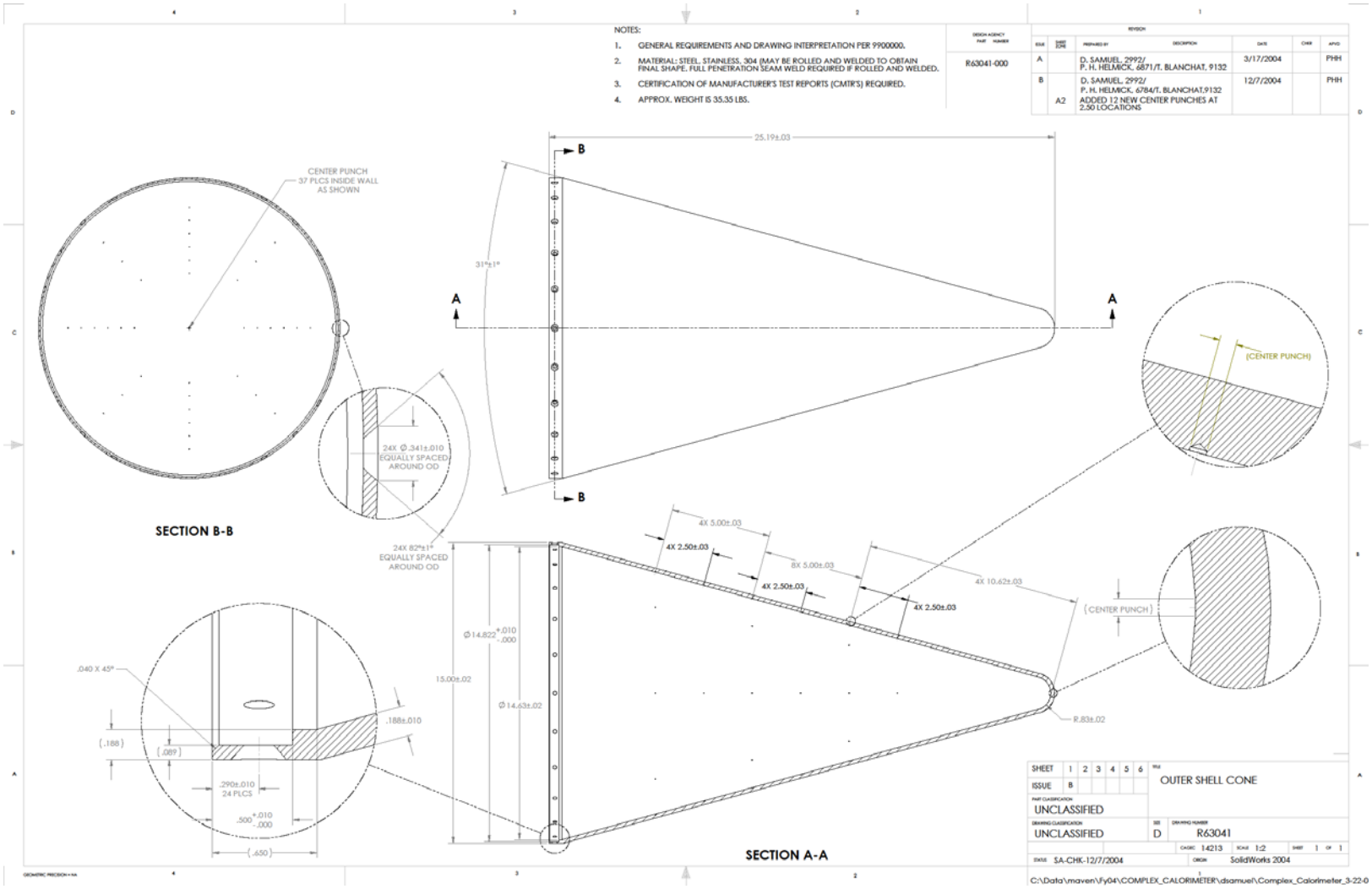
NOTES:
1. GENERAL REQUIREMENTS AND DRAWING INTERPRETATION PER 9900000.
2. MATERIAL: STEEL, STAINLESS, 304 (MAY BE ROLLED AND WELDED TO OBTAIN FINAL SHAPE. FULL PENETRATION SEAM WELD REQUIRED IF ROLLED AND WELDED.
3. CERTIFICATION OF MANUFACTURER'S TEST REPORTS (CMTR'S) REQUIRED.
4. APPROX. WEIGHT IS 35.35 LBS.
DESIGN AGENCY PART NUMBER
R63041-000
REVISION
A D. SAMUEL, 2992/ P. H. HELMICK, 6871/T. BLANCHAT, 9132 3/17/2004 PHH
B A2 D. SAMUEL, 2992/ P. H. HELMICK, 6784/T. BLANCHAT,9132 ADDED 12 NEW CENTER PUNCHES AT 2.50 LOCATIONS 12/7/2004 PHH
CENTER PUNCH 37 PLCS INSIDE WALL AS SHOWN
SECTION B-B
24X Ø .341±.010 EQUALLY SPACED AROUND OD
24X 82°±1° EQUALLY SPACED AROUND OD
25.19±.03
31°±1°
A
B
(CENTER PUNCH)
4X 5.00±.03
4X 2.50±.03
8X 5.00±.03
4X 10.62±.03
Ø14.822 +.010 -.000
15.00±.02
Ø14.63±.02
R.83±.02
.040 X 45°
.188±.010
(.188)
(.089)
.290±.010 24 PLCS
.500 +.010 -.000
(.650)
SECTION A-A
SHEET 1 2 3 4 5 6
ISSUE B
OUTER SHELL CONE
PART CLASSIFICATION UNCLASSIFIED
DRAWING CLASSIFICATION UNCLASSIFIED
SIZE D
DRAWING NUMBER R63041
CAGE/RC 14213
SCALE 1:2
SHEET 1 OF 1
STATE SA-CHK-12/7/2004
ORIGIN SolidWorks 2004
C:\Data\maven\Fy04\COMPLEX_CALORIMETER\dsamuel\Complex_Calorimeter_3-22-0

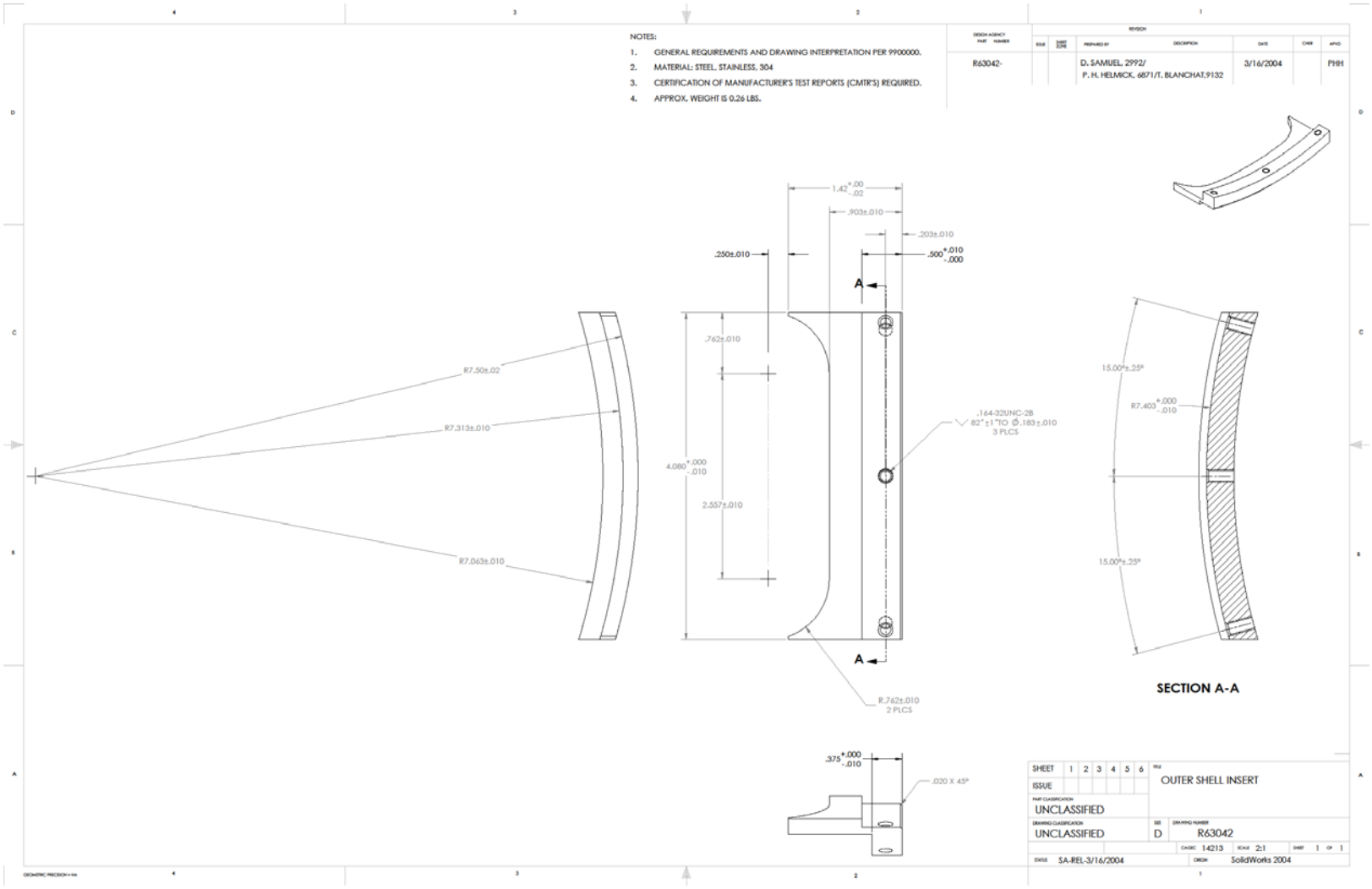
NOTES:
1. GENERAL REQUIREMENTS AND DRAWING INTERPRETATION PER 9900000.
2. MATERIAL: STEEL, STAINLESS, 304
3. CERTIFICATION OF MANUFACTURER'S TEST REPORTS (CMTR'S) REQUIRED.
4. APPROX. WEIGHT IS 0.26 LBS.
DESIGN AGENCY PART NUMBER
R63042-
REVISION
ISSUE
DATE
PREPARED BY
DESCRIPTION
DATE
CHKR
APVD
D. SAMUEL, 2992/
P. H. HELMICK, 6871/T. BLANCHAT,9132
3/16/2004
PHH
1.42 +.00 -.02
.903±.010
.203±.010
.250±.010
.500 +.010 -.000
A
R7.50±.02
R7.313±.010
R7.063±.010
.762±.010
4.080 +.000 -.010
2.557±.010
.164-32UNC-2B
82°±1° TO Ø.183±.010
3 PLCS
R.762±.010
2 PLCS
15.00°±.25°
R7.403 +.000 -.010
SECTION A-A
.375 +.000 -.010
.020 X 45°
SHEET 1 2 3 4 5 6
ISSUE
PART CLASSIFICATION
UNCLASSIFIED
DRAWING CLASSIFICATION
UNCLASSIFIED
TITLE
OUTER SHELL INSERT
SIZE
D
DRAWING NUMBER
R63042
CAGE CODE 14213
SCALE 2:1
SHEET 1 OF 1
STATE SA-REL-3/16/2004
ORIGIN SolidWorks 2004

NOTES:

1. GENERAL REQUIREMENTS AND DRAWING INTERPRETATION PER 9900000.
2. MATERIAL: STEEL, STAINLESS, 304
3. CERTIFICATION OF MANUFACTURER'S TEST REPORTS (CMTR'S) REQUIRED.
4. APPROX. WEIGHT IS 4.6 LBS.

DESIGN AGENCY PART NUMBER	REVISION						
	ISSUE	SHEET ZONE	PREPARED BY	DESCRIPTION	DATE	CHKR	APVD
R63043-			D. SAMUEL, 2992/ P. H. HELMICK, 6871/T. BLANCHAT,9132		3/17/2004		PHH

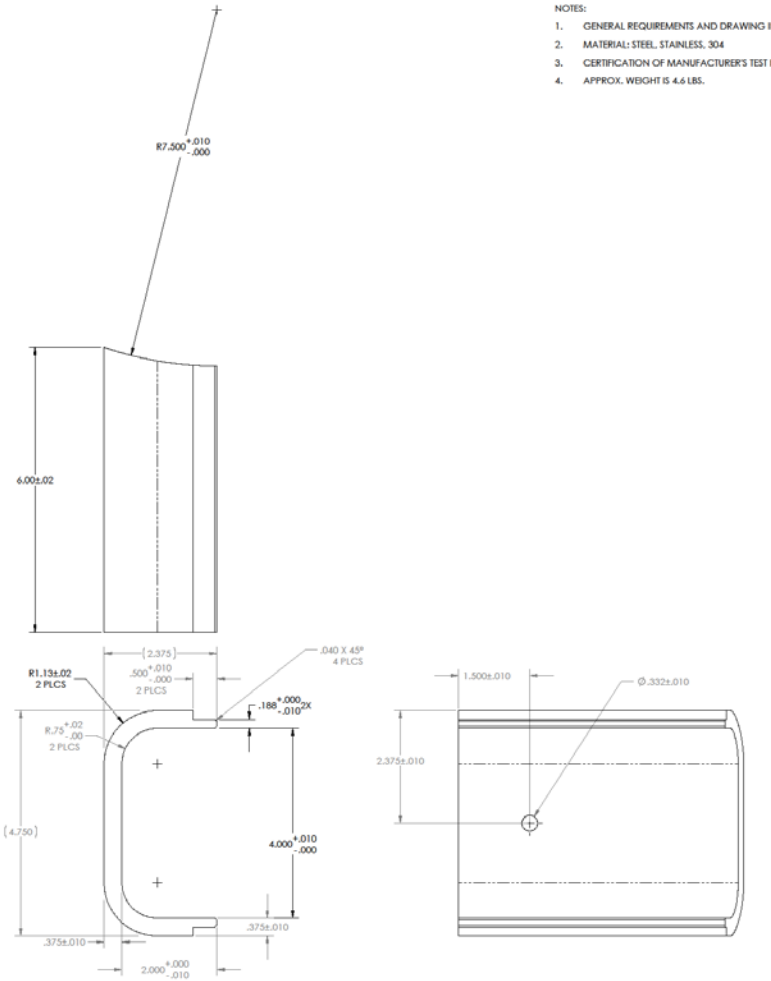

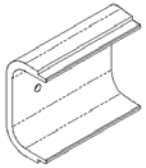

SHEET	1	2	3	4	5	6	TITLE	SUPPORT TUBE COLLAR, LEFT	
ISSUE									
PART CLASSIFICATION UNCLASSIFIED									
DRAWING CLASSIFICATION UNCLASSIFIED							SIZE D	DRAWING NUMBER R63043	
							CAGE NO. 14213	SCALE 1:1	SHEET 1 OF 1
STATUS SA-REL-3/17/2004							ORIGIN SolidWorks 2004		

NOTES:

1. GENERAL REQUIREMENTS AND DRAWING INTERPRETATION PER 9900000.
2. MATERIAL: STEEL, STAINLESS, 304
3. CERTIFICATION OF MANUFACTURER'S TEST REPORTS (CMTR'S) REQUIRED.
4. APPROX. WEIGHT IS 5.2 LBS.

DESIGN AGENCY PART NUMBER	REVISION						
	ISSUE	SHEET ZONE	PREPARED BY	DESCRIPTION	DATE	CHKR	APVD
R63044-			D. SAMUEL, 2992/ P. H. HELMICK, 6871/T. BLANCHAT,9132		3/17/2004		PHH

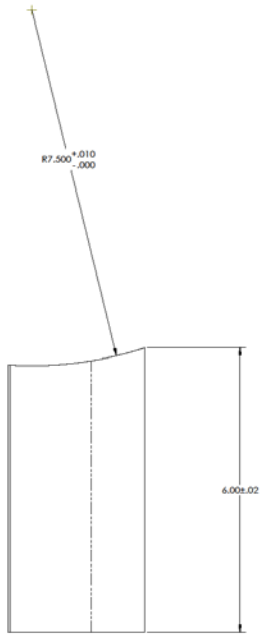

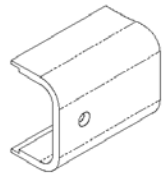

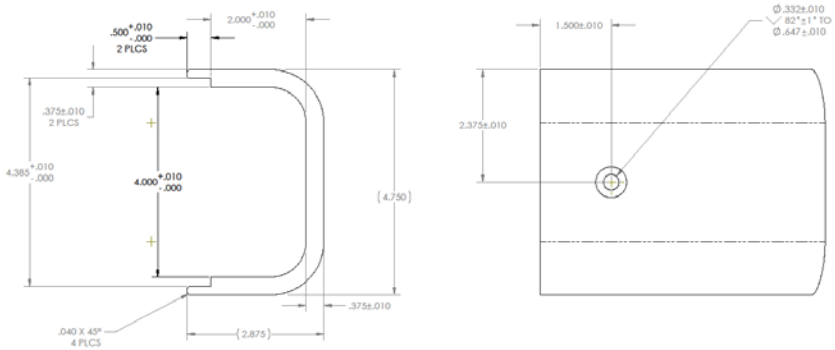

SHEET 1 2 3 4 5 6		TITLE	SUPPORT TUBE COLLAR, RIGHT
ISSUE			
PART CLASSIFICATION	UNCLASSIFIED		
DRAWING CLASSIFICATION	UNCLASSIFIED	SIZE D	DRAWING NUMBER R63044
		CAGE/C 14213	SCALE 1:1 SHEET 1 OF 1
STATE SA-REL-3/17/2004		ORIGIN SolidWorks 2004	

NOTES:

1. GENERAL REQUIREMENTS AND DRAWING INTERPRETATION PER 9900000.
2. MATERIAL: KOAWOOL BLANKET
3. CERTIFICATION OF MANUFACTURER'S TEST REPORTS (CMTR'S) REQUIRED.
4. SHAPE TO BE OBTAINED BY WRAPPING DURING ASSEMBLY PROCESS.
5. APPROX. WEIGHT IS 19.0 LBS.

DESIGN AGENCY PART NUMBER	REVISION						
	ISSUE	SHEET ZONE	PREPARED BY	DESCRIPTION	DATE	CHKR	APVD
R63045-000			D. SAMUEL, 2992/ P. H. HELMICK, 6871		3/17/2004		PHH

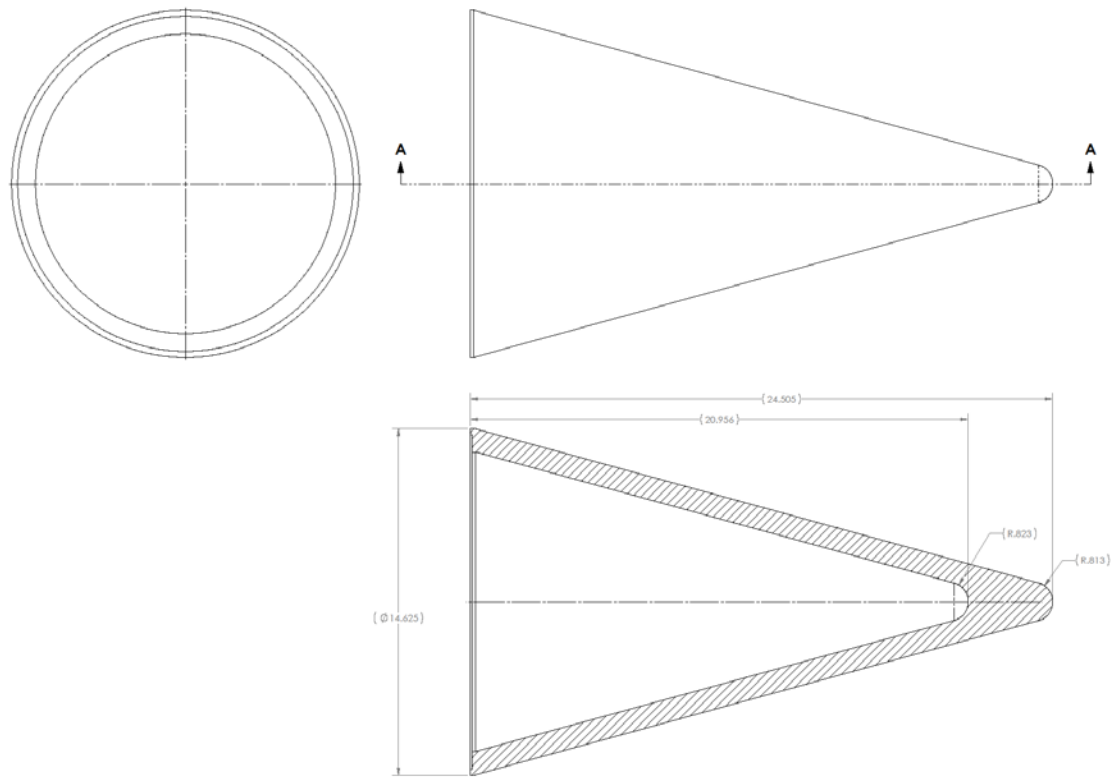

SECTION A-A

SHEET 1 2 3 4 5 6	TITLE INSULATION, CONE		
ISSUE			
PART CLASSIFICATION UNCLASSIFIED			
DRAWING CLASSIFICATION UNCLASSIFIED	SIZE D	DRAWING NUMBER R63045	
	CAGE/RC 14213	SCALE 1:2	SHEET 1 OF 1
STATUS SA-REL-3/17/2004	ORIGIN SolidWorks 2004		

NOTES:

1. GENERAL REQUIREMENTS AND DRAWING INTERPRETATION PER 9900000.
2. MATERIAL: KOAWOOL BLANKET
3. CERTIFICATION OF MANUFACTURER'S TEST REPORTS (CMTR'S) REQUIRED.
4. SHAPE TO BE OBTAINED BY WRAPPING DURING ASSEMBLY PROCESS.
5. APPROX. WEIGHT IS 8.5 LBS.

DESIGN AGENCY PART NUMBER	REVISION						
	ISSUE	SHEET ZONE	PREPARED BY	DESCRIPTION	DATE	CHKR	APVD
R63046-000			D. SAMUEL, 2992/ P. H. HELMICK, 6871		3/17/2004		PHH

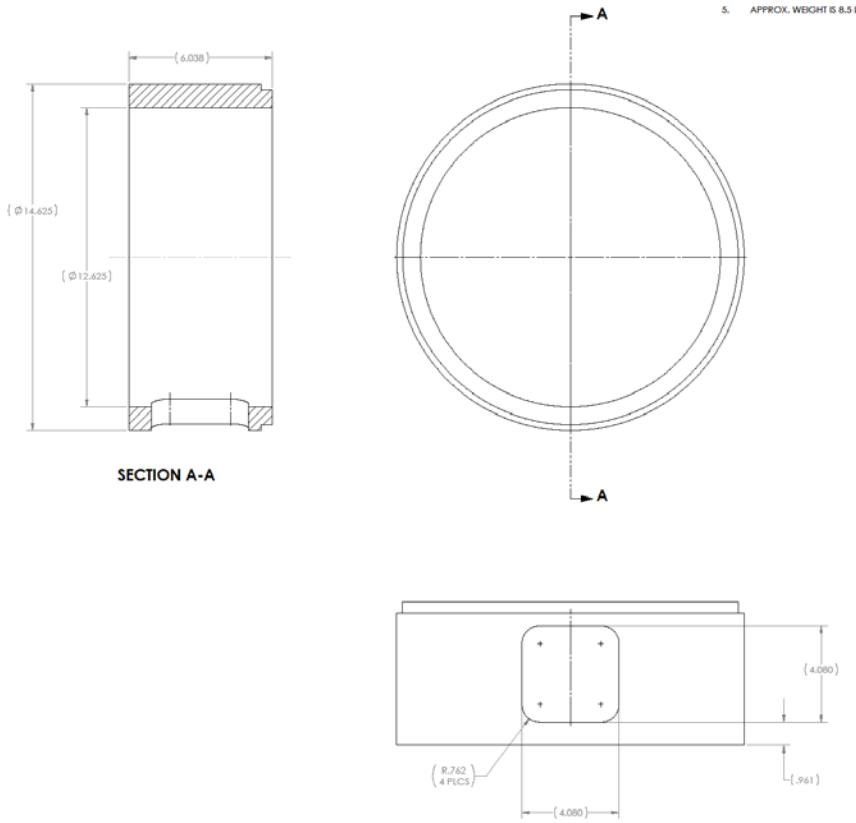

SHEET 1 2 3 4 5 6		TITLE	INSULATION, MID SECTION
ISSUE			
PART CLASSIFICATION	UNCLASSIFIED		
DRAWING CLASSIFICATION	UNCLASSIFIED	SIZE D	DRAWING NUMBER R63046
		CAGE/RC 14213	SCALE 1:2 SHEET 1 OF 1
STATUS	SA-REL-3/17/2004	ORIGIN	SolidWorks 2004

NOTES:

1. GENERAL REQUIREMENTS AND DRAWING INTERPRETATION PER 9900000.
2. MATERIAL: KOAWOOL BLANKET
3. CERTIFICATION OF MANUFACTURER'S TEST REPORTS (CMTR'S) REQUIRED.
4. SHAPE TO BE OBTAINED BY WRAPPING DURING ASSEMBLY PROCESS.
5. APPROX. WEIGHT IS 13.0 LBS.

DESIGN AGENCY PART NUMBER	REVISION						
	ISSUE	SHEET ZONE	PREPARED BY	DESCRIPTION	DATE	CHKR	APVD
R63047-000			D. SAMUEL, 2992/ P. H. HELMICK, 6871		3/17/2004		PHH

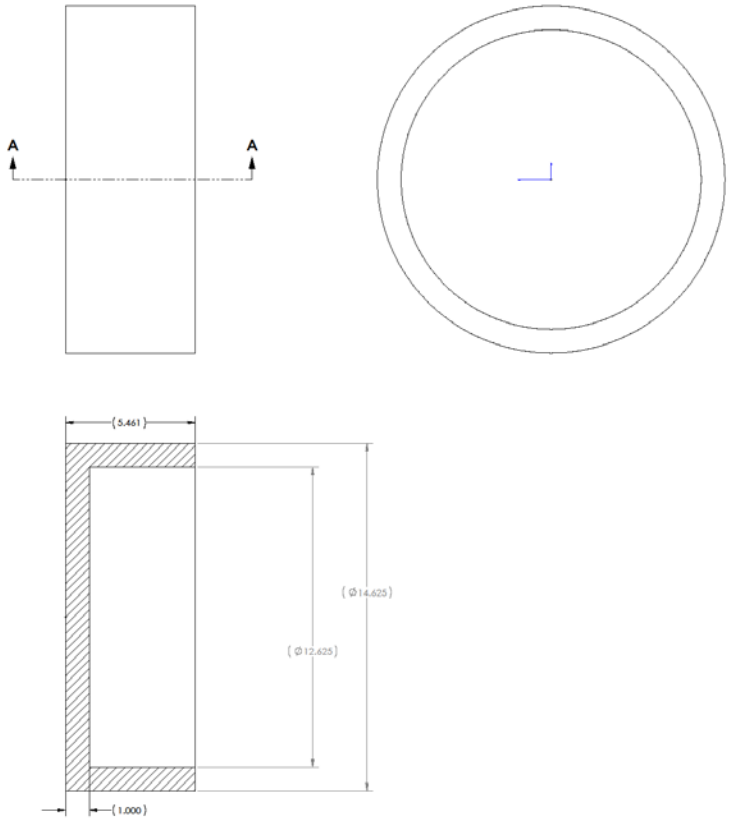

SECTION A-A

SHEET 1 2 3 4 5 6		TITLE	INSULATION, BACK
ISSUE			
PART CLASSIFICATION	UNCLASSIFIED		
DRAWING CLASSIFICATION	UNCLASSIFIED	SIZE D	DRAWING NUMBER R63047
		CAGE/RC 14213	SCALE 1:2 SHEET 1 OF 1
STATUS SA-REL-3/17/2004		ORIGIN SolidWorks 2004	

APPENDIX B COMPLEX CALORIMETER THERMOCOUPLE LOCATIONS

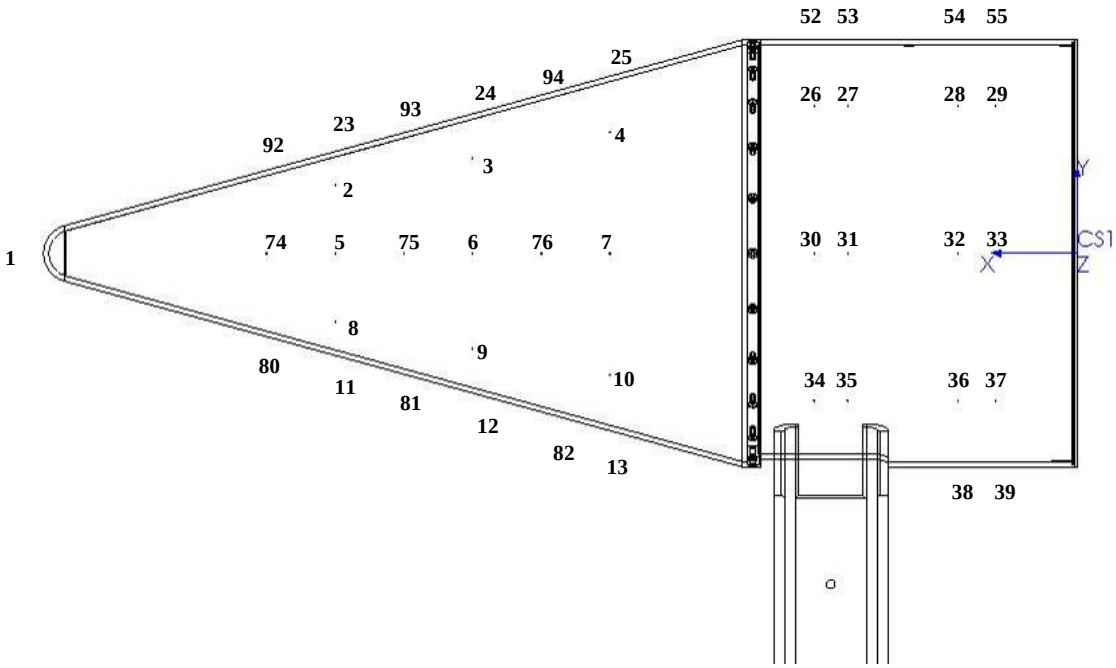

Figure 1. Outer shell (-z side)

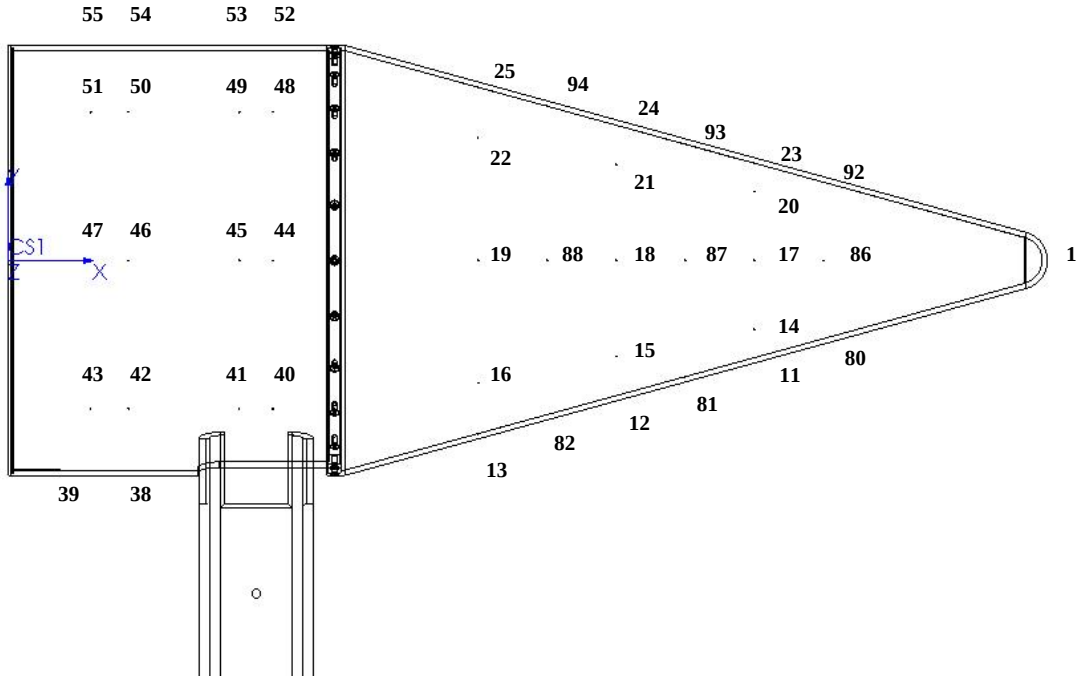

Figure 2. Outer shell (+z side)

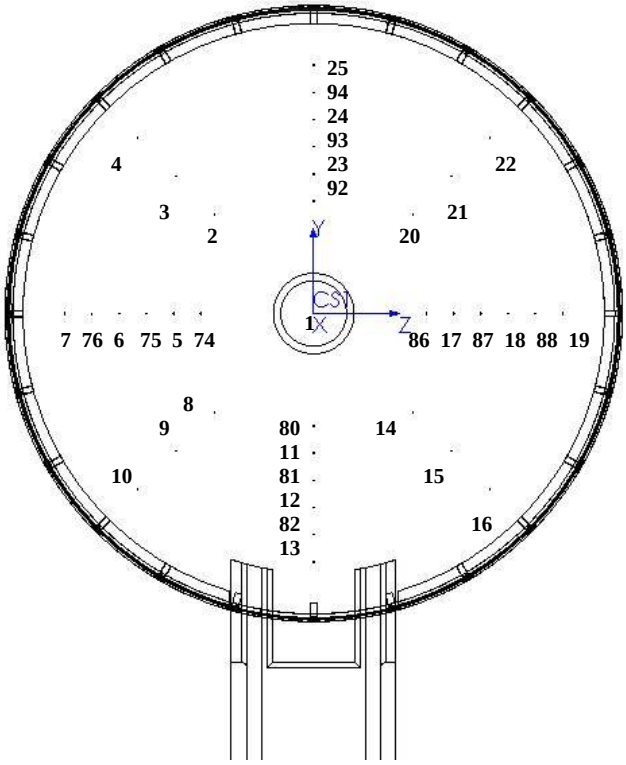

Figure 3. Outer shell cone (inside view)

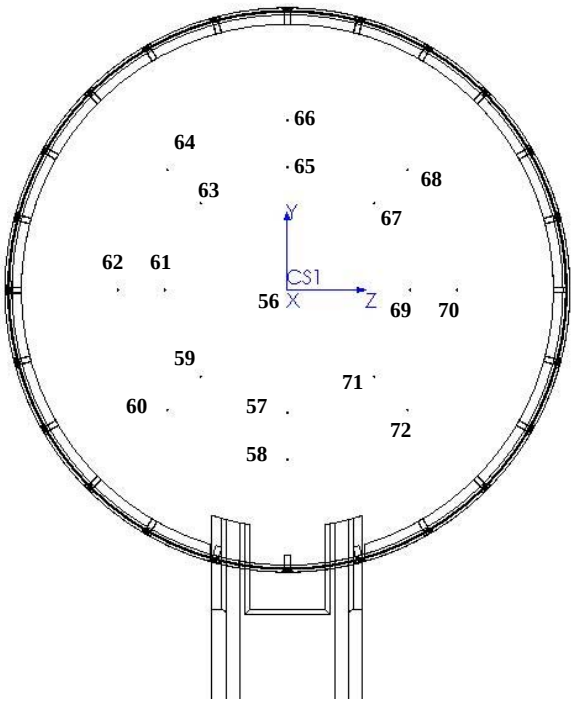

Figure 4. Outer shell bottom plate (outside view)

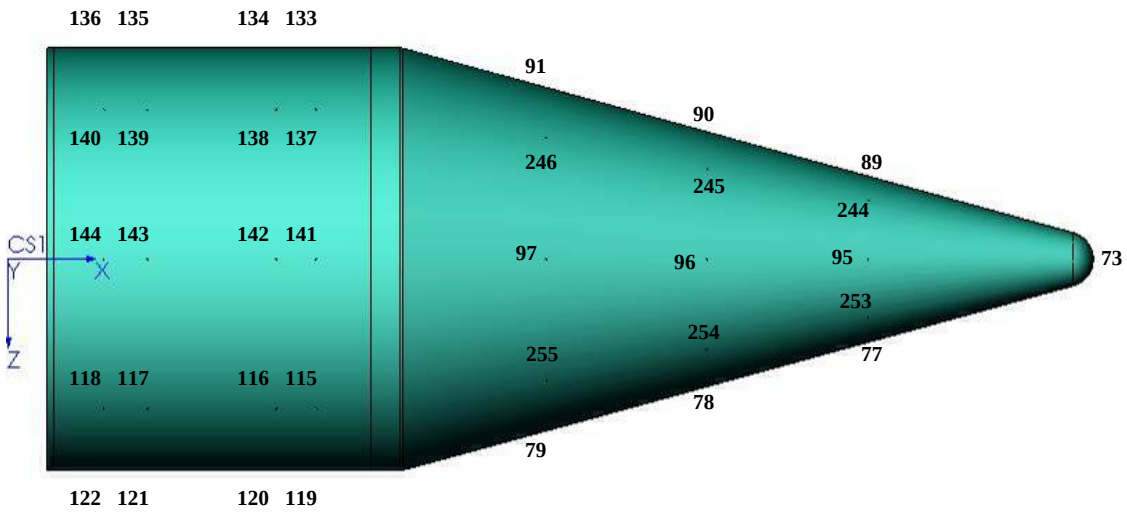

Figure 5. Inner shell (top view)

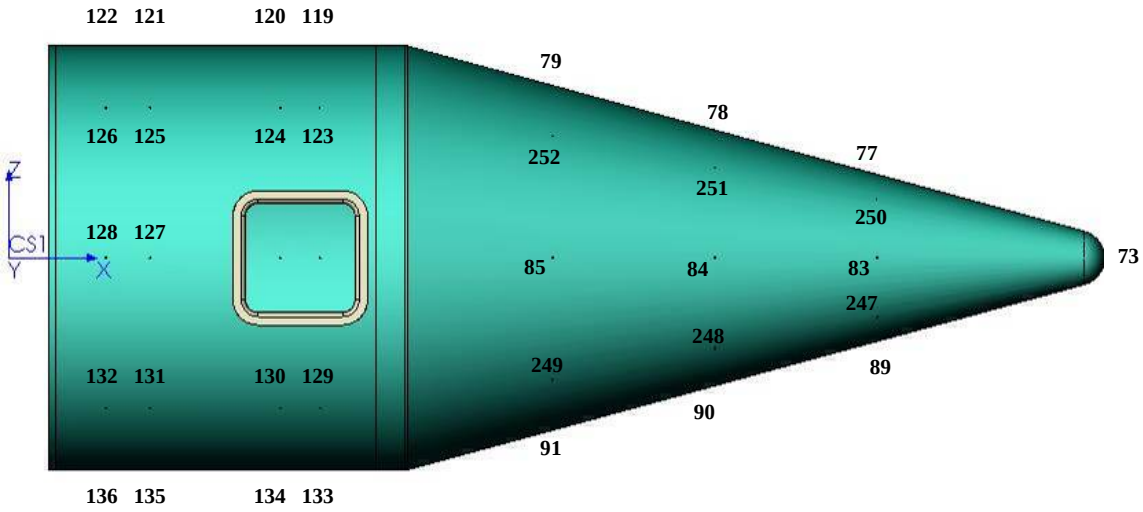

Figure 6. Inner shell (bottom view)

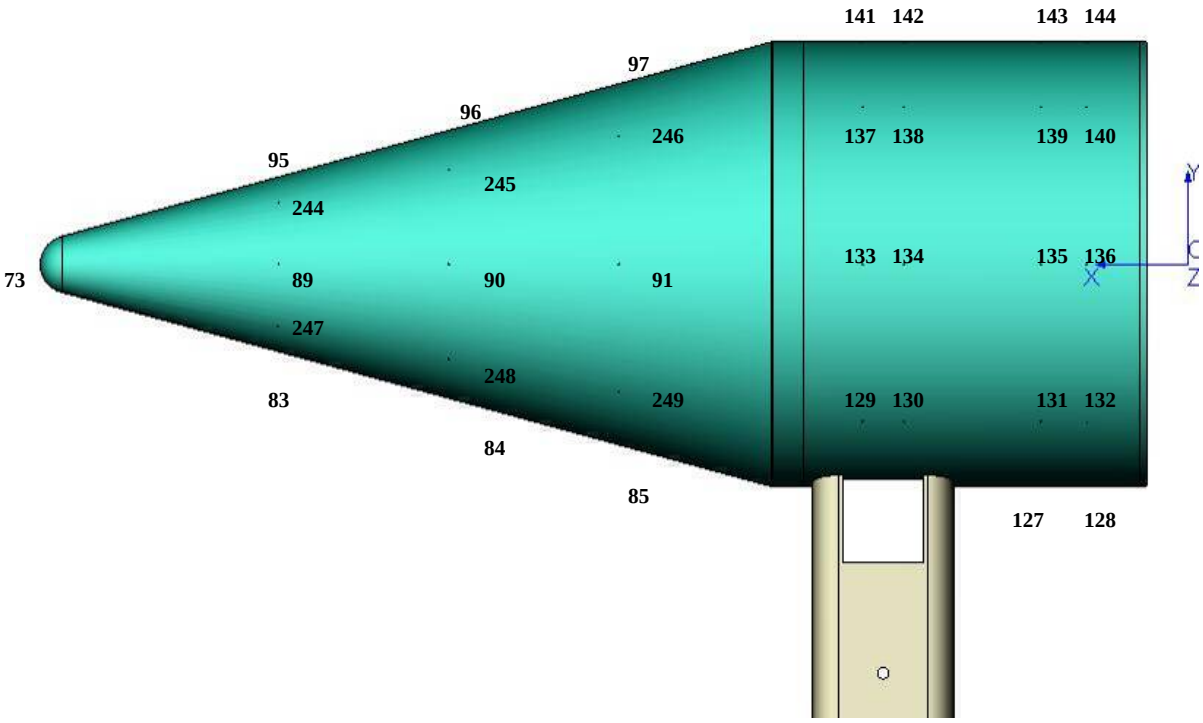

Figure 7. Inner shell (-z side)

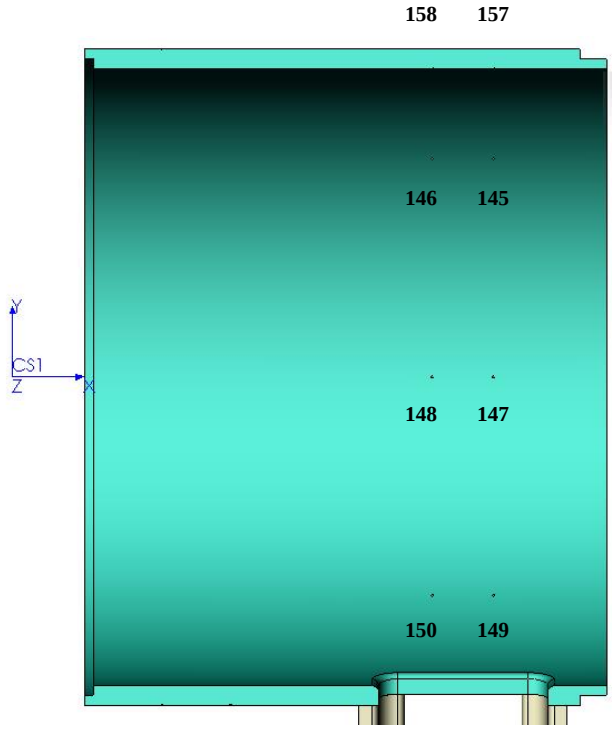

Figure 8. Inner shell inner surface (-z side)

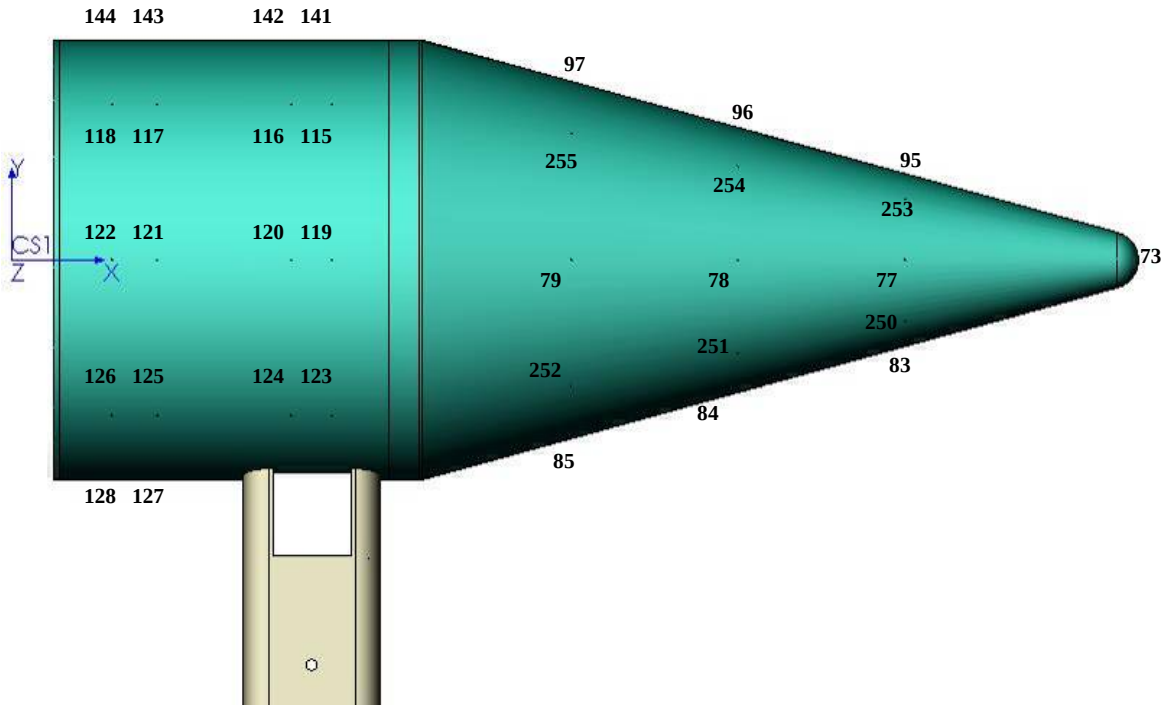

Figure 9. Inner shell (+z side)

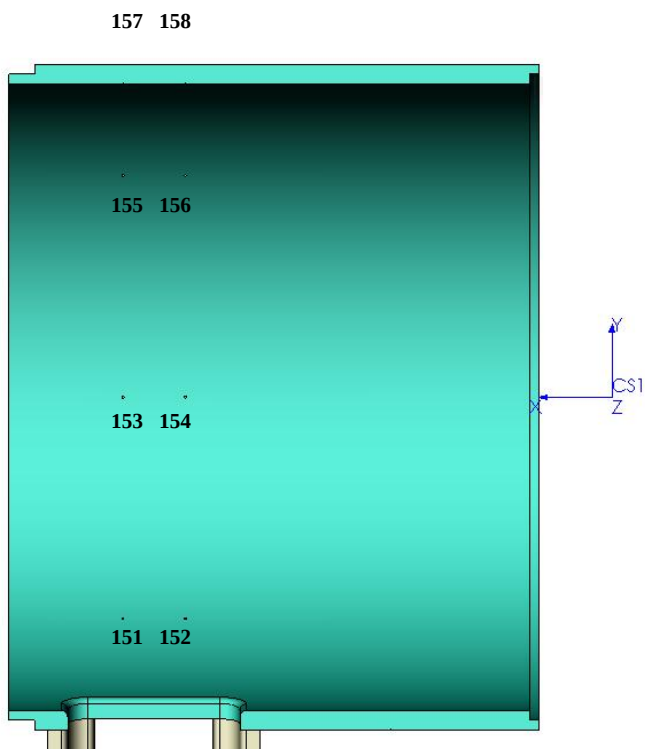

Figure 10. Inner shell inner surface (+z side)

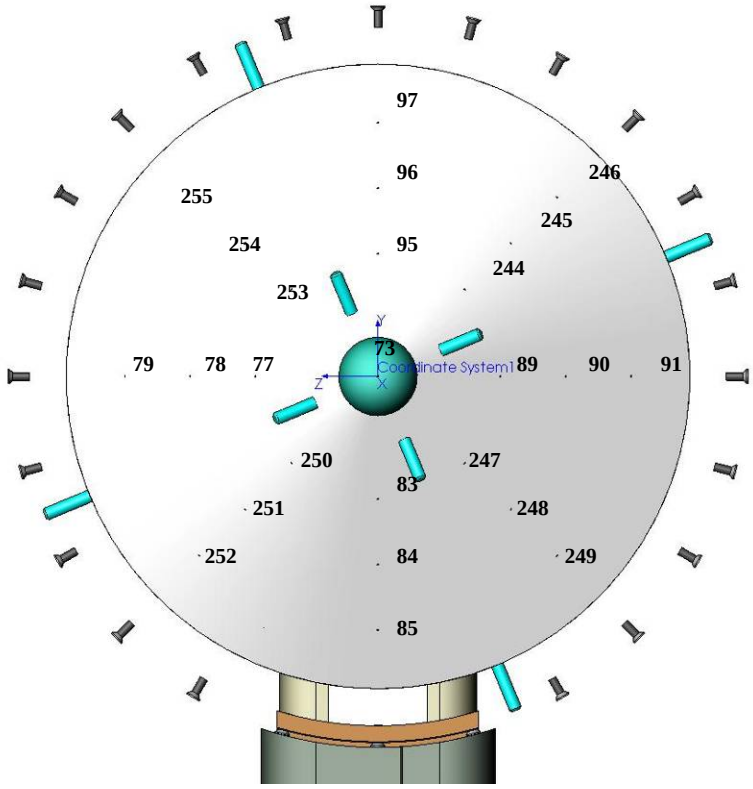

Figure 11. Inner shell cone (outside view)

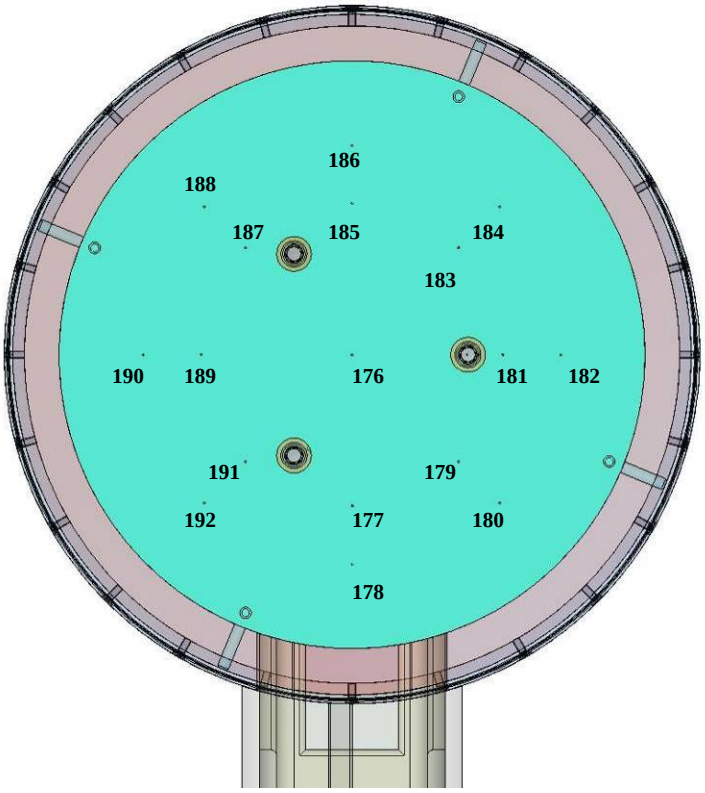

Figure 12. Inner shell bottom plate (outside view)

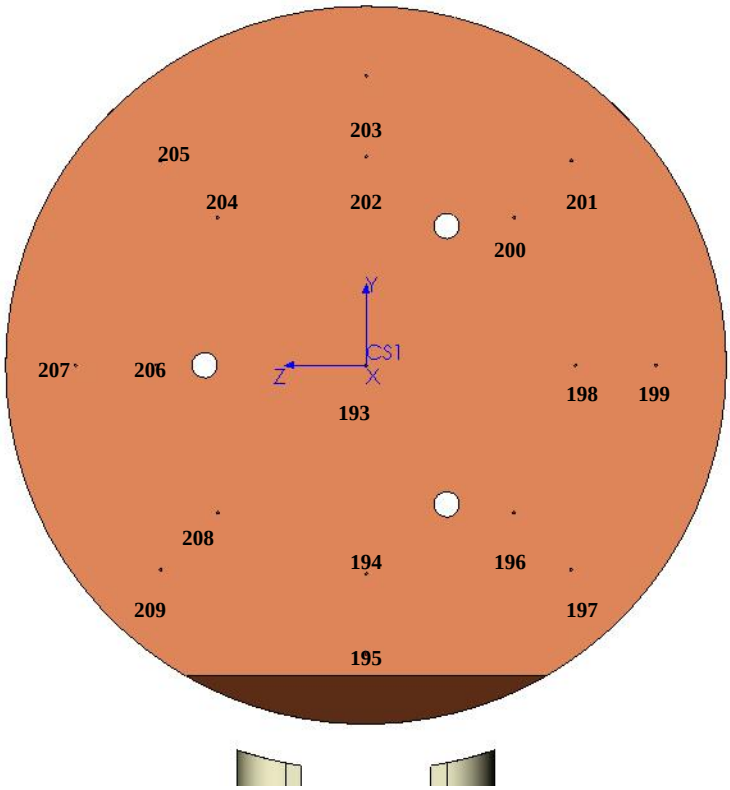

Figure 13. Blivet cone side

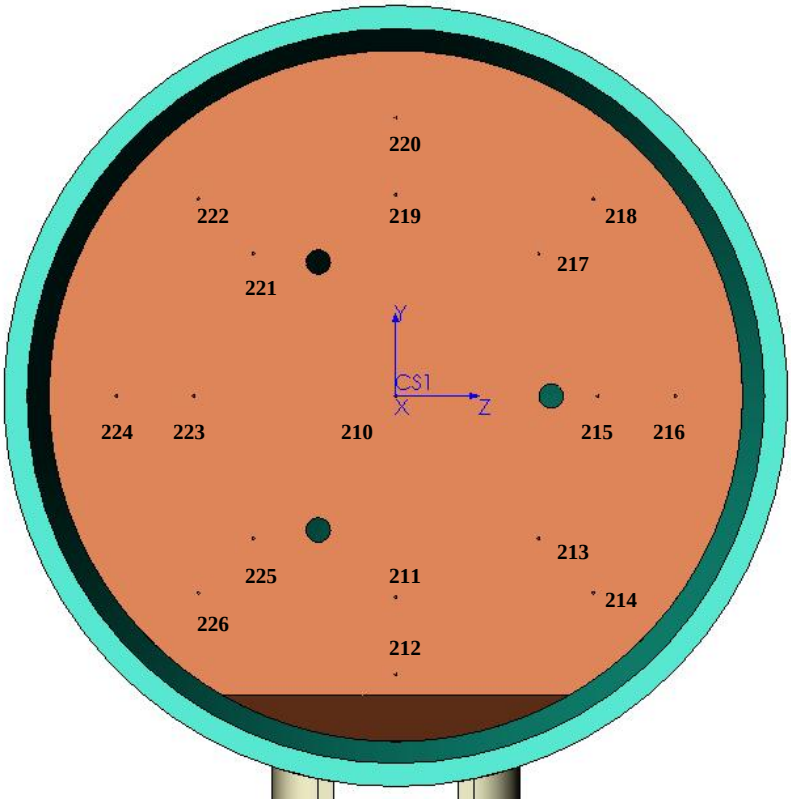

Figure 14. Blivet cylinder side

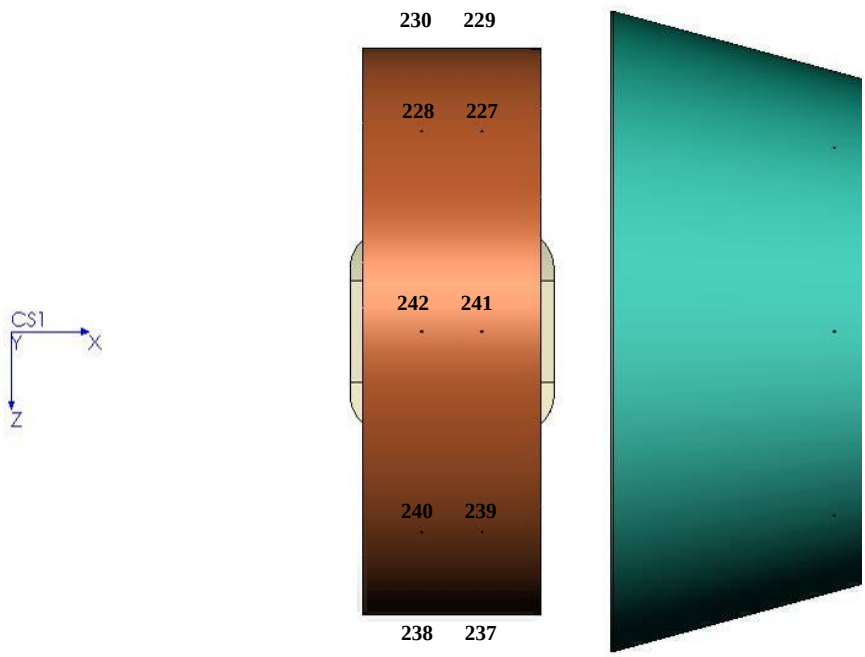

Figure 15. Blivet top side

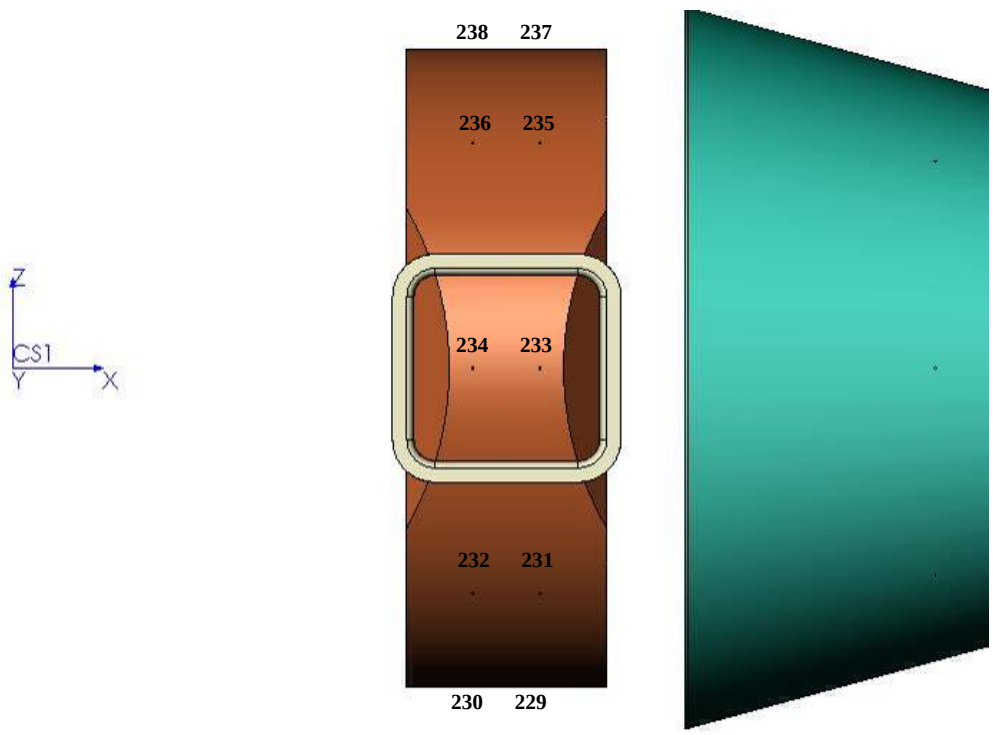

Figure 16. Blivet bottom side

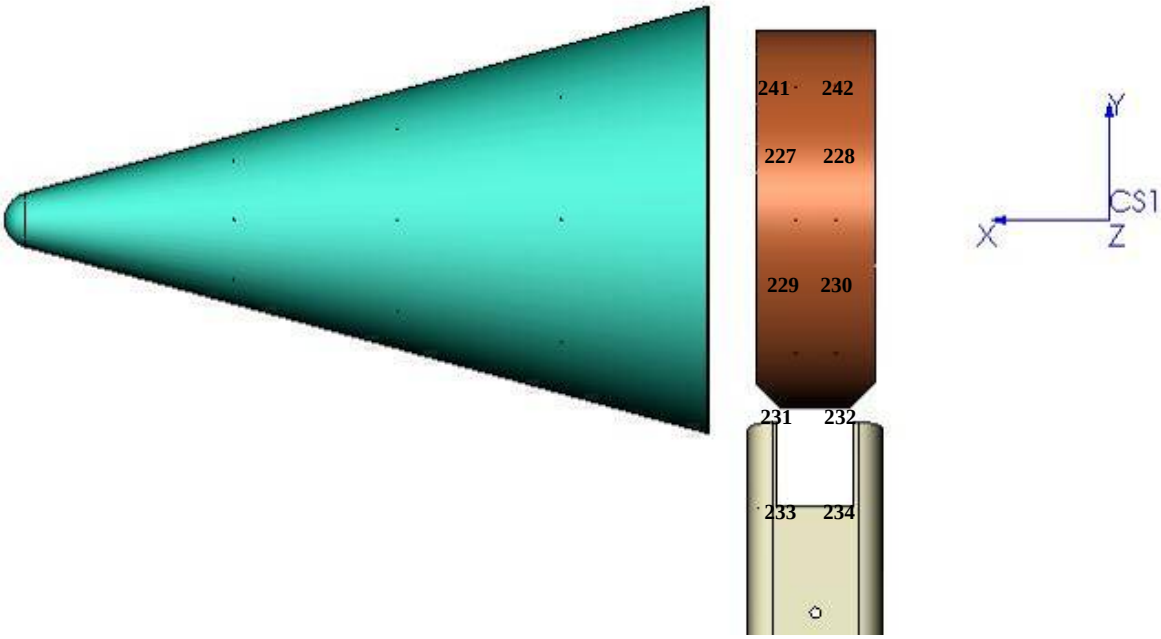

Figure 17. Blivet (-z side)

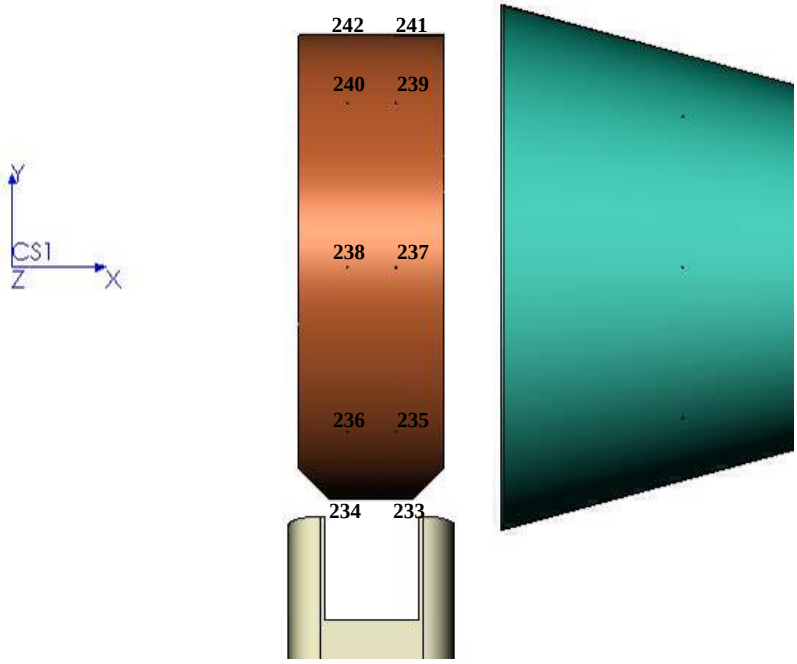

Figure 18. Blivet (+z side)

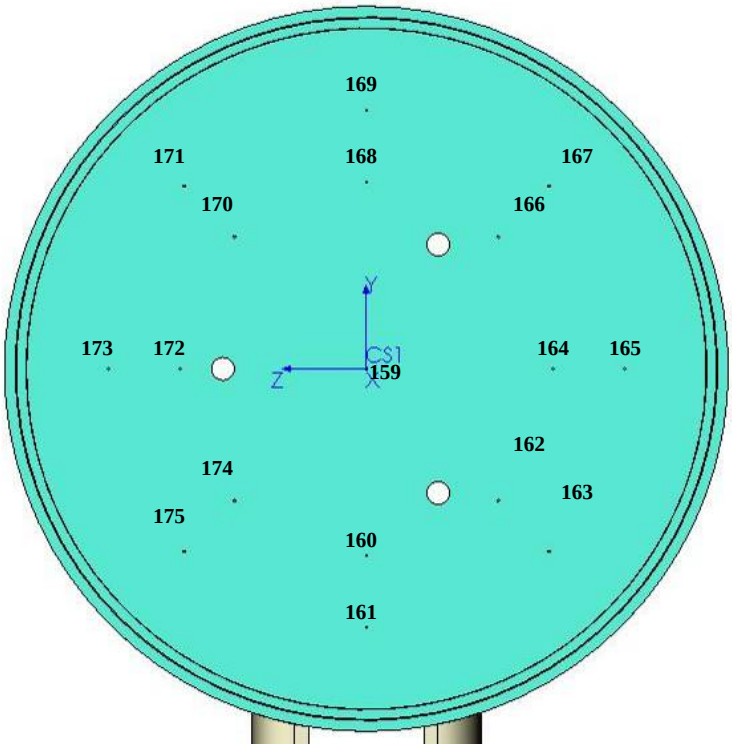

Figure 19. Inner shell cylinder plate to blivet

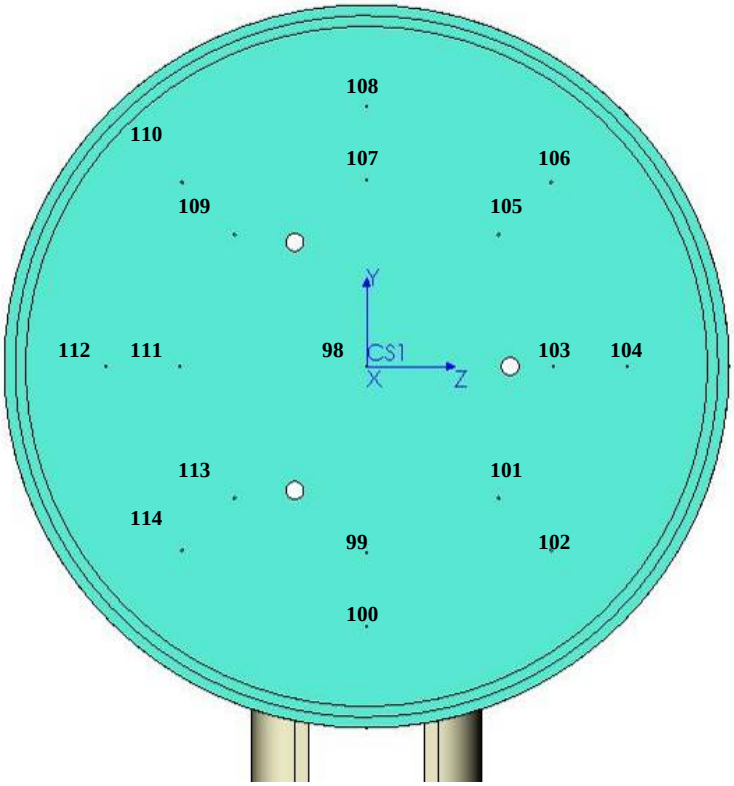

Figure 20. Inner shell cone plate to blivet

The following table gives the name of each thermocouple (TC), color coded to a surface. Each TC has a corresponding data acquisition (DAQ) number, a TC number, and a location number matching to the above drawings. The coordinate system (in inches) is the same as the global Cartesian coordinate system used in the CALORE model.

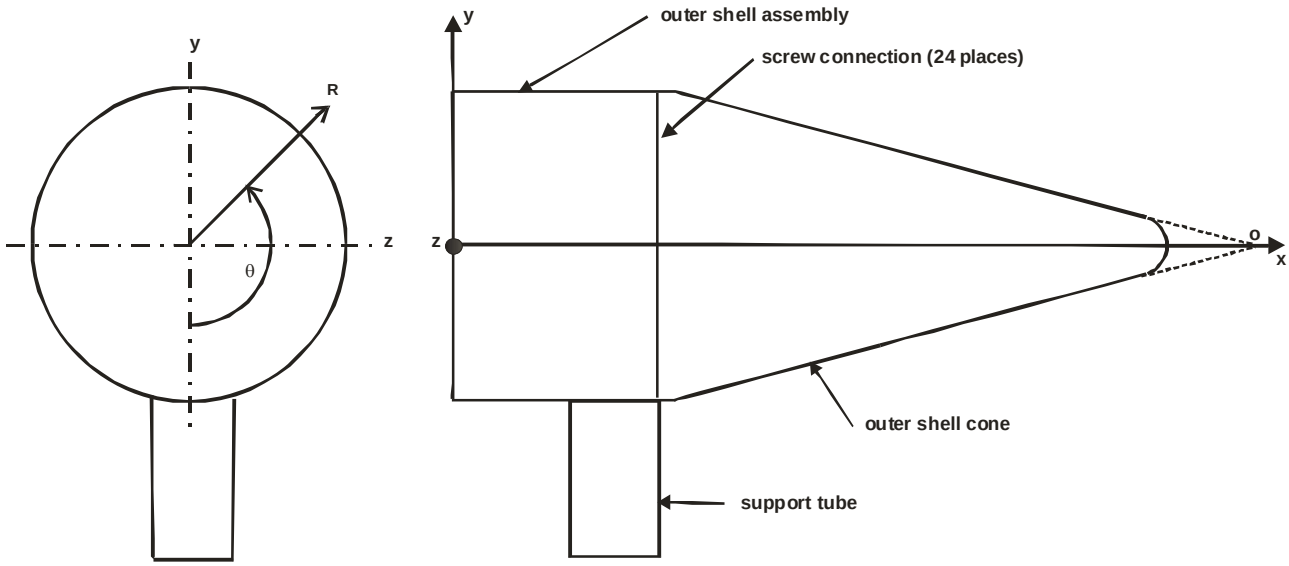

Coordinate systems for complex calorimeter

name	daq #	tc #	loc #	x calore	y calore	z calore
Inner bucket/outer surface unrolled	DAQ1	128	LOC128	2.87	-6.30	0.00
Inner bucket/outer surface unrolled	DAQ2	130	LOC130	8.06	-4.46	-4.46
Inner bucket/surface below blivit	DAQ3	162	LOC162	5.89	-2.30	-2.30
Inner bucket/outer surface unrolled	DAQ4	125	LOC125	4.18	-4.46	4.46
Inner bucket/surface below blivit	DAQ5	161	LOC161	5.89	-4.50	0.00
Inner bucket/surface below blivit	DAQ6	171	LOC171	5.89	3.18	3.18
Inner bucket/inner surface unrolled	DAQ7	149	LOC149	9.23	-4.20	-4.20
Inner bucket/outer surface unrolled	DAQ8	134	LOC134	8.06	0.00	-6.30
Inner bucket/Bottom Side	DAQ9	182	LOC182	1.19	0.00	4.50
Inner bucket/outer surface unrolled	DAQ10	115	LOC115	9.23	4.46	4.46
Inner bucket/surface below blivit	DAQ11	169	LOC169	5.89	4.50	0.00
Inner bucket/outer surface unrolled	DAQ12	143	LOC143	4.18	6.30	0.00
Inner bucket/inner surface unrolled	DAQ13	157	LOC157	9.23	5.94	0.00
Inner bucket/outer surface	DAQ14	142	LOC142	8.06	6.30	0.00

unrolled						
Inner bucket/outer surface unrolled	DAQ15	139	LOC139	4.18	4.46	-4.46
Inner bucket/outer surface unrolled	DAQ16	141	LOC141	9.23	6.30	0.00
Inner bucket/inner surface unrolled	DAQ17	152	LOC152	8.06	-4.20	4.20
Inner bucket/Bottom Side	DAQ18	185	LOC185	1.19	3.25	0.00
Inner bucket/surface below blivit	DAQ19	163	LOC163	5.89	-3.18	-3.18
Inner bucket/Bottom Side	DAQ20	176	LOC176	1.19	0.00	0.00
Inner bucket/inner surface unrolled	DAQ21	158	LOC158	8.06	5.94	0.00
Inner bucket/inner surface unrolled	DAQ22	145	LOC145	9.23	4.20	-4.20
Inner bucket/outer surface unrolled	DAQ23	138	LOC138	8.06	4.46	-4.46
Inner bucket/outer surface unrolled	DAQ24	135	LOC135	4.18	0.00	-6.30
Inner bucket/Bottom Side	DAQ25	186	LOC186	1.19	4.50	0.00
Inner bucket/outer surface unrolled	DAQ26	133	LOC133	9.23	0.00	-6.30
Inner bucket/outer surface unrolled	DAQ27	144	LOC144	2.87	6.30	0.00
Inner bucket/Bottom Side	DAQ28	184	LOC184	1.19	3.18	3.18
Inner bucket/Bottom Side	DAQ29	191	LOC191	1.19	-2.30	-2.30
Inner bucket/outer surface unrolled	DAQ30	118	LOC118	2.87	4.46	4.46
Inner bucket/Bottom Side	DAQ31	189	LOC189	1.19	0.00	-3.25
Inner bucket/surface below blivit	DAQ32	168	LOC168	5.89	3.25	0.00
Inner bucket/surface below blivit	DAQ33	173	LOC173	5.89	0.00	4.50
Inner bucket/inner surface unrolled	DAQ34	155	LOC155	9.23	4.20	4.20
Inner bucket/outer surface unrolled	DAQ35	136	LOC136	2.87	0.00	-6.30
Inner bucket/inner surface unrolled	DAQ36	154	LOC154	8.06	0.00	5.94
Inner bucket/outer surface unrolled	DAQ37	140	LOC140	2.87	4.46	-4.46
Inner bucket/outer surface unrolled	DAQ38	137	LOC137	9.23	4.46	-4.46
Inner bucket/inner surface unrolled	DAQ39	156	LOC156	8.06	4.20	4.20
Inner bucket/Bottom Side	DAQ40	181	LOC181	1.19	0.00	3.25
Inner bucket/Bottom Side	DAQ41	190	LOC190	1.19	0.00	-4.50
Inner bucket/inner surface unrolled	DAQ42	153	LOC153	9.23	0.00	5.94
Inner bucket/outer surface unrolled	DAQ43	119	LOC119	9.23	0.00	6.30
Inner bucket/outer surface unrolled	DAQ44	116	LOC116	8.06	4.46	4.46
Inner bucket/Bottom Side	DAQ45	183	LOC183	1.19	2.30	2.30
Inner bucket/Bottom Side	DAQ46	177	LOC177	1.19	-3.25	0.00
Inner bucket/inner surface unrolled	DAQ47	147	LOC147	9.23	0.00	-5.94

Inner bucket/Bottom Side	DAQ48	178	LOC178	1.38	-4.50	0.00
Inner bucket/Bottom Side	DAQ49	188	LOC188	1.19	3.18	-3.18
Inner bucket/surface below blivit	DAQ50	170	LOC170	5.89	2.30	2.30
Inner bucket/Bottom Side	DAQ51	187	LOC187	1.19	2.30	-2.30
Inner bucket/inner surface unrolled	DAQ52	146	LOC146	8.06	4.20	-4.20
Inner bucket/surface below blivit	DAQ53	167	LOC167	5.89	3.18	-3.18
Inner bucket/surface below blivit	DAQ54	174	LOC174	5.89	-2.30	2.30
Inner bucket/inner surface unrolled	DAQ55	151	LOC151	9.23	-4.20	4.20
Inner bucket/outer surface unrolled	DAQ56	122	LOC122	2.87	0.00	6.30
Inner bucket/outer surface unrolled	DAQ57	126	LOC126	2.87	-4.46	4.46
Inner bucket/surface below blivit	DAQ58	165	LOC165	5.89	0.00	-4.50
Inner bucket/surface below blivit	DAQ59	166	LOC166	5.89	2.30	-2.30
Inner bucket/Bottom Side	DAQ60	192	LOC192	1.19	-3.18	-3.18
Inner bucket/surface below blivit	DAQ61	164	LOC164	5.89	0.00	-3.25
Inner bucket/outer surface unrolled	DAQ62	117	LOC117	4.18	4.46	4.46
Inner bucket/Bottom Side	DAQ63	180	LOC180	1.19	-3.18	3.18
Inner bucket/surface below blivit	DAQ64	160	LOC160	5.89	-3.25	0.00
Inner bucket/Bottom Side	DAQ65	179	LOC179	1.19	-2.30	2.30
Inner bucket/inner surface unrolled	DAQ66	148	LOC148	8.06	0.00	-5.94
Inner bucket/outer surface unrolled	DAQ67	121	LOC121	4.18	0.00	6.30
Inner bucket/outer surface unrolled	DAQ68	132	LOC132	2.87	-4.46	-4.46
Inner bucket/outer surface unrolled	DAQ69	123	LOC123	9.23	-4.46	4.46
Inner bucket/surface below blivit	DAQ70	159	LOC159	5.89	0.00	0.00
Inner bucket/surface below blivit	DAQ71	172	LOC172	5.89	0.00	3.25
Inner bucket/inner surface unrolled	DAQ72	150	LOC150	8.06	-4.20	-4.20
Inner bucket/outer surface unrolled	DAQ73	131	LOC131	4.18	-4.46	-4.46
Inner bucket/outer surface unrolled	DAQ74	120	LOC120	8.06	0.00	6.30
Inner bucket/outer surface unrolled	DAQ75	129	LOC129	9.23	-4.46	-4.46
Inner bucket/outer surface unrolled	DAQ76	124	LOC124	8.06	-4.46	4.46
Inner bucket/outer surface unrolled	DAQ77	127	LOC127	4.18	-6.30	0.00
Inner bucket/surface below blivit	DAQ78	175	LOC175	5.89	-3.18	3.18
Blivit/Side	DAQ79	235	LOC235	9.23	-3.95	3.95
Blivit/Side	DAQ80	242	LOC242	8.06	5.58	0.00
Blivit/Side	DAQ81	231	LOC231	9.23	-3.95	-3.95
Blivit/Bottom	DAQ82	225	LOC225	6.90	-2.30	-2.30
Blivit/Top	DAQ83	195	LOC195	10.39	-4.50	0.00
Blivit/Top	DAQ84	194	LOC194	10.39	-3.25	0.00
Blivit/Side	DAQ85	241	LOC241	9.23	5.58	0.00

Blivit/Bottom	DAQ86	224	LOC224	6.90	0.00	-4.50
Blivit/Top	DAQ87	197	LOC197	10.39	-3.18	-3.18
Blivit/Bottom	DAQ88	220	LOC220	6.90	4.50	0.00
Blivit/Side	DAQ89	227	LOC228	9.23	3.95	-3.95
Blivit/Top	DAQ90	193	LOC193	10.39	0.00	0.00
Blivit/Side	DAQ91	234	LOC233	9.23	-5.58	0.00
Blivit/Top	DAQ92	196	LOC196	10.39	-2.30	-2.30
Blivit/Side	DAQ93	232	LOC232	8.06	-3.95	-3.95
Blivit/Side	DAQ94	240	LOC240	8.06	3.95	3.95
Blivit/Side	DAQ95	228	LOC227	8.06	3.95	-3.95
Blivit/Side	DAQ96	238	LOC238	8.06	0.00	5.58
Blivit/Side	DAQ97	233	LOC234	8.06	-5.58	0.00
Blivit/Top	DAQ98	209	LOC209	10.39	-3.18	3.18
Blivit/Side	DAQ99	230	LOC229	9.23	0.00	-5.58
Blivit/Top	DAQ100	198	LOC198	10.39	0.00	-3.25
Blivit/Bottom	DAQ101	222	LOC222	6.90	3.18	-3.18
Blivit/Top	DAQ102	203	LOC204	10.39	4.50	0.00
Blivit/Top	DAQ103	202	LOC202	10.39	3.25	0.00
Blivit/Top	DAQ104	208	LOC208	10.39	-2.30	2.30
Blivit/Top	DAQ105	201	LOC201	10.39	3.18	-3.18
Blivit/Bottom	DAQ106	219	LOC219	6.90	3.25	0.00
Blivit/Bottom	DAQ107	217	LOC217	6.90	2.30	2.30
Blivit/Top	DAQ108	200	LOC200	10.39	2.30	-2.30
Blivit/Top	DAQ109	205	LOC205	10.39	3.18	3.18
Blivit/Bottom	DAQ110	216	LOC216	6.90	0.00	4.50
Blivit/Side	DAQ111	239	LOC239	9.23	3.95	3.95
Blivit/Top	DAQ112	206	LOC207	10.39	0.00	3.25
Blivit/Top	DAQ113	207	LOC206	10.39	0.00	4.50
Blivit/Top	DAQ114	204	LOC203	10.39	2.30	2.30
Blivit/Bottom	DAQ115	211	LOC211	6.90	-3.25	0.00
Blivit/Bottom	DAQ116	218	LOC218	6.90	3.18	3.18
Blivit/Bottom	DAQ117	214	LOC214	6.90	-3.18	3.18
Blivit/Side	DAQ118	229	LOC230	8.06	0.00	-5.58
Blivit/Top	DAQ119	199	LOC199	10.39	0.00	-4.50
Blivit/Bottom	DAQ120	215	LOC215	6.90	0.00	3.25
Blivit/Side	DAQ121	236	LOC236	8.06	-3.95	3.95
Blivit/Bottom	DAQ122	226	LOC226	6.90	-3.18	-3.18
Blivit/Bottom	DAQ123	210	LOC210	6.90	0.00	0.00
Blivit/Bottom	DAQ124	221	LOC221	6.90	2.30	-2.30
Blivit/Bottom	DAQ125	213	LOC213	6.90	-2.30	2.30
Blivit/Bottom	DAQ126	223	LOC223	6.90	0.00	-3.25
Blivit/Side	DAQ127	237	LOC237	9.23	0.00	5.58
Blivit/Bottom	DAQ128	212	LOC212	6.90	-4.50	0.00
Inner Cone	DAQ129	253	LOC253	25.79	1.75	1.75
Inner Cone	DAQ130	244	LOC244	25.79	1.75	-1.75
Inner Cone	DAQ131	254	LOC254	20.97	2.69	2.69
Inner Cone	DAQ132	95	LOC95	25.79	2.48	0.00
Inner Cone	DAQ133	255	LOC255	16.15	3.62	3.62
Inner Cone	DAQ134	248	LOC248	20.97	-2.69	-2.69
Inner Cone	DAQ135	83	LOC83	25.79	-2.48	0.00

Inner Cone	DAQ136	252	LOC252	16.15	-3.62	3.62
Inner Cone	DAQ137	77	LOC77	25.79	0.00	2.48
Inner Cone/Bottom Plate	DAQ138	99	LOC99	11.42	-3.25	0.00
Inner Cone	DAQ139	97	LOC97	16.15	5.12	0.00
Inner Cone	DAQ140	96	LOC96	20.97	3.80	0.00
Inner Cone	DAQ141	245	LOC245	20.97	2.69	-2.69
Inner Cone	DAQ142	73	LOC73	32.55	0.00	0.00
Inner Cone	DAQ143	79	LOC79	16.15	0.00	5.12
Inner Cone	DAQ144	250	LOC250	25.79	-1.75	1.75
Inner Cone	DAQ145	78	LOC78	20.97	0.00	3.80
Inner Cone	DAQ146	247	LOC247	25.79	-1.75	-1.75
Inner Cone/Bottom Plate	DAQ147	104	LOC104	11.42	0.00	4.54
Inner Cone/Bottom Plate	DAQ148	111	LOC111	11.42	0.00	-3.25
Inner Cone	DAQ149	84	LOC84	20.97	-3.80	0.00
Inner Cone	DAQ150	249	LOC249	16.15	-3.62	-3.62
Inner Cone	DAQ151	89	LOC89	25.79	0.00	-2.48
Inner Cone	DAQ152	246	LOC246	16.15	3.62	-3.62
Inner Cone/Bottom Plate	DAQ153	98	LOC98	11.42	0.00	0.00
Inner Cone	DAQ154	90	LOC90	20.97	0.00	-3.80
Inner Cone	DAQ155	91	LOC91	16.15	0.00	-5.12
Inner Cone/Bottom Plate	DAQ156	112	LOC112	11.42	0.00	-4.54
Inner Cone/Bottom Plate	DAQ157	107	LOC107	11.42	3.25	0.00
Inner Cone/Bottom Plate	DAQ158	113	LOC113	11.42	-2.30	-2.30
Inner Cone/Bottom Plate	DAQ159	103	LOC103	11.42	0.00	3.25
Inner Cone	DAQ160	251	LOC251	20.97	-2.69	2.69
Inner Cone	DAQ161	85	LOC85	16.15	-5.12	0.00
Inner Cone/Bottom Plate	DAQ162	243	LOC101	11.42	-2.30	2.30
Inner Cone/Bottom Plate	DAQ163	114	LOC114	11.42	-3.21	-3.21
Inner Cone/Bottom Plate	DAQ164	105	LOC105	11.42	2.30	2.30
Inner Cone/Bottom Plate	DAQ165	100	LOC100	11.42	-4.54	0.00
Inner Cone/Bottom Plate	DAQ166	110	LOC110	11.42	3.21	-3.21
Inner Cone/Bottom Plate	DAQ167	108	LOC108	11.42	4.54	0.00
Inner Cone/Bottom Plate	DAQ168	102	LOC102	11.42	-3.21	3.21
Inner Cone/Bottom Plate	DAQ169	109	LOC109	11.42	2.30	-2.30
Inner Cone/Bottom Plate	DAQ170	106	LOC106	11.42	3.21	3.21
Outer Bucket/Bottom plate	DAQ171	65	LOC65	0.19	3.25	0.00
Outer Bucket/Bottom plate	DAQ172	63	LOC63	0.19	2.30	-2.30
Outer Bucket/inner surface unrolled	DAQ173	55	LOC55	2.87	7.31	0.00
Outer Bucket/inner surface unrolled	DAQ174	29	LOC29	2.87	5.17	-5.17
Outer Bucket/Bottom plate	DAQ175	66	LOC66	0.19	4.50	0.00
Outer Bucket/inner surface unrolled	DAQ176	36	LOC36	4.18	-5.17	-5.17
Outer Bucket/inner surface unrolled	DAQ177	47	LOC47	2.87	0.00	7.31
Outer Bucket/inner surface unrolled	DAQ178	54	LOC54	4.18	7.31	0.00
Outer Bucket/inner surface unrolled	DAQ179	32	LOC32	4.18	0.00	-7.31
Outer Bucket/Bottom plate	DAQ180	69	LOC69	0.19	0.00	3.25
Outer Bucket/inner surface	DAQ181	46	LOC46	4.18	0.00	7.31

unrolled						
Outer Bucket/inner surface unrolled	DAQ182	27	LOC27	8.06	5.17	-5.17
Outer Bucket/inner surface unrolled	DAQ183	48	LOC48	9.23	5.17	5.17
Outer Bucket/inner surface unrolled	DAQ184	42	LOC42	4.18	-5.17	5.17
Outer Bucket/inner surface unrolled	DAQ185	33	LOC33	2.87	0.00	-7.31
Outer Bucket/inner surface unrolled	DAQ186	30	LOC30	9.23	0.00	-7.31
Outer Bucket/inner surface unrolled	DAQ187	28	LOC28	4.18	5.17	-5.17
Outer Bucket/inner surface unrolled	DAQ188	39	LOC39	2.87	-7.31	0.00
Outer Bucket/Bottom plate	DAQ189	71	LOC71	0.19	-2.30	2.30
Outer Bucket/inner surface unrolled	DAQ190	37	LOC37	2.87	-5.17	-5.17
Outer Bucket/inner surface unrolled	DAQ191	52	LOC52	9.23	7.31	0.00
Outer Bucket/inner surface unrolled	DAQ192	43	LOC43	2.87	-5.17	5.17
Outer Bucket/Bottom plate	DAQ193	56	LOC56	0.19	0.00	0.00
Outer Bucket/inner surface unrolled	DAQ194	53	LOC53	8.06	7.31	0.00
Outer Bucket/inner surface unrolled	DAQ195	34	LOC34	9.23	-5.17	-5.17
Outer Bucket/inner surface unrolled	DAQ196	40	LOC40	9.23	-5.17	5.17
Outer Bucket/Bottom plate	DAQ197	62	LOC62	0.19	0.00	-4.50
Outer Bucket/Bottom plate	DAQ198	59	LOC59	0.19	-2.30	-2.30
Outer Bucket/Bottom plate	DAQ199	67	LOC67	0.19	2.30	2.30
Outer Bucket/Bottom plate	DAQ200	61	LOC61	0.19	0.00	-3.25
Outer Bucket/inner surface unrolled	DAQ201	41	LOC41	8.06	-5.17	5.17
Outer Bucket/inner surface unrolled	DAQ202	35	LOC35	8.06	-5.17	-5.17
Outer Bucket/inner surface unrolled	DAQ203	38	LOC38	4.18	-7.31	0.00
Outer Bucket/inner surface unrolled	DAQ204	51	LOC51	2.87	5.17	5.17
Outer Bucket/Bottom plate	DAQ205	68	LOC68	0.19	3.18	3.18
Outer Bucket/Bottom plate	DAQ206	72	LOC72	0.19	-3.18	3.18
Outer Bucket/Bottom plate	DAQ207	64	LOC64	0.19	3.18	-3.18
Outer Bucket/inner surface unrolled	DAQ208	26	LOC26	9.23	5.17	-5.17
Outer Bucket/Bottom plate	DAQ209	57	LOC57	0.19	-3.25	0.00
Outer Bucket/inner surface unrolled	DAQ210	50	LOC50	4.18	5.17	5.17
Outer Bucket/Bottom plate	DAQ211	58	LOC58	0.19	-4.50	0.00
Outer Bucket/inner surface unrolled	DAQ212	44	LOC44	9.23	0.00	7.31
Outer Bucket/inner surface unrolled	DAQ213	31	LOC31	8.06	0.00	-7.31

Outer Bucket/Bottom plate	DAQ214	60	LOC60	0.19	-3.18	-3.18
Outer Bucket/Bottom plate	DAQ215	70	LOC70	0.19	0.00	4.50
Outer Bucket/inner surface unrolled	DAQ216	45	LOC45	8.06	0.00	7.31
Outer Bucket/inner surface unrolled	DAQ217	49	LOC49	8.06	5.17	5.17
Outer Cone	DAQ218	86	LOC86	28.44	0.00	2.76
Outer Cone	DAQ219	23	LOC23	26.03	3.42	0.00
Outer Cone	DAQ220	92	LOC92	28.44	2.76	0.00
Outer Cone	DAQ221	24	LOC24	21.21	4.76	0.00
Outer Cone	DAQ222	21	LOC21	21.21	3.37	3.37
Outer Cone	DAQ223	1	LOC1	36.10	0.00	0.00
Outer Cone	DAQ224	5	LOC5	26.03	0.00	-3.42
Outer Cone	DAQ225	18	LOC18	21.21	0.00	4.76
Outer Cone	DAQ226	20	LOC20	26.03	2.42	2.42
Outer Cone	DAQ227	2	LOC2	26.03	2.42	-2.42
Outer Cone	DAQ228	14	LOC14	26.03	-2.42	2.42
Outer Cone	DAQ229	25	LOC25	16.39	6.10	0.00
Outer Cone	DAQ230	74	LOC74	28.44	0.00	-2.76
Outer Cone	DAQ231	22	LOC22	16.39	4.31	4.31
Outer Cone	DAQ232	93	LOC93	23.62	4.09	0.00
Outer Cone	DAQ233	7	LOC7	16.39	0.00	-6.10
Outer Cone	DAQ234	17	LOC17	26.03	0.00	3.42
Outer Cone	DAQ235	13	LOC13	16.39	-6.10	0.00
Outer Cone	DAQ236	15	LOC15	21.21	-3.37	3.37
Outer Cone	DAQ237	4	LOC4	16.39	4.31	-4.31
Outer Cone	DAQ238	76	LOC76	18.80	0.00	-5.43
Outer Cone	DAQ239	87	LOC87	23.62	0.00	4.09
Outer Cone	DAQ240	16	LOC16	16.39	-4.31	4.31
Outer Cone	DAQ241	19	LOC19	16.39	0.00	6.10
Outer Cone	DAQ242	10	LOC10	16.39	-4.31	-4.31
Outer Cone	DAQ243	3	LOC3	21.21	3.37	-3.37
Outer Cone	DAQ244	94	LOC94	18.80	5.43	0.00
Outer Cone	DAQ245	80	LOC80	28.44	-2.76	0.00
Outer Cone	DAQ246	75	LOC75	23.62	0.00	-4.09
Outer Cone	DAQ247	12	LOC12	21.21	-4.76	0.00
Outer Cone	DAQ248	11	LOC11	26.03	-3.42	0.00
Outer Cone	DAQ249	9	LOC9	21.21	-3.37	-3.37
Outer Cone	DAQ250	88	LOC88	18.80	0.00	5.43
Outer Cone	DAQ251	82	LOC82	18.80	-5.43	0.00
Outer Cone	DAQ252	6	LOC6	21.21	0.00	-4.76
Outer Cone	DAQ253	8	LOC8	26.03	-2.42	-2.42
Outer Cone	DAQ254	81	LOC81	23.62	-4.09	0.00

DISTRIBUTION

MS0384	D.B. Dimos, 1500
MS1139	D.L. Miller, 1530
MS1135	R.D. Watkins, 1532
MS1135	T.K. Blanchat, 1532 (5)
MS0836	S.R. Tieszen, 1532
MS0826	W. Gill, 1532
MS1135	J.T. Nakos, 1532
MS1135	D. Jernigan, 1532
MS0828	V.J. Romero, 1544
MS0828	A.R. Black, 1544
MS0836	S.P. Domino, 1541
MS0340	S.E. Slezak, 2141
MS9042	A.R. Ortega, 8005
MS9001	C. Moen, 8775
MS0899	Technical Library, 9536 (electronic copy)